# Compliance, locomotion and local computation in (self-) reconfigurable modular robots

Thèse N° 9578

Présentée le 9 août 2019

à la Faculté des sciences et techniques de l'ingénieur
Laboratoire de biorobotique
Programme doctoral en robotique, contrôle et systèmes intelligents

pour l'obtention du grade de Docteur ès Sciences

par

Simon Lukas HAUSER

Acceptée sur proposition du jury

Prof. J. Paik, présidente du jury
Prof. A. Ijspeert, directeur de thèse
Prof. J. Bongard, rapporteur
Prof. J. Rossiter, rapporteur
Prof. D. Floreano, rapporteur

2019

ÉCOLE POLYTECHNIQUE
FÉDÉRALE DE LAUSANNE

But there is still a catch.
Computer simulations can not account for everything,
like the complexities of gravity.
— in a video of the *Nature* magazine on why to do experiments in the real world

In honor of the moments where dedication is driven by the will to advance science.

# Acknowledgements

This chapter is dedicated to saying thanks to all the people that paved the way for my pursuit of a doctoral degree.

I would like to first thank my advisor Prof. Auke Jan Ijspeert. It was a unique opportunity to work in his Biorobotics Laboratory, and he actively contributes to a fruitful research ground, scientifically and socially. He left me all the freedom I wished for and supported all ideas with constructive feedback and positive thinking, making life as a Ph.D. a pleasant experience. His general care and initiative for many lab outings and team building events made the atmosphere in the lab an enjoyable workplace. Further, I would like to thank the members of my thesis committee, Prof. Josh Bongard, Prof. Jonathan Rossiter, Prof. Dario Floreano, and Prof. Jamie Paik, for their time and their valuable suggestions and comments on the thesis. In addition, thanks to EPFL and the Swiss National Science Foundation (SNSF) for supporting my work.

The next thanks goes to my Ph.D. colleague and partner in crime, Mehmet Mutlu. I had the pleasure of being hired on a project in a team and could not have wished for a better teammate. Mehmet's helpfulness has no boundaries and he patiently would explain me his world of electronics, which ultimately brought life into my mechanical designs. Together we managed to create a variety of fun robots and projects. Here I also would like to acknowledge the invaluable help of our technician François Longchamp, who always had an ear and two crafty hands to help me with designs and ideas.

Of course the whole lab deserves credit for a very friendly work environment as well as unforgettable social events. I specifically would like to thank Robin for the many night talks on the bikes, Tomislav for his down-to-earth opinions, Shravan for the introduction into the Indian community, Behzad for his general knowledgeable advice, Ale for everything he does to keep things running, and Sylvie for her invaluable work behind the scenes. Special thanks to Massimo and Stéphane for their guidance in the first phase of my PhD, and to all current and previous members of BioRob who positively influenced my Ph.D. with fruitful discussions and collaborations. Thanks to the students I had the pleasure to supervise, in particular Rui and Matthieu who significantly advanced my research, and Jérémy for his help in software development.

The next thanks goes to friends and family. To my boys from the gymnasium; I am very fortunate to keep in contact with you and call you my friends, and spending time with you

never fails to bring me back to life. To my brother, who secretly shares my enthusiasm for robotic toys and motivates me. To my sister, who challenges me to justify my work from different perspectives. And to their partners and families for their opinions and support.

I would like to thank Wiola for all her love and patience. Two PhDs at the same stage often meant double the trouble, but also allowed us to have a full understanding of each other's challenges. Thank you for the continuous, unconditional support, the unique holiday experiences and the great time we had and have together. I am proud of us that we went through this together, and our writing time in Oberried will always have a special place in my heart.

Lastly, an enormous thanks to my parents. I am grateful for all they have done to enable me to be where I am today, keeping me motivated in good and difficult times, and never losing faith in my abilities.

Thank you all!

*Lausanne, 21th June 2019* S. H.

# Abstract

Animals display an enormous versatility and a remarkable ability to adapt to changes in environment and terrain. Research in bio-inspired robotics strives to transfer these skills to robots, including legged systems. Even though animals seemingly effortlessly perform most of their activities on rough terrain, this feature seems to be particularly difficult to achieve in their robotic counterparts. We hypothesize that perturbations caused by e.g. rough terrain are not handled by the central nervous system, but rather by local modifications of the locomotion system such as legs and feet. Modifications can include changing mechanical properties such as spring and damping characteristics, as well as adjustments in the movement pattern of the locomotion. In this thesis, we isolate instances where a specific component, in our view, needs such modifications to fulfill different functionalities in a locomotion cycle. Further, we introduce the concept of mode-switches: a local computation is performed to induce these changes in functionalities by changing the dynamical response of the component. We then present one mode-switch method in hardware, jamming of granular media, that can switch the functionality of a foot between "impact damping" and "propulsion force transmission", and we show how this regularizes step sizes on rough terrain. We then present one mode-switch method in control, a force feedback strategy named "tegotae". This switches the functionality of leg movement between "displacing the leg" and "displacing the body", and we show how this informs the controller about which legs are bearing less weight and thus are more suited to be moved. We suggest that these methods can be applied to any legged structure and use modular robots to demonstrate these concepts. In parallel, we also improved our previously developed self-reconfigurable modular robot platform "Roombots" such that they perform a variety of tasks centered around adaptive and assistive furniture with up to 12 modules. This includes demonstrations of self-reconfiguration, mobile furniture, object manipulation, interaction capabilities and the development of a user interface. With these improvements, this platform can in the future also be used for further locomotion research where the shape-shifting ability could be of major importance.

Key words: self-reconfiguration, modular robots, universal gripper, jamming of granular media, locomotion control, rough terrain, tegotae, arbitrary morphologies, local computation, robotics.

# Zusammenfassung

Die Fortbewegung von Tieren zeigt eine enorme Vielseitigkeit und eine bemerkenswerte Fähigkeit, sich an ändernde Umgebungen und Bodenstrukturen anzupassen. Die Forschung an biologisch inspirierten Robotern hat zum Ziel, solche Fähigkeiten auf Laufroboter zu übertragen. Obwohl es scheint, also ob Tiere ihre Bewegungen mühelos auch auf unebenem Untergrund ausführen, haben Laufroboter gerade mit dieser Eigenschaft einige Schwierigkeiten. Wir stellen die Hypothese auf, dass Störungen durch beispielsweise solche Unebenheiten nicht hauptsächlich vom zentralen Nervensystem bearbeitet werden, sondern von lokalen Modifikationen am Bewegungsapparat wie zum Beispiel Beinen und Füssen. Solche Modifikationen beinhalten Veränderungen von mechanischen Eigenschaften wie Federsteifigkeit und Dämpfungsverhalten sowie auch Veränderungen am Bewegungsmuster der Fortbewegung. Wir betrachten Fälle, in denen eine bestimmte Komponente im Bewegungsapparat eine solche Veränderung benötigt, um durch eine Änderung ihrer dynamischen Reaktion eine unterschiedliche Funktionsweise zu erzeugen. Wir führen das Konzept Modus-Wechsel ein, welches eine Art von lokaler Berechnung ausführt, um solche Wechsel in der Funktionsweise einzuleiten. Mit "Verklemmung durch granulare Medien" präsentieren wir eine mechanische Modus-Wechsel-Strategie, welche einen Fuss zwischen der Funktionweise "Aufpralldämpfung" und "Übertragung von Antriebskräften" hin und her schalten kann, und wir zeigen, wie dadurch die Schrittweite auf unebenem Grund verregelmässigt werden kann. Mit "Tegotae", einer speziellen Sensorrückführung von Antriebskräften, präsentieren wir dann eine Modus-Wechsel-Strategie in der Regelung. Diese Strategie kann eine Beinbewegung zwischen den Funktionsweisen "Bewegung des Beins" und "Bewegung des Körpers" hin und her schalten. Dies informiert die Steuerung darüber, welche Beine gerade weniger Gewicht tragen und daher besser bewegt werden können. Diese Strategien sind auf weitere Laufroboter übertragbar. Dazu verwenden wir modulare Roboter, die wir in unterschiedliche Konfigurationen zusammenbauen. Parallel beschreiben wir Verbesserungen an unserem selbst-rekonfigurierbaren modularen Robotersystem "Roombots" und demonstrieren eine Vielzahl von Aufgaben im Bereich "anpassungsfähige Möbel" mit bis zu 12 Modulen. Dazu gehören Selbst-Rekonfiguration, mobile Möbel, Objekthandhabung, Interaktionsfähigkeiten sowie Entwicklung einer Benutzeroberfläche. Diese Verbesserungen stellen dieses Robotersystem auch für zukünftige Forschung an der Fortbewegung bereit.

Stichwörter: Selbst-Rekonfiguration, Modulare Roboter, Universeller Greifer, Verklemmung durch granulare Medien, Fortbewegung, unebener Untergrund, Tegotae, beliebige Morphologie, lokale Berechnung, Robotik.

# Résumé

Les animaux font preuve d'une énorme versatilité et d'une capacité remarquable à s'adapter aux changements d'environnement et de terrain. La recherche en robotique bio-inspirée cherche à transférer ces capacités en robotique, y compris sur des systèmes à pattes. Bien que les animaux effectuent sans effort apparent la plupart de leurs activités sur terrain accidenté, cette capacité semble particulièrement difficile à transposer sur leurs équivalents robotiques. Nous émettons l'hypothèse que les perturbations engendrées p.ex. par un terrain accidenté ne sont pas gérées par le système nerveux central, mais plutôt par des changements locaux du système locomoteur comme les pattes et les pieds. Ces changements peuvent inclure des modifications des propriétés mécaniques telles que les caractéristiques de ressort et d'amortissement, ou des ajustements du schéma de mouvement de la locomotion. Dans cette thèse, nous isolons des cas particuliers dans lesquels un composant spécifique, selon nous, requiert de tels changements pour remplir différentes fonctions lors d'un cycle de locomotion. En outre, nous introduisons le concept de changements de mode : un calcul local est effectué afin d'induire ces modifications de fonctionnalité par un changement de la réponse dynamique du composant. Nous présentons ensuite une méthode matérielle de changement de mode, le coincement d'un milieu granulaire, qui permet le changement de la fonctionnalité d'un pied entre "amortissement d'impact" et "transmission de force de propulsion", et nous montrons comment ceci rend les tailles des pas régulières sur un terrain accidenté. Nous présentons par la suite une méthode de changement de mode dans le contrôle, une stratégie de feedback de force nommée "tegotae". Celle-ci commute la fonction du mouvement des pattes entre "déplacer la patte" et "déplacer le corps", et nous montrons comment ceci informe le contrôleur sur quelles pattes supportent le moins de poids et sont donc plus adaptées à être déplacées. Nous suggérons que ces méthodes peuvent être appliquées à toute structure à pattes, et nous utilisons des robots modulaires pour démontrer ces concepts. En parallèle, nous avons amélioré la plateforme modulaire auto-recofigurable "Roombots", développée par le passé, de manière à implémenter sur jusqu'à 12 modules une série de tâches liées à des meubles adaptatifs ou d'assistance. Ceci inclut des démonstrations d'auto-reconfiguration, des meubles mobiles, de la manipulations d'objets, des capacités d'interaction, et le développement d'une interface utilisateur. Cette plateforme pourra ainsi servir pour d'autres recherches sur la locomotion pour lesquelles la capacité à changer de forme pourrait être d'importance majeure.

Mots clés : auto-reconfiguration, robots modulaires, dispositif préhenseur universel, coincement d'un milieu granulaire, contrôle de locomotion, terrain accidenté, tegotae, morphologies arbitraires, calcul local, robotique.

# Contents

**Acknowledgements** v

**Abstract (English/Deutsch)** vii

**List of figures** xvii

**List of tables** xxi

**Introduction** 1

Industrial Revolution, car tires, and the knee joint . . . . . 1
Locomotion and local functionality changes . . . . . 3
Robots for biology and vice versa . . . . . 4
A word about the *reality gap* . . . . . 5
Thesis organization and main contributions . . . . . 6

**I Roombots: 3D self-reconfiguration** 9

**Topic of Part I** 11

Overview . . . . . 11
Robots-building robots: Modularity and self-reconfiguration . . . . . 11
Roombots: modular self-reconfiguration in three dimensions . . . . . 13

**1 Advancements and applications of the 3D SRMR Roombots** 15

1.1 Goal of the improvements . . . . . 16
1.2 Related work: 3D SRMRs, tracking and smart homes . . . . . 18
1.3 Advancements and supplementary systems . . . . . 20
1.3.1 Mechanics, motors and connection . . . . . 20
1.3.2 Sensors . . . . . 21
1.3.3 Spotlight LED . . . . . 23
1.3.4 Universal Gripper . . . . . 23
1.3.5 Electronics . . . . . 24
1.3.6 Motor control . . . . . 25
1.3.7 Connection control . . . . . 26
1.3.8 Graphical User Interface (GUI) . . . . . 27

1.3.9 RGB-D vision system . . . . . . . . . . 29
1.3.10 Robotic-enhanced furniture . . . . . . . . . . 29
1.4 Demonstrations of the five key-tasks . . . . . . . . . . 30
1.4.1 Easy-to-use user interface: the GUI . . . . . . . . . . 30
1.4.2 Scalable self-reconfiguration . . . . . . . . . . 31
1.4.3 Mobile furniture . . . . . . . . . . 33
1.4.4 Manipulating furniture . . . . . . . . . . 37
1.4.5 Interactive furniture . . . . . . . . . . 39
1.5 Discussion and Future work of the Roombots project . . . . . . . . . . 41
1.6 Conclusion: state of Roombots . . . . . . . . . . 42
1.7 Acknowledgments . . . . . . . . . . 43

**II Mode-switch in hardware: jamming of granular media 45**

**Topic of Part II 47**
Functionalities in jamming systems . . . . . . . . . . 47
Variable stiffness to change mechanical properties . . . . . . . . . . 48
Jamming of granular media . . . . . . . . . . 48
Controllable variable stiffness with compliant granules . . . . . . . . . . 49

**2 JammJoint: mobile jamming for variable stiffness 51**
2.1 Inspiration: Wearable joint support device . . . . . . . . . . 52
2.2 Description of the JammJoint device . . . . . . . . . . 52
2.3 Full-device characterization . . . . . . . . . . 53
2.3.1 Setup for stiffness measurements of the full device . . . . . . . . . . 53
2.3.2 Bending and torsion in the full device . . . . . . . . . . 55
2.4 Sub-component characterization . . . . . . . . . . 57
2.4.1 Setup for stiffness measurements of the sub-components . . . . . . . . . . 57
2.4.2 Stiffness of the column and ring sub-components . . . . . . . . . . 58
2.5 Properties of JammJoint . . . . . . . . . . 58
2.5.1 Change of spring stiffness . . . . . . . . . . 58
2.5.2 Additional modes . . . . . . . . . . 60
2.5.3 Passive adaptability, safety and operation time . . . . . . . . . . 60
2.6 Conclusion and Future Work . . . . . . . . . . 61

**3 Climbing with compliant grippers 63**
3.1 Inspiration: Legged climbing . . . . . . . . . . 63
3.2 Compressive stiffness characterization . . . . . . . . . . 64
3.2.1 Materials: Oblong latex membrane . . . . . . . . . . 64
3.2.2 Change of Young's modulus $E$ . . . . . . . . . . 65
3.3 Friction force on walls . . . . . . . . . . 67
3.3.1 Materials: Smooth and irregular walls . . . . . . . . . . 67
3.3.2 Vacuum-dependent and shape-adapted friction . . . . . . . . . . 68

3.4 Climbing vertical shafts . . . . . . . . . . . . . . . . . . . . . . . . . . . . . . . . . . . 70
3.4.1 Materials: Robotic Platform . . . . . . . . . . . . . . . . . . . . . . . . . . . . 70
3.4.2 Open-loop climbing on varying shaft layouts . . . . . . . . . . . . . . . . 73
3.5 Conclusion and Future Work . . . . . . . . . . . . . . . . . . . . . . . . . . . . . . 76

**4 Compliant Universal Grippers as adaptive feet 79**
4.1 Inspiration: Jamming membranes as feet . . . . . . . . . . . . . . . . . . . . . . . 80
4.1.1 Contact point vs. contact area . . . . . . . . . . . . . . . . . . . . . . . . . 80
4.1.2 Tackling the stiffness dilemma . . . . . . . . . . . . . . . . . . . . . . . . 82
4.2 Feet comparison . . . . . . . . . . . . . . . . . . . . . . . . . . . . . . . . . . . . 84
4.2.1 Feet in nature . . . . . . . . . . . . . . . . . . . . . . . . . . . . . . . . . . 84
4.2.2 Feet in currently used robots . . . . . . . . . . . . . . . . . . . . . . . . . 85
4.2.3 Foot design based on granular media . . . . . . . . . . . . . . . . . . . . 85
4.3 Static jamming: Are jamming feet viable? . . . . . . . . . . . . . . . . . . . . . . 86
4.3.1 Effects of jamming on contact friction and impact damping . . . . . . . . 86
4.3.2 Effects of jamming on speed and locomotion behavior with “Oncilla” . . 89
4.3.3 Conclusion of static jamming experiments . . . . . . . . . . . . . . . . . 91
4.4 Dynamic jamming: fast state-switch at touchdown . . . . . . . . . . . . . . . . . 92
4.4.1 Preliminary evacuation mechanism . . . . . . . . . . . . . . . . . . . . . 93
4.4.2 Evacuation speed . . . . . . . . . . . . . . . . . . . . . . . . . . . . . . . . 93
4.4.3 Effects on ground reaction force . . . . . . . . . . . . . . . . . . . . . . . 93
4.4.4 Conclusion of fast state-switching experiments . . . . . . . . . . . . . . . 96
4.5 Dynamic jamming: adaptive feet for rough terrain . . . . . . . . . . . . . . . . . 96
4.5.1 The MODOK quadruped robot platform . . . . . . . . . . . . . . . . . . . 96
4.5.2 Improved evacuation mechanism . . . . . . . . . . . . . . . . . . . . . . . 99
4.5.3 Rough terrain . . . . . . . . . . . . . . . . . . . . . . . . . . . . . . . . . . 101
4.5.4 Validation: Evacuation speed 2 . . . . . . . . . . . . . . . . . . . . . . . . 101
4.5.5 Validation: Altering ground reaction forces 2 . . . . . . . . . . . . . . . . 102
4.5.6 Locomotion on rough terrain . . . . . . . . . . . . . . . . . . . . . . . . . 106
4.6 Conclusion: jamming membranes as adaptive feet . . . . . . . . . . . . . . . . . 109

**III Mode-switch in control: phase oscillators 111**

**Topic of Part III 113**
Locomotion with Central Pattern Generators (CPGs) . . . . . . . . . . . . . . . . . . . 113
Functionalities in leg movements . . . . . . . . . . . . . . . . . . . . . . . . . . . . . . 114
Control framework for arbitrary legged morphologies . . . . . . . . . . . . . . . . . . 114

**5 Compliance through tegotae: stabilization and rough terrain locomotion 117**
5.1 Inspiration: Compliance in locomotion . . . . . . . . . . . . . . . . . . . . . . . . 118
5.2 Body compliance: Energy efficiency through joint compliance distribution . . . 118
5.2.1 MODOK configuration . . . . . . . . . . . . . . . . . . . . . . . . . . . . . 118
5.2.2 Effects of joint compliance distribution . . . . . . . . . . . . . . . . . . . 119

5.2.3 Conclusions of joint compliance distribution experiments . . . . . . . . 120
5.3 Control compliance: Stability through tegotae . . . . . . . . . . . . . . . . . . . . 120
5.3.1 Tegotae, the rule of good feedback . . . . . . . . . . . . . . . . . . . . . . . . . 121
5.3.2 MODOK configuration . . . . . . . . . . . . . . . . . . . . . . . . . . . . . . . . . 122
5.3.3 Emergence of gaits: convergence to walking trot . . . . . . . . . . . . . . 122
5.3.4 Steady state limit cycle behavior . . . . . . . . . . . . . . . . . . . . . . . . . . 124
5.3.5 Gait adaptation to morphological modifications . . . . . . . . . . . . . . 124
5.3.6 Conclusions of stability through tegotae . . . . . . . . . . . . . . . . . . . . 129
5.4 Stability on rough terrain: Tegotae and joint compliance . . . . . . . . . . . . . 129
5.4.1 MODOK configuration . . . . . . . . . . . . . . . . . . . . . . . . . . . . . . . . . 129
5.4.2 Performance metrics . . . . . . . . . . . . . . . . . . . . . . . . . . . . . . . . . . 131
5.4.3 Locomotion on flat surface, rough surface and rough inclination . . . . . 133
5.5 Conclusions of tegotae for rough terrain locomotion and Future Work . . . . . . 139

**6 Learning to move in arbitrary morphologies 141**
6.1 Inspiration: Locomotion adaptation in animals . . . . . . . . . . . . . . . . . . . 142
6.1.1 Recovery of locomotion ability . . . . . . . . . . . . . . . . . . . . . . . . . . . 142
6.1.2 Approaches in robotics . . . . . . . . . . . . . . . . . . . . . . . . . . . . . . . . 142
6.1.3 Application of tegotae in arbitrary morphologies . . . . . . . . . . . . . . 143
6.1.4 Prerequisites for multi-legged tegotae . . . . . . . . . . . . . . . . . . . . . . 144
6.2 The ARBITER robotic platform . . . . . . . . . . . . . . . . . . . . . . . . . . . . . . 145
6.2.1 Modular motors and modular sensors . . . . . . . . . . . . . . . . . . . . . . 145
6.2.2 Costs . . . . . . . . . . . . . . . . . . . . . . . . . . . . . . . . . . . . . . . . . . . . 146
6.3 Controller strategy: twitching, learning and tegotae . . . . . . . . . . . . . . . . 146
6.3.1 Full process: building to walking . . . . . . . . . . . . . . . . . . . . . . . . . . 146
6.3.2 Model simplifications at the current stage of the project . . . . . . . . . . 147
6.3.3 Spontaneous Motor Activity . . . . . . . . . . . . . . . . . . . . . . . . . . . . . 148
6.3.4 Number of limbs . . . . . . . . . . . . . . . . . . . . . . . . . . . . . . . . . . . . 148
6.3.5 Motor-sensor correlations . . . . . . . . . . . . . . . . . . . . . . . . . . . . . . 149
6.3.6 Internal kinematic model . . . . . . . . . . . . . . . . . . . . . . . . . . . . . . . 151
6.3.7 Accelerations . . . . . . . . . . . . . . . . . . . . . . . . . . . . . . . . . . . . . . 155
6.3.8 Assignment of oscillator parameters . . . . . . . . . . . . . . . . . . . . . . . 156
6.3.9 Simulation . . . . . . . . . . . . . . . . . . . . . . . . . . . . . . . . . . . . . . . . 157
6.4 Conclusion and Future work . . . . . . . . . . . . . . . . . . . . . . . . . . . . . . . 157

**Conclusion and Future Work 159**
Roombots as a self-reconfigurable modular robot platform . . . . . . . . . . . . . . . 160
Summary and outcomes . . . . . . . . . . . . . . . . . . . . . . . . . . . . . . . . . . 160
Future Work . . . . . . . . . . . . . . . . . . . . . . . . . . . . . . . . . . . . . . . . . 161
Distributed intelligence for locomotion . . . . . . . . . . . . . . . . . . . . . . . . . . . 161
Summary and outcomes . . . . . . . . . . . . . . . . . . . . . . . . . . . . . . . . . . 161
Future Work . . . . . . . . . . . . . . . . . . . . . . . . . . . . . . . . . . . . . . . . . 164

**A Further applications with Roombots** **165**
A.1 Application: Playdough to Roombots . . . . . 165
A.1.1 Purpose . . . . . 165
A.1.2 Summary of the work . . . . . 166
A.2 Application: natural user interface . . . . . 169
A.2.1 Purpose . . . . . 169
A.2.2 Summary of the work . . . . . 169
A.3 Application: virtual reality for reconfigurable rooms . . . . . 170
A.3.1 Purpose . . . . . 170
A.3.2 Summary of the work . . . . . 170

**B Correlation maps** **173**

**Bibliography** **190**

**Curriculum Vitae** **191**

# List of Figures

1 Thesis topics . . . . . . . . . . . . . . . . . . . . . . . . . . . . . . . . . . . . . . . 7

1.1 Roombots framework with five main tasks . . . . . . . . . . . . . . . . . . . . . . . . 17
1.2 Design of a single Roombots module . . . . . . . . . . . . . . . . . . . . . . . . . . 20
1.3 Modifications of the connection plates . . . . . . . . . . . . . . . . . . . . . . . . . 22
1.4 Integration of a Universal Gripper into a Roombots hemisphere . . . . . . . . . 24
1.5 Roombots electronics . . . . . . . . . . . . . . . . . . . . . . . . . . . . . . . . . . . 25
1.6 Pitch angle compensation . . . . . . . . . . . . . . . . . . . . . . . . . . . . . . . . 27
1.7 Screenshots of the GUI . . . . . . . . . . . . . . . . . . . . . . . . . . . . . . . . . . 28
1.8 RGB-D camera and furniture used in the sub-tasks . . . . . . . . . . . . . . . . . 30
1.9 Circle walk demonstration . . . . . . . . . . . . . . . . . . . . . . . . . . . . . . . . 32
1.10 Snapshots of the chair formation sequence . . . . . . . . . . . . . . . . . . . . . . 33
1.11 Following chair . . . . . . . . . . . . . . . . . . . . . . . . . . . . . . . . . . . . . . 34
1.12 Assistive furniture makes space . . . . . . . . . . . . . . . . . . . . . . . . . . . . . 35
1.13 Active slope compensation . . . . . . . . . . . . . . . . . . . . . . . . . . . . . . . . 36
1.14 Overcoming a ledge . . . . . . . . . . . . . . . . . . . . . . . . . . . . . . . . . . . . 36
1.15 Table picking up an object . . . . . . . . . . . . . . . . . . . . . . . . . . . . . . . . 38
1.16 Two RB gripper modules passing a pen in mid-air . . . . . . . . . . . . . . . . . . 39
1.17 A gripper metamodule assisting in opening a PET water bottle . . . . . . . . . . 40
1.18 Interaction with tracking and lighting . . . . . . . . . . . . . . . . . . . . . . . . . 40

2.1 The JammJoint device . . . . . . . . . . . . . . . . . . . . . . . . . . . . . . . . . . 53
2.2 Silicone sleeve . . . . . . . . . . . . . . . . . . . . . . . . . . . . . . . . . . . . . . . 54
2.3 Schematics of the full JammJoint system . . . . . . . . . . . . . . . . . . . . . . . 54
2.4 Setups for stiffness characterization of JammJoint and sub-components . . . . 55
2.5 Characterization experiments . . . . . . . . . . . . . . . . . . . . . . . . . . . . . . 57
2.6 Spring stiffness increase . . . . . . . . . . . . . . . . . . . . . . . . . . . . . . . . . 59

3.1 Setup of the characterization experiments . . . . . . . . . . . . . . . . . . . . . . 65
3.2 Meta-material characterization . . . . . . . . . . . . . . . . . . . . . . . . . . . . . 67
3.3 Two wall types . . . . . . . . . . . . . . . . . . . . . . . . . . . . . . . . . . . . . . . 68
3.4 Friction on wall experiments . . . . . . . . . . . . . . . . . . . . . . . . . . . . . . . 69
3.5 Climbing robot with jamming end effectors . . . . . . . . . . . . . . . . . . . . . . 71
3.6 Shaft layouts . . . . . . . . . . . . . . . . . . . . . . . . . . . . . . . . . . . . . . . . 74

3.7 Current consumption of the climbing robot . . . . . . . . . . . . . . . . . . . . . 76
3.8 Climbing sequence . . . . . . . . . . . . . . . . . . . . . . . . . . . . . . . . . . . . . 77

4.1 Hard vs. soft foot . . . . . . . . . . . . . . . . . . . . . . . . . . . . . . . . . . . . . 82
4.2 The stiffness dilemma . . . . . . . . . . . . . . . . . . . . . . . . . . . . . . . . . . 83
4.3 Feet of two robots in comparison to an animal foot . . . . . . . . . . . . . . . . 84
4.4 Schematics of the membrane foot . . . . . . . . . . . . . . . . . . . . . . . . . . . 86
4.5 Plastic deformation of jamming membranes . . . . . . . . . . . . . . . . . . . . . 88
4.6 Snapshots of the damping tests . . . . . . . . . . . . . . . . . . . . . . . . . . . . 89
4.7 Snapshot of Oncilla . . . . . . . . . . . . . . . . . . . . . . . . . . . . . . . . . . . . 89
4.8 Complete setup (top view) . . . . . . . . . . . . . . . . . . . . . . . . . . . . . . . 94
4.9 Normal and drag forces . . . . . . . . . . . . . . . . . . . . . . . . . . . . . . . . . 95
4.10 Images extracted from high-speed recordings . . . . . . . . . . . . . . . . . . . . 95
4.11 The MODOK platform . . . . . . . . . . . . . . . . . . . . . . . . . . . . . . . . . . 97
4.12 Open-loop CPG, transformation and trajectory . . . . . . . . . . . . . . . . . . . 98
4.13 Schematics of the system . . . . . . . . . . . . . . . . . . . . . . . . . . . . . . . . 99
4.14 Validation: evacuation speed and impact forces . . . . . . . . . . . . . . . . . . . 105
4.15 Foot trajectories of the configurations OF, JMSS, JMA and JMV . . . . . . . . . . 108
4.16 Snapshots of the stance behavior of JMSS . . . . . . . . . . . . . . . . . . . . . . 108

5.1 Joint compliance distribution experiments . . . . . . . . . . . . . . . . . . . . . . 119
5.2 Closed-loop CPG and influence of tegotae . . . . . . . . . . . . . . . . . . . . . . 121
5.3 Force measurements of each limb . . . . . . . . . . . . . . . . . . . . . . . . . . . 123
5.4 Convergence characteristics . . . . . . . . . . . . . . . . . . . . . . . . . . . . . . . 123
5.5 Initial Morphology (Symmetric) . . . . . . . . . . . . . . . . . . . . . . . . . . . . 125
5.6 Exp. 1 (small asymmetry) . . . . . . . . . . . . . . . . . . . . . . . . . . . . . . . . 126
5.7 Exp. 2 (distinct asymmetry) . . . . . . . . . . . . . . . . . . . . . . . . . . . . . . 128
5.8 Exp. 4 (small hind limbs) . . . . . . . . . . . . . . . . . . . . . . . . . . . . . . . . 128
5.9 MODOK configuration . . . . . . . . . . . . . . . . . . . . . . . . . . . . . . . . . . 130
5.10 Evaluation of the proposed metrics . . . . . . . . . . . . . . . . . . . . . . . . . . 135
5.11 Ground reaction force and the orientation of the force . . . . . . . . . . . . . . . 136
5.12 Foot trajectories during locomotion on the flat surface . . . . . . . . . . . . . . . 138
5.13 Phase evaluation of fore and hind right limbs . . . . . . . . . . . . . . . . . . . . 138

6.1 Quadruped prototype with the ARBITER platform . . . . . . . . . . . . . . . . . . 146
6.2 Raw and processed sensory responses . . . . . . . . . . . . . . . . . . . . . . . . 149
6.3 Weight convergence and Hinton map . . . . . . . . . . . . . . . . . . . . . . . . . 152
6.4 Overall effect of a motor to each loadcell . . . . . . . . . . . . . . . . . . . . . . . 153
6.5 Effect of a motor on the z-direction of each loadcell . . . . . . . . . . . . . . . . . 154
6.6 Loadcell-limb map inversion . . . . . . . . . . . . . . . . . . . . . . . . . . . . . . 155
6.7 Simulation of the ARBITER quadruped . . . . . . . . . . . . . . . . . . . . . . . . 157

A.1 The cycle from an inspiration to the final Roombots shape . . . . . . . . . . . . 166

A.2 Stages of playdough-to-Roombots . . . . . . . . . . . . . . . . . . . . . . . . . . . . . 168
A.3 Benchmarking objects for playdough-to-Roombots . . . . . . . . . . . . . . . . . . 168
A.4 Setup of the spotlight user interface . . . . . . . . . . . . . . . . . . . . . . . . . . . . 170
A.5 Virtual Reality setup . . . . . . . . . . . . . . . . . . . . . . . . . . . . . . . . . . . . . . 171

B.1 Full hinton diagram . . . . . . . . . . . . . . . . . . . . . . . . . . . . . . . . . . . . . . . 174

# List of Tables

3.1 Friction force for end effectors . . . . . . . . . . . . . . . . . . . . . . . . . . . . . . . 70
3.2 Completion of first climbing cycle . . . . . . . . . . . . . . . . . . . . . . . . . . . . . 74

4.1 Results of characterization tests . . . . . . . . . . . . . . . . . . . . . . . . . . . . . . 88
4.2 Speed results of on-robot experiments . . . . . . . . . . . . . . . . . . . . . . . . . 91
4.3 Slope tests . . . . . . . . . . . . . . . . . . . . . . . . . . . . . . . . . . . . . . . . . . . . . 92
4.4 Speed comparison on different terrains . . . . . . . . . . . . . . . . . . . . . . . . . 107

5.1 Gait adaptation analysis . . . . . . . . . . . . . . . . . . . . . . . . . . . . . . . . . . . 125

6.1 Cost of ARBITER . . . . . . . . . . . . . . . . . . . . . . . . . . . . . . . . . . . . . . . . 147
6.2 Limb assignment . . . . . . . . . . . . . . . . . . . . . . . . . . . . . . . . . . . . . . . . 153

# Introduction

## Industrial Revolution, car tires, and the knee joint

The two most dominant engineering materials of the 20th century were concrete and iron. On the one hand, the first and second industrial revolutions (1760 - 1830 and 1870 - 1914 respectively) introduced iron and steel for machinery and production lines, and war machinery during the First and Second World Wars was heavily based on metal production and usage. On the other hand, since its patenting in 1824, concrete became the number one building material, with a steep exponential growth rate since the 1950s, starting from the peace period that followed the wars.

The common property of these two materials is mechanical durability. For both materials, it is all about strength. Iron, and especially steel, as a strong metal enabled the development of machines that could outlast many production cycles, and concrete as a building material is able to withstand the forces of nature.

In contrast, biological systems, specifically animals, seem to never consist of only hard material; virtually every living creature contains some form of softness. This brings us to a fundamental question: what is the purpose of this softness? And if we were to use nature's example as a design principle, how should we combine hard and soft materials in robots?

My answer to these questions is that hard and soft materials are used to trade-off power and adaptability. Whereas the previous examples of iron and concrete are used to for resilience and strength, they have a rather linear application. Industrial production lines usually produce a single product, and the duty of concrete structures is to provide stable housing. Biological systems arguably are less resilient (hence the invention of the other materials), however they demonstrate an adaptability that so far is unmatched by engineered systems: ducks can adapt to move in the three different media: water, earth and air.

Such increased adaptive capabilities can stem directly from the combination of hard and soft materials. A bone, made for structural rigidity, still possesses a certain flexibility. A purely hard bone would be too brittle and break on impacts, e.g. during walking or running. Although the inclusion of collagen reduces the bone's overall mechanical strength, it can now withstand a wide range of mechanical perturbations. An example from the engineering world could be that of tires: while Formula 1 cars have soft tires that adapt to the track to create grip, they lose several 100 g of rubber and need to be replaced multiple times during a race. Regular car tires are less soft, sacrificing some friction for an increase in lifetime, up to several thousands of kilometers.

But what is the actual effect of having different mechanical properties? It is, in my view, *to obtain a different dynamical response* of the system to perturbations. Hard and soft materials react fundamentally differently to perturbations: while a hard material counteracts the external disturbance and exerts and transmits forces, a soft material embraces the disturbance and absorbs forces, and thus the two materials have an entirely different *functionality*. This lies at the root of the emergence of the recent field of soft robotics [87, 94] that currently is creating a new generation of robots. These robots work and react differently than what has been developed in industry in the last 100 years because they focus on a different functionality, such as wearability, safety, adaptability, etc. It is no surprise that control strategies, optimized for industrial robots, need to be rethought to accommodate this major difference.

However, if the aim is to obtain a set of functionalities, I would argue that it is not the actual mix of hard and soft materials but rather the switch between hard and soft modes that enables elements to function in a multi-modal manner. In a dark room, we can use our arms as sensors to detect obstacles; the arms are in “soft” mode. We can use the same arms to break bones during a boxing match; the arms are in “hard” mode, displaying two very different functionalities with two very different mechanical properties. In general, a mode-switch can be a gradual transition or a rapid change, depending on how different the functionalities are and how fast they need to be obtained.

When building nature-inspired machines [125] to solve tasks with the simplicity, elegance and efficiency optimized (or deemed “good enough”) by nature during evolution, a rich set of functionalities is usually a desired property, reflecting the actual biological inspiration more accurately. A set is also interesting from an engineering viewpoint, as a new task that requires a new functionality does not imply the integration of additional elements, but an adaptation of the existing components, either by hardware modifications or control methods. Further, like animals, such machines should be able to interact with the environment, and it is not by chance that contact interactions are predestined to invoke a change in functionality. For example, in the dark, the contact with a wall is first detected in the soft mode of the arms, but an actual collision is avoided by applying a breaking force to the wall, requiring the hard mode.

Changes in the dynamical response of a system can be achieved by modifying mechanical properties in hardware or by influencing control parameters (which can also be interpreted as affecting mechanical properties). A knee joint behaves like a normal hinge for a certain movement range, but locks (i.e. infinite stiffness due to a mechanical lock) in one direction when stretched, resulting in the functionalities of enabling bipedal locomotion in the former case and efficient balancing while standing in the latter case (since no active muscle control is needed to keep the knee locked in the stretched position). In contrast to this hardware-caused change in mechanical properties, a wrist joint is made stiffer by co-contracting the muscles on both sides of the joint through the control of muscle activations, changing the functionality - as described above - from assisting in obstacle detection to assist in obstacle destruction.

With this introduction in mind, in this thesis I define a *mode-switch method* as a method to *gradually or rapidly modify the dynamical response* of a system in order to *change the functionality* of that system.

## Locomotion and local functionality changes

The question now becomes, how and where to implement such mode-switches in a robot. As for the "how", a mode-switch in hardware could be the implementation of (variable) series elastic elements (SEA) that change spring/damping properties of structural elements. A control switch mechanism could be the change from position control of motors to force/torque control, allowing modification of the spring/damping characteristics of joints. However, other methods will be presented in the thesis. As for the "where", there are essentially two options: *centralized*, meaning that a central element has access to and can influence every possible switch, or *local*, with multiple decentralized elements (each potentially less "powerful" or "capable" than the centralized version) exhibiting a certain autonomy in controlling their assigned switch mechanism.

Intuitively, it is clear that mode-switches in hardware by design are local since they can only affect their own properties, e.g. the locking of the knee joint does not affect the movement ability of other joints. There are cases where multiple joints are affected by a single switch through specific mechanical coupling (e.g. biarticular muscles), however the usual case is a localized effect. I understand this as being the essence of *mechanical intelligence*: a *mode-switch method in hardware to locally permit a manifold of dynamical responses*. Note that according to this definition, a simple spring can already provide mechanical intelligence, since depending on the state of the spring it can be better suited for adaptability (soft state) or force transmission (hard state). The purpose of mechanical intelligence is to simplify lower-level control: if appropriately chosen (a not so well-defined condition), mechanical intelligence can take over a certain "computation", either saving energy or freeing up computational power for other tasks. Locking the knee joint for maintaining balance during standing removes otherwise necessary control of this action, saving both muscle energy and removing control computation in the process. The computation performed by a physical system by utilizing its own physical dynamics such as shape, stiffness, and material properties is dubbed *morphological computation* [124, 123, 43]. Some of the systems presented in this thesis perform morphological computation, however here the focus is not on the computation part but mainly on the mode-switch method itself.

Given by the usual use of a central control unit, mode-switches in control on the contrary are rather centralized, depending where the actual computation takes place. Nevertheless, a part of this thesis aims at demonstrating that lower-level control simplifications can likewise be achieved by local effects through local computation of mode-switches in control, and we analogously define *control intelligence* as a *mode-switch method in control to locally permit a manifold of dynamical responses.* This also has biological evidence, for example the spinal cord processes low-level feedback from the foot and activates ankle muscles for propulsion during a walking cycle autonomously, which allows the brain to focus on other and computationally intensive tasks (e.g. vision). Note that the spinal cord not only takes over the task of muscle activation from the brain, activating muscles in a "blind" manner (this alone wouldn't qualify as control intelligence); it locally performs computation (e.g. reflexes caused by force feedback), only then demonstrating control intelligence.

The range of dynamical responses that should be permitted depends on the desired or required functionality change of the element. The stiffness modification of locking the knee joint is an extreme example, however already less drastic switches can have significant global effects. We investigate such global effects in the task of *legged locomotion* as one of the fundamental movement patterns of animals. We are especially interested in locomotion on rough terrain since this is what biological, legged systems most often deal with. Objectively, it seems that locomotion on rough terrain does not differ greatly from locomotion on smooth terrain. Given the complex movement pattern already needed for locomotion on smooth terrain, the comparatively small modification from smooth to rough terrain intuitively should likewise only require a small modification in the movement behavior and not an entirely different locomotion strategy. We hypothesize that parts of the body temporarily change their functionality over a locomotion cycle, causing such small modifications by inducing subtle adjustments occurring due to continuously shifting dynamical responses: a continuous exchange between power and adaptability, the working principle of mode-switches as described above. This defines our main research question:

*Can local computation through mode-switches be beneficial for locomotion in general and specifically for legged locomotion on rough terrain, and if so, what are the effects of them and how do they improve locomotion?*

## Robots for biology and vice versa

To answer this question and based on the idea of bio-inspired robotics to use robotic tools to advance the understanding of biological systems, we apply approaches of mode-switches to robot systems. The aim of this research is to find generic strategies to enable or simplify locomotion on smooth and rough terrain, independent of robot parameters such as body proportions and number of legs. To test our strategies on a variety of morphologies, the main class of robots used in this thesis is *reconfigurable modular robots* [48, 179, 181] as they can adopt many different expressions of legged robots. In the ideal case, a generic strategy could even create locomotion patterns for arbitrary legged morphologies; reconfigurable modular robots then are the obvious choice to build the corresponding hardware.

Concerning the actual robot hardware used in this thesis, we selected two modular robotic platforms. Most of the research is done with a customized version of the commercial off-the-shelf modular system *Bioloid Kit* [134] that provides a number of simple, 1-DoF (degree of freedom) hinged servo motors and structural parts that can manually be assembled and wired together. This platform allowed a rapid execution of a large number of experiments due to its flexibility and simplicity. In parallel, over the last 10 years the Biorobotics Laboratory has developed special kinds of modular robots with the ability to perform reconfiguration autonomously. In the future, this could lead to interesting research such as autonomously transforming structures that can adjust their configuration task dependently. This self-reconfigurable modular robot system, *Roombots* [148], is still in development, thus a part of my time was invested in advancing the platform for future research. We detail these advancements and demonstrate selected example applications, however only research that required the self-reconfiguration ability is performed with this platform.

## A word about the *reality gap*

A major selling point of reconfigurable modular robots is their ability to “quickly” be configured into various morphologies. For the topic and research question of this thesis, this includes different expressions of legged morphologies and the locomotion thereof. The versatility of such a system however loses some of its “rapid prototyping ability”-aspect if a newly built structure requires a lengthy procedure of modeling and simulation optimizations to obtain an appropriate locomotion controller to achieve movement. Moreover, if the general approach is to transfer the best simulated controller to the robot because extensive tests with the real hardware are too time consuming, such controllers will likely suffer from the so-called *reality gap* [76]. In the best case, the reality gap could reduce the robot’s performance compared to its simulated self because of unmodeled deteriorating effects. In the worst case, it can render the controller entirely infeasible for application in the real world.

It is currently an unsolved issue of how to best cross the reality gap. Detailing the simulation with more real world effects is an option, as well as finding “robust” controllers that do not depend on a particular interaction in simulation not present in the real world, or that can deal with real world noise. Ultimately, the goal of any strategy should be to make a robot perform in the real world, and so the path we chose is to research locomotion directly in hardware. Because of the aforementioned time-consuming process of performing a large number of experiments in hardware, it thus was necessary to formulate general concepts that ideally work on various robots, i.e. can be applied to arbitrary legged morphologies.

## Thesis topics, organization and main contributions

This thesis presents one mode-switch method in hardware and one in control on two modular robotic platforms and is split into three parts, followed by a final chapter that concludes with reviewing the tasks in each chapter and with an outlook for future research.

**Part I** describes advancements in hardware and control of our self-reconfigurable modular robot *Roombots*, a controller used to enable reliable docking of a single module, and example applications of such robots (blue blocks and arrows in Fig. 1).

**Part II** focuses on the hardware mode-switch method *jamming of granular media*, showcasing first a wearable joint support device before its application to the tasks of climbing and locomotion on smooth and rough terrain with quadrupedal structures (orange blocks and arrows in Fig. 1).

**Part III** introduces the control mode-switch method *tegotae*, a force feedback control strategy used together with phase oscillators, also applied to ground locomotion on smooth and rough terrain of a quadruped robot. Further, it discusses a combination of tegotae and a biological learning method to move towards a generic strategy for creating locomotion patterns in arbitrary morphologies (green blocks and arrows in Fig. 1).

**Main contributions**

- We describe the advancement of our self-reconfigurable modular robot system (SRMR) Roombots, detailing modifications in mechanics and control
- We demonstrate applications of SRMRs, namely adaptive and assistive furniture, and present user interfaces developed for these applications
- We enabled jamming of compliant granules for a mobile, wearable joint support device
- We introduce jamming of compliant granules as a variable stiffness method in end-effectors and show that the different states achieve different functionalities beneficial in locomotion:
  - enabling climbing on irregular walls by transitioning between shape adaptability and force transmissibility
  - improving ground locomotion on rough terrain (flat and inclined) with a faster version of the same concept
- We use tegotae force feedback in phase oscillators and show its stabilizing properties in locomotion on rough terrain
- We combine hebbian learning and tegotae force feedback to move towards a generic control method that allows locomotion in arbitrary modular morphologies

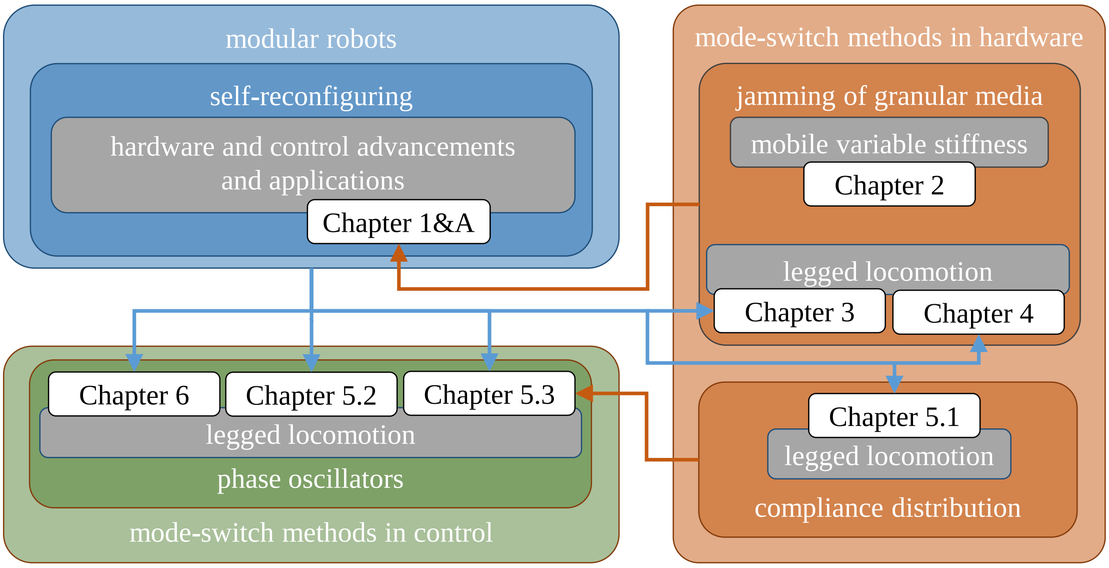
modular robots
self-reconfiguring
hardware and control advancements and applications
Chapter 1&A
mode-switch methods in hardware
jamming of granular media
mobile variable stiffness
Chapter 2
legged locomotion
Chapter 3
Chapter 4
Chapter 6
Chapter 5.2
Chapter 5.3
legged locomotion
phase oscillators
mode-switch methods in control
Chapter 5.1
legged locomotion
compliance distribution

Figure 1 – Thesis topics. Grey blocks: application/task. Blue blocks and arrows: robot hardware *(self-) reconfigurable modular robots* used in the indicated chapters. Orange blocks and arrows: *jamming of granular media* and its usage as a hardware mode-switch method in the indicated chapters. Green blocks and arrows: control mode-switch method *phase oscillators* used in the indicated chapters.

# Roombots: 3D self-reconfiguration

# Part I

# Topic of Part I

## Overview

The first part focuses on the work done with our self-reconfigurable modular robot (SRMR) “Roombots”. The development of Roombots started in 2008 with the first concept. In the following years, the hardware was continuously improved such that the major functionalities of an SRMR could be demonstrated in [153]. Many of the presented tasks were shown as a proof-of-concept to validate the design and control of Roombots, such as relatively simple reconfiguration and locomotion. However, to verify the suitability of Roombots as self-reconfigurable furniture - the grand vision of the system - more modules and a few modifications were needed. Thus one of the main tasks of my research was to identify the needed module improvements based on the experience of previous research and build a new set of modules such that larger-scale structures could be formed. Chapt. 1 describes these improvements - both in hardware and control - and presents demonstrations around adaptive and assistive furniture, performed with up to 12 modules (of which 11 were newly built). Chapt. A in the appendix briefly presents more work done with Roombots that are not the main focus of this thesis but were carried out alongside.

## Robots building robots: Modularity and self-reconfiguration

Modular robots (MRs) are the “Swiss army knives” of robotics. Instead of designing a specialized robot for a single task, the idea of modular robotics in general is to provide functionalities in robotic “modules”, and a robot can be constructed out of these modules. The advertised advantages of modular robots are threefold (based on [156]):

1. versatility: different tasks require different functionalities; in a modular robot, these functionalities can be put together by assembling the according modules.
2. robustness: if a module fails, only the functionality of this specific module is affected; the rest of the robot still can operate normally and the failing module can easily be replaced.
3. low-cost: since each module is thought to only perform a simple function, it is in principle also simple in design, allowing cheap manufacturing; additionally, modules can more easily be mass-produced for wide availability, helping to reduce module costs.

There is an ongoing discussion if the current state of modular robots yet delivers any of these advantages: it can be challenging to realize a function in a compound of modules; more single robotic agents means more potential for failure; and most modular systems are still in their prototype stage, making them expensive to produce. Only the future development of the modular robotics field in general will show if the concept is able to overcome current limitations with more research, new ideas and new technologies. The research presented in this first part focuses on this topic.

Among modular robots, self-reconfigurable modular robots (SRMRs) form a special class. Not only are the modules now reconfigurable, meaning they can be assembled into different morphologies, but the system has the ability to perform the reconfiguration autonomously. This could potentially make such a system extremely independent since it could transform its morphology and add and remove functionalities all by itself, leading to an uncomfortable question: what would be the limitations of such a system? This inspired many fictional scenarios over the years, most recently in the Walt Disney movie “Big Hero 6” (2014) where the tiny “microbots” are shown to have almost omnipotent powers when working together in clusters of many thousands of modules.

As physical robots have to deal with real world effects however, namely gravity and other physical effects, such scenarios are far from being realistic and will remain fiction for the foreseeable future. Nevertheless, research on SRMR retains a futuristic touch, and in practise SRMRs pose interesting interdisciplinary challenges in hardware, control and their application for an end user.

The hardware presents an engineering challenge. The general idea of modular robotics is to combine “simple” modules into larger, more complex and thus usually more capable structures that possess the required functionality of a task at hand. A true reversible modular robotic system (meaning no permanent state-change) has three key functionalities: reversible connection between two modules, reversible disconnection between two modules, and actuation (either within one module or in a structure as a whole). Note that reversible connection does not automatically include disconnection as there can be different mechanical systems for both connection and disconnection. For the design of each of these systems, the overall dimensions of a module should be defined, which often are linked to the expected tasks. Lastly, one has to consider if all the sub-units are exact copies of each other (homogeneous MR) or if specialized units collaborate together (heterogeneous MR) [3]. In manually reconfigurable modular robot systems [3], the connection and disconnection procedures are outsourced to a human such that an MR mainly has to care only about the actuation system. This means that each module can take on almost any form with any mechanical properties, including soft modules. In contrast, SRMR [3] systems have to perform the connection and disconnection procedures autonomously, which introduces additional constraints on the rigidity. To enable (or at the very least simplify) self-reconfiguration, each module should be structurally rigid such that some form of alignment between modules is achievable - a usually necessary condition for self-connection - yet provide some form of movement to initiate self-reconfiguration. The balance between these two properties is already challenging to achieve in 2D SRMR systems and adds a significant level of difficulty in 3D SRMR systems. Soft modules (e.g.[53]) can have their own form of connection and disconnection methods, however a 3D self-reconfigurable modular soft robot has yet to be developed due to the constraint above.

The control requires algorithms to deal with decentralized systems. It needs to be defined if one module acts as a master commanding all other modules in the system, if each module has the same amount of control, or if there is a main external controller unit. Additionally, a way for a human to intuitively interact with one or more groups of modules may have to be developed such that the current state of the modular system can be understood and a future desired state can be communicated.

Lastly, one has to consider for which application the robotic platform is to be developed. Even though SRMR can shape-shift into various morphologies, this does not necessarily mean that one module should be as small as possible to build any arbitrary morphology; one module should be as small as the smallest unit required by the application. We must also define the added value of self-reconfiguration to justify the effort to overcome the challenges mentioned above: what is the utility of self-reconfiguration?

## Roombots: modular self-reconfiguration in three dimensions

As one example that aims at addressing some of these challenges, over the last decade we developed “Roombots” (RB), a 3D self-reconfigurable modular robot system with the application - among others - of serving as adaptive and assistive furniture. In this framework, multiple groups of modules adapt to the needs of a user by creating different pieces of furniture or augmenting the capabilities of existing furniture. Additionally, such pieces of furniture can also act somewhat autonomously and provide assistance specifically to the elderly by for example preventing falls as a result of a following chair, picking up and holding objects, and bringing items, all while retaining their functionality as furniture. This part focuses on the advancements made to the initial Roombots module design and control. Eleven new, modified modules were built (yielding 13 in total) to show the full capabilities of our SRMR that we demonstrate in different applications, most importantly that of adaptive and assistive furniture.

# 1 Advancements and applications of the 3D SRMR Roombots

The hardware and design considerations of Roombots are described in detail in [153], thus the main focus of this chapter is on the hardware modifications and control advancements of the last four years and the application of Roombots to adaptive and assistive furniture.

**Reference publications**

- This chapter is based on ***Simon Hauser**, Mehmet Mutlu, Pierre-Alexandre Léziart, Hala Khodr, Alexandre Bernardino and Auke Jan Ijspeert. "Roombots extended: challenges of the next generation of self-reconfigurable modular robots and their application in adaptive and assistive furniture."* Submitted to Journal of Robotics and Autonomous Systems.

  **My original contributions**

  - Building the hardware
  - Supervision of student projects on Roombots
  - Supervision of GUI development
  - Guiding and planning of experiments
  - Performing of experiments
  - Writing the manuscript
- Parts of the text and figures of *Hala Khodr, Mehmet Mutlu, **Simon Hauser**, Alexandre Bernardino, and Auke Ijspeert. "An optimal framework to deploy self-reconfigurable modular robots." Submitted to IEEE International Conference on Intelligent Robots and Systems (IROS), 2019.* have been reorganized in this chapter.

  **My original contributions**

  - Co-supervision of the master thesis of Hala Khodr
  - Planning of experiments
  - Manufacturing and preparation of hardware equipment
  - Inputs to the manuscript

## 1.1 Goal of the improvements

The aim of the improvements was to reach the goals proposed in the SNF project grant "Roombots: using reconfigurable robots to construct adaptive and assistive furniture" (Project 153299). The following sections will briefly explain the scenarios therein and show their demonstration in hardware.

The first generation of Roombots proposed the general hardware design of our SRMR together with algorithmic work on reconfiguration, locomotion, user interfaces [150, 148, 151, 147, 149, 152, 153, 16, 15, 17, 18, 171, 119]. As a proof-of-concept, only a limited number of modules was needed to demonstrate the three key functions connection, disconnection and movement. However, to further the vision of using Roombots as adaptive furniture, more modules were needed and a few adaptations in hardware and control had to be made based on the experience with the developed prototypes. To showcase some of the new capabilities of the upgraded Roombots system, we propose five tasks that we regard as core functionalities of adaptive and assistive furniture: self-reconfiguration, mobility, manipulation, human-module-interaction, and developing a user interface. Each of these tasks is demonstrated by Roombots, often through various sub-tasks (see Fig. 1.1).

The first task described herein is scalable *self-reconfiguration* which stands at the core of an SRMR system and fits well into the vision of creating adaptive furniture. For this demonstration, a loose group of RB modules self-reconfigures into a shape resembling that of a common piece of furniture. It should be noted that while this task essentially reduces to a series of connection, disconnection and movement actions which already have been demonstrated in e.g. [153], performing it with a larger number of modules is not trivial due to the scalability of the robotic system: continuous reliable reconfiguration with a group of modules rather than an isolated reconfiguration with two modules adds significant challenges in hardware and control to deal with real world physical phenomenons that only occur for larger groups of modules. In the case of Roombots, the first hardware iteration experienced major elastic deformations and misalignment issues such that the autonomous formation of larger structures was not possible. Due to the various hardware modifications presented in section 1.3.1 and closed-loop control described in section 1.3.7, such tasks lie now within or at least much closer to the capabilities of the present hardware iteration.

Second, adaptive furniture should possess a certain degree of *mobility* such that pieces of furniture can dynamically move within a living space. Depending on the functionality of the structure, mobility can require certain adaptation of the furniture to the environment as well as autonomy to react to changes in the environment. We performed a set of demonstrations to showcase the mobility aspect, ranging from following and evading pieces of furniture to slope compensation and even stair climbing.

To fulfill more of the assistive aspects of the Roombots vision, robotic-enhanced furniture must possess a way to *manipulate objects*. Simple actions such as holding a book can already provide assistance, and it is clear that many of such actions require a method for manipulation,

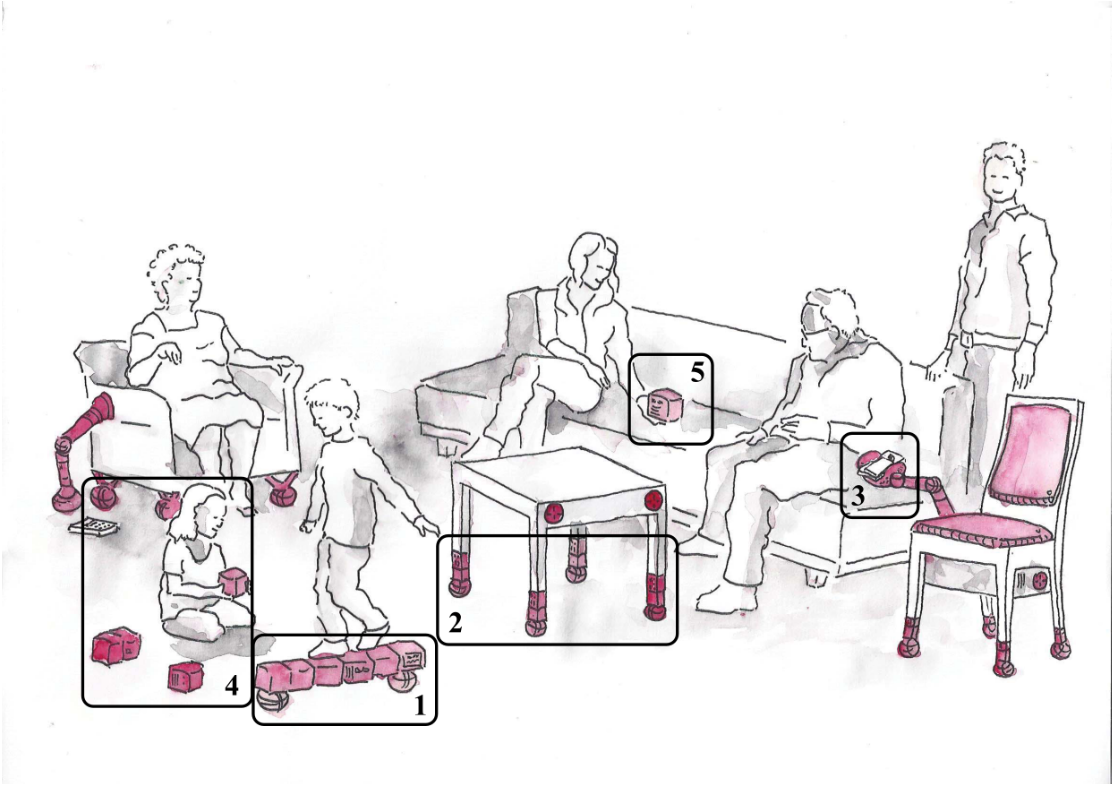

Figure 1.1 – Roombots framework with the five tasks indicated. 1) self-reconfiguration of a group of Roombots modules into a shape to function as a toy. 2) mobile furniture where an existing piece of furniture has been enhanced with RB modules to enable it to move around in the living space. 3) object manipulation where furniture is able to assist in simple tasks such as picking up and holding a remote control. 4) interactive furniture, allowing users to work together with robotic-enhanced furniture, and 5) an easy-to-use user interface (UI) to monitor the current state of the robotic system.

i.e. a gripper. Such a gripper can, for instance, be used for fetching a remote controller fallen on the ground. For the integration of a gripper into the RB framework - which should be able to manipulate a wide range of everyday objects - we revisited the concept of granular jamming that was used to develop a “Universal Gripper”. By miniaturizing the mechatronic components, we were able to equip selected modules with this gripper and demonstrate common tasks such as a piece of furniture picking up an object from the ground and an RB structure helping to open a water bottle. Two gripper modules further are able to pass objects from one module to another, which will also be briefly discussed.

Users need an intuitive way of *interacting with modules*. Interaction could be through e.g. speech recognition where modules react to spoken commands, or through gesture control as e.g. in [119, 105, 112] where commands are created through the tracking of gestures. Further, modules should provide feedback to the environment such that the current state of a single module or a group of modules can easily be understood. A simple way to achieve this is through light where different colors can be assigned to different states. We revisited our approaches in the past and demonstrate again the interaction capabilities of RB.

Lastly, when complete information about the state of the modules is required, an appropriate *visualization tool* is needed. We describe the development of a Graphical User Interface (GUI) that allows for easy control of RB modules. The GUI greatly facilitated the development of many of the presented demonstrations and will simplify the development of future challenges. Such challenges (e.g. RB metamodule locomotion on-grid) are identified along with this work and analyzed and discussed in section 1.5.

## 1.2 Related work: 3D SRMRs, tracking and smart homes

Over the years, a large variety of 2D and 3D proof-of-concept SRMR systems has been developed. A comprehensive list of both mechanical designs and algorithms of SRMR can be found in [3] and [2]. If research includes experiments with prototype hardware modules, the basic functions of connection and disconnection are in many cases shown with a minimal number of modules, often in an isolated experiment involving two to five modules. Larger reconfigurations with more modules are usually shown in simulation, whereas structures in hardware experiments with more modules (e.g. some form of collaborative behavior) are mostly manually assembled, e.g. PolyBot [180], SMORES [38], UBot [35], SUPERBOT [141], CoSMO [95], 3D M-Blocks [137], Soldercubes [111] and AMAS [160].

With Roombots, the focus is not only task execution with prepared structures, but also the actual formation process in 3D. While some of the systems in [3] and [2] certainly will mature further and with additional development will be able to demonstrate larger reconfigurations in hardware, most (if not all) SRMR systems have difficulties when the number of modules is increased, especially for 3D systems. Because of significant hardware challenges, only a limited number of such SRMR systems are able to perform 3D self-reconfiguration with more than five modules where all modules are involved in the self-reconfiguration, allowing for a more comprehensive understanding of the potential of reconfigurable systems.

As Roombots are thought to work in groups that can involve up to tens of modules (task 1), we more closely inspect the largest structures formed through self-reconfiguration with 3D SRMRs, and could only find two examples where the formation (or reconfiguration) is explicitly stated in literature: (i) M-TRAN III [91] formed a mesh structure with 24 modules (48 DoF) that locomotes by disconnecting modules from one side of the mesh and reattaching them on the other side, and (ii) ATRON presents a self-reconfiguration sequence with three, three-unit meta-modules in [23], resulting in 9 modules (9 DoF). We aim to show that Roombots is one of the few systems where 3D reconfiguration with 10 modules (30 DoF) and more is possible.

Challenges still remain even after a structure is formed. The shape-shifting capabilities of SRMRs raise the question of how humans can interact with such complex robot systems [176]. For humans, vision is one of the most powerful senses that enables accurate remote sensing and allows for interaction. Particularly the sense of depth plays a crucial role in almost all of our fundamental sub-tasks such as grasping and locomotion. Similar to humans, robotics systems can benefit from vision too. One of the easiest ways of getting the depth map information is by using RGB-D cameras. There exists numerous ways to utilize RGB-D cameras for human tracking [27, 59, 97], detecting gestures [131] as well as other human motion [178] or learning object affordances [88]. Modular robots can benefit from vision as well, although the integration of a vision system into a modular robot system is not straightforward. There are several possibilities (e.g. integrated in a module, a specialized module, an external system), each with their own advantages and disadvantages and engineering difficulties. A recent use of RGB-D sensor in the scope of SRMR has been reported in [162] where a system made out of SMORES carries the RGB-D sensor around and uses it for closed-loop self-reconfiguration as well as navigation. The simplest way for tracking however is to keep the RGB-D camera external. Such an external camera could be placed on top of a structure built out of modular robots as e.g. in [98]. However, because the camera in this work is used to track multiple objects in a simulated living space, we use a stationary mounted external camera with an overhead view.

Concerning the vision of providing assistance in everyday tasks, robots started entering houses to do chores much later than their industrial counterparts used in process automation. One of the pioneering assistive robots which became widely available is Roomba [47]. Although consumer robots are not very widespread, there is a deep literature on the research of assistive robots reporting various tasks such as cloth folding [99, 165], social interaction with humans [25, 101, 39], doing a combination of different chores [12, 154, 9] and helping disabled people with an autonomous wheelchair [29] or bidepal robot [158]. All of those robots embody either a partial generic human form, or are specifically designed for a given task. Here, we explore the possibility whether such tasks can be attempted by distributed systems such as SRMRs, specifically in the scope of creating an assistive environment.

Whereas conventional furniture consists of passive elements that stay where they are placed, advancements in technology and robotics call for smarter and interactive houses. Examples include a robotic ottoman system guessing your intention and responding to your needs [145] or a robotic wardrobe to modulate living space to the needs of the user [114]. Thanks to the expansion of the internet of things, there is an increasing number of architectural efforts to sensorize furniture using cameras and other complementary sensors [52] and in designing actuation systems for furniture [55, 182].

The vision of Roombots is to introduce dynamically reconfigurable furniture into our future living space, redefining room arrangements and available space. In this work, we show proof-of-concepts of functionalities enabled by such reconfigurable furniture, namely dynamic adaptivity and assistance. We are aware that our current work does not contain much quantitative data; we rather report qualitative data by showcasing the many abilities of a reconfigurable system. We believe that such progress is also important to report as it can serve as a benchmark for future iterations and generations of reconfigurable systems.

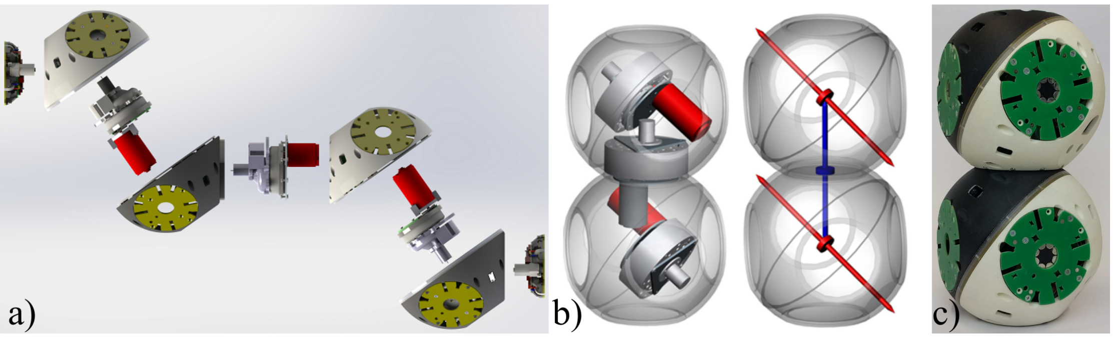

Figure 1.2 – Design of a single module with a) an exploded view of the main components Active Connection Mechanism ACM (2), hemispheres (4) and motor units (3), b) arrangement of the motor units inside the assembled module and orientation of the rotation axes (red and blue axes), and c) fully assembled Roombots module of the newest iteration with dimensions 11x11x22 cm. Parts of this image have been adapted from [148].

## 1.3 Advancements and supplementary systems

The following subsections describe the different modifications of the RB hardware and control in detail: the adaptations on the module itself, the added sensors and the new control possibilities, the new gripper, added electronics, the Graphical User Interface (GUI), the external RGB-D camera and the passive parts (furniture).

### 1.3.1 Mechanics, motors and connection

The overall design and dimensions of one Roombots module are kept as the original design described in [153], thus only the main features are described here. One RB module consists of 4 interconnected half-spheres (hemispheres) that can continuously rotate around each other by 3 motor units. Each module has 10 connection plates of which (due to space constraints) two possess actively retractable hooks that can latch onto any other connection plate. This Active Connection Mechanism (ACM) is the mechanism that allows one module to attach to another module or to any surface equipped with our connection plate, forming dynamic multi-module structures such as adaptive furniture. One module contains all necessary electronics for operation, a bluetooth module for communication and batteries, making it fully autonomous. Fig. 1.2 gives an overview of the design of a single module.

As already pointed out in [153], a stiffer construction and stronger actuators were needed to overcome some of the limitations of the initial design. From previous iterations of the hardware, it became clear that the design needed major improvements in three areas: output torque, control precision, and docking reliability. As a first step, the material of the three main gearboxes that are driving each module was changed from plastic to brass together with replacing the respective motors to more powerful ones. On the one hand, this significantly increased the torque of the Degrees of Freedom (DoFs) of one module (19% increase for the middle DoF with a Maxon RE-max 24 DC motor to 4.3 Nm, and 70% increase for the outer DoF with a Maxon RE 25 DC motor to 8.4 Nm, [168]). On the other hand, due to the much more precise metal gearboxes, the backlash from each gearbox was reduced by a factor of 10 (from 2 ° to 0.2 °) which was necessary to improve the control precision and thus the connection reliability of a module. Many difficulties in the ACM caused by the use of 3D-printed parts and plastic gearboxes also required a change of material. This mechanical latch needs to withstand the full weight of a few connected modules. Thus, we decided to also implement metallic gearboxes and manufacture the structural parts of the ACM out of aluminum which also helped to increase the connection reliability of a module.

In an effort to compensate for small misalignments during reconfiguration, we reconsidered the hybrid ACM mentioned in [153] in which permanent magnets are used to assist the connection action. It consisted of one permanent magnet in the middle of the ACM and connection plates that would need a specific polarity to create attraction, thus unfavorably changing the hermaphrodite ACM into a gendered connection mechanism. We achieved a hermaphrodite connection with permanent magnets by creating a *ring* of magnets whose polarities are oriented in a specific manner (see Fig. 1.3) such that an attraction is created every 90 ° which corresponds to how two modules can connect to each other. A standard ring (for a non-ACM connection plate) is formed by 8 disk-shaped magnets with alternating poles facing the surface; due to space constraints caused by the gears of the ACM, a ring in an ACM connection plate only contains 6 magnets. Each ACM and every possible connection plate both of a module and of a passive grid structure has been equipped with this ring of permanent magnets. Taken together, this helps to form an aligned contact between two connection plates that are supposed to be touching. This magnetic connection is strong enough to form a small region of attraction when two plates are close, however it is not capable of transferring any load and the connection is easily broken by any movement of a module. The researches in [91] and [38] use a similar magnetic ring idea as a main connection method. Using permanent magnets as main connection method results in a harder disconnection process. However, the magnet ring is used as only a complementary method to the mechanical ACM in Roombots. Thus, advantages of both methods are integrated while minimizing disadvantages of each approach.

In the end, we built 11 new fully functional modules with the presented hardware modifications (with a total of 13 modules with 2 modules of the previous iteration).

### 1.3.2 Sensors

The most important sensorization was done on the rotary joints by adding absolute encoders (12-bit capacitive absolute encoder AMT203). Initially, Roombots had relative encoders which meant that modules were supposed to be powered up only after all joints were manually aligned to a certain angle such as 0°. New absolute encoders ensure that the control of a module no longer depends on the initial position when switched on, thus the initialization

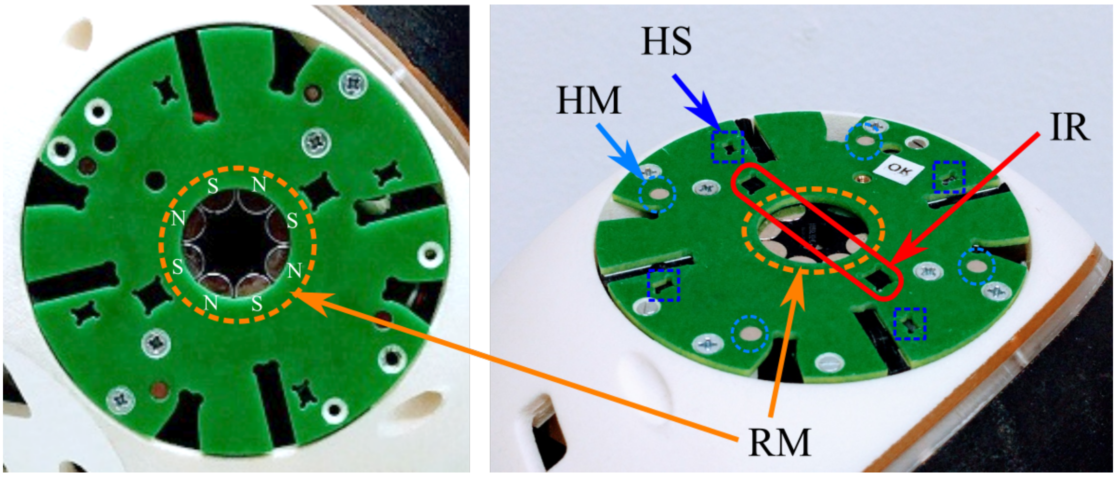

Figure 1.3 – Modifications of the connection plates. In the middle of each plate, a ring of permanent magnets with alternating poles (N and S) facing the surface (RM; 8 magnets for a standard non-ACM connection plate, 6 magnets for an ACM connection plate) assists in forming contact between two plates. Two infrared sensors (IR) give information about the proximity of neighboring plates or the environment whereas four pairs of a hall-effect sensor (HS) and corresponding magnet (HM) indicate if two touching plates are oriented appropriately such that a connection with the ACM can be formed.

of experiments became easier. Although both relative and absolute encoders could have been used in conjunction to increase the control precision due to the higher resolution of the relative encoders, they have been removed to provide space for stronger DC motors.

There has been a high demand for proximity sensors on Roombots for various applications, particularly for reliable self reconfiguration. Each ACM plate is equipped with two infrared (QRE1113GR) and four single-axis linear hall-effect sensors (DRV5053RA) (shown as IR and HS respectively in Fig. 1.3). Infrared sensors detect existence and distance of a nearby object within the range of 1 mm to 15 mm. The reading of the infrared sensor relies on the reflectivity and orientation of a facing surface. On the other hand, hall effect sensors report the magnetic flux, $\Phi_B$, crossing the sensor area which correlates to the proximity of a magnet. The actual $\Phi_B$ reading depends on distance, strength, orientation and misalignment of a facing magnet. Every possible docking surface (matching surface of ACMs) are equipped with four cylindrical magnets with a diameter of 3 mm (illustrated as HM in Fig. 1.3). All four magnets are situated right in front of the hall effect sensors when an ACM is connected. Thus, the viability of docking can be assessed. Additionally, each ACM is equipped with a three-axis accelerometer (ADXL337) to detect the gravity vector. The gravity vector helps to detect external disturbances or internally accumulated errors such as gear backlashes, manufacturing/assembly misalignments or local control imperfections. The use of similar sensors has been reported in different modular robots too. For instance Sambot in [174] uses infrared sensors, accelerometer and gyroscope integrated in modules whereas [183] presents a non-actuated sensor module just for carrying linear hall effect sensors and a camera.

### 1.3.3 Spotlight LED

A powerful RGBW-spotlight LED board has been developed to illuminate a workspace whenever the ambient lighting is insufficient. This spotlight can be integrated within any Roombots module. Particularly when Roombots need to incorporate a camera, the environment needs to be well-lit. Whenever there is a lack of light, a module can carry the spotlight to the desired location and enable the computer vision approaches. Furthermore, such a colourful and strong light can be used to induce emotions by playing with color and intensity functions. For example creating a sunset effect in a bedroom without any windows or fireplace engenders good feeling in a living room without a fireplace.

### 1.3.4 Universal Gripper

In the vision of Roombots as depicted in Fig. 1.1, the functionality of object manipulation had to be implemented in the Roombots platform. There were essentially two options available: a manipulator either could be designed as a standalone system that can be attached to a module with the ACM, or it can be implemented directly into a module. For the first option, the method of manipulation is more open since the space needed for it is not restricted as a standalone gripper unit could have arbitrary dimensions. As a disadvantage, a new power management and communication line would have to be designed for such a system. For the latter option, only methods that do not require much space can be considered as everything has to fit into one hemisphere, however power and communication can be shared from the module itself. This advantage led to the decision to integrate a manipulator into a module, and thus an appropriate gripper technology had to be found with two constraints: (i) to work in limited space and (ii) to be able to manipulate a variety of everyday objects (glasses, remote control, USB stick, cutlery, etc.). After much consideration, the interesting concept of granular jamming was used to develop a “Universal Gripper” (UG) similar to the one in [26]. This gripper consists of a closed, flexible membrane (often a party latex balloon) filled with small granules (e.g. sand, ground coffee, etc.). The membrane is normally soft and adapts to the shape of an object when pushed onto it. The actual gripping is achieved by transitioning the fluid state of the granules into the solid (jammed) state by creating a vacuum inside the membrane. This effectively locks the shape of the membrane which now is able to exert a gripping force on the object. Due to this interplay of a soft, shape-adapting state and a solid, gripping state, this gripper is capable of manipulating a wide range of objects as demonstrated in various previous works (e.g. [26, 7, 8]).

Integrating a UG into a Roombots hemisphere still posed a number of challenges, mostly around downsizing the mechatronic components, especially the required and usually large vacuum pump. A careful selection of a miniature vacuum pump (Schwarzer SP 100 EC) and small-scale solenoid valves (SMC S070C-SAG-32) resulted, to the best of our knowledge, in the first-of-its-kind mobile jamming gripper integration within an MR. Two modules have been equipped with this type of gripper which is filled with ground coffee as in the original version

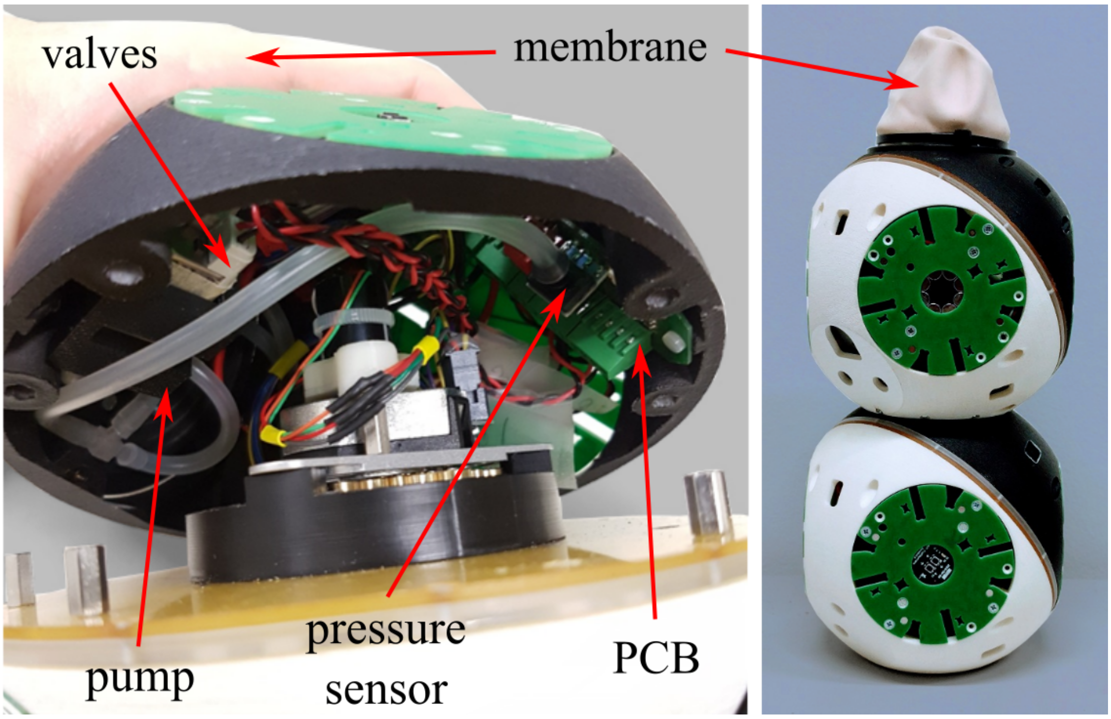

Figure 1.4 – Integration of a Universal Gripper into a Roombots hemisphere. Left: a miniature vacuum pump and small-scale solenoid valves allowed the components to be fully contained and a specialized gripper PCB alike the existing electronics measures and controls the pressure inside the flexible membrane. Right: a gripper module with the Universal Gripper sticking out on top, replacing one of the ACMs.

in [26]. In addition of being able to manipulate various objects, the control of the gripper is extremely simple and robust where the vacuum pump - with the solenoids - either inflates or deflates the membrane to set pressures, measured by a single pressure sensor (Honeywell 015PAAA5). Details of the implementation are depicted in Fig. 1.4 left, and the final Roombots gripper module is shown in Fig. 1.4 on the right. Although the Universal Gripper is very capable, it has a few limitations such as the object size and weight which depends on the size of the gripper, pressure in the membrane chamber, and type of granules and membrane. Furthermore, it needs to press against the object, which can be difficult with a limited DoF system. Hence, it is not always suitable to handle standing objects that have sensitive balance, or soft objects.

### 1.3.5 Electronics

A considerable part of the electronics was redesigned to accommodate for hardware changes (see Fig. 1.5 for details). The power board, motor control boards and ACM control boards went through major updates. The technology of communication with the modules (Bluetooth) as well as the communication bus inside a module (RS-485) were kept the same. Three new

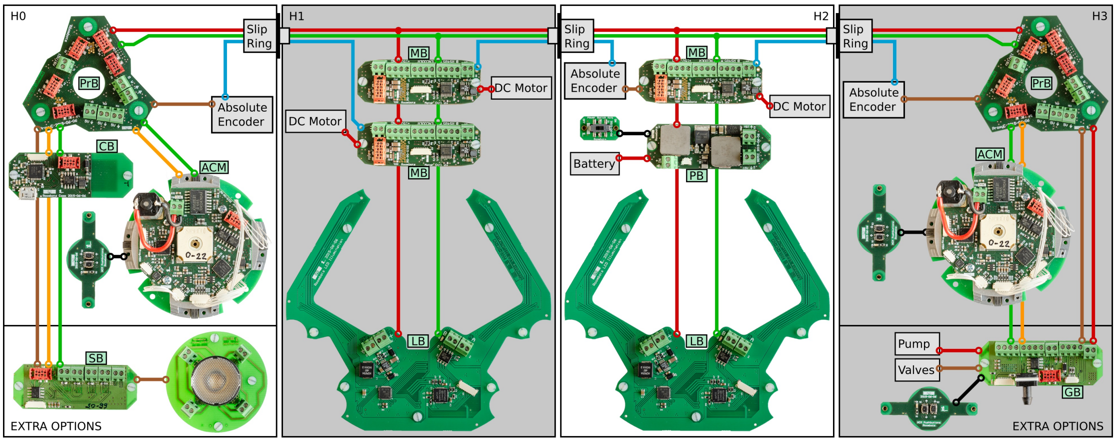

Figure 1.5 – Roombots electronics is also modular and distributed throughout a module in hemispheres H0-H3. The background of each hemisphere region is shaded to match colors of the real hemispheres. In each Roombots module, there exists 3 motor driver boards (MB), 2 active connection mechanisms boards (ACM), 2 proxy boards (PrB, used to convert voltages and ease assembly), 2 LED boards (LB, used to give feedback to the operator), 1 communication board (CB, provides Bluetooth connection and drives the inner RS-485 bus) and 1 power regulation board (PB). Furthermore, each module can support extra options such as spotlight board (SB) or Universal Gripper control board (GB) in the outer hemispheres. Extra option slots are identical and each electro-mechanical subsystem can be placed in either of the outer hemispheres. The extra options are not considered as essential for the basic operation of Roombots modules; only selected modules are equipped with them. Electrical connections within a module are illustrated with different colors: Red (15V), orange (6V), brown (5V), green (RS-485 bus), blue (SPI) and black (support boards for easy user access). Each physical connection is shown with a circle whereas unconnected lines pass through a board without a circle.

board types were designed to control the additional hardware. The hemisphere with an integrated Universal Gripper contains a gripper board that is responsible for controlling the pressure inside the membrane by using a pressure sensor, vacuum pump and valves. Further, a specialized spotlight board controls the powerful RGBW-LED integrated in one hemisphere which is used for illumination purposes in different colors and brightness. Finally, an LED-ring board gives feedback to a nearby user (this board has been developed in [119]).

Further, readout boards for other new sensors have been integrated in Roombots. The values of the proximity sensors and accelerometer are not directly used by modules, however they can be reported to an external PC which can execute higher level controllers (as e.g. in [84] for a local connection search algorithm, summarized in section 1.3.7).

### 1.3.6 Motor control

Changing the hardware led to changes in the firmware of various boards in Roombots. The nature of the new absolute encoders is that they give a much lower number of ticks per rotation than relative encoders which particularly affected the derivative control. Hence, the frequency of the control loop was reduced and PID parameters were adapted. Absolute encoders read over SPI and the communication channel is going through slip rings. Although the communication with absolute encoders is mostly smooth, rare encoder reading errors can occur. Various reading error detection and safety procedures have been implemented. For instance, all the DC motors are disabled if the position error gets unexpectedly large which may occur due to external disturbances or persistent erroneous encoder readings.

### 1.3.7 Connection control

The proximity sensors and accelerometer data can be used to check the validity of a connection. A connection can only be formed if two plates are close enough and correctly oriented which can be checked by the IR-sensors and hall effect sensors. Additionally, in a lattice-type configuration, the gravity vector must be collinear to either the global x-, y- or z-coordinate, measured by the accelerometer; other directions indicate non-idealities such as body elasticity, local control error, or gear and ACM backlashes.

These properties are used in [84] to develop a local search algorithm for reliable connections that has two stages. In our case, the condition for a successful connection is the proper alignment of the four hall effect sensors. Since their values are maximal when directly opposite a magnet, it is enough to threshold the sum of the four sensors to validate a possible connection. If the sum is above the threshold when a connection sequence is initiated, the command list continues normally. If the sum is below the threshold, the first stage of the local search engages, where the accelerometer data is converted into a *pitch* angle. The pitch then is used to generate motor commands for a new desired angle by an inverse kinematics model of the module (Fig. 1.6) to reorient the plates orthogonally. If this is still not satisfying the threshold condition due to elasticity in the module and docking plates, the second stage with random movements engages. This is because the occurrence of ACM misalignments strongly depends on the movement history of each module such that modeling this effect is infeasible. Instead, one of the three motors is randomly chosen and moves by either +1° or -1°, followed by a new evaluation of the hall effect sensor values. This process is repeated until the threshold condition is satisfied.

The result of this local search algorithm was a drastic improvement of single-module on-grid locomotion: while one module before could only locomote on a tabletop and had a 0% success rate for certain movements on a wall or ceiling, the new connection control was tested in three of the most challenging scenarios: (i) going up when attached to a ceiling, (ii) going up when attached to a side wall, and (iii) going left when attached to a side wall. Each scenario was repeated 10 times. The new docking position search method works with a 100% reliability for all movements (average convergence time for a connection by random movement is 43.53 s), a crucial property for any self-reconfiguration with the hardware.

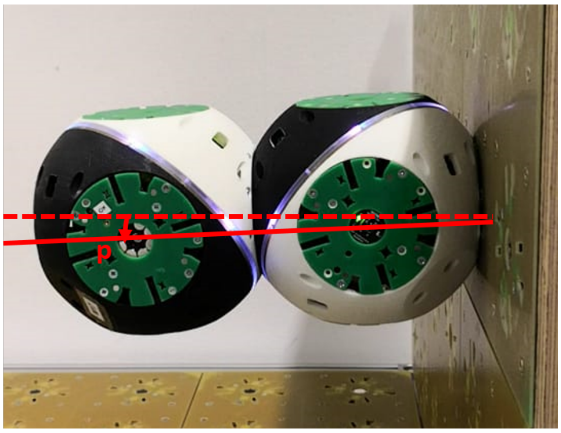

Figure 1.6 – Pitch angle compensation. The accelerometer detects deviations (red solid line) from the global orthogonal frame (red dashed line) and uses an inverse kinematics model of the module to correct imperfect attachments and module deflections. If this compensation does not result in a valid connection, a second stage with small random module movements engages, aiming at aligning the hall-effect sensors with the corresponding connection plate.

### 1.3.8 Graphical User Interface (GUI)

For designing different complex tasks as outlined in section 1.1, an easy-to-use User Interface (UI) was needed. Different user interfaces with Roombots were already explored in the past, e.g. using Playdough to form structures (see section A.1 and [107]) and an approach based on Virtual Reality (VR) (see section A.3 and [112]), however these previous works could not be adapted to larger scale dynamic formations. The Playdough interface does not work in real-time, and the VR only allows a limited kinematic range for reasons of simplicity. Since Roombots are able to form complex geometrical structures, it seemed natural to develop a Graphical User Interface (GUI) to be able to visualize such formations. This GUI has been developed by Jérémy Blatter under my supervision. Unity[1] is used, a 3D animation software that often is used for creating video games. Even though Unity has the capability to function as a physics simulator, we only use the visualization aspect of the software. Naturally, the visualization does not always represent the real configuration of modules perfectly due to the physics present in the real world, causing e.g. elastic deformation of modules and attachment plates under load. This effect as well as others arguably could be modeled and hence included in the visualization. However, throughout our experience with the real modules, we found these effects and other sources of noise to be too stochastic for modeling and decided to implement control routines in the modules to account for discrepancies. These routines will be discussed below in section 1.4.1; the GUI itself was kept simple and assumes perfect conditions. At the current state of the project, our system focuses on forming viable connections of single modules, for which the development of these routines was feasible. Connection sequences of multi-module formations likely will nevertheless need additional modeling effort, which remains a future challenge.

---

[1] https://unity3d.com

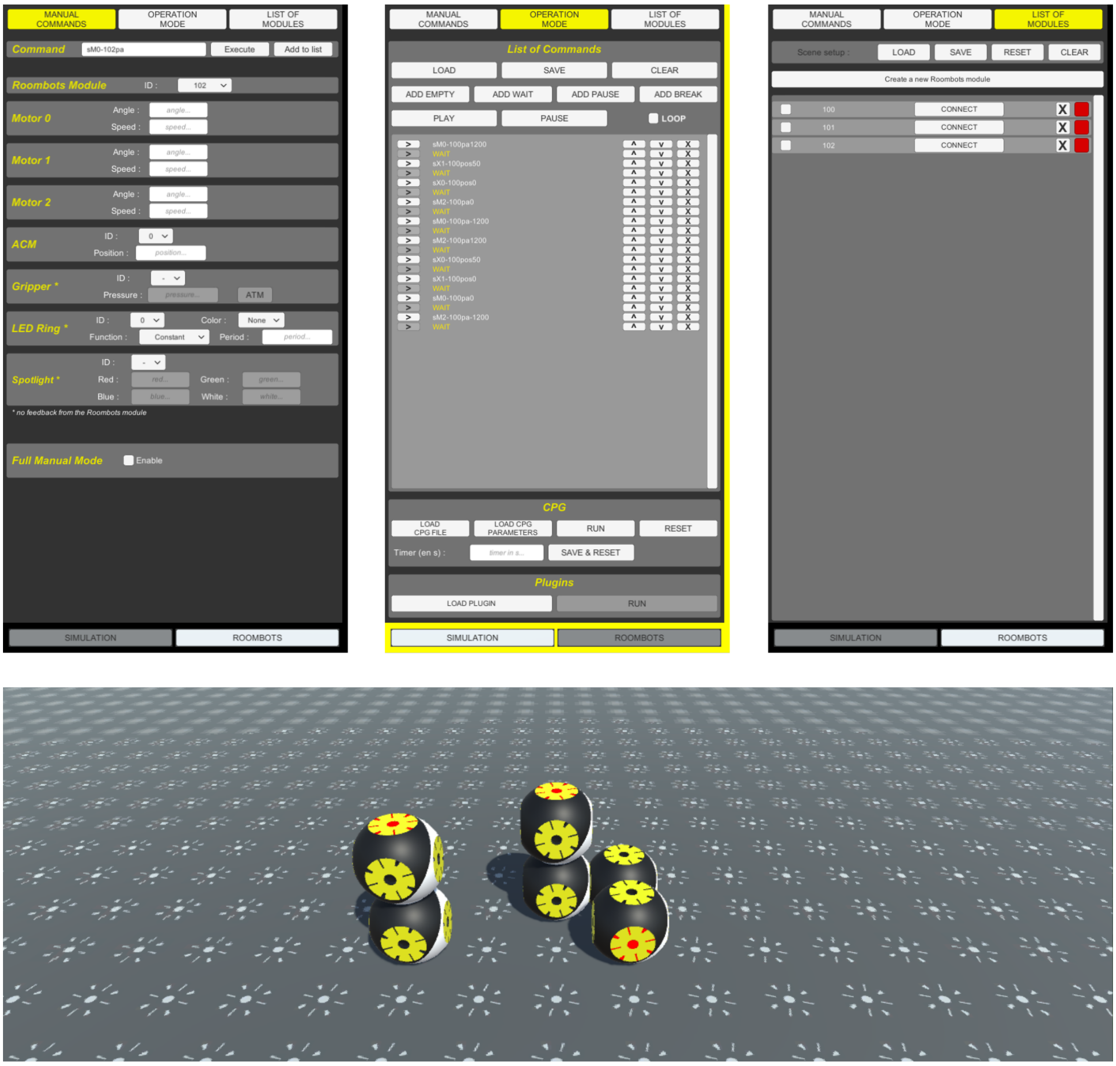

Command: sM0-102pa

Roombots Module ID: 102

ACM ID: 0

Gripper * ID: -

LED Ring * ID: 0 Color: None Function: Constant

Spotlight * ID: -

* no feedback from the Roombots module

```
sM0-100pa1200
WAIT
sX1-100pos50
WAIT
sX0-100pos0
WAIT
sM2-100pa0
WAIT
sM0-100pa-1200
WAIT
sM2-100pa1200
WAIT
sX0-100pos50
WAIT
sX1-100pos0
WAIT
sM0-100pa0
WAIT
sM2-100pa-1200
WAIT
```

MANUAL COMMANDS
OPERATION MODE
LIST OF MODULES
Command
Execute
Add to list
Roombots Module
Motor 0
Angle :
Speed :
Motor 1
Motor 2
ACM
Position :
Gripper *
Pressure :
ATM
LED Ring *
Color :
Function :
Period :
Spotlight *
Red :
Green :
Blue :
White :
Full Manual Mode
Enable
SIMULATION
ROOMBOTS
List of Commands
LOAD
SAVE
CLEAR
ADD EMPTY
ADD WAIT
ADD PAUSE
ADD BREAK
PLAY
PAUSE
LOOP
CPG
LOAD CPG FILE
LOAD CPG PARAMETERS
RUN
RESET
Timer (en s) :
SAVE & RESET
Plugins
LOAD PLUGIN
Scene setup :
Create a new Roombots module
100
101
102
CONNECT

Figure 1.7 – Screenshots of the GUI. The control panel can be switched between "manual commands" where specific commands can be sent to single modules, "operation mode" where a sequence of commands can be played and additional modes are available (transfer of parameters of a CPG network, and external plug-ins), and "list of modules" where all modules are listed and can be connected by bluetooth to real Roombots modules. On the bottom, a visualization panel shows a Roombots arrangement, and a message panel below can display various information during runtime (not shown here).

Fig. 1.7 shows screenshots of an example usage of the GUI. There are three main parts: control panel, visualization panel and message panel. The control panel has three sub-categories: manual commands, operation mode and list of modules. In “manual commands” (left), single commands (motor, ACM, LED, gripper, spotlight) can be created and sent to specific modules. These commands can also be added to a list which is created on the fly. In “operation mode” (second left), this list of commands is stored, and it can be executed in a single sequence to perform a specific task. Command lists also can be saved and loaded here. This category also allows the execution of predefined movements of a Central Pattern Generator (CPG) [73] as well as executing external plug-ins, e.g. control of a motor with a computer keyboard. The yellow border around the panel indicates that the control has been switched from the virtual modules to the actual real world modules. Connected modules provide real-time feedback of all the motor and sensor states which then are displayed in the GUI. In “list of modules” (second right), all virtual modules are listed and modules can be created or deleted. The current state and positions of all modules can be exported as a “scene”, and scenes can also be imported again, allowing a quick setup for new tasks. Here, each virtual module can also be connected to a real module by bluetooth, which then allows an easy switch between performing a list of commands with the virtual modules only or also with the real connected modules. On the bottom, the visualization panel with an arrangement of virtual Roombots modules is visible. This panel also contains a (empty) message panel to display warnings and other messages are visible (not shown here).

### 1.3.9 RGB-D vision system

Some of the proposed tasks require an external system that tracks a user and any furniture present in a setup. We have already used the Microsoft Kinect sensor in previous work for tracking purposes and reimplemented the same system also for the current work. Here, a Kinect v2 sensor is mounted on the ceiling and observes a designated ground area. It functions as a depth sensor and can distinguish objects with different heights in the scene. It is assumed that the highest object in the scene is the user, and multiple pieces of furniture are marked in specific ways to make them unique and define their orientation. Fig. 1.8 a) and b) give an overview of the tracking system.

### 1.3.10 Robotic-enhanced furniture

As two example pieces of furniture to demonstrate the proposed tasks, we equipped a small table and a chair with Roombots modules to extend their functionalities. The chair is put on passive caster wheels such that it can roll in any direction, and two modules use their outer hemispheres as wheels to drive the chair similar to a differential drive. Since the main load is borne by the passive wheels, a user can sit on the chair, however the chair is only moved by the modules under no additional load. For the table, each leg is extended by one module, and by again using the outer hemispheres for rolling, it gives the table the ability to move forward and backward and to rotate. Additionally, a gripper structure consisting of one gripper module in

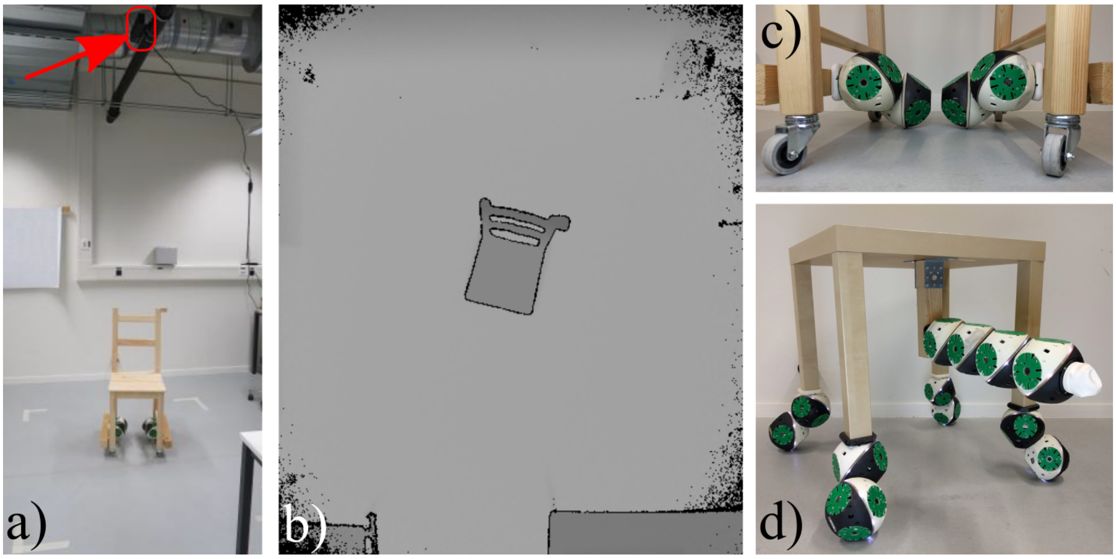

Figure 1.8 – RGB-D camera and furniture used in the sub-tasks. a) An overhead Microsoft Kinect depth sensor (red arrow) can track objects within the area marked with masking tape. A chair is shown in this area. b) View of the camera; depth is mapped onto pixel gray-scale with black edges, making the chair easily identifiable. c) Close-up view of the caster wheels and the differential drive-like wheel modules of the chair. d) The table with four wheel modules and a meta-module with a gripper attached underneath.

series with a standard module can be mounted underneath the table. This allows the table to pick up objects from the ground and place them onto itself as will be shown later. Fig. 1.8 c) and d) show both pieces of furniture.

## 1.4 Demonstrations of the five key-tasks

To demonstrate the augmented capabilities of the modified RB system, we designed five main tasks which are demonstrated in various sub-tasks. The results of these experiments are presented in this section.

### 1.4.1 Easy-to-use user interface: the GUI

For the sake of clarity, we present the GUI first. As an example to present the work flow of the GUI from task definition to hardware execution, we here describe the development of a simple demonstration that we call "circle walk", i.e. a sequence of movement commands that make a module locomote on-grid in a circular manner.

At the start, the GUI visualization area is empty, and a new virtual RB module is added. A module usually is initialized with both ACMs opened and all motors in their zero state, and by default is placed in the GUI vertically onto the grid with one ACM facing the grid. First, an initialization script is loaded into the GUI that attaches the module to the grid and brings the motors in the correct position to start the circular loop. Then, the main list is loaded and the loop-box ticked which makes the full sequence loop as long as needed. This main list of commands consists of a predefined series of opening and closing ACMs and performing 90 ° rotations of motors in between where looping these actions makes the module move in a circular fashion on a single 2x2 grid plate. The top row in Fig. 1.9 shows the initialization and the first half of the circle walk demonstration in the GUI.

Once the demonstration has been developed in the GUI, it is only a matter of connecting a real module to the virtual module in the GUI. Once connected, the mode is switched from "Simulation" to "Roombots" to send commands to the bluetooth connection, and the demonstration is performed with the hardware (bottom row of Fig. 1.9). Additional control routines are implemented to increase the rate of success for executing commands. The GUI continuously crosschecks the setpoints of motors and ACMs with the actual values fed back from the module and resends commands for values that do not lie within a small margin. In particular, the most crucial part of a reconfiguration is forming the connection to a new attachment point. Handling misalignments during this process required more elaborate strategies. In our case, the sensors implemented on the ACM plates give the necessary information concerning the correct alignment. If a misalignment is detected, a search algorithm performs small, random actions around the setpoints that usually results in a successful connection. Details of this algorithm can be found in [84].

The GUI possesses more features, e.g. forcing the starting point for the forward kinematics of connected RB modules in simulation, adding pauses to a sequence of commands, running CPG networks and external plugins and more. The described example only present the basic functions of the GUI which are enough to make the development of simple demonstrations relatively quick and easy.

Research on most of the (SR)MR systems begins with simulation to study the feasibility of the system because simulation is easier and faster to set up compared to robot hardware and can give valuable information. Moreover, very complex scenarios can be explored in simulation. Most of the modular robotic systems are accompanied with simulation/GUI tools. For instance, [90] explains a simulation environment for a modular system whereas [92] includes self-reconfiguration steps too. One of the most comprehensive and recent SRMR GUI (VSPARC) is designed for Smores in [80]. It uses Unity engine similar to our approach. Most of the features presented for VSPARC also exists in the Roombots GUI, but adapted for the Roombots hardware.

### 1.4.2 Scalable self-reconfiguration

As an example of a larger self-reconfiguration task (i.e. with more modules and more steps) that goes together with the application of adaptive furniture, we show the formation of a small chair with 12 modules. The details of the planning of this demonstration can be found in [84].

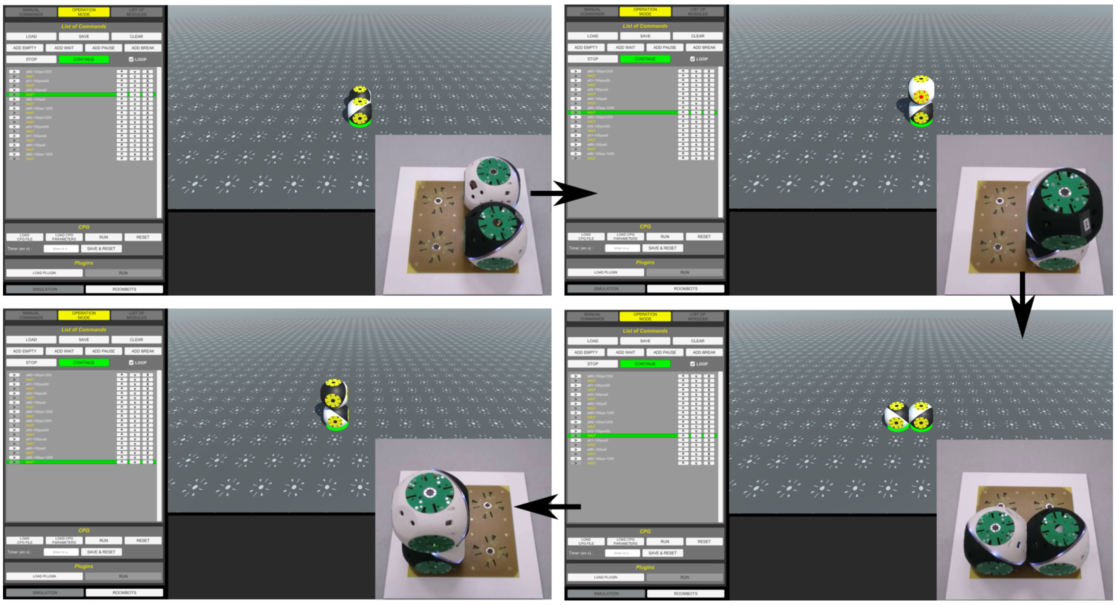

Figure 1.9 – Circle walk demonstration. The GUI is shown in “operation mode” where a preprogrammed list of commands is executed in sequence. The first half of the circle walk is shown; looping the script makes one module go around on a 2x2 grid. The corresponding hardware configuration is shown as insets.

The work includes the development of a local search algorithm and closed-loop control during the connection process that enabled more reliable reconfiguration, as well as the derivation of an A* search algorithm that finds the motor command sequence to form a given structure from arbitrary initial conditions.

Here, only the final formation sequence is shown, starting from 12 modules standing on a flat grid. In order to decrease the number of nodes on the search tree for such a large number of possible motor actions at each state, pruning methods are included in the search algorithm to avoid exploring unpromising branches. The formation of the full chair is divided in to 6 sub-configurations (manually preprocessed by an operator) that must be reached in a specified order and build up the chair in stages. Fig. 1.10 shows snapshots of the formation process.

In 3D SRMRs, we could only find a few systems that demonstrated self-reconfiguration with more than 8 modules. M-TRAN demonstrated cluster flow with 24 modules (48 DOF total) in [91]. However, in most of the demonstrations of M-TRAN, the structure stays connected. ATRON [23] presents a sequence with 9 DoF. Similarly, SMORES demonstrate a system with from 6 up to 9 modules (4 DOF each) and considerable autonomous (closed-loop) shape changing with disconnections and re-connections as reported in [162] and [37]. Although M-TRAN, ATRON, SMORES and various other SRMR are potentially capable of showing a similar application shown in Fig. 1.10, to the best of our knowledge this is the first time a 3D self-reconfiguration is shown using more than 30 DOF (36) with all modules initially detached.

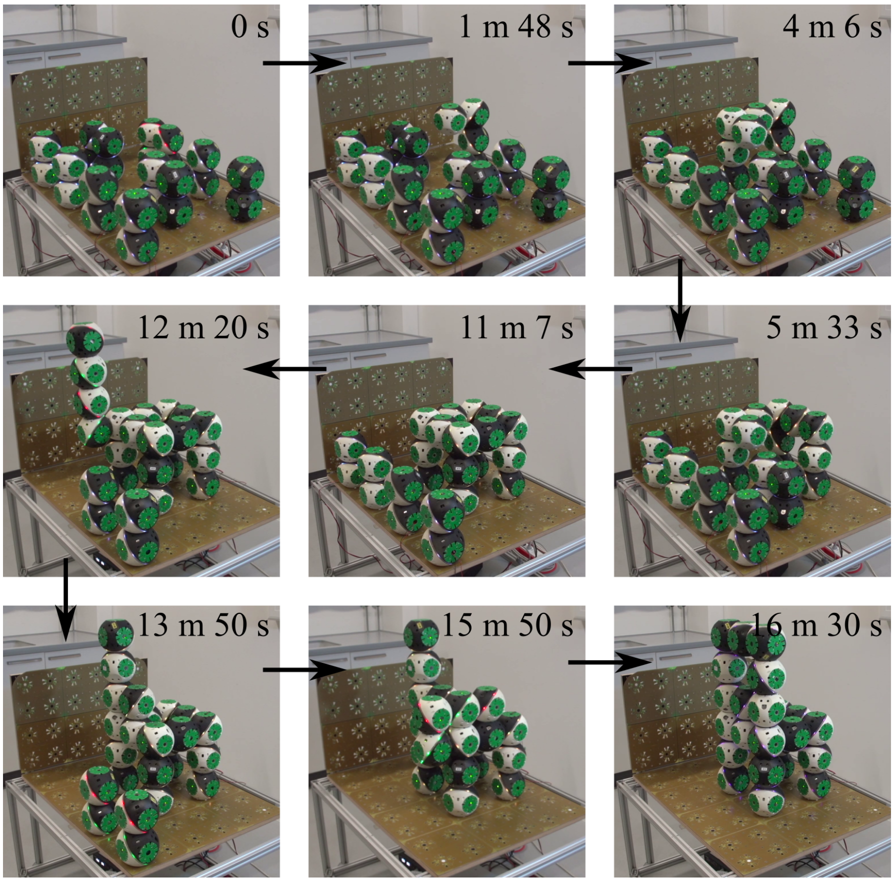

Figure 1.10 – Snapshots of the chair formation sequence. The chair is built in 6 stages (4 for the legs and 2 for the backrest). The large time loss in the middle is caused by a manual intervention to connect the leg segments, however as shown in the supplementary video, the self-reconfiguration is largely autonomous.

### 1.4.3 Mobile furniture

The potential task of mobile furniture is demonstrated with four sub-tasks: following chair, evading chair, adaptation to environment and overcoming obstacles.

#### Following chair

We explore the possibility of an assistive chair that follows a user to always be available in case of the user needing to rest. The system is aimed at preventing falls and providing assistance for manual recovery after a fall. It consists of an RGB-D camera tracking the position and orientation of the user and of the chair in a predefined area. Two Roombots modules are attached to the chair allowing it to move anywhere and in any orientation in the area, similar to a two-wheeled differential drive robot. A controller (PC) computes the difference between the position and orientation of the user and the chair and sends movement commands to the modules such that the chair is always next to the user (Fig. 1.11).

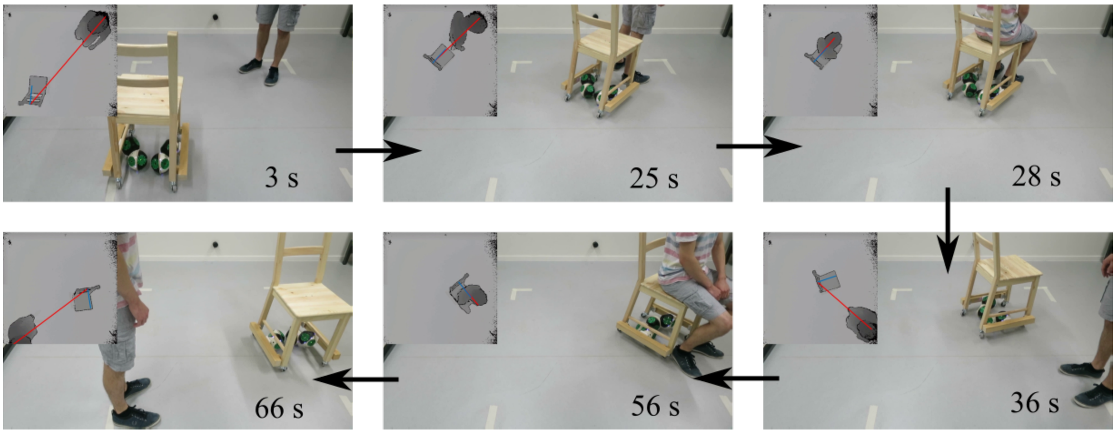

Figure 1.11 – Following chair. An overhead Kinect (top left panels in each snapshot) tracks the position and orientation of an assistive chair (short blue line) and the path to the patient (long red line). The user can sit whenever needed as the chair follows the user inside the predefined area.

#### Evading chair

We also demonstrate the inverse scenario where Roombots furniture has to make space to let a user pass. This scenario could take place in a packed apartment where the available space is limited and shared between user and furniture, or a user is physically unable (e.g. in a wheelchair) to move furniture out of the way. We again used the depth map to track a user and the same chair as in the previous demonstration. The chair initially is located in the middle of a defined area and the user would like to cross this area. A controller (PC) extrapolates the desired path of the user and moves the chair orthogonally to this path out of the way to make space for the user to pass. After creating enough space and the user passing, the chair moves back to its original position (Fig. 1.12).

It is important to note that both "following and evading chair" demonstrations are not complete and comprehensive solutions to solve the problem. The full solution would require significantly more research which falls out of the scope of this paper and the SRMR field. Such a solution would involve detailed intention detection considering a much wider spectrum of actions and would incorporate safety and emergency protocols. Nevertheless, they serve as a proof-of-concept that SRMR can be used in such applications.

#### Adaptation to environment

Roombots-enhanced furniture can have additional functionalities besides providing mobility to existing furniture. In this demonstration, we equip a small table with four modules, fixed to the end of each leg of the table. We use the outer hemispheres (one DoF) as wheels to enable the table to move forward and backward and to rotate. In this specific example, the two other DoFs of a module can move in a null-space such that the total height of a leg can

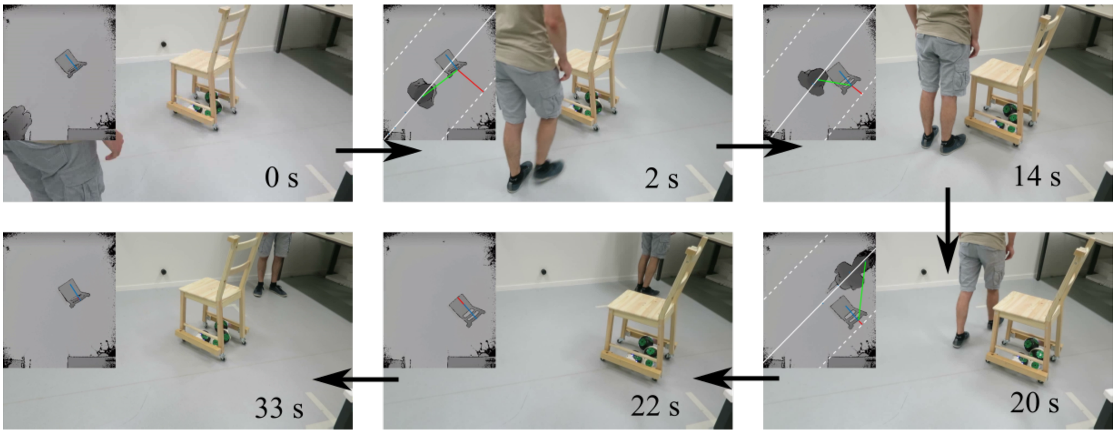

Figure 1.12 – Assistive furniture makes space. An overhead RGB-D camera (top left panels in each snapshot) tracks an assistive chair (short blue line) and the user's location with respect to the chair (green line). It extrapolates the path of the user (white lines) and moves the chair orthogonally to it (short red line) before returning to its original position after letting the user pass.

be varied. The table transports a set of objects and this height adjusting ability can be used to keep the tabletop horizontal on uneven terrain to prevent the objects from falling off the tabletop. We let the table drive from a straight area into a sloped area. In the first case without adaptation, the set of objects falls off the table after a short distance on the slope area. If the slope compensation is activated, the tabletop can be kept closer to the horizontal plane which prevents the objects from falling when the table is on the sloped area. Fig. 1.13 depicts snapshots of both cases.

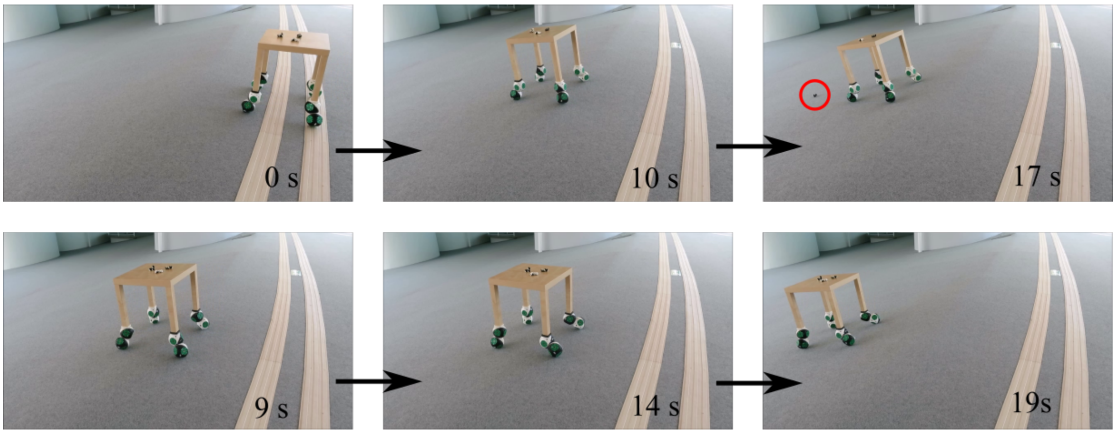

Figure 1.13 – Active slope compensation. Top row: a table driving over a sloped area tilts its tabletop, causing objects on top of it to fall (red circle). Bottom row: the attached RB modules can partly compensate for the slope by shortening the hind legs of the table, keeping the tabletop more horizontally such that the objects stay on top.

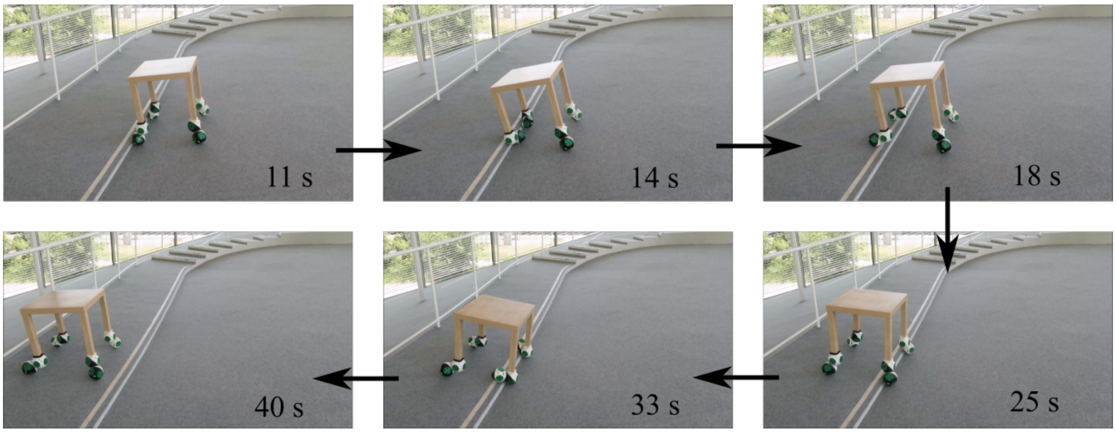

Figure 1.14 – Overcoming a ledge. A table drives until its front legs touch the ledge. The attached RB modules then perform a rotation around their attachment point, causing them to move on top of the ledge in the process. The same movement then is repeated for the hind legs after which the table has overcome the ledge.

#### Overcoming obstacles

For the table in the previous demonstration, an additional behavior is available by “rotating” the RB modules around their attachment point at the end of each leg. This causes a module to move in a circular manner around the tip of the leg, performing a movement similar to a step. We use this movement to demonstrate climbing a small ledge that the table cannot drive over. The table drives towards the ledge until the front legs are aligned and touch the ledge. The front RB modules then rotate, moving on top of the ledge by doing so. The same process then repeats for the hind legs, after which the table has successfully overcome the ledge (Fig. 1.14). Here, the table is piloted by a human and the sequences are manually initiated.

### 1.4.4 Manipulating furniture

One of the most needed and repeated task in daily life (as well as industrial settings) is object manipulation. Hence, it is an implicit requirement for a SRMR to be able to manipulate surrounding objects, particularly when humans and SRMR need to cohabit.

#### Object pick-up

A small table is equipped with one module on each leg for wheeled locomotion. Additionally, a meta-module structure with an implemented Universal Gripper is attached to the underside of the table. The task is to start at location X, pick up a pen at location Y and bring it to location Z. The table is again manually controlled and rolls into position to pick up the pen. The gripping sequence is preprogrammed and executed once the table is in the correct position. It picks up the pen from the ground and puts it on top of the table which then rolls to the final location. Fig. 1.15 shows snapshots of this manipulation task.

#### Passing objects

One of the advantages of the Universal Gripper is that it can grip objects basically regardless of their shape and orientation (within a size limit given by the size of the gripper). This is promising for passing objects from one gripper to another since the passing sequence does not need to take the object’s shape or orientation into account. In the framework of multiple RB furniture pieces collaborating with each other, such a scenario of passing an object between pieces of furniture can easily be imagined. We adopt this task in a simpler setup where an object is passed from one RB gripper module to another. The first module picks up an object (pen) from a tabletop and rotates its gripper to face the gripper of the second module. In this position, it is important to notice that simply making the two grippers touch orthogonally causes issues for the second gripper to actually grip the object as it would require the surface on the object that is currently occupied by the first gripper. There are several ways to deal with this issue; here we present the preliminary results of inducing a “shift” such that the second gripper touches a free part of the object (this also requires that the object is somewhat

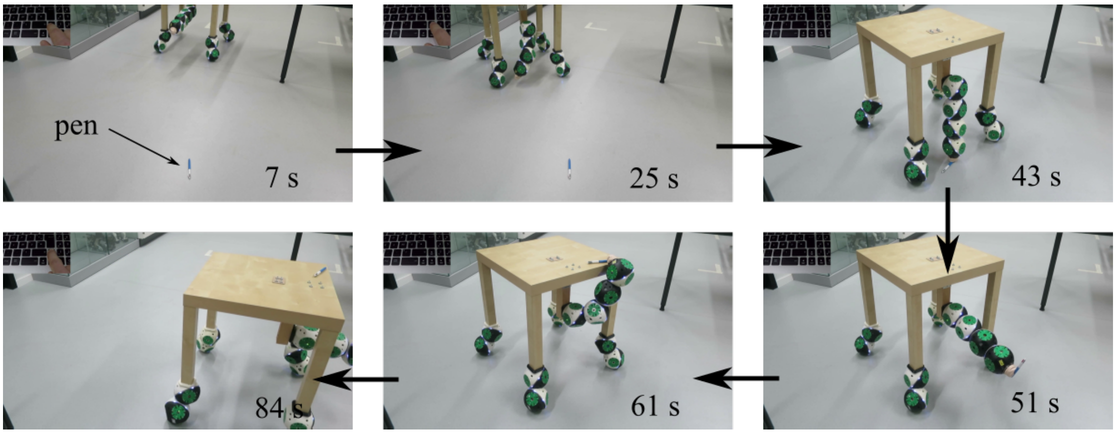

Figure 1.15 – Table picking up an object. An assistive table with manipulating capabilities moves towards a pen dropped on the floor. It picks up the pen with a Universal Gripper, places it on top of the table and brings it to the user.

elongated to possess such a free part). The second gripper then grips the object upon which the first gripper releases, transferring the object to the second gripper. Fig. 1.16 shows snapshots of transferring a pen from one to another module.

Even though we only show one example of such mid-air sensor-less passing of objects between two modules, we see much potential in using this unique way of object transfer in a collaborative environment as depicted in Fig. 1.1.

### Opening water bottle

The third demonstration in this task concerns a more assistive subtask of manipulation. Here, we briefly validate if a gripper structure can help with opening a PET water bottle. A user has to hold the bottle and push it into the gripper of a waiting RB structure. The gripper then actively grips the cap of the bottle and performs a rotation to open the cap. Once opened, the user can remove the bottle and the modules place the cap on the table (Fig. 1.17).

### Object manipulation capabilities of SRMRs

Almost all SRMRs have means of connecting and detaching to each other. Some use magnetic attraction whereas a big portion of them use mechanisms. For example, the Active Connection Mechanism (ACM) is the mechanical latch Roombots use for the purpose of connection. In theory, this connection mechanism - and similar ones in other systems - could also be used for object manipulation. However, most of the times these self-reconfiguration methods are not suitable for manipulating arbitrary objects. It is possible to design a gripper module as an extension for almost all of the SRMRs similar to [23]. Also, some SRMRs have already integrated gripper modules such as [104] and [56]. An integrated universal manipulator is demonstrated for the first time with this work.

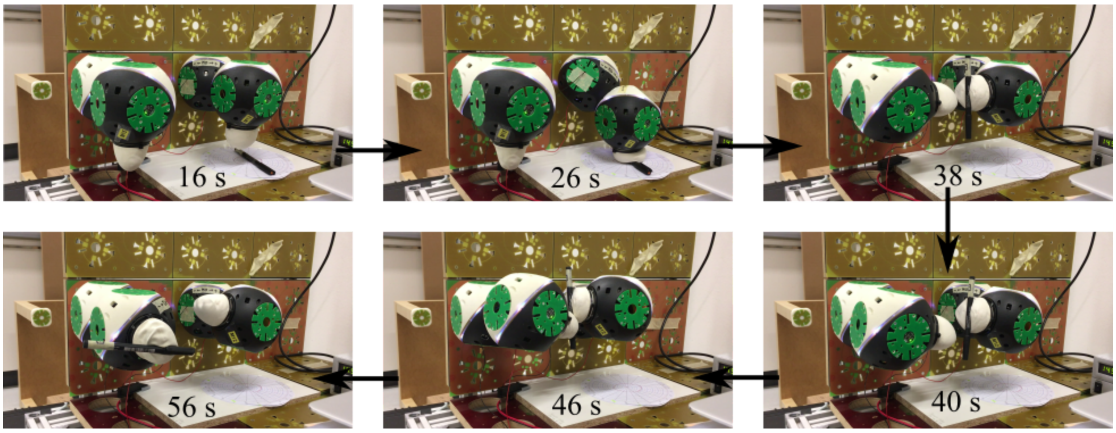

Figure 1.16 – Two RB gripper modules passing a pen in mid-air. The first module picks up the pen from the table and orients it to face the gripper of the second module. A shifting motion then takes place such that the second gripper has a free part of the pen to grab onto. The first module then presses the pen into the gripper of the second module and releases it after the pass is completed.

### 1.4.5 Interactive furniture

#### Kinect tracking control

We can couple movement control of RBs with the tracking abilities of the Kinect. Using depth information and the body segregation method of the Kinect, we can define e.g. intuitive hand gestures for certain commands. Such a user interface already has been explored in [119], however not in real-time. There, a user would first point to an RB module and then to a desired goal position, and a planning algorithm then computes and executes a movement sequence. Here, we use real-time inverse kinematics to convert the position of a users hand, tracked by the Kinect, into movements commands to make a meta-module follow the hand. The top row of Fig. 1.18 gives an example of this interaction.

#### LED capabilities

At last, we showcase LED lighting capabilities as an interaction method. Each module contains two rings of 6 RGBW-LEDs that can be used to e.g. display the state of a module to a user or indicate if an ACM is open or closed. Additionally, one module possesses a powerful RGBW-LED that can be used as a spotlight to illuminate a specific region (as already discussed in [105]). In the bottom row of Fig. 1.18, some lighting examples are shown.

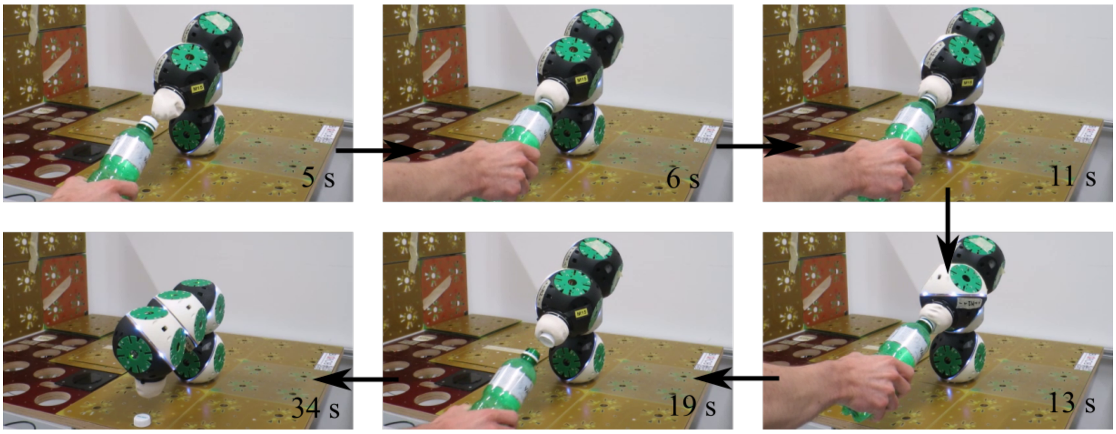

Figure 1.17 – A gripper metamodule assisting in opening a PET water bottle. The user pushes the bottle into the gripper which grips the cap and then performs a rotating movement to open the bottle.

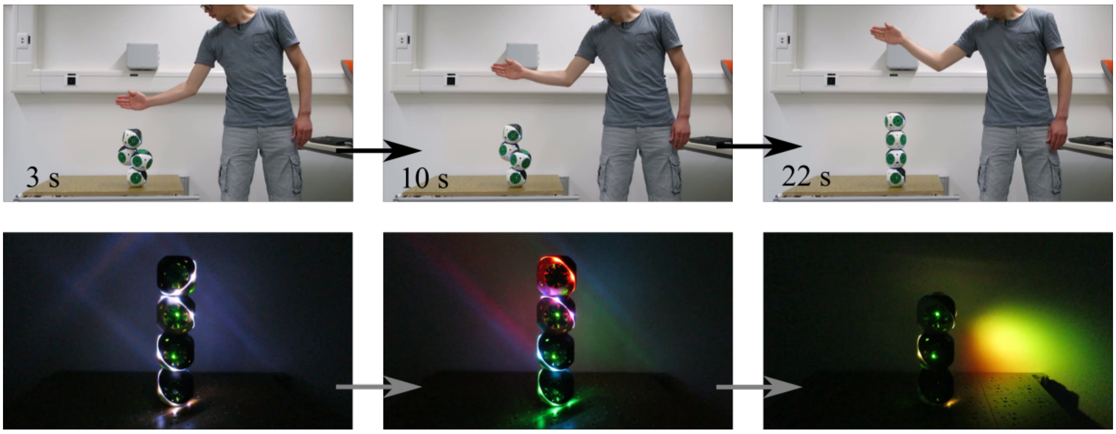

Figure 1.18 – Interaction with tracking and lighting. Top row: a users hand is tracked with the Kinect sensor and its position converted into inverse kinematic commands that make the meta-module follow the hand. Bottom row: lighting capabilities of Roombots with the integrated LED-rings and the powerful RGBW-spotlight.

## 1.5 Discussion and Future work of the Roombots project

The presented hardware demonstrations showcase the capabilities of the upgraded Roombots modules. We are aware that the outcomes of the demonstrations are rather of qualitative than of quantitative nature as this work aims at exploring a potential use of (SR)MR for adaptive and assistive furniture. In this context, we successfully presented proof-of-concept demonstrations of RB modules completing a large and complex self-reconfiguration task involving a significant number of autonomous connections with minimal human assistance. Further, RB modules are used to create mobile furniture that can follow and evade users, adapt to the environment and can overcome obstacles. Manipulation tasks involved RB modules picking up a pen, opening a PET bottle and a proof-of-concept demonstration of passing objects between two modules. At last, RB modules possess various LED lighting capabilities, and we showed examples of how to use simple gestures to control an RB metamodule and developed a dedicated GUI for easy monitoring of modules and creation of demonstrations.

The challenges for the presented experiments were to increase the connection reliability and to develop an interface to quickly create demonstrations with a large number of modules. For the reliability, on the one hand we could significantly improve the movement precision of all DoFs by changing the materials of the main gearbox and ACM from plastic to aluminum and by integrating a new absolute encoder. The increase in weight was compensated for with stronger motors. On the other hand, reconfiguration sequences now use a closed-loop controller to better align an ACM with a neighboring plate thanks to the integration of infrared and hall-effect sensors. Additionally, a ring of permanent magnets locally helps to form a connection while retaining the hermaphroditism of the ACM. Concerning the interface, the developed GUI contains all the key functionalities to rapidly develop Roombots scenarios. It allows for the safe creation of motor sequences in its virtual mode, and due to the improved connection reliability, the switch from virtual to real modules has a high chance of correctly performing the demonstration despite the disturbances present in the real world.

While a single module now works effectively, reliable position control of multiple modules in series remains a challenge. With Roombots, an example are the necessary more complex on-grid locomotion capabilities of a meta-module to perform a self-reconfiguration as in task 1, for which the capabilities of a single module are too limiting. Even though the mechanics have been upgraded to cause less gearbox backlash, there are two main sources of misalignment that hinders the autonomy of this functionality: (i) the connection between two modules possesses unidentified mechanical play, and (ii) two modules in series still cause significant elastic deformation of the module shells.

For the experiments in this work, only the chair reconfiguration task involved meta-module reconfiguration where human assistance thus was needed in a few cases. Nevertheless, we regard the successful demonstration of the autonomous chair formation using 12 modules as a significant milestone in the Roombots project. It validates both the capabilities of the hardware and the self-reconfiguration framework. It should be noted that relatively minor human intervention during the hardware demonstration was needed despite the efforts for autonomy: three manual interventions were needed in 107 executions of motor commands and connection or deconnection events (of which 16 events are independent connections only). In particular, the random local search algorithm to align the ACMs does not handle all possible cases equally well and may not converge because the positions of the two connecting plates are initially too misaligned due to elastic deformations and mechanical play. As a result, the local motor actions caused by the algorithm do not allow a meaningful quantitative comparison of the sensory feedback to steer the connection to a more aligned state, in which case the external assistance was needed. A more elaborate algorithm together with a proper modeling of all physical effects could be able to bring the reconfiguration to true autonomy. However, the Roombots robotic platform in its current form has rather reached a limit in terms of complexity and weight, making it difficult to investigate such research. Further hardware validation would thus likely require a new platform which could be part of future research in the topic of SRMRs.

Another major future work is the integration of additional structural passive parts. In the full Roombots vision, furniture consists not only of RB modules but also of lightweight structural parts that will help to reduce the weight of the formations and allow the creation of larger pieces of furniture such as a table. The addition of such passive parts requires a close collaboration of RB modules to position them appropriately in a structure for which new reconfiguration algorithms will have to be developed and tested, such as e.g. in [17].

By operating the upgraded Roombots design at the limitations of the platform through successfully running the many different sub-tasks, we could identify the following additional hardware and control challenges: (i) exploration of machine vision capabilities (such as e.g. in visual servoing for autonomous docking) to allow modules to perceive their environment, (ii) autonomous adaptation of morphology according to the task, either with visual feedback and/or other means, (iii) exploring safe human-module interaction for a safe integration of modular robots into our living space, (iv) improved autonomy and self-reconfiguration performance through deeper research on AI methods, potentially with a new design of an SRMR.

The continuous development of SRMRs gives us insights into current challenges and limitations of the general concept of reconfigurable systems. In the long term, we could imagine the technology being used in many more applications, e.g. reconfigurable factory lines where it could be used both for reducing factory space and manufacture costs through machine reconfiguration, or futuristic visions of reconfigurable satellites, exploration space robots or even space stations where autonomous reconfiguration systems could prove invaluable for their versatility and robustness.

## 1.6 Conclusion: state of Roombots

In this chapter, we presented the capabilities of the latest generation of our self-reconfigurable modular robotic system “Roombots”. We outlined five key tasks that we consider relevant to the vision of modular robotics for adaptive and assistive furniture and were able to successfully demonstrate various sub-tasks in hardware. This required significant design improvements - especially in the mechanics of the modules - which are described in detail.

Concerning the demonstrations, modules performed a large-scale self-reconfiguration into a chair and provided mobility capabilities - such as following and evading a patient and overcoming obstacles - to off-the-shelf pieces of furniture by being used similarly to omnidirectional wheels. Specialized gripper modules were used to demonstrate basic manipulation capabilities such as picking up a pen, and could show the passing of objects between two modules. Interaction functionalities with colored LED and with the use of a Kinect depth camera were presented and we discussed the development of an easy-to-use Graphical User Interface (GUI) to control and monitor groups of modules.

Much of the presented results are of a qualitative nature with a set of Roombots modules achieving a defined sub-task. Our goal in this work was not to optimize a single task leading to quantitative data to analyze, but to show the versatility of our SRMR system in many different scenarios. We were interested in the capabilities as well as limitations of the current iteration of our system to build new experience in hardware experiments that can be used for future development of this or another SRMR, creating a benchmark of demonstrations that other systems can compare to. Even though some of the demonstrations were partly controlled by a human operator, autonomy is only one aspect of SRMRs and all of the presented demonstrations have been crucial milestones for this project.

While the majority of the presented demonstrations is focused on adaptive and assistive furniture, the tasks in general share the main challenges present in generic SRMR functionalities in mechanics (connection, disconnection, movement, alignment), electronics (autonomy, communication, sensors), software (control, computation, robustness, safety) and interaction (user interface, user feedback). Roombots as a system presents one approach in tackling these various and interdisciplinary challenges, which could inspire other systems with the solutions described here, and we hope that this work stimulates the general field of modular robots.

As for the future of the Roombots project, we envision the design and integration of lightweight passive, structural parts that can be used in conjunction with active RB modules to form larger furniture for our everyday environment. New collaboration algorithms (i.e. adapting the existing control framework or creating a new distributed control framework) will need to be developed, especially regarding safety when interacting with modules, coming one step closer to the integration of such robotic systems into our living space.

## 1.7 Acknowledgments

We gratefully acknowledge the help of Ahmet Safa Öztürk, Stéphane Bussier, Quentin Golay and Théo-Tim Denisart for their contribution to the Roombots project. Special thanks to Jérémy Blatter for the development of the GUI. Further, we are enormously thankful to François

Longchamp for his technical support in the design of the modules.

This project was funded by the Swiss National Science Foundation (Project 153299) and the Fundação para a Ciência e Tecnologia (FCT) agency of Ministry for Education and Science of Portugal (PD/BD/105781/2014).

# Part II

# Mode-switch in hardware: jamming of granular media

# Topic of Part II

## Functionalities in jamming systems

The development of the Universal Gripper for manipulation tasks for the Roombots system revealed that jamming of granular media can be a viable strategy for mechanical stiffness variability due to the two distinct states of such materials: granular media behaves fluid-like and is soft in free space, and behaves solid-like and is hard in confined space. Even though this state-switch already allows for a variety of gripping tasks, the method lacks controllability. On the one hand, the state-switch is somewhat binary, transferring the system from the non-jammed state into the jammed state without much leeway in between. On the other hand, the final stiffness of the solid state (given by the mechanical properties of the ground coffee) is rather hard, potentially too hard for further applications. Previous research on this subject introduced a specially shaped compliant granule that enabled a greater stiffness control in jamming. These new properties allow new applications that will be explored in the following chapters.

In all jamming systems, the state-switch characteristic corresponds exactly to a mode-switch in hardware as described in the introduction through the change in the dynamic response, and thus it can be used to achieve different functionalities. In the case of the Universal Gripper, these functionalities are of the binary form of “shape adaptation” and “force transmission”. With the improved controllability in jamming, we can also target states in between these extremes. In Chapt. 2, we look at the more general functionalities from “free movement” to “freeze movement” and everything in between. We developed JammJoint, a wearable joint support device that uses these functionalities to allow free joint movement, joint stiffening or joint freezing. In Chapt. 3, we reconsider the functionalities of the Universal Gripper “shape adaptation” and “force transmission” - now in their extended, compliant form - to create end effectors that allow climbing in a particular, uneven terrain. Chapt. 4 then uses a much more rapid version of the same concept to create a novel foot for legged locomotion that is able to switch its functionality from “impact damping” (with shape adaptation as a side effect) to “force transmission” during the stance phase of a quadruped robot, which is shown to have a significant effect on rough terrain locomotion.

## Variable stiffness to change mechanical properties

In the case where energy efficiency is a crucial design feature of a robot or a robot is required to safely interact with humans, new compliant actuator designs are better suited than classical, stiff robot designs which typically excel in pick-and-place applications. Such compliant actuators have the ability to reduce impact forces, store and release energy through their compliance, and add safety. Thus, these actuators are the preferred choice in various applications such as rehabilitation, prostheses, manipulation, bio-inspired robotics and wearable robotics [58]. However, the compliance in the system often needs to be well-tuned to a specific task. If a robot is to perform a variety of tasks, a corresponding prescription of different compliance settings is required, giving rise to variable stiffness mechanisms.

The design of variable stiffness manipulators and joints is an active field and many prototypes have been developed in the past. Some of them use pretensioning of a spring to stiffen a joint [102]. A review of variable stiffness actuators (VSA) that have an integrated compliant element can be found in [177]. For highly articulated robots (e.g. [144]), the stiffness usually cannot be changed unless a compliant element is integrated in the design [169]. This essentially represents a series elastic actuator (SEA) which has the ability to adjust its stiffness by changing the elastic element [136]. For continuum robots [133], tightening tendons [164] and Shape Memory Polymers (SMP) [44] are used to vary the stiffness. Magneto-rheological dampers can adjust their damping properties which in turn also has an effect on their spring stiffness (e.g. [57]). This can be also considered as a variable stiffness joint, although rather as a side effect.

## Jamming of granular media

Recently, the field of granular jamming is receiving more attention since it offers stiffness variability through state switching, i.e. a transition from a soft to a hard state. In an open area, a granular medium (e.g. sand) behaves fluid-like where the granules can freely slide around each other. By confining the space around the granules, the inter-particle friction increases drastically, transforming the pack of granules into a solid-like state, resulting in a hard structure [96]. Even though the concept has been known for many years, it regained popularity through the development of the Universal Gripper [26]. It uses ground coffee enclosed in a flexible membrane (a latex balloon) to create a ball that could grip an impressive variety of objects by letting it adapt to the shape of the object in the fluid state and using the solid state to apply a sufficient gripping force.

Switching between the two states of the Universal Gripper means switching between two different sets of spring and damping characteristics. The soft state possesses shape adaptation capabilities and strong damping properties, whereas the solid state is stiffer and thus better suited to transmit forces. Interestingly, but not surprisingly, it is the material of the granules and their geometrical shape that define the medium's overall mechanical properties, in particular the spring and damping characteristics. In an experiment involving a latex tube filled with hard granules, [77] demonstrated that this system is able to significantly change the stiffness in relation to the internal pressure. In a similar experiment with a silicone membrane filled with hard granules in [10], it was demonstrated that different levels of vacuum can change the damping coefficient of an oscillating beam. Though dealing with slightly different conditions, the field of granular dampers is related to this property (e.g. in [66],[146],[120]).

## Controllable variable stiffness with compliant granules

The research in [79] presents an in-depth analysis of the bending stiffness variability of a finger-like structure. An experimental characterization is performed because even though considerable effort has been put into deriving mathematical models to describe the reaction of granular material to external load, they most often concern spherical or elliptical granules (both rigid and soft, e.g. [30, 161, 166]), but are not yet applicable to other geometric shapes. In contrast, [79] used compliant, cubic rubber granules which resulted in an approximately linear dependence of the bending stiffness to the vacuum applied, which deviates from the often non-linear state transition observed with other granules. As stiffness and damping are coupled in jamming, this also applies to the damping properties.

This translates to a better and easier control over the stiffness and damping of a jamming membrane, opening up the method for potential applications where a specific stiffness or damping characteristic is required. Together with the aim of creating mobile and autonomous robots, Part II presents three such applications that use the same three key ingredients for this “compliant mobile jamming”: a small-scale vacuum pump that can be powered by a battery to induce jamming, a latex balloon as the flexible membrane, and cubic rubber granules with a side length of 4 mm (Neukadur ProtoFlex HS 75) as granules.

# 2 JammJoint: mobile jamming for variable stiffness

The evacuation of the flexible membrane in jamming is usually achieved by a vacuum pump. Depending on the size and geometry of the granules, this pump needs to be of significant strength and therefore size and weight which often results in a bulky system. Due to the development of the Universal Gripper for Roombots and specifically the integration of the required mechatronic components into a limited space, we were able to demonstrate that mobile jamming can be used as a new approach for stiffness variability. This chapter shows the development of the JammJoint, a variable stiffness device for wearable joint support, enabled by using a miniature vacuum pump and small-scale solenoid valves together with a wearable silicone sleeve. The functionalities that this device can exhibit range from "free movement" to "freeze movement" and everything in between.

**Reference publication**

This chapter is based on ***Simon Hauser***, *Matthew Robertson, Auke Ijspeert, and Jamie Paik. "Jammjoint: A variable stiffness device based on granular jamming for wearable joint support." IEEE Robotics and Automation Letters 2, no. 2 (2017): 849-855.*

This work was created in collaboration with Jamie Paik's Reconfigurable Robotics Laboratory (RRL).

**My original contributions**

- Development of concept
- Manufacturing of device
- Design and performing of experiments
- Analysis of results
- Writing of manuscript

## 2.1 Inspiration: Wearable joint support device

In [77], the proposition of a variable stiffness joint based on granular jamming of compliant granules can be found. Their idea was to fix an array of finger-like membranes around a joint and vary the stiffness by controlling the pressure in these columns. The joint can either be active (actuated by inflating the columns) or passive (the columns only vary their stiffness but do not provide actuation).

This concept was the inspiration for creating the proposed JammJoint, which is designed to support and stabilize human joints during post-injury rehabilitation or for daily assistance of chronic biomechanical impairment. Similar to existing orthotic devices for this purpose, this device provides constraints to joint motion in selected directions to reduce unwanted loading and motion, while allowing free or low impedance motion in other directions for maintaining principal joint functionality. In general, most existing devices are only uni-axial, providing support and restriction in all but one direction, or they offer only fixed or manually adjustable levels of supporting stiffness. The JammJoint enables automated tuning of both the direction and magnitude of joint axis support by applying distributed, independently controlled variable stiffness elements in parallel with the biological joint. The variable stiffness is enabled by vacuum induced jamming of compliant granules. The novelty of the design is that the structural part of the device doubles as the enclosing membrane to enable the jamming, which also directly facilitates its wearability around a joint. Additionally, in contrast to other applications of granular jamming where a large, powerful external vacuum pump is required, JammJoint uses a miniature vacuum pump directly integrated in the device. This makes the system unique in the field of granular jamming as it is wearable and - adding a battery to power the electronics - portable and autonomous. The complete device can be seen in Fig. 2.1 (except for the required smartphone for controlling the device) and each separate part is described in detail below.

## 2.2 Description of the JammJoint device

**Silicone sleeve:** The sleeve is made out of highly stretchable silicone (Ecoflex 00-30) and consists of three parts. The main section is cylindrical with four evenly distributed hollow columns integrated along the cylinder, with a total height of 210 mm. These columns are coupled together by tubes and share the same pressure. The diameter of the hollow cavity in the columns is 20 mm. On each side of the cylinder, hollow rings are attached, also with a hollow cavity of 20 mm and coupled together. Both rings and the hollow sections of the cylinder are filled with cubic rubber granules with a side length of 4 mm (Neukadur ProtoFlex HS 75). Schematics of the sleeve are depicted in Fig. 2.2. The figure displays the active controllable 2 DoF of the system: 2 rings and 4 columns are independently controlled.

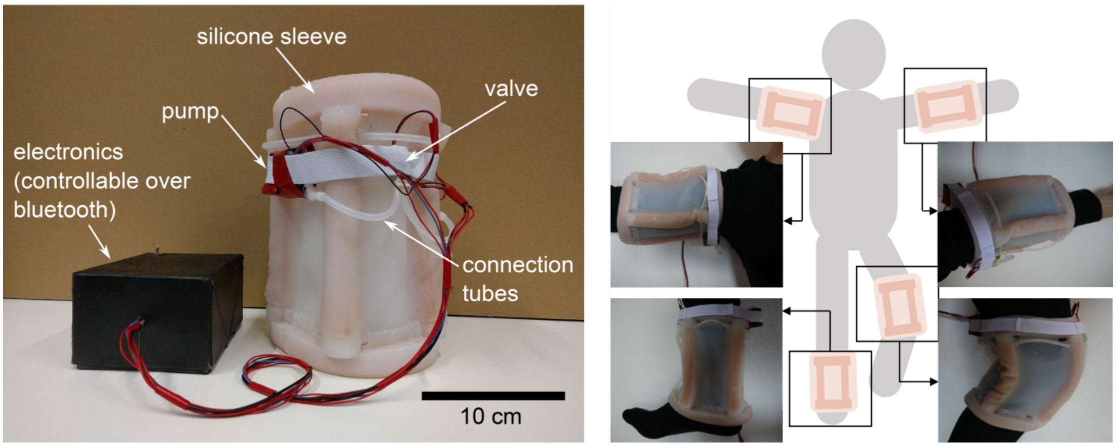

Figure 2.1 – The JammJoint device. Left: the electronic box on the left contains a microcontroller, bluetooth module and battery. A miniature pump, small-scale valves and connection tubes are mounted directly on the silicone sleeve. The sleeve with pump and valves weighs 700 g, and the electronic box is 250 g of which the battery weights 100 g. Right: application examples of the JammJoint device on different human joints.

**Pump and valves:** A miniature pump (Schwarzer SP 100 EC-DU, serial configuration) creates a vacuum up to 800 mbar below atmospheric pressure inside the rings and columns (200 mbar absolute pressure). The airflow of the pump is controlled with three miniature solenoid valves (SMC S070C-SAG-32) and the level of vacuum is measured with a single pressure sensor (Honeywell 015PAAA5).

**Electronics and bluetooth interface:** A microcontroller (Arduino Nano V3.0) controls the pump, valves and pressure sensor. Additionally, a bluetooth module (JY-MCU) is attached to the microcontroller, allowing a bluetooth serial communication. The electronics are powered by a 12 V LiPo battery (Conrad energy BEC 11.1V 1300 mAh 12C). A bluetooth enabled smartphone can establish a connection to the bluetooth module. For this work, the free app BlueTerm2[1] has been used. The device is controlled with a few simple commands: “r” and “c” direct the airflow either to the rings or columns, the numbers 1-8 are used to set the pressure in the respective section from 900 mbar to 200 mbar absolute pressure and the number 0 sets a section to atmospheric pressure. The complete system can be seen in Fig. 2.3. The smartphone is the only external hardware; JammJoint is fully autonomous otherwise.

## 2.3 Full-device characterization

### 2.3.1 Setup for stiffness measurements of the full device

The objective of the experimental measurement of the complete device is to obtain the range of its stiffness variability. Since the device is designed for use on human joints, these joints are

---

[1] available for Android in Google Play store

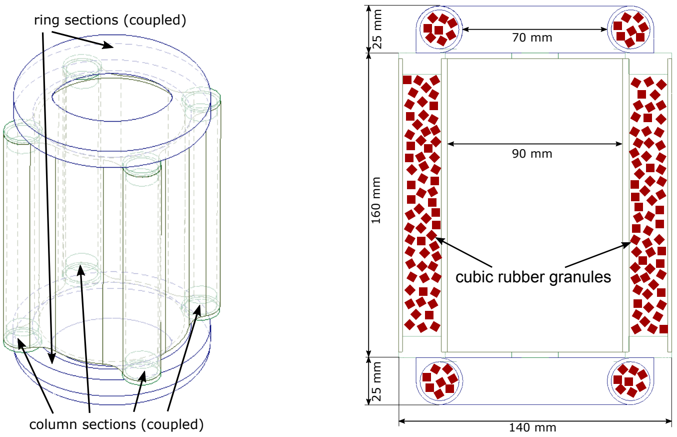
ring sections (coupled)
column sections (coupled)
25 mm
70 mm
90 mm
160 mm
cubic rubber granules
25 mm
140 mm

Figure 2.2 – Silicone sleeve. Left: The complete sleeve. Two hollow rings (blue; coupled to share the same pressure) are attached at each end of a cylinder with four integrated, hollow columns (green; coupled to share the same pressure). Right: Cross-section of the sleeve. The hollow sections in the rings and columns are filled with cubic rubber granules.

approximated by ball joints for the purpose of this investigation. A ball joint has 3 degrees of freedom: 2 rotations around the joint in 2 perpendicular planes (henceforth called “bending”) and 1 rotation around the main axis of the joint (henceforth called “torsion”). Whereas the torsion movement is symmetric in the case of the device, bending is directional, depending on the orientation of the bending plane to the columns. For these experiments, only bending where the bending plane is in between two columns is analyzed (see Fig. 2.4a). This is expected to more evenly distribute the bending torques as each column is engaged in a similar way, to simplify both quantitative and qualitative results. The case where the bending axis coincides with a column is not studied, as one column would receive a large compressive force and one column a large strain respectively, compared to the columns located outside the bending plane. This type of loading is likely to yield unique stiffness characteristics, including enhanced buckling. However this is considered to only be important for a full quantification of the device’s stiffness and is beyond the intention of this study.

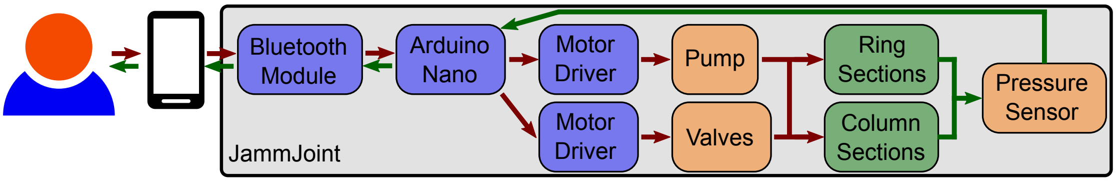
Bluetooth Module
Arduino Nano
Motor Driver
Pump
Ring Sections
Pressure Sensor
Motor Driver
Valves
Column Sections
JammJoint

Figure 2.3 – Schematics of the full JammJoint system. A user (on the left) inputs the desired commands into a smartphone which communicates with a bluetooth module attached to the Arduino microcontroller. It controls the pump and valves over motor the drivers, changing the pressure level inside the ring and column sections. The pressure is measured by a sensor and fed back to the microcontroller, which also shares this information with the user over the smartphone interface.

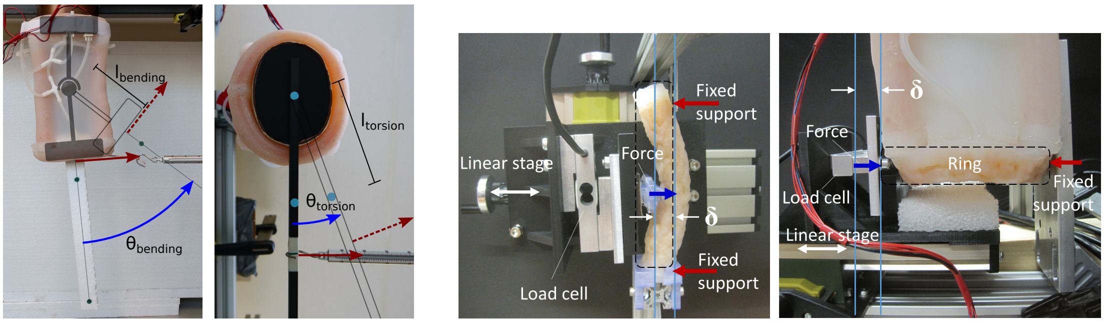

(a) Full-device characterization. The red arrows show the direction of the force at resting position; the silhouette and the red dashed arrows show the orientation of the lever and the direction of the force at the rotation angle $\theta_{bending/torsion}$ (blue arrow). Left: Side view of the bending setup. The mechanics of the balljoint is overlaid in gray. Right: Bottom view of the torsion setup.

(b) Sub-component characterization. Left: A 3-point bending setup is used apply a force at the centerpoint of a single variable stiffness column. A single-axis load cell records the force applied to the column. Right: The same apparatus is reconfigured to apply a force to the variable stiffness ring segment. In both experiments a linear stage is manually advanced and the deflection, $\delta$, is recorded at 2 millimeter intervals from 0-20 mm, equal to the width or diameter of a single column.

Figure 2.4 – Setups for stiffness characterization of JammJoint and sub-components.

It is important to note that in a ball joint, all possible movements can be superposed. This is also achievable with the device. The two rings only serve as the way of fixing the device on the respective joint through passive adaptation and solidifying. Only the level of vacuum in the columns determines the final stiffness, therefore coupling both bending and torsional stiffness. The experimental procedure for the experiments is defined as follows: (i) fit the device around the joint, (ii) pair the JammJoint with a smartphone, (iii) solidify the rings by setting the pressure inside the rings to the lowest value (200 mbar absolute pressure), (iv) increase the level of vacuum inside the columns in steps of 100 mbar from atmospheric pressure (approx. 1000 mbar absolute pressure) to 200 mbar absolute pressure by selecting the desired pressure on the smartphone and (v) measure the torque for different angles of rotation. Fig. 2.4a shows the experimental setup. A camera takes pictures of the device and a force meter. Two colored dots allow the calculation of the rotation angle through image analysis and the force meter provides the applied torque, given the length of the lever.

## 2.3.2 Bending and torsion in the full device

### Experiments

**Bending torque:** For measuring the bending torque, the device is placed over a ball joint where torsion is restricted. The two rings are both fit over circular disks, each with the height of the ring (25 mm). The joint is located exactly in the middle of the device, resulting in a lever length $l_{bending}$ of 105 mm. The upper part of the joint is fixed to a table. Each configuration is tested 3 times. A force is applied perpendicularly to the lower part of the joint until the rotation angle reaches approximately 45 deg. The force then is slowly released back to zero to measure any potential hysteresis in the rotation angle caused by the displacement of granules. This leads to a different resting angle because the displacement of granules generates plastic deformation of the device. After every test, the columns therefore are set to atmospheric pressure to allow a manual “reset” of the position of the granules inside the columns. Although this only considers the most ideal loading case and does not represent real operation conditions where a reset would not take place (and thus hysteresis effects would occur), preventing the rearrangement of granules will be further discussed in section 2.6. Effects caused by the viscoelacity of the silicone have been neglected as the response time of silicone is roughly between 50 ms and 200 ms [139]. This is assumed to be one order of magnitude faster than the expected movement of a human joint. The results of this series are normalized to the initial resting angle of the respective test (meaning that initially, zero applied force results in zero rotation angle).

**Torsion torque:** For measuring the torsion torque, the balljoint is removed, keeping only the upper circular disk. To avoid slipping, the upper part of the device is additionally secured and the lower circular disk is replaced by an ellipsoid. This change is assumed to have only a minor influence on the measurements. The ellipsoid has a lever attached (lever length $l_{torsion}$ is 150 mm) where the force is applied in a rotational manner, twisting the device. The number of trials (3) and measurement methods are kept the same as in the previous experiments.

### Results

**JammJoint performance in bending:** Fig. 2.5a shows the results of the experiments performed in the bending series. Each curve is calculated with the interpolated average of the three trials per vacuum level and for each curve, the stretching phase (solid), relaxation phase (gray) and the maximum torque (red cross) is indicated. From these curves, the increase in torque needed for a certain rotation angle is clearly visible. However, especially in higher vacuum, a buckling of the columns under compression can be observed, leading to a decrease of torque with larger angles. The buckling also plastically deforms the columns by rearranging the position of granules, which in turn changes the loading conditions for the relaxation phase. This can be seen from the increase in resting angles after relaxation where a hysteresis of several degrees starts to form. As the resting angle gets shifted, the respective torque at certain deflection values is lower in the relaxation phase compared to the stretching phase. Resetting the granules after each trial ensured that this hysteresis would not transfer into the next trial.

**JammJoint performance in torsion:** In Fig. 2.5b, the results of the torsion experiments are shown. Similar to Fig. 2.5a, the interpolated average is shown for the stretching (solid) and relaxation phase (gray) together with the maximum torque (red crosses). The increase of the required torque is not as pronounced as in the case of bending but nevertheless observable. In contrast to the previous experiments, no buckling occurs and a hysteresis in resting angles is less noticeable.

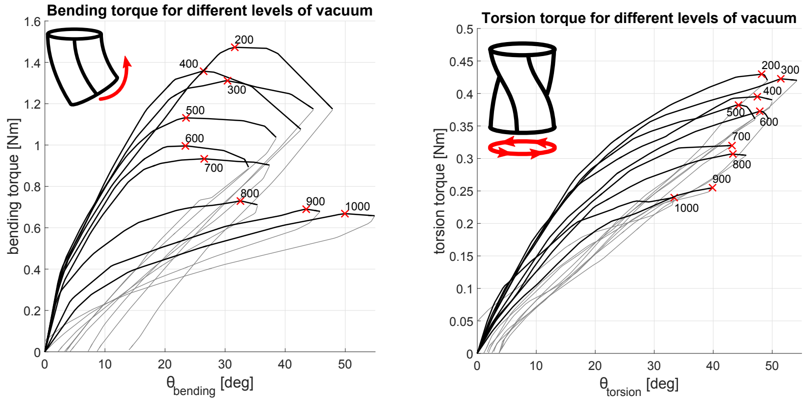

(a) Bending angle versus bending torque; buckling and hysteresis effect observable.

(b) Torsion angle versus torsion torque.

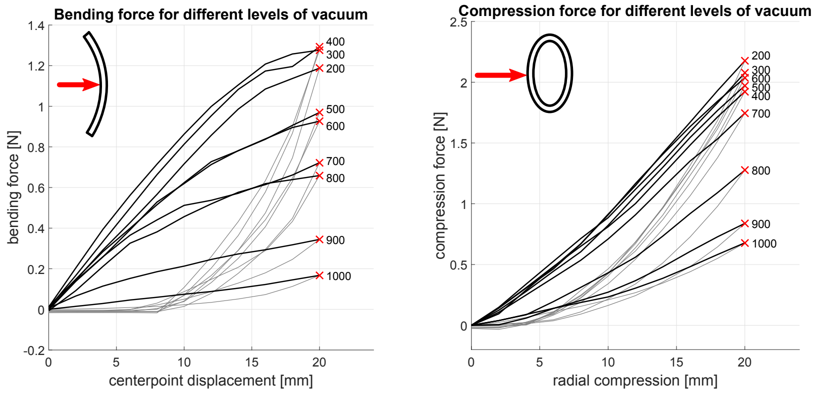

(c) Force versus column deflection; hysteresis effect observable.

(d) Force versus ring deflection.

Figure 2.5 – Characterization experiments. Red cross: maximum torque per curve with the level of vacuum in mbar; Solid: measurements during stretching; Gray: measurements during relaxation. In all experiments, increasing the level of vacuum results in an increased reaction torque/force.

## 2.4 Sub-component characterization

### 2.4.1 Setup for stiffness measurements of the sub-components

Additionally, experimental measurements are taken to individually characterize the change in stiffness of the sub-components of the wearable device: the rings and the columns. The setup for each characterization test can be seen in Fig. 2.4b.

### 2.4.2 Stiffness of the column and ring sub-components

#### Experiments

**Column characterization:** A three point bending setup is used to apply a linear force at the center of a single column segment supported at the ends, while the applied force in [N] is recorded through a displacement range in [mm] and different pressures.

**Ring characterization:** Similarly to the column measurements, the stiffness profile of a single ring segment is measured across a range of displacements and pressures.

#### Results

**Stiffness variation of a single column:** The results from characterization of a single column at different pressures is shown in Fig. 2.5c. While the force and displacement measurements can be used to estimate the true angular bending stiffness of a column following analytic beam bending models, only the linear transverse stiffness of the column as directly tested is reported to illustrate the qualitative effect of pressure variation on column stiffness. Each curve shown represents the average of three separate trials taken for each pressure. The curves show a nearly linear stiffness relationship during stretching with a maximum force at the maximum deflection. There is also a large hysteresis observed, resulting from plastic deformation at high vacuum pressures.

**Stiffness variation of a ring:** The stiffness profile generated from the ring sub-component measurements can be seen in Fig. 2.5d. The compressive force applied across the ring is used to calculate the overall radial stiffness of the structure. The radial stiffness of the ring can be seen to be very nearly linear, with minimal plastic deformation at any pressure, and hence minimal hysteresis upon unloading.

## 2.5 Properties of JammJoint

### 2.5.1 Change of spring stiffness

The results of Fig. 2.5a and 2.5b are summarized in Fig. 2.6a where the change of the respective spring stiffness is shown. For each curve in the previous experiments, the maxima (red crosses) are connected to the origin with a straight line. The slope of each line can be regarded as a hypothetical linear spring stiffness with $D_{\text{bending/torsion}} = \Delta\text{torque}/\Delta\text{angle}$ where $\Delta$torque is the maximal torque in [Nm], $\Delta$angle the angle in [deg] corresponding to the maximal torque and $D_{\text{bending/torsion}}$ the spring stiffness coefficient in [Nm/deg]. Fig. 2.6a shows these spring stiffnesses for bending and torsion for the different levels of vacuum with the error bars calculated from the standard deviation of the interpolated average at the maxima. For bending, the increase in the spring stiffness is significant: the experiments show an almost fourfold increase (from 0.0134 Nm/deg to 0.0514 Nm/deg) with the maximum stiffness value being

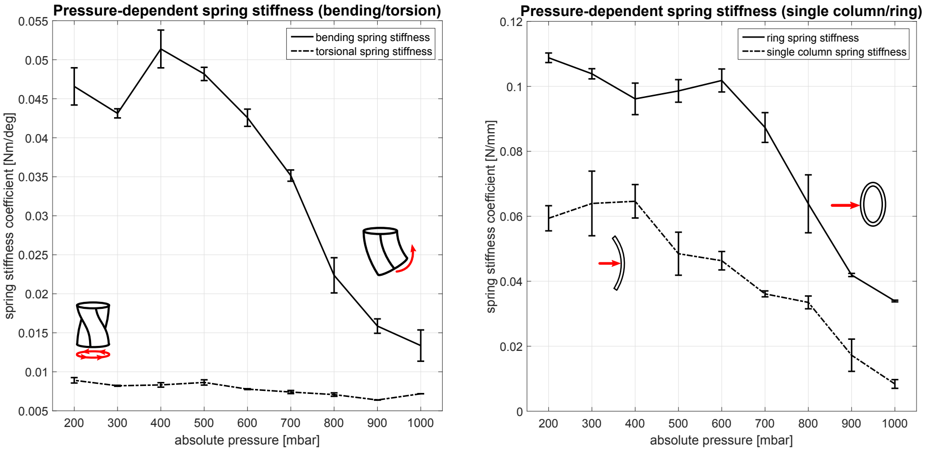

(a) Spring stiffness increase depending on the level of vacuum for bending and torsion.

(b) Spring stiffness increase depending on the level of vacuum for a single column and ring sub-component.

Figure 2.6 – Spring stiffness increase. The values of the curves are calculated by approximating the spring behavior of each experiment with a linear spring stiffness coefficient from the origin to the maximal torque from Fig. 2.5a and Fig. 2.5b. for bending and torsion, and from Fig. 2.5c and Fig. 2.5d for the single column and ring sub-components.

reached at 400 mbar. For torsion, the difference is much smaller, with an increase of torsional spring stiffness of 40% (from 0.0064 Nm/deg to 0.0089 Nm/deg). Even though these results are obtained by simple linear approximations of the nonlinear spring stiffness coefficients where the true “instantaneous” stiffness is angle dependent, the goal of this study was not to precisely define the stiffness (possibly with the help of models) but rather to give an overview of what qualitative overall stiffness change the system can achieve.

Likewise, the results of Fig. 2.5c and Fig. 2.5d are summarized in Fig. 2.6b. For each curve in the respective experiments, the maxima (red crosses) are again connected to the origin with a straight line. The slope of each line is obtained as $D_{\mathrm{column/ring}} = \Delta\mathrm{force}/\Delta\mathrm{deflection}$ where Δforce is the maximal force in N, Δdeflection the distance in mm corresponding to the maximal force and $D_{\mathrm{column/ring}}$ the spring stiffness coefficient in N/mm. Error bars are calculated from the standard deviation of three measurements taken at each pressure level. Both trends for the column and ring show a significant change in stiffness for different pressures. The ring stiffness increases more than threefold from 0.0339 to 0.1088 N/mm following a pressure change from 1000 to 200 mbar. Over the same pressure range, the column stiffness changes from 0.0084 to 0.0646 N/mm; the maximum stiffness value is again observed at an intermediate pressure of 400 mbar. The maximum range indicates that an increase of stiffness over a factor of seven is possible.

Ideally, these changes in spring stiffness are linked to a change in intrinsic material properties. In the case of jamming, the applied level of pressure suggests that the pack of granules changes its Young's modulus $E$ which is closely related to the overall spring behavior. However, modeling the effect of jamming on the Young's modulus $E$ has not been investigated as such characterizations usually require unidirectional loading of the substrate (typically compression and tension). The performed experiments were not specifically designed for such cases. Therefore, instead of a change in intrinsic material properties, only the simple comparison of these changes to a linear spring stiffness are presented here. It is the subject of further research to model inter-particle reactions and define which experiments qualify for material property characterizations in different loading scenarios.

### 2.5.2 Additional modes

Firstly, besides a coupled bending-torsion-mode, an additional bending-only mode is available. This can be achieved by fitting one ring around the base of a joint and only loosely fitting the second ring (by enlarging it to a slightly larger diameter than the other joint base). This results in the device being held in place by the fit ring but leaving the torsion rotation of the joint unrestricted. The bending stiffness still can be adjusted in the same manner as in the normal mode.

Secondly, the initial orientation of the device can be freely chosen and does not need to be known beforehand. For the purpose of the performed experiments, the initial orientation was chosen to be straight. However, with the rings solidified but the columns under atmospheric pressure, the joint can easily be moved into any desired orientation where it can be fixed by solidifying the columns. This process is reversible and can be repeated whenever required.

### 2.5.3 Passive adaptability, safety and operation time

The soft silicone of the sleeve and the nature of the granules allow the JammJoint to passively adapt to the wearer's anatomy. Moreover, the rings and cylinder can easily be stretched to twice their circumference, making the device applicable to different joints. This also applies to joint shapes which are not circular where the rings conform around them. Once fit, after solidifying the rings to attach the device to the joint, the rings keep their conformed shape without further power. Additionally, thanks to the soft silicone, the solidified rings and columns still possess a certain softness, allowing a certain deformation of the joint e.g. through moving muscles or blood flow. The examples in Fig. 2.1 depict the application of the device on elbow, shoulder, ankle and knee joints.

Since the device - except the miniature pump and valves - is entirely made out of soft materials, the risk of injury for the user is greatly diminished. Moreover, since the functionality of the device relies on successfully maintaining a vacuum, puncturing any part of the silicone sleeve simply results in a slow inflation of the section to atmospheric pressure. The device therefore loses its functionality without harming a potential user (as opposing to e.g. a technology based on inflation where puncturing a membrane might result in explosion of the section). These properties are promising for the usage of such a device as joint support.

Concerning the operation time, most of the battery power is consumed when the pump is evacuating. Even though the evacuation time is somewhat slow (roughly 20 seconds) as a result of the usage of a miniature vacuum pump with low airflow, it has been assumed that the application of joint assistance does not require a rapid change in stiffness. On the contrary, the advantage of the pump to be powerful but portable was regarded as being more important. It is important to notice that a set pressure level in the sections is held without power by the off-position of the valves (assuming the sections are airtight; the current device inflates at around 25 mbar per minute due to sealing imperfections). Thus, the operation time depends almost only on the number of evacuation cycles the pump is able to perform with one battery charge. All testing and experiments were performed with one single charge of the used LiPo-battery, performing roughly 150 evacuation cycles without completely discharging the battery.

## 2.6 Conclusion and Future Work

In this work, a joint assistance device based on the jamming of granular media is presented. Cubic rubber granules are filled into two separate hollow sections of a silicone sleeve, rings and columns. These sections can independently be evacuated to a desired level of vacuum by a powerful miniature vacuum pump directly integrated into the device. A small LiPo-battery powers the electronics and the microcontroller with an attached bluetooth module. This enables the system to communicate with, for example, a bluetooth enabled smartphone, making it portable and autonomous.

The level of vacuum inside the sections varies the stiffness property of the device, measured for two different modes: bending stiffness and torsional stiffness. Decreasing the pressure from 1000 mbar to 200 mbar absolute pressure results in an almost fourfold increase in bending stiffness and a 40% increase in torsional stiffness. Additionally, besides the normal mode of a coupled bending-torsional stiffness change, a bending-only mode is available. Individually, the subsections of the wearable device are shown to have high versatility with a large range of stiffness adjustment available (up to seven times stiffer) for alternate deformation modes, including simply supported bending and radial compression. Further, due to the jamming of granular media, the device can be moved in any orientation when the sections are under atmospheric pressure and fixed in that orientation by solidifying (evacuating) the sections. The pressure level then can be kept without additional power. And lastly, the highly stretchable silicone in combination with rubber granules creates a safe to use, adaptable, versatile device which can be applied to different joint sizes and shapes.

For future work, different directions could be followed. The mechanical design of the sleeve could be changed to include more columns to make their distribution more uniform for bending. If required, the columns could be separated from each other to control the vacuum in each column independently (contrary to the current design where all the columns are connected together to share the same pressure). Although this would require more valves, the independent control of multiple columns in parallel would also increase the robustness and reliability of the total system [132]. Designing custom electronics would allow for a full integration into the sleeve, eliminating the need for additional cables. A different design to increase the torsional stiffness could be tested. Alternate mechanical configurations with different combinations of sub-component elements (columns and rings) might also be used to create entirely new forms of a variable stiffness wearable device.

Further, the materials used for the sleeve and granules can be subject to future studies. While the soft silicone enables the jamming of the granules, it also adds much softness to the system even when the sections are under the highest vacuum. If necessary, a harder material or a different combination of materials could further increase the overall stiffness and the achievable change in both bending and torsional stiffness. Although it has not been tested here, the method of jamming does not interfere with actuation through inflation. Thus, with the integration of additional valves only, the same system can be used to provide active actuation. The design and choice of materials might change if inflation is also considered. One issue in the current design is that if the columns are inflated, the granules collect on the bottom of the enlarged cavity. Since jamming assumes uniformly distributed granules, this makes further jamming impossible. Thus, a way of preventing such an undesirable rearrangement in the enlarged volume has to be developed. This could also enable automatic resetting of the granules (e.g. under atmospheric pressure) to diminish hysteresis effects, as described in section 2.3.2.

Lastly, further experiments are needed to provide the basis to model changes in intrinsic material properties such as Young's modulus $E$. Such experiments will be discussed in the following chapter 3 where jamming of compliant granules is used in end effectors that require more specific stiffness characteristics.

# 3 Climbing with compliant grippers

We now return to the usage of jamming as a gripping method as in the Universal Gripper. It possesses a soft state that has the capability to be used for shape adaptation, and a solid state that is more suitable for force transmission. Due to the development of a mobile jamming system in the previous chapter, we were interested in using compliant Universal Grippers in a mobile, untethered robot system to perform a particular type of locomotion where gripping is implicitly necessary: climbing. This chapter describes the development of a robot that climbs vertical shafts with non-trivial wall structures. As will be shown, the additional features due to the usage of the cubic compliant granules play a crucial role in offloading complex contact computation from the controller unit to the mechanics of jamming membranes (also referred to as *morphological computation*).

**Reference publication**

This chapter is based on ***Simon Hauser****, Mehmet Mutlu, Frédéric Freundler, and Auke Ijspeert. "Stiffness variability in jamming of compliant granules and a case study application in climbing vertical shafts." In 2018 IEEE International Conference on Robotics and Automation (ICRA), pp. 1559-1566. IEEE, 2018.*

**My original contributions**

- Development of concept
- Design of robot
- Design and performing of experiments
- Analysis of results
- Writing of manuscript

## 3.1 Inspiration: Legged climbing

The experiments around the stiffness variability of a finger-like structure in [79] have been performed to characterize the *bending* stiffness, however the method of granular jamming is not restricted only to such type of deformations. To provide a more complete characterization for multi-directional loading scenarios, in the first part of this Chapter we perform a similar set of experiments to characterize the variability of the *compressive* stiffness of the same material. As a proof-of-concept, we then apply the method of compliant granular jamming to a climbing task. Locomotion on walls is a challenging task that can be done with robotic systems in various ways depending on the environmental requirements. Two major factors in wall climbing are the surface material and smoothness (e.g. ferromagnetic, smooth, with grooves, etc.). A large literature on climbing robots is available (see e.g. [31] for a review). To make use of the characterized compression stiffness, shaft-climbing (considered equivalent to in-pipe climbing) has been chosen as the climbing challenge, as one of the available strategies for climbing is to push against the shaft walls to increase friction, inducing compression. The industrial in-pipe climbing robots have various forms and [135] gives different classes of in-pipe inspection robots as well as the design of a wheeled pipe inspection robot. Although legged robots are not widely used in pipe locomotion due to much higher power consumption compared to wheeled ones, [110] give a spider-inspired in-pipe robot to demonstrate the adaptation capabilities of legged robots. They mention that even though legs can be advantageous over wheels in complex pipe layouts including steps and sharp turns, the main challenge is the more complex control which usually involves advanced force and position control. Therefore, the last part of this work addresses the simplification of the control of legged shaft climbing by replacing the active force control with a mechanical impedance and focusing on simple open-loop movements.

As such, a robotic platform is designed with jamming membranes as end effectors. We chose vertical shaft climbing with both smooth and irregularly shaped walls as it involves both deformation modes of compression (end effector pushing against the shaft walls to increase friction) and bending (end effector counteracting gravitational force). Further, for the legged morphology, we chose a bio-inspired structure by relating the morphology to a humanoid shape.

## 3.2 Compressive stiffness characterization

### 3.2.1 Materials: Oblong latex membrane

A cylindrically shaped oblong latex membrane with a diameter of $d_0$ = 45 mm and a length of $l_0$ = 90 mm in its relaxed state (natural dimensions of the membrane) is filled with the cubic rubber granules. At the start of each experiment, described in subsection 3.2.2, the atmospheric pressure inside the membrane causes the granules to be in their fluid state where they would deform the required cylindrical shape. Thus, a way to ensure that the measurements are taken under roughly the same shape conditions had to be implemented. We used a hard, removable 3D-printed shell to form the required cylinder (Fig. 3.1 left). An airtight seal is formed by clamping the membrane between two disks, allowing control of the pressure inside the membrane and thus enable the jamming. A manual valve allowed for detaching the membrane from the pumping system, making it easier to place it into the

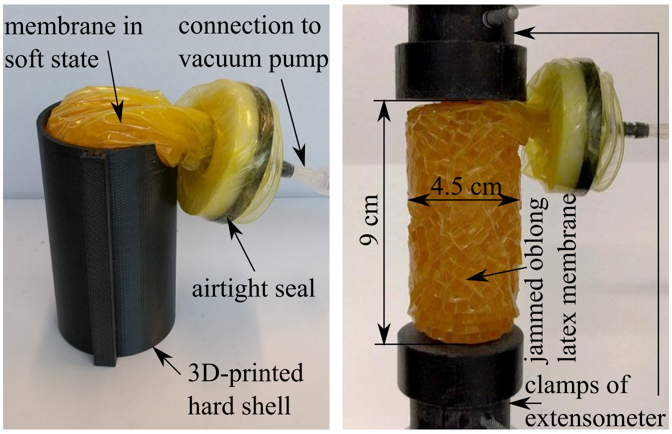

Figure 3.1 – Setup of the characterization experiments. Left: the oblong latex membrane is put into the cylindrical shape with the help of a 3D-printed hard shell. Right: after evacuating the membrane, the hard shell is removed and the membrane is put into the compression area of the extensometer.

compression area (Fig. 3.1 right). An extensometer (Instron AVE 2) logged the loading force and compressive deflection during a compression experiment.

### 3.2.2 Change of Young's modulus $E$

**Experiments**

Fig. 3.1 shows the setup of the compressive tests. Similar to the bending tests performed in [79], the goal was to relate the change in spring stiffness to the Young's modulus $E$. Even though $E$ usually is a defined intrinsic property of a material and itself does not change for either of the two materials of the end effector (latex membrane and rubber granules) under vacuum, we regarded the combination of the membrane and many granules as a *meta-material* where a change of the Young's modulus $E$ is feasible.

When deforming a granular material, the relative position of each granule can change, effectively rearranging granules into a different shape. In the case of the compression experiments, this is an unwanted effect as the meta-material and therefore the loading conditions would change during the test and would manifest in sudden discontinuities in the force-deflection profiles and plastic deformation. To avoid this, a maximal compressive deflection of 3 mm (strain $\epsilon = 3.33$ %) has been applied. It has been assumed that deflections of the membranes of the robot climber are comparable. The results in the next section may change if rearrangement of the granules and plastic deformation is expected. After shaping the membrane (see Fig. 3.1), the pressure inside the membrane then is set from atmospheric pressure (approximately 1000 mbar absolute pressure) to 0 mbar absolute pressure in steps of 100 mbar. The miniature pump used in the climber is able to lower the pressure to 200 mbar absolute pressure, hence an external, more powerful pump was used to achieve the two last pressure values of 100 mbar and 0 mbar. Each vacuum pressure configuration has been repeated five times with resetting the cylindrical membrane to atmospheric pressure between trials, and the deflection in [mm] and the applied load in [N] have been logged at 10 Hz.

### Results

Fig. 3.2 shows the results of the load experiments. On the left, the data gathered by the extensometer is depicted for the different levels of vacuum pressure. The black part represents the loading phase until the maximal compressive deflection of 3 mm, and the gray part represents the relaxation phase. Each curve is the average over the five trials performed. In this loading scenario, the maximal force also corresponds to the maximal deflection, which is marked by the red crosses, with each vacuum pressure level indicated next to its maximum. Overall, a very linear trend can be seen in the loading phase with a hysteresis observable for every curve, likely due to slight creep. This indicates that the meta-material has an almost linear force-deflection relationship for every vacuum pressure level, similar to the bending results in [79]. To relate these results to Young's modulus $E$, the following formula was used:

$$E = \frac{\sigma}{\epsilon} = \frac{F_{max}/A_0}{\Delta l/l_0} = \frac{F_{max} \cdot l_0}{\Delta l \cdot A_0} \tag{3.1}$$

where $E$ is the Young's modulus in [N/mm$^2$], $\sigma$ is the stress in [N/mm$^2$] and $\epsilon$ the strain, $F_{max}$ the maximal force in [N], $L_0$ the initial length of the cylinder in [mm], $\Delta l$ the length difference in [mm] to the initial length when the maximal load is experienced and $A_0$ the (constant) cross-sectional area in [mm$^2$]. With $d_0 = 2 \cdot r_0 = 45$ mm, $A_0$ is given by $A_0 = r_0^2 \cdot \pi = d_0^2 \cdot \pi/4 = 1'590.4$ mm$^2$, $l_0 = 90$ mm and $\Delta l = 3$ mm. Note that Eq. (3.1) only considers one single point in the force-deflection-graphs to calculate $E$ which implicitly assumes a linear force-deflection relationship. The linearity present was assumed to fulfill this criterion; separate linear approximations of each loading phase led to $R^2_{loading} > 0.93$ for all configurations. Thus, only the maximal force at the maximal deflection has been used for the calculations.

On the right in Fig. 3.2, the change of $E$ is displayed, calculated for each vacuum pressure level with error bars representing the standard deviation of the 5 trials of the maximal force at maximal deflection. For visibility reasons, $E$ has been converted to [MPa]. A linear model ($E_{lin} = -0.00166 \frac{MPa}{mbar} \cdot p_{vac} + 1.644$ MPa) is fit over the data with a correlation coefficient of $R^2 = 0.91$. This indicates that the stiffness change of the meta-material can fairly accurately be described by a linear function of the vacuum pressure level. Additionally, the change of $E$ achieved by the range of the vacuum pressure is considerable: $E$ of 0 mbar is 62 times higher than $E$ of 1000 mbar. It has to be noted that even though a strong vacuum of (almost) 0 mbar could be achieved, the meta-material under this vacuum is still far from the characteristics of a fully cast, solid cylinder with the same shape and material. Using the formula given in [103], a material with Shore A 75 results in $E \approx 6.5$ MPa, which is roughly 3.5 times higher than the measured $E$ of 1.9 MPa at 0 mbar. This likely can be explained by airless voids present in the jammed meta-material, stemming from the stochasticity of the orientation

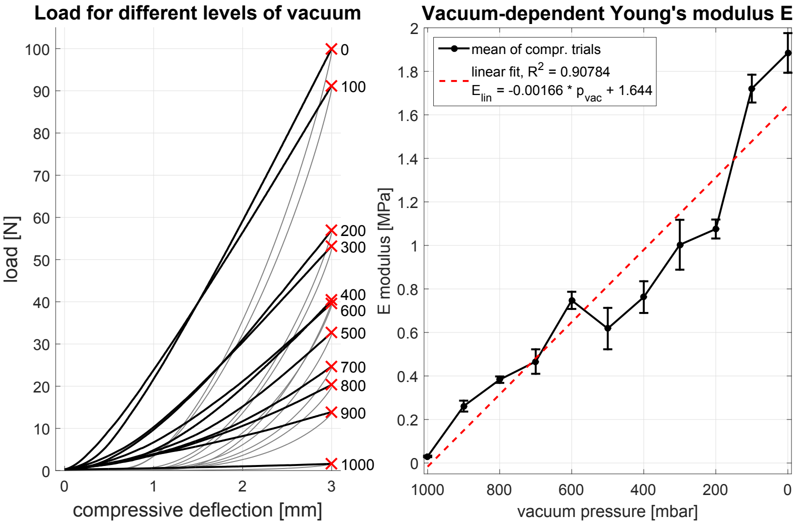

Figure 3.2 – Meta-material characterization. Left: Force versus deflection with loading phase (black), relaxation phase (gray) and the maximum force (red cross) indicated for each vacuum pressure level. Right: Change of Young's modulus $E$ over the vacuum pressure levels with a linear model approximation.

of the granules. In contrast to the fully cast solid material, these voids can be occupied by the meta-material through small reorientations of the granules during loading. This poses less resistance against the loading, resulting in the decrease of $E$. In practice, the highest $E$ achievable by the miniature vacuum pump is around 1 MPa at 200 mbar which, subjectively, feels fairly hard. The climbing experiments use this limited range of $E$.

## 3.3 Friction force on walls

### 3.3.1 Materials: Smooth and irregular walls

Smooth and irregularly shaped walls are used in this work. Both types are first used to investigate the effect of the stiffness variation in *bending* and afterwards as shaft walls in the climbing experiments. For the smooth wall, a textile tape (tesa extra Power Eco) creates the surface of a wall (left in Fig. 3.3). For irregular walls, there are two variants: (i) irregular, straight walls and (ii) irregular, ramped walls which exhibit two flat regions connected by an angled ramp. The irregularity is formed by spherical pebbles of roughly 1 cm in diameter. These pebbles are put onto a rectangular panel of plywood (50 cm by 60 cm) and covered with a sheet of textile. The loaded plywood then is put into a vacuum bag (usually used to store clothes). When the seal of the bag is closed and the bag evacuated with a vacuum cleaner, the bag conforms to and around the pebbles, forming irregular bumps and valleys in a continuous fashion. Fig. 3.3 shows the example of a panel with a ramp on the right. Styrofoam is shaped into a ramp shape with an angle of 15 deg, elevating the flat terrain by 3 cm within approximately 15 cm (shape outline in Fig. 3.3); we use two straight and two ramped panels.

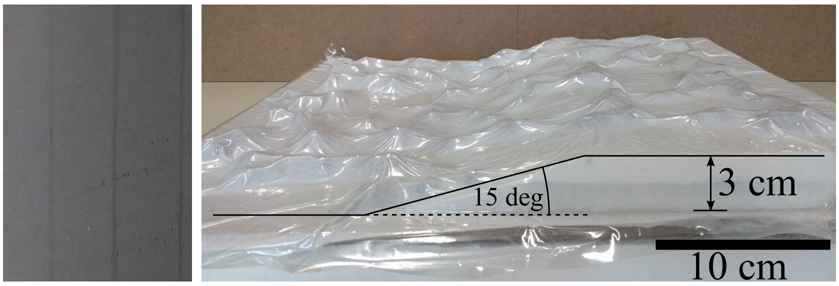

Figure 3.3 – The two wall types. Left: Smooth textile tape on a flat surface. Right: Spherical pebbles (approx. 1 cm in diameter) are put on a flat piece of plywood, covered with a layer of textile and enclosed in a vacuum bag. Applying a vacuum makes the bag adapt to the pebbles, forming bumps and valleys. Additionally, ramped sections can be created by building ramps out of Styrofoam on top of the plywood.

### 3.3.2 Vacuum-dependent and shape-adapted friction

**Experiments**

Due to the shape adaptation capability of a jamming membrane in its soft state, the development of the method of jamming-based climbing aims at irregularly shaped walls which is one of the more challenging tasks. However, climbing on smooth walls should nevertheless be possible. Therefore, the effect of jamming to counteract the gravitational force pulling on the robot is investigated in this series of experiments by measuring the static friction force that the end effector applies to the wall. A spherically shaped end effector design is used, together with the designed wall type. For an easier setup, we rotated the experimental setup such that the shaft wall lies horizontally. Similar to [61], the shaft wall is fixed on top of a 3-axis force plate. The lever of a hinge joint places a single end effector onto the wall and restricts the movement to the z-direction (see Fig. 3.4 a) for the experimental setup). The weighted lever applies a normal force of approximately 5 N ± 0.3 N to the end effector and wall, depending on the contact point or midpoint of the contact area respectively. The static friction force has to support the weight of the robot of 1.6 kg. As a first approximation, if only Coulomb friction with a friction coefficient of $\mu = 1$ is assumed, then in static equilibrium the robot has to at least exert $F_{friction} = \mu \cdot F_{robot} = 16$ N to the wall which ideally is split equally between the four end effectors, hence 4 N per end effector. An additional 1 N has been added to this value.

To cover the wide range of possible spring stiffnesses in Fig. 3.2 and take into account the pump limitations, we performed these experiments with four selected levels of vacuum of 1000 mbar (atmospheric pressure), 800 mbar, 500 mbar and 200 mbar absolute pressure. Additionally, as a comparison to purely passive end effectors, we also repeated the experiments with a spherical sponge (on the soft side of the stiffness spectrum) and a ball cast from the same material as the granules (on the hard side of the stiffness spectrum). Both types of walls - the smooth textile covered wall and the straight irregular wall - have been considered (Fig. 3.4 b) and c)). The experimental procedure is as follows. After putting an end effector in its

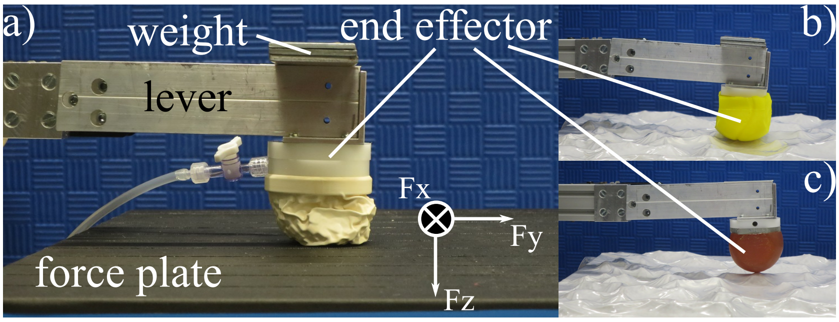

Figure 3.4 – Friction on wall experiments. a) Setup: a weighted lever places the end effectors on the force plate which is moved in negative direction of $F_x$. Jamming membrane on smooth wall. b) Sponge and c) rubber ball on irregular wall fixed on top of the force plate.

initial state (atmospheric pressure for the jamming membranes) onto a respective wall, it was brought to its vacuum pressure (if applicable). Then, the force plate was continuously moved laterally in the negative x-direction until the end effector slipped. In the context of the climbing movement, this would mean that the end effector has lost its grip to the wall and the robot is sliding down. The friction force in the x direction in [N] is logged at 10'000 Hz. Each experiment is repeated 10 times.

#### Results

To extract the static friction of the end effectors against the walls, the profile of the force measurements has been analyzed (not shown here). All graphs first show a monotonically rising force curve until the point where static friction abruptly breaks and a lower, dynamic friction force is observable. The maximal force at this switching point has been recorded for each experiment. Table 3.1 summarizes the experimental data, indicating both the average and standard deviation of each configuration. It can be seen that both the sponge and the jamming membrane at 1000 mbar apply an insufficient friction force to the wall; they describe a "rolling" motion which is depicted in more detail in 4.3.1. Further, the friction force tends to increase with a harder end effector, peaking with the rubber ball on the smooth wall. However, for the irregular walls, the jamming membranes at 500 mbar and 200 mbar apply a very similar friction force, with 200 mbar even outperforming the rubber ball. At last, the rubber ball suffers from a large standard deviation: because of the single point contact, its performance is highly dependent on the location on the irregular wall. If placed exactly on top of, or on the downwards slope of a bump, then the shape of the wall influences the transmittable friction force negatively. The lower standard deviations for the jamming membranes indicate that this issue occurs less and the transmittable friction force is more consistent regardless of the shape of the wall due to the increased contact area created in the soft state and the shape adaptation. The actual shape adaptation part is a morphological computation of the end effector to match the irregularities of the wall. While this is also the case for the sponge, it is too soft to make use of the irregularities. For the membranes, more often than not they manage to *actively* use the

| end effector | wall type | mean friction force | std. deviation |
|---|---|---|---|
| sponge | smooth | 0.62 N | 0.18 N |
| | irreg. | 0.42 N | 0.14 N |
| 1000 mbar | smooth | 0.91 N | 0.18 N |
| | irreg. | 0.76 N | 0.16 N |
| 800 mbar | smooth | 2.52 N | 0.86 N |
| | irreg. | 2.20 N | 0.70 N |
| 500 mbar | smooth | 3.83 N | 0.92 N |
| | irreg. | 3.00 N | 1.09 N |
| 200 mbar | smooth | 3.56 N | 0.55 N |
| | irreg. | 3.41 N | 0.67 N |
| rubber ball | smooth | 4.67 N | 0.83 N |
| | irreg. | 3.28 N | 1.72 N |

Table 3.1 – Friction force for end effectors

irregularities in the wall. This and the overall transmitted friction force are promising aspects for the successful implementation of jamming-based climbing.

It should be mentioned that almost all forces are smaller than the required 4 N. Even though the robot is tuned to apply roughly the same normal force, it geometrically increases the normal force with its own weight (see Fig. 3.8). The values in Tab. 3.1 therefore would change. However, the qualitative results are expected to still hold true.

## 3.4 Climbing vertical shafts

### 3.4.1 Materials: Robotic Platform

**Morphology with Bioloid modules:** The morphology of the robot is inspired by a real human both for the proportions and joint placements, scaled to a height of approximately 50 cm and a weight of 1.6 kg. It has been chosen to partly imitate the versatility of a legged morphology: the scenario in which the robot could be operating may only partially be composed of climbing and it must perform many other tasks that a specialized climbing robot might not be able to do; the legs and jamming membranes could serve in a multi-modal way. The robot consists of a trunk, which houses most of the electromechanical parts, and four limbs with three joints each. The joints are simplified to hinge joints due to the usage of simple position controlled servo motors (Dynamixel AX-12+) from a Bioloid kit [134]. For an arm, three servo motors form the shoulder, elbow and wrist, where the lower and upper arm are of equal length ($l_{as} = 6.7$ cm). For a leg, three servo motors form the hip, knee and ankle, where the upper and lower thigh are of equal length ($l_{ls} = 9.3$ cm). The hinge joints can only perform movements in 2D

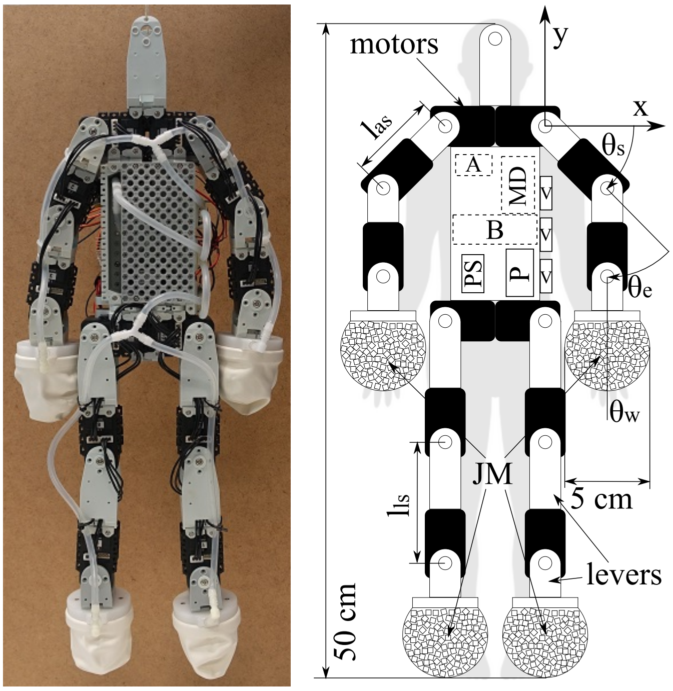

Figure 3.5 – Climbing robot with jamming end effectors. Left: the real robot made out of Bioloid modules. Right: schematics of the design. The proportions of body and limbs roughly correlate to the proportions of a human body (silhouette in gray). The trunk houses the pump (P) and pressure sensor (PS) while the arduino (A), motor drivers (MD) and the battery (B) are mounted on the back of the robot. The valves (V) are visible on the left side of the robot. Latex balloons filled with cubic rubber granules form the jamming membranes (JM). The robot weights 1.6 kg.

and as all servo motors are in series with the same orientation, the whole robot does not have the capability to move limbs sagitally; the movements are restricted to the coronal plane. This is not unlike a human climber solving the same task where the knees are rotated outwards. Fig. 3.5 shows the schematics of the robot with the corresponding dimensions. The outline of the shape of a human is indicated as a comparison.

**Jamming end effectors:** Four identical jamming membranes represent hands and feet of a humanoid, consisting of a spherical latex balloon with a diameter of roughly 5 cm filled with the cubic rubber granules (see Fig. 3.5).

**Pump and valves:** A miniature pump (Schwarzer SP 100 EC-DU, serial configuration) directs the airflow over a series of three solenoid valves (SMC S070C-SAG-32) to specific end effectors and a single pressure sensor (Honeywell 015PAAA5). The pump is able to create a vacuum up to -800 mbar versus atmospheric pressure inside the end effectors (200 mbar absolute pressure). Depending on the state of the valves, the end effectors are affected in different ways. The basic states are evacuation, hold or reset of both feet and evacuation, hold or reset of both hands. Hold means holding the current vacuum pressure and reset means equalizing the membrane pressure to atmospheric pressure. Section 3.4.1 explains how these states are used during a climbing cycle.

**Electronics:** An on-board microcontroller (Arduino Nano V3.0) controls the motors, pump, valves and pressure sensor. The electronics are powered by an on-board 12 V LiPo battery (Conrad energy BEC 11.1V 1300mAh 12C), making the robot fully autonomous.

**Control:** The movement sequence is inspired by real climbers and can be split into periodic cycles. The cycle starts from the state where all four extremities are in contact with the wall after the climbing movement with both arms stretched downwards and the legs in an intermediate position with all jamming membranes in a hardened state. First, both legs perform a symmetric movement, release the wall contact, reset their membranes and raise the feet towards the height of the hip. During this state, the robot represents an inverted pendulum in its stable equilibrium position (viewed from the side). The soft feet then are slowly and simultaneously moved horizontally towards the walls where the wall contact is detected by the pressure sensor when the membranes get compressed upon impact. Both feet then harden by evacuating the membranes.

In this state, it is important to notice that the same strategy of symmetric movements cannot be applied to reposition the arms without intervention, as by releasing the arms the robot represents an inverted pendulum in its unstable equilibrium position and thus would fall forward or backward. Human climbers in a similar scenario solve this issue by raising the arms sequentially such that one arm always can stabilize the coronal plane. This either requires elaborate movements of the whole body in the case where only pushing forces to the wall are allowed (as in the case of the robot). More often however, a human is able to also apply a pulling force to the wall by actually gripping an area which facilitates the sequential arm movement. For the sake of simplicity, as this experiment only represents a proof-of-concept for jamming-based climbing, only the simplified symmetrical movement of the arms has been implemented. To prevent the robot from falling forward or backward in the unstable case, a string is manually pulled on the top of the robot. During this external stabilization period, both arms symmetrically release the wall contact, reset their membranes and raise the hand to shoulder level. Analogue to the legs, the hands move horizontally until they touch the wall, upon which the string is released again. Both hands then harden and the robot has now all four end effectors in wall contact in their hardened state, ready to execute the climbing movement.

The servo motors are position controlled and the movement is performed by inverse kinematics. Eqs. (3.2) to (3.4) give the calculations for the left arm:

$$x = l_{as}\,(cos(\theta_s + \theta_e) + cos(\theta_s)) \tag{3.2}$$

$$y = l_{as}\,(sin(\theta_s + \theta_e) + sin(\theta_s)) \tag{3.3}$$

$$\theta_w = -(\theta_s + \theta_e) \tag{3.4}$$

where $x$ and $y$ define the position of the wrist joint in Eq. (3.2) and Eq. (3.3) and $\theta_s$, $\theta_e$ and

$\theta_w$ are the servo motor angles around the zero position. Eq. (3.4) ensures that the jamming membrane is always confined to the horizontal plane during climbing. The movements of the arm (and similarly for the other limbs) are constrained differently during the climbing cycle. When approaching a wall, $y = 0$ and $x$ is incremented until stopped at $x_{wall}$ by the feedback from the pressure sensor. When performing the climbing movement, $x = x_{wall}$ and $y$ is incremented until the arm is fully stretched at $\theta_e = 0$. It is assumed that the shaft width is within a minimal and maximal value such that the robot fits in between and can reach both shaft walls. Note that the legs touch the wall in a position such that the maximal movement of the arms, limited by the shorter arm segments, can always be executed. This completes the movement cycle and the robot is back to its initial position. During the climbing cycle, feedback is only provided by the pressure sensor. It regulates the vacuum pressure level inside the jamming membranes and provides the starting point of solving the inverse kinematic equations by stopping the horizontal limb movement. The threshold for the pressure sensor to stop this movement is hand tuned to roughly match the force requirements, previously described in section 3.3.2. The robot otherwise is not provided with any information about the shaft width, structure or layout, and the actual climbing movement is performed open-loop.

### 3.4.2 Open-loop climbing on varying shaft layouts

#### Experiments

For the climbing experiments, a current sensor (Texas Instruments INA169) measures the total current consumed by the whole system. This includes the consumption of the microcontroller as well as the pump when it is evacuating. The majority of power however is consumed by the 12 servo motors. The current measurement is expected to give insight into how climbing performance is affected by the hardness of the end effectors. Additionally, video recordings of the climbing sequences qualitatively show if the climbing is successful, or capture the type of failure.

The viability of climbing shafts has been investigated with the following four layouts of shaft walls (as shown in Fig. 3.6). Based on the results of the friction experiments in section 3.3.2, 5 trials for absolute vacuum pressures of 800 mbar, 500 mbar and 200 mbar have been performed for each layout.

1. Straight smooth shaft: A straight shaft with a width of 45 cm and the smooth textile-tape as walls.
2. Straight irregular shaft: A straight shaft with a width of 45 cm and the straight vacuum-pebble-panels as walls.
3. Enlarging irregular shaft: Two irregular, ramped panels form a shaft with a width of 42 cm which enlarges to 48 cm within a distance of 15 cm.
4. Narrowing irregular shaft: Two irregular, ramped panels form a shaft with a width of 50 cm which narrows to 44 cm within a distance of 15 cm.

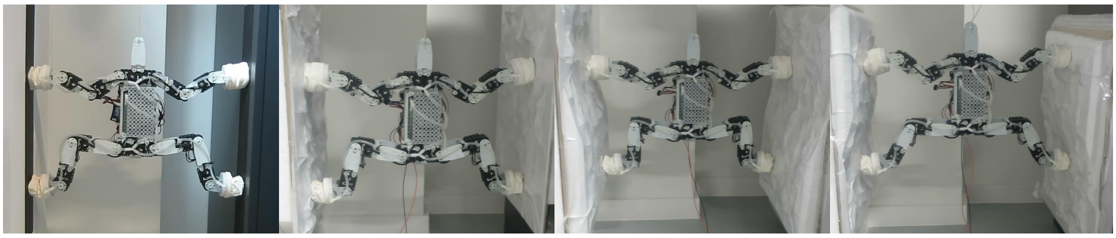

Figure 3.6 – Shaft layouts: smooth, straight, enlarging, narrowing

| Vacuum pressure | successful | slippage | overload |
|---|---|---|---|
| 800 mbar | 11 | 8 | 1 |
| 500 mbar | 14 | 0 | 6 |
| 200 mbar | 10 | 0 | 10 |

Table 3.2 – Completion of first climbing cycle

### Results

The results of the climbing experiments are rather of a qualitative nature as the robot was designed to simply validate the approach of climbing with jamming end effectors. As such, it was able to perform a climbing step on all four shaft wall layouts, considering the method of external stabilization by the string during the unstable phase in the climbing cycle. Tab. 3.2 summarizes the successful climbing sequence or indicates the failure mode otherwise.

The best vacuum pressure level of the tested configurations was 500 mbar, which enabled the robot to solve all three layouts the most consistently. At 800 mbar, the membranes are often simply not stiff enough and deform under the weight and movement of the robot, losing their shape adaptation to the wall. This causes the robot to fall. At 200 mbar, the robot was able to climb the layouts but would often run into the issue of servo motor overload which is discussed below. Lastly, the focus of the experiments was to demonstrate the multi-modal properties of jamming membranes. In the context of the climbing scenario presented, the membranes act in three different modalities:

**Sensors:** Even though the inverse kinematics of the climbing step is open-loop, the horizontal positions of the end effectors (providing one constraint to solve the inverse kinematic equations) are determined by the membranes sensing the wall. During the horizontal movement of the extremities, upon wall contact, the movement effectively compresses the membranes, which is detected as a pressure increase by the pressure sensor (Fig. 3.8 (c) and (e)).

**Grippers:** As the membranes are in their soft state during the compression from forming wall contact, the membranes passively adapt to the irregular terrain. After hardening the membranes through jamming, the shape adaptation allows the climber to *actively* use the irregularities in the terrain to create the necessary friction forces for climbing (Fig. 3.8 (a)-(e)). This enables the robot to also climb over convex sections (see supplementary video of this thesis): provided that the irregularities form certain angled edges or bumps, a jamming membrane hitting such edges is able to advantageously exploit the irregularity (contrary to, for instance, avoiding them or failing).

**Force dissipators:** Most of the time, the climber is in contact with the wall with all four extremities, which, during climbing up, ideally should not move vertically nor horizontally. In any case, non-perfect position following of the position controlled servo motors and other sources of noise can lead to motor commands that cause unintentional pushing forces of the limbs against the walls. Since the walls provide a hard constraint on the movement, the servo motors ultimately can end up acting against each other, causing the build-up of internal forces (closed kinematic chains). This can cause damage to both robot and environment. The membranes in their hardened state are able to dissipate such forces while still maintaining their main functionality of providing grip to the wall: they act as omni-directional springs as long as the granules do not rearrange.

We call this phenomenon “compliant gripping” and consider this a form of morphological computation, however in a different manner than the shape adaptation computation. Here, the morphological computation is redistributing and absorbing forces to avoid the build-up of large internal forces in the closed kinematic chains. This is visualized in Fig. 3.7 with the current consumption of the robot during a specific period. The case of climbing irregular, straight walls is shown for one trial for the two vacuum pressure levels 500 mbar and 200 mbar absolute pressure. The period starts with both legs in their hardened state in wall contact just as the arms are about to experience the compression caused by forming contact with the wall (Fig. 3.8 (e)). The string preventing the robot from tilting is also released at the same time, making the robot fully support its own weight. The membrane compression and the following movement with inverse kinematics cause the build-up of force chains which is visible in the increase of the current consumption. At 500 mbar, the consumption briefly rises when the hands form contact with the wall. After evacuation, more current is consumed during the inverse kinematics movement. The three peaks visible at the end are caused by the leg movements of the following climbing sequence, where the consumption decreases again due to releasing the two feet membranes and therefore some of the internal forces. At 200 mbar, the consumption after forming contact with the wall rises to a level that can cause an overload shutdown of a servo motor. This occurs when the current exceeds a threshold during a certain duration, which here is the case when the weight of the robot and the force chains are acting against an impedance which is too stiff. During evacuation of the hand membranes, one servo motor in the leg shuts off, causing a sudden drop in the current consumption, and causing the robot to fall. The consumption drops to zero after the robot is switched off.

Although Fig. 3.7 depicts a selected case and the effect of overload is not always as visible as in this example, it provides an indication when the build-up of internal forces occurs and how it is dealt with in the different levels of vacuum. Measuring the current consumption for each servo motor separately was out of scope for this work but could provide a better insight into the subject of force dissipation. Also, if the control of the robot is switched from position

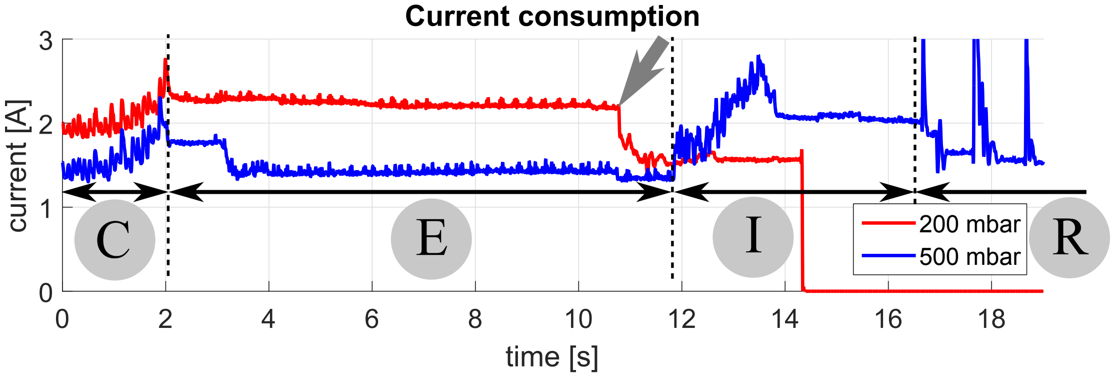

Figure 3.7 – Current consumption with all four membranes in contact with the wall. The consumption initially rises during the wall contact formation phase (C). At 200 mbar during evacuation phase (E), it exceeds a threshold during a certain duration, causing one motor to shut down (approximately at 11 s, gray arrow), followed by a sudden drop in the consumption and falling of the robot. In contrast, the consumption at 500 mbar is lower during evacuation and the climbing step can be performed by inverse kinematics (phase I). It drops again once the legs release their grip at the end of the graph where a new climbing sequence starts (phase R).

controlled to torque controlled servo motors (though not feasible with the servo motors used in this setup), the force dissipation characteristic may differ.

## 3.5 Conclusion and Future Work

This work presents the characterization of the compressive stiffness change of compliant granular jamming and a case study application to jamming-based climbing in vertical shafts. First, compressive load tests ($\epsilon = 3.33$ %) with an oblong latex membrane filled with cubic rubber granules were performed over a vacuum pressure range of 1000 mbar to 0 mbar absolute pressure. By regarding the combination of membrane and granules as a metamaterial, the stiffness variation can be described by a change in its Young's modulus $E$. The results of the first part show that the Young's modulus $E$ can fairly accurately be described by a linear relationship to the vacuum pressure level. Then, the capability of the jamming membranes to create friction forces on a smooth and an irregular surface has been investigated. By comparing different vacuum pressure conditions to passive end effectors such as a sponge and a rubber ball, it was found that the jamming membranes exert a comparable friction force as the best performing case of the rubber ball, and that a stronger jamming tends to transmit higher friction forces. Moreover, for an irregular surface, the jamming membranes even outperform the rubber ball and are able to more consistently apply a high friction force. This is due to their shape adaptation that lets them actively exploit the irregularities.

Lastly, these findings were used to design a small autonomous humanoid robot that can climb vertical shafts with both smooth and irregular shaft walls. The robot is equipped with

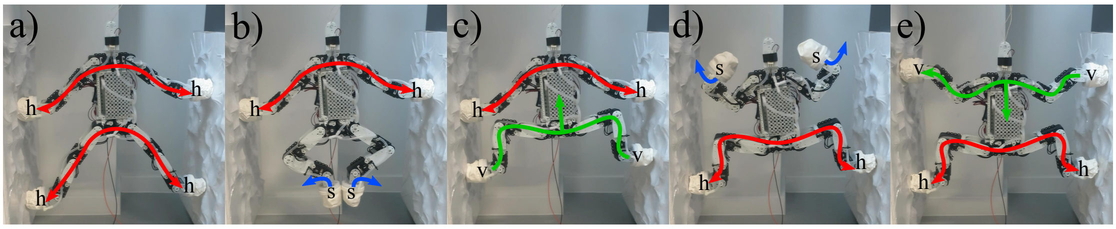

Figure 3.8 – Climbing sequence. (a) After the climbing movement, all membranes in their hardened state [h] in wall contact. (b) Repositioning of the legs and resetting their membranes to the soft state [s]. The robot forms an inverted pendulum in its stable equilibrium point. (c) The legs form wall contact by exceeding a pressure threshold when the membranes get compressed upon wall impact. The feet then are evacuated [v]. (d) Repositioning the arms and resetting their membranes. The robot forms an inverted pendulum in its unstable equilibrium point and thus is stabilized by a string at the head of the robot during this phase only. (e) The arms form wall contact by exceeding a pressure threshold when the membranes get compressed upon wall impact. The hands then are evacuated. The robot now is ready to perform the climbing step with inverse kinematics. Red arrows: closed air system; Blue arrows: air system opened to atmospheric surrounding; Green arrows: air system connected to pressure sensor and vacuum pump.

four jamming membranes as end effectors and an on-board microcontroller, pump-valve-system and battery. In four different shaft layouts, including a convex case, the robot is able to perform a climbing step with success depending on the chosen stiffness of the jamming membranes: the robot cannot support its own weight if the membranes are too soft and servo motor overload can occur if the membranes are too stiff. The experiments demonstrate a multi-modal effect of the jamming membranes: they enable a simple pressure sensor to detect the wall impact; they can act as universal grippers that provide the necessary grip to the wall in their hardened state, additionally benefiting from the passive shape adaptation in their soft state; they can act as force dissipators in their role as an impedance, performing “compliant gripping” which dissipates internal forces caused by closed kinematic chains (in turn formed by position controlled servo motors) without losing wall contact.

The jamming membranes are shown to perform two kinds of morphological computation. The first computation happens during the shape adaptation to the terrain irregularity, and the second computation is the redistribution and absorption of forces to avoid high internal forces in the closed kinematic chains. Since these computations happen on different mechanical properties of the membranes, and thus during their different functionalities, this could be classified as a *variable morphological computation* [140]. A more in-depth analysis would be needed on this subject.

As future work, the prototype design of the robot could be adjusted (e.g. stronger servo motors or torque control instead of position control with different servo motors). The implementation of a sequential arm movement could also lead to fully autonomous climbing. More experiments with different levels of vacuum pressure could suggest an optimal membrane stiffness in terms of current consumption and climbing success. Testing the robot in more climbing situations is expected to provide a better understanding of the limits of granular jamming in the application of climbing and in other forms of locomotion. This includes legged ground locomotion, which will be the subject of the following chapter. There, shape adaptation is shown to be one of the key features for using jamming membranes as feet for simplifying locomotion control on rough terrain. Also, while in this chapter the mode-switch was a gradual transition between two functionalities because the focus was not on speed climbing, the dynamics of legged locomotion occur at a faster timescale. We thus describe next the development of a fast version of the same concept.

# 4 Compliant Universal Grippers as adaptive feet

In ground locomotion, a specific element that can make good use of variable spring and damping characteristics is the foot. It has different functionalities during a gait cycle: at touchdown, the foot dampens the impact forces to instantaneously create a clean ground contact without bounces (fluid state, “impact damping”), whereas during stance and takeoff, the foot transmits propulsion forces to the ground to advance (solid state, “force transmission”). With a Universal Gripper as a foot, there are two possibilities for how to control these characteristics. A specific, gait-tuned level of jamming can strike just the right balance between impact damping and force transmission. This strategy, referred to as “static jamming”, is presented in section 4.3 of this chapter. It describes the first implementation of jamming membranes as feet in a quadruped robot and discussing the effects of changing the physical characteristics of the membranes in preliminary locomotion experiments. The second possibility is to change the physical characteristics during the gait cycle, referred to as “dynamic jamming”, such that the advantages of both states can be utilized maximally. In this method, the foot is able to rapidly switch between the two states, which will be described in sections 4.4 and 4.5, again together with the implementation in a simple quadruped robot platform for analysis.

**Reference publications**

This chapter is based on

- ***Simon Hauser***, *Peter Eckert, Alexandre Tuleu, and Auke Ijspeert. “Friction and damping of a compliant foot based on granular jamming for legged robots.” In 2016 6th IEEE International Conference on Biomedical Robotics and Biomechatronics (BioRob), pp. 1160-1165. IEEE, 2016.*
- ***Simon Hauser***, *Kamilo Melo, Mehmet Mutlu, and Auke Ijspeert. “Fast state-switching of a jamming-based foot.” The 8th International Symposium on Adaptive Motion of Animals and Machines (AMAM), 2017.*
- ***Simon Hauser***, *Mehmet Mutlu, Pol Banzet, and Auke Jan Ijspeert. “Compliant universal grippers as adaptive feet in legged robots.” Advanced Robotics 32, no. 15 (2018): 825-836.*

**My original contributions**

- Development of concept
- Design of mechatronic system
- Design and performing of experiments
- Analysis of results
- Writing of manuscripts

## 4.1 Inspiration: Jamming membranes as feet

Biologically inspired robots that are used to research the animal and the technological domains are becoming increasingly refined. Control schemes for sensor-less and sensorized robots have been developed that are able to handle torque control and sometimes even adapt to a changing task set. Further, mechanics and electronics have evolved and take part in more reliable and robust bio-inspired robots. Robots reproduce animal structures or use bio-mechanical principles to excel in a specific task. Nevertheless, during this evolution of robots, the feet are often oversimplified. This chapter centers around the foot as a bio-mechanically complex but extremely important end effector. The foot is often implemented as a simple ball-foot [68] out of various materials with different friction coefficients, or a simple compliant bending structure [152, 175] (Fig. 4.3). This gives the freedom to the controller to use the approximate ground contact as a discrete point or line. In consequence, high performing control-schemes such as the spring loaded inverted pendulum (SLIP) model [130] were developed. Moving away from flat terrain often results in the use of sensory feedback to alter foot trajectories to ensure a precise ground contact. If we look at our biological inspiration, feet seem to be the opposite of their robotic counterparts: complex, highly actuated and sensorized, adaptable and maybe most importantly made out of soft as well as hard tissue. The latter leads to the ability of changing ground contact points dynamically during stance phase. We speculate that this property plays an important role in the open-loop adaptation of the foot to perturbations and uneven terrain.

### 4.1.1 Contact point vs. contact area

In many closed-loop locomotion cases with force feedback, the centralized-control approach usually requires three parts: (i) precise force sensing that accurately measures the ground reaction forces, (ii) precise tracking of joint angle trajectories by the mechatronic system of the robot to execute a planned trajectory and (iii) relatively high computational power to collect all the sensor data, process them and plan and adjust the foot trajectories. On the one hand, these requirements can make the application of such a control system to legged robots infeasible due to the sever computational cost. On the other hand, even though such systems are able to perform well in certain conditions, the results do not necessarily represent animal-like behavior. Partly due to the feet's inability to adapt, in such systems the roughness of the terrain has to be individually dealt with on a computational level through constantly and extremely quickly changing trajectories, which rather deteriorates the performance of a robot. For example, when a foot unexpectedly hits a rough patch while still in forward swing motion, the controller immediately needs to adapt the trajectory to stop the forward motion. Otherwise, the foot could either bounce off the ground or - in case it creates sufficient friction - could induce the build up of internal forces due to closed kinematic chains in the feet touching the ground that eventually get released, potentially causing e.g. a change of the direction of heading. While a potential way out of this issue is the explicit allowance of slippage (disabling closed kinematic chains), this mostly reduces performance and hence is undesired. Thus, damping and mechanical adaptability in the feet could have the potential to reduce the need for complex control by offloading terrain adaptation, trajectory imperfections and dealing with unexpected gait events from the main computational unit to the feet and hence simplifying the control while still retaining favorable friction properties. This is the same morphological computation described in the previous chapter, where the end effectors adapt their shape to the irregularities of the climbing walls.

However, the design of adaptive feet for legged robots on rough terrain remains a challenge. One available strategy is to increase the number of contact points per foot (as opposed to only one contact point in the case of “rigid” spherical feet) by e.g. splitting the foot into independent sections and let each contact point form ground contact individually. This distributes the roughness to multiple points where the final orientation of the foot is determined by an averaged influence of each point [11, 65, 82]. Other works focused on replicating the main features of human feet [143, 126, 109, 46] and animal feet [28, 1].

Interestingly, some of the research presented is arguably focused on *avoiding* the unevenness of the terrain by creating multiple contact points. Our proposition is that creating an actual contact *area* is more beneficial for the locomotion performance as such an area may actively use the features of the ground (which may be unfavorable for a few contact points or not covered at all) for improved friction and propulsion, thus *seeking* unevenness. Additionally, the weight of a robot is more evenly distributed over a contact area rather than focused on contact points, potentially allowing the robot to also locomote on soft ground (e.g. sand or snow).

Intuitively, it is clear that a spatial conformation of the foot to uneven terrain requires compliance, and thus a soft foot seems desirable, as illustrated in Fig. 4.1. A foot with a single contact point (or line) can suffer from inconsistent friction transmissibility depending on where it touches unevenness, as well as vertical shift caused by it. A compliant foot with a contact area is able to “assimilate” the unevenness, making the friction independent of it and eliminating vertical shifts (the ankle joint is not considered in this example). However, as it is described in [113] and further analyzed in [126], a purely soft foot creates new issues. A compliance below a critical level is no longer able to stabilize the system as the support polygon becomes instable. Applying a required force within the support polygon to compensate for a slight shift of the center of gravity of the robot gets absorbed by the compliance, resulting in the robot falling.

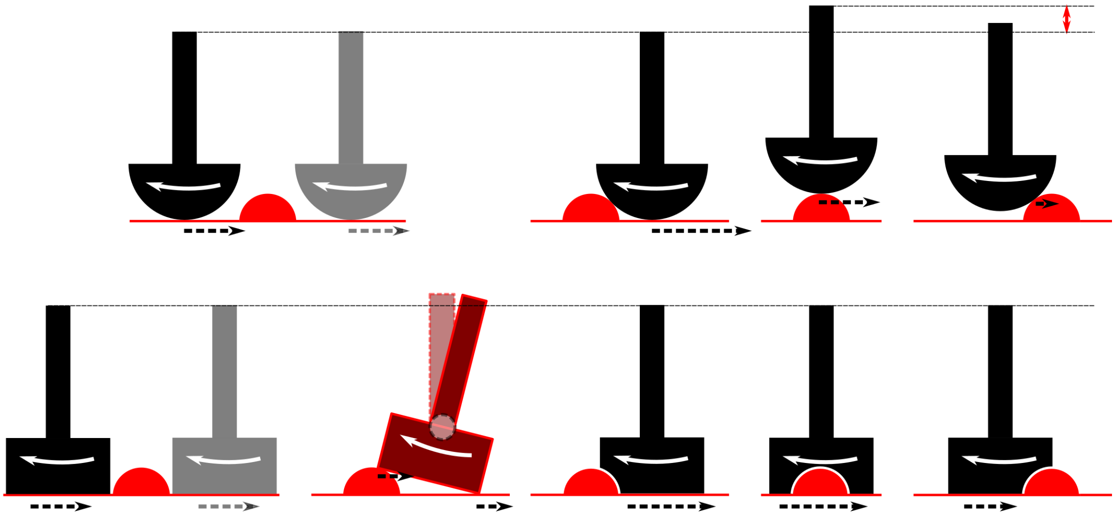

Figure 4.1 – Hard vs. soft foot. Top row: a hard foot with only one contact point applies a varying friction force to the ground (arrows below the feet), heavily depending on the location of roughness present (red half-sphere). Additionally, the foot may shift upwards when it encounters a rough area. Bottom row: a soft foot is able to apply a more consistent friction force due to the conformation of the foot to the roughness. Also, no shift occurs (the option with an implemented ankle is not considered).

Moreover, propulsion forces orthogonal to the contact area get absorbed as well: instead of pushing a robot forward, the movement of e.g. a step will simply exchange energy with the compliance without resulting in a net forward motion. A compromise seems unavoidable: a foot should be soft enough to adapt and stiff enough to allow propulsion.

### 4.1.2 Tackling the stiffness dilemma

One possibility to deal with this dilemma is to separate two distinct functionalities of a foot during stance phase. First, the foot must adapt to the uneven terrain and damp the impact with the ground to ensure an undisturbed ground contact without slipping and bouncing (caused either by bouncy mechanics or unexpectedly hitting an uneven area). Then, it must use the shear forces transmittable in the formed contact area to create the necessary propulsion forces. As discussed above, these two actions seem to be somewhat opposed to each other: while adaptation and damping requires a certain softness in the system, controlled force transmission prefers a stiff system.

The research in [113] states the importance of such a state-switch and employs a clever mechanism in the foot that passively achieves the state transition using the weight of the robot. Their developed foot consists of four separate fingers that are unconstrained at touchdown to enable terrain adaptation (the research does not mention damping). The weight of the robot then engages a brake (interestingly related to the principle of jamming) that locks the finger arrangement in place to perform locomotion. Although the work is motivated by developing a

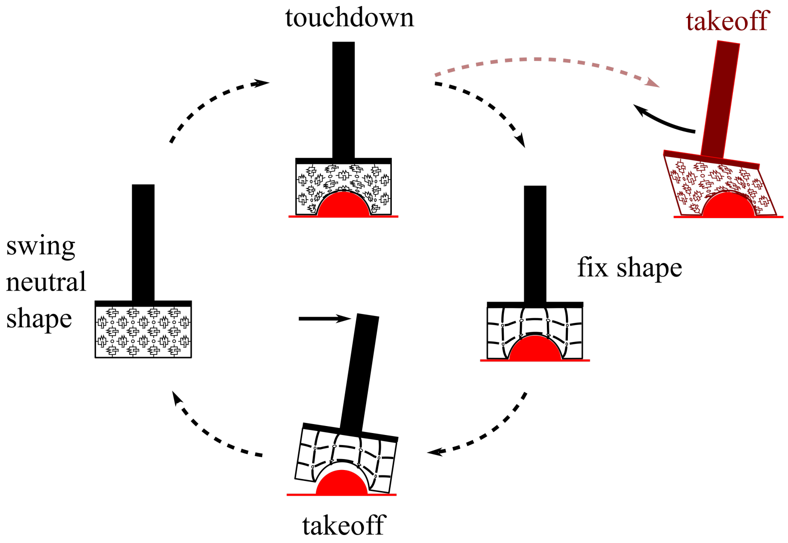

Figure 4.2 – The stiffness dilemma. A foot should be soft at touchdown to enable shape adaptation. A purely soft foot however is not ideal to provide propulsion as the input of propulsion movement simply will exchange energy with the compliance. A reversible shape-fixing mechanism that makes the foot stiff can solve the stiffness dilemma.

“sole” that enlarges the support polygon of the robot during stance, the mechanism creates four contact points per foot without creating an actual contact area - as in animal feet - that could interact as a whole with the structure of the terrain.

In the case of a dog paw, we hypothesize that the adaptive capabilities of the paw-pads stem from a complex, local interplay of bones, tissues and muscles which is able to form a contact area that can smoothly transition between soft and hard states. As a result, this leads to extremely versatile locomotion capabilities [32], although the mechanisms are not yet fully understood. In humans, recent research indicates how the transition could function. The bones and muscles together with the surrounding tissue form an inherently compliant structure which can act as a damper at touchdown. A group of bones known as the *tarsal bones* near the end of the tibia has the ability to change its structural rigidity from flexible to rigid through a rotation of the foot, rearranging these bones in such a way that an interlocked structure is formed. The rotation happens passively during stance phase and is assisted by the contraction of the muscles in the foot that keep the bones in their interlocked arrangement. This allows the transmission of the propulsion force to the ground until takeoff when the foot becomes compliant again [13, 41].

The goal of this chapter is to understand how a change of foot stiffness can be used to switch between the functionalities of the foot during stance, thus improving the locomotion performance of legged robots. We abstract the mechanism and design and implement it in a quadruped robot. The abstraction aims at simplifying the mechanical construction, as a replication of the complex anatomy would be too challenging. Jamming of granular media was selected as the enabling technology due to its state-switching capabilities, mechanical and control simplicity, and relative similarity to a compound of muscles and tissues, specifically for forming an interlocked system like the tarsal bones. Further, it is worth mentioning that in [41] the unlocked configuration of the tarsal bones is described as ‘a loose bag of bones’, unconsciously hinting at the idea of approximating the structure with macroscopic granules.

The numerical simulation of compliant, shape-changing objects is a difficult problem to tackle and moreover likely suffers largely from the reality gap [76]. As our aim is to understand how legged animals could use a change in foot stiffness during locomotion with the help of real robots, we decided to conduct this experimental study in hardware only.

## 4.2 Feet comparison

### 4.2.1 Feet in nature

Feet in animals are highly adapted to their living environment and the mode of usage. Structures range from highly articulated feet in cats with soft paw-pads and retractable claws, to horse feet that consist of combined toes forming a single solid structure, to specialized feet as for e.g. geckos. Our robot foot design takes inspiration and links to the soft pads in multiple animal paws, such as those of cats and dogs. These structures are used to increase traction, protect the fine bones and joints of the foot from impacts, and sense the surface. The pads consist of a layer of harder skin, enclosing multiple layers of soft tissue with nerves and blood vessels (Fig. 4.3a).

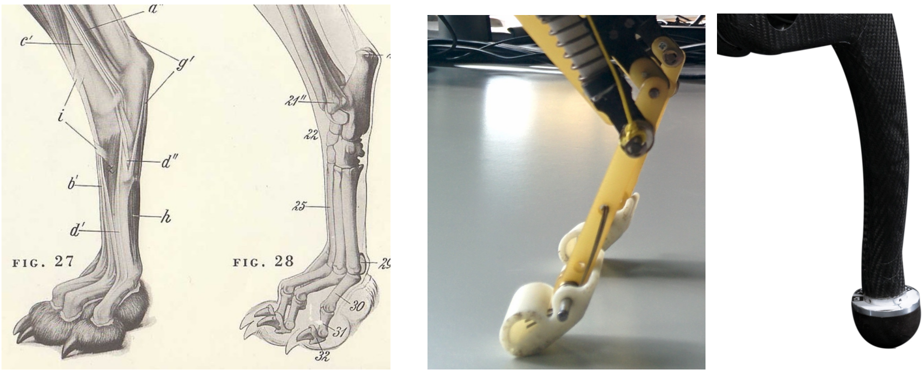

(a) (b) (c)

Figure 4.3 – Feet of two robots in comparison to an animal foot; (a) 1950’s drawing of a dog paw with soft paw-pads, claws, interior bones, muscles and ligaments[a], (b) Cheetah-Cub-S foot with rigid 3D-printed ABS structure contacting the ground in a line with a cylindric shape [175], (c) ANYmal foot with a spherical shaped OptoForce sensor [68].

---

[a] http://tinyurl.com/1950dogpaw

### 4.2.2 Feet in currently used robots

The design of feet in robots is often oversimplified. Independent of gait, speed, weight, or size, most modern quadruped robots use very simple feet. Shapes often used in robots include ball- [68, 128, 129, 142, 69] or half-cylinder-like structures [152, 175, 71, 70, 159, 85, 42]. Nevertheless, most of these feet feature a slight elasticity, either through use of springs or the choice of elastic material.

### 4.2.3 Foot design based on granular media

A compliant jamming membrane as the foot could prove an enabling technology to open up the possibilities of high friction locomotion on uneven terrain. On the one hand, the damping property (fluid-like state) could benefit the ground contact. On the other hand, a semi-solid state of the granules could allow for movements parallel to the ground without losing ground contact. This could serve as an additional degree of freedom to solve imperfect control, e.g. in the closed kinematic chain mentioned above. In this case, internal forces could be dissipated through the additional degree of freedom. Lastly, a terrain-adapted solidification of the foot could enable exploitation of the features of the terrain to increase its “grip”. The proposed foot design takes these effects into consideration and consists of a spherical latex balloon filled with the cubic rubber granules. Fig. 4.4 shows a schematic of the mechanical design. An airtight seal is created with a closing lid where a silicone tube is attached, leading to a vacuum pump.

The reasons to use compliant cubes as granules instead of e.g. ground coffee are threefold. First, it has been shown by [79] that cubic granules perform a *geometrical* jamming due to their shape, which enables jamming with less pressure difference. This results in less demanding specifications for the pump, i.e. a smaller, lighter pump which could prove beneficial for such a mobile jamming application. Second, the same research as well as Chapt. 3 show that these compliant granules have the ability to change the overall stiffness of the membrane linearly with the applied vacuum pressure. Even though evacuation to different vacuum pressure levels has not been implemented in the following projects, a change in membrane stiffness could become important especially in different gait patterns and higher frequencies. Third, bigger granules result in less memory effect which occurs by the pack of granules sustaining the shape adaptation even after the deformation of the membrane. Resetting the granules to their initial, unpacked arrangement can be achieved by a burst of positive pressure (e.g. [7]) which would require a separate positive pressure reservoir. In order to keep the evacuation system as light as possible, only a vacuum reservoir has been implemented, and the membrane reset to only atmospheric pressure showed a sufficient mitigation of the memory effect.

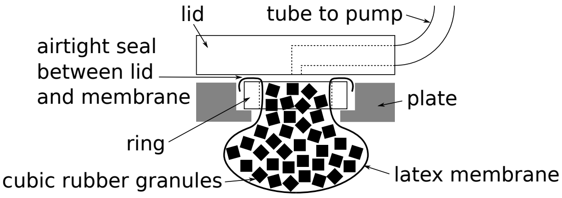

Figure 4.4 – Schematics of the membrane foot. A latex membrane is filled with cubic rubber granules and wrapped around a plastic ring. The plate presses the ring against the lid and forms an airtight seal. A silicone tube connects the membrane to the vacuum pump.

## 4.3 Static jamming: Are jamming feet viable?

For the locomotion experiments performed in this section, the quadrupedal robot Oncilla (Fig. 4.7) is used. Oncilla is a compliant quadruped robot developed cooperatively during the AMARSI program[1]. It normally features force sensors serving as feet. These OptoForce[2] (OF) sensors consist of a semi-sphere made out of hard silicon rubber and an aluminum base frame, similar to the feet used in many other robots. The foot trajectory is controlled open-loop and taken from [4]. This way, the results are more likely to reflect the behaviors produced by the foot mechanics and not the possible influence of closed-loop control. In the experiments, Oncilla is either equipped with the OptoForce feet or with four jamming feet (latex membrane with diameter of ≈ 3 cm, filled with the cubic rubber granules) and a vacuum pump (Schwartzer SP 620 EC-L) powered by a 9 V battery. The pump creates a pressure of -180 mbar versus atmospheric pressure (measured with a pressure sensor, Honeywell015PAAA5) which is the level of vacuum applied in the static jamming experiments. The mass of the foot is 46 g, which is comparable to the weight of an OptoForce sensor (54 g), keeping the inertia of the legs approximately the same. The mass of the silicone tubes, battery and pump together is 285 g which is added to the trunk of the robot. The control is kept the same for all experiments.

### 4.3.1 Effects of jamming on contact friction and impact damping

#### Experiments

For characterization purposes of the OptoForce and jamming membrane feet, the first series of experiments focuses on the friction between the foot and a flat smooth surface. Moreover, the damping behavior of the foot when dropped onto hard ground is observed. Both these effects occur during locomotion. The touch down of a foot involves a certain damping of the impact forces. Once on the ground, friction allows the robot to propel.

Four different cases - two cases for the previously used foot designs and two cases with different levels of pressure and thus changed mechanical properties for the proposed membrane foot design - are compared:

---

[1] https://www.amarsi-project.eu/

[2] http://optoforce.com/

1. Ball-shaped compliant OptoForce sensors (OF)
2. Ball-shaped compliant OptoForce sensors covered with Socks (OFS)
3. Ball-shaped Jamming Membrane foot at Atmospheric pressure (JMA)
4. Ball-shaped Jamming Membrane foot Vacuumized (JMV)

The series involved observing (i) sliding friction behavior on a flat, smooth surface and potential elastic and plastic deformation of the feet during and after the test, and (ii) the damping property when falling on hard ground and consequent elastic and plastic deformation.

The experimental setup is kept as simple as possible to avoid unknown sources of error. Two pairs of the respective feet are mounted under a plastic plate and charged with the same weight as Oncilla. For measuring sliding friction, the platform is manually pulled sideways and transitioned into a steady-state sliding motion. The sliding friction force is measured with a digital scale (Burgwächter Tara PS 7600). Each setup is recorded with a high speed camera at 240 fps in HD-quality. Plastic and elastic deformations are observed during and after the test and classified qualitatively using snapshots of the high speed camera videos. The friction experiments were only performed on one type of smooth surface (plastic coated wood). For damping, we let the platform fall onto a concrete floor from a height of 5 cm. Analyzing the high speed videos, we determine the time from the first ground contact until none of the feet loses ground contact caused by bouncing off the ground (where a 0 would mean that the first ground contact does not bounce off) and count the maximum number of bounces occurring during this time. A measurement of the more conventional coefficient of restitution would require a more advanced experimental setup which was not developed for these experiments. Each experiment is repeated five times and, if applicable, the mean and standard deviation are given in Tab. 4.1. For the maximum number of bounces, the median is given.

### Results

The experiments concerning the friction between the foot and the ground revealed that the silicone OptoForce sensors possess the best adherence to the ground, although drastically reduced when covered with socks. Jamming membranes also show good adherence properties which are comparable to the silicone OptoForce sensor. The differences lie in the magnitude of elastic and plastic deformations as depicted in Table 4.1. While OF are affected very little in both configurations, JMA and JMV undergo large elastic and especially plastic deformation (of the entire foot, not only the membrane, see Fig. 4.5). The granules conform even better to the ground under atmospheric pressure than under vacuum.

OF experience strong bouncing that can be reduced by covering them with socks (OFS). Interestingly, both jamming membranes show a different behavior. The impact energy rearranges the granules, which converts the kinetic energy into heat dissipation through friction between the granules. This leads to large plastic deformations. Granules under atmospheric pressure are able to profit the most from this phenomenon, whereas granules under vacuum, due to their confined arrangement, exhibit it to a lesser degree (Fig. 4.6). At the same time the spring

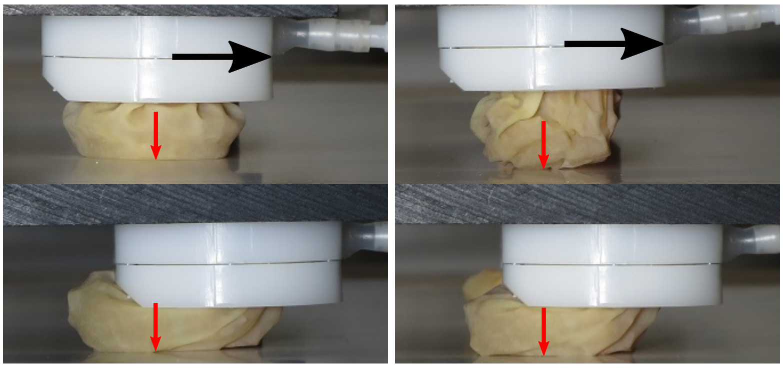

Figure 4.5 – Plastic deformation of JMA (left column) and JMV (right column). The first row shows the foot before applying force sideways (arrow). The second row shows the plastic deformation of the same foot after releasing the force. The red arrows approximate the central contact point. When applying the force to the feet, it is not directly transferred to the ground but transitioned into the plastic deformation, causing a horizontal shift. This could serve as the before mentioned additional degree of freedom.

behavior is changed. The level of vacuum controls both properties at the same time. This could lead to experiments where e.g. static gaits require stronger damping and dynamic gaits require higher spring stiffness, which both are controlled over the vacuum applied.

In summary, the four different feet can be described as follows: (i) OF are bouncy feet with high friction and very low plastic deformation; (ii) OFS are less bouncy with low plastic deformation and low friction; (iii) JMA are extremely plastically deformable feet with high friction and high damping abilities and (iv) JMV are plastically deformable feet with high friction and relatively strong damping abilities.

| Test | OF | OFS | JMA | JMV |
|---|---|---|---|---|
| Friction force [N] | 59.3 ± 1.2 | 10.5 ± 0.5 | 54.9 ± 3.3 | 47.2 ± 3.1 |
| el. deform. | − | −− | ++ | + |
| pl. deform. | −− | −− | ++ | + |
| Damping time [s] | 0.6 ± 0.045 | 0.54 ± 0.049 | 0.27 ± 0.005 | 0.35 ± 0.04 |
| bounces | 5 | 4 | 2 | 3 |
| el. deform. | + | + | −− | − |
| pl. deform. | −− | −− | ++ | + |

Table 4.1 – Results of characterization tests; qualitative comparison from large deformation (++) to no deformation (−−)

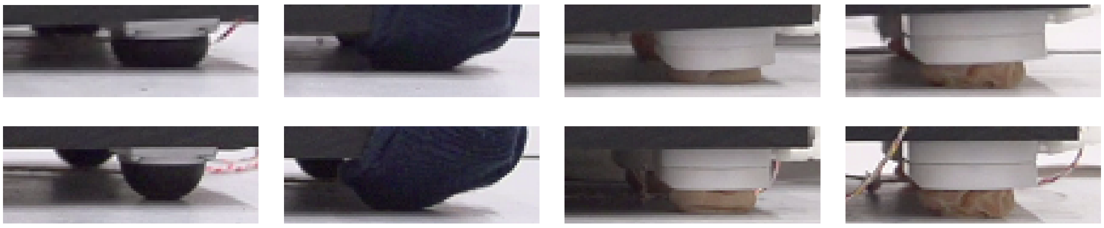

Figure 4.6 – Snapshots of the damping tests. The first row shows the elastic and plastic deformation of one foot during the first compression after releasing the platform from 5 cm. The second row shows the plastic deformation of the same foot after the platform comes to a rest. 1. column - OF, 2. column - OFS, 3. column - JMA, 4. column - JMV

### 4.3.2 Effects of jamming on speed and locomotion behavior with "Oncilla"

#### Experiments

The second series of experiments focuses on the locomotion behavior of the robot. The gait used for all experiments is the fastest open-loop trotting gait found for OFS on flat ground [4]. The following test series were performed: (i) Forward and backward locomotion on flat ground, and (ii) forward and backward locomotion on an inclined smooth surface.

These experiments were again recorded with a high speed camera at 240 fps and aimed towards speed, which was determined by running the robot for a predefined distance and measuring the time. These speed tests were performed on linoleum with similar friction properties as the surface of the previous experiments. Each configuration was repeated three times. The second outcome that is derived from the high speed camera is the quality of the used gait, meaning if it meets the characteristics of a walking-trot shown in [64], such as a symmetric footfall pattern, ground clearance and stride cycle behavior. In Tab. 4.2, the mean speed is noted and descriptions of the gaits are given in section 4.3.2.

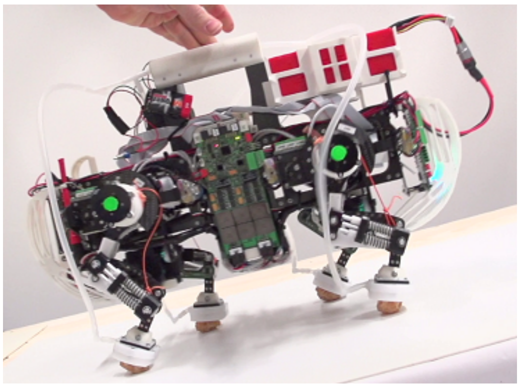

Figure 4.7 – Snapshot of Oncilla running backwards on a slope with 14° inclination; used foot configuration is JMV

The experiments on the inclined surface aimed only at testing the ability of climbing up the slope. The inclination was measured manually and chosen such that the feet using the OFS could not climb the slope due to slippage. Table 4.3 summarizes the different configurations with a short description if climbing the slope was successful and indicating the reason of failure otherwise. Because the open-loop gait is tuned for flat ground, the robot would fall backwards when run on the slopes. Thus, we introduced an offset which modifies the foot trajectory. By shifting the trajectory backwards (negative offset), the robot leans forward, enabling it to keep its balance on the slope in forward locomotion.

#### Results

To assess the robot's behavior on even ground, speed is an important metric. Additionally, the quality of the gait in terms of conformity to the animal gait should be evaluated. Hence the walking trot gait implemented here should show symmetrical movement, with the diagonally opposite feet striking the ground at the same time instant, with no flight phases [64]. Analyzing the similarity to the animal gait it has to be noted that backwards trotting is very unusual in nature. Here the animal would turn around and advance head first. Referencing Table 4.2, forward gaits are generally slower than their backward counterpart although the foot trajectory was not specially adapted. The explanation for this behavior is rather found in the structure of the leg than the influence of the ball shaped feet. When running backwards, the angle of the touchdown is much steeper than forwards, resulting in better transmission of the force to the ground and thus in increased propulsion. It is important to notice that the proposed foot design solely focuses on mimicking the soft paw-pads of e.g. cat feet and does not take the role of toes into account, which are expected to play a key role in the transmission of forces, possibly improving especially the forward locomotion. Looking at forward locomotion, OFS yields the fastest speed as the socks allow the robot to slide forward if ground contact already happens during protraction. All other designs show slightly slower movement. Backwards, JMV leads with the fastest speed followed by the OFS. The OFS have low surface friction due to the socks and the JMV allow for elastic deformation due to the soft rubber cubes forming a better ground contact of a half cylindrical shape. The slight advantage of the JMV can be explained by the increased friction compared to the slightly slipping OFS in the very last moment of the stance phase, allowing it to use maximum propulsion. Looking at the walking trot gait characteristics, most of the feet and locomotion directions show good similarity, including simultaneous touchdown and liftoff of the diagonal feet, no jumping off the ground and expected ground clearance during swing. This is especially the case for the backward moving JMV, where the gait features can be very clearly recognized. The only exception are the OF during forward and backward movement, and the JMA during backward locomotion. The OF sometimes show little to no lift off during swing phase (protraction), resulting in stick-slip. Furthermore this breaking motion loads the leg springs in an unwanted way, making the robot partly jump and perturb the touchdown synchronization between the legs. The parallel spring of the legs is very often fully extended and serves especially in the backward motion as a buffer to partly compensate for this unwanted perturbation. Oncilla with the JMA in backward

| | OF | OFS | JMA | JMV |
|---|---|---|---|---|
| Speed forwards [m/s] | 0.49 | 0.56 | 0.48 | 0.46 |
| Speed backwards [m/s] | 0.82 | 0.86 | 0.79 | 0.87 |

Table 4.2 – Speed results of on-robot experiments

locomotion exhibits an almost full contact sliding gait that is only able to work due to the high elasticity of the rubber membrane. This gait cannot be characterized as a trot.

After the success of certain configurations, the experiments were also repeated on a steeper slope. In all of the cases, forward locomotion did not result in a successful ascent of the slope. We only considered an attempt as successful if the robot could ascend the slope straight in multiple trials. Although the heading of the robot is in open-loop control, turning away from the slope has been regarded as an indication that the foot contact is not uniform for all feet and imperfect foot placement is not compensated. The backwards locomotion of OF, JMA and JMV for both offsets were all successful for the flatter 14° slope. OF and JMV both managed to ascend the steeper 24° slope in the backwards configuration with a higher offset of the foot trajectory. This is particularly promising for the JMV. Despite its friction being lower than that of OF, it still could climb up the steep slope, indicating the potential of our foot design. At higher inclinations, the current mechanical design of the new feet interferes with the foot trajectories, making further experiments unfeasible.

### 4.3.3 Conclusion of static jamming experiments

We investigated and compared friction and damping properties of four different feet currently in use on the quadruped robot Oncilla. Both proposed novel jamming membrane configurations possess friction similar to the one obtained by the OptoForce sensor. Contrary to the bouncy OptoForce configurations, the jamming membranes show high damping abilities by undergoing large plastic deformation. Locomotion experiments on flat ground demonstrated that the jamming membranes achieve speeds similar to the fastest gait found for the robot Oncilla. A qualitative analysis of high speed videos revealed that most gaits of both jamming membranes and OFS resemble the desired trotting gait, while OF display a rather jumpy behavior. JMA as the exception exhibits a full contact sliding gait when moving backwards. Ascending a smooth slope was possible in multiple configurations including JMA and JMV, indicating that the jamming membrane is a promising foot design for legged locomotion.

| Foot | Dir. | $\Delta x$ | $\Phi$ = 14 [deg] | $\Phi$ = 24 [deg] |
|---|---|---|---|---|
| OF | f | -0.03 | turning | 0 |
| | | -0.05 | turning or falls | 0 |
| | b | 0.03 | successful | falls |
| | | 0.05 | successful | successful |
| OFS | f | -0.05 | not enough friction, slides | 0 |
| | b | 0.05 | not enough friction, slides | 0 |
| JMA | f | -0.03 | unsuccessful, feet frames touch ground | 0 |
| | | -0.05 | not enough friction, slides | 0 |
| | b | 0.03 | successful | turning |
| | | 0.05 | successful | unsuccessful, feet frames touch ground |
| JMV | f | -0.03 | unsuccessful, feet frames touch ground | 0 |
| | | -0.05 | foot clearance too small | 0 |
| | b | 0.03 | successful, feet frames touch ground | keeps position on slope |
| | | 0.05 | successful, feet frames touch ground | successful |

Table 4.3 – Slope tests; f - forwards, b - backwards, $\Delta x$ - offset of foot trajectory [m], 0 - test not performed

## 4.4 Dynamic jamming: fast state-switch at touchdown

Whereas the last section only showed the effects of static jamming on locomotion performance, the jamming ideally should act dynamically on the feet during the stance phase: the membrane has the best damping properties in its soft state to absorb the impact energy of a touchdown, but the solid state provides better force transmissibility. This section describes a mechanism to quickly switch from the soft to the solid state of a jamming-based foot and discusses the effects of this transition on locomotion forces. Our aim is the application of such a system in mobile, untethered robots which could make the use of a usual vacuum pump unpractical. To enable mobile jamming, we here propose a mechanism that uses an air storage system and a magnetic solenoid for fast state-switching.

### 4.4.1 Preliminary evacuation mechanism

The setup is shown in Fig. 4.8. The foot is formed by compliant cubic granules enclosed in a spherical latex membrane (diameter ≈ 2 cm). The membrane is connected to an air container (Fortuna Optima All Glass Syringe, 50 ml) whose volume can be changed, forming a closed air system with the membrane. Starting from atmospheric pressure where the granules are in their fluid state, enlarging the volume of the air container by pulling the piston lowers the vacuum pressure in the whole system, transitioning the foot into its hardened state. The piston of the glass syringe is attached to the anchor of a magnetic solenoid (ITS-LZ 2560, ≈ 15 W) which, when activated, pulls on the piston with a strong magnetic force. A microcontroller (Arduino Nano) controls the activation of the solenoid by measuring the pressure inside the membrane with a pressure sensor (Honeywell 030PAAA5). When overpressure is detected in the membrane caused by e.g. touchdown of the foot, the solenoid immediately gets activated and the membrane evacuated. Two batteries in series (Conrad energy 7.4 V, 1200 mAh, 10 C) power the electronics. The foot - imagined on a real robot - acts in the following manner: In swing phase, the foot is in its soft state which enables damping of the impact at touchdown and passive shape adaptation to structured terrain. Upon touchdown, the foot immediately hardens, allowing the transmission of locomotive/friction forces. In swing phase, the foot then can be brought back to its soft state (not shown here).

### 4.4.2 Evacuation speed

#### Experiments

To measure the evacuation time, the position of the solenoid with respect to the syringe was chosen such that the enlargement of the volume (caused by pulling the piston) resulted in a pressure difference of -180 mbar versus atmospheric pressure (same as in section 4.3). The time to reach this pressure difference was recorded in 5 trials.

#### Results

The results showed that the solenoid achieves the desired pressure in 62.2 ± 3.6 ms. As a comparison, for a walking trot gait at 1 Hz with a dutyfactor of 0.5, this would correspond to 12.4 % of the stance duration which was regarded as fast enough to perform the experiments on ground reaction forces.

### 4.4.3 Effects on ground reaction force

#### Experiments

To investigate the ground reaction forces, a series of experiments with three different feet were performed: the previously used OptoForce sensors (OF), the proposed foot in atmospheric

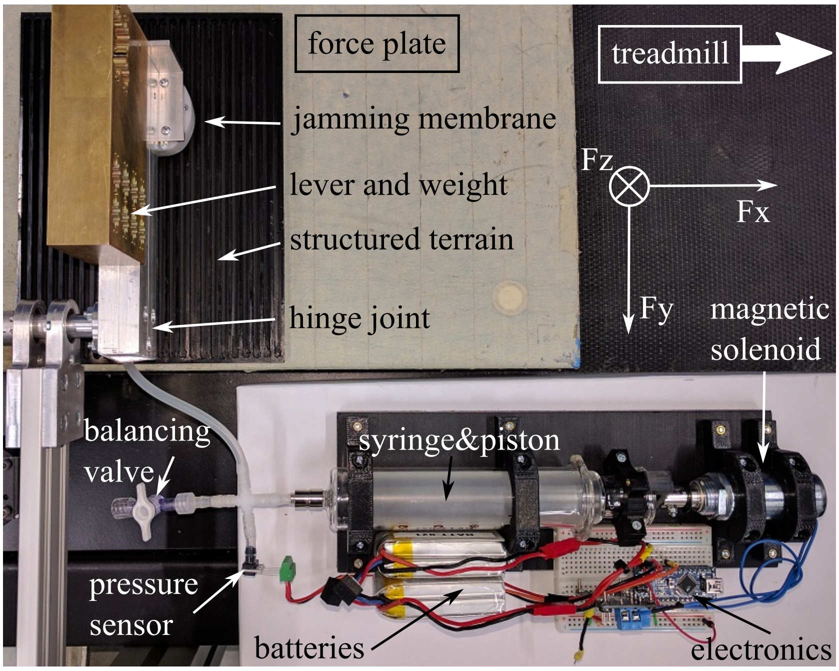

Figure 4.8 – Complete setup (top view). A jamming membrane is attached to a simplified leg (hinge joint and lever) and connected to an airtight glass syringe whose piston is fixed to the anchor of a magnetic solenoid. A treadmill moves a structured terrain, mounted on a force plate, at a constant speed. The membrane is dropped onto the ground, causing the pressure sensor to trigger the evacuation of the membrane upon ground contact. The solenoid and electronics are powered by two batteries. The manual balancing valve is used for a reset to atmospheric pressure.

pressure (soft state) only (JMA) and the proposed foot with state-switching (JMSS). A structured ground (grooves perpendicular to the locomotion direction) is moved with a constant speed of 0.1 km/h (0.028 m/s) on a treadmill to simulate steady-state locomotion. A simplified leg (hinge joint and lever) drops an attached foot from a height of 2 cm perpendicular to the ground plane. The forces in z- and x-direction in [N] (see Fig. 4.8) are measured by a force plate at 10’000 Hz starting at touchdown and onward until the foot transitions into a steady-state sliding motion, and the touchdowns are recorded with a high-speed camera at 960 fps.

### Results

Fig. 4.9 depicts the time evolution of the normal and drag force for one trial of each foot. The force profile of the normal force as well as the high-speed recording reveal that OF bounces off the ground several times before it is able to transmit drag force, which in steady-state sliding motion is comparable to the drag forces of JMA and JMSS. The steady-state normal force is approximately 8 N is all cases. Both JMA and JMSS barely show any rebound, leading to improved damping properties and almost immediate drag force transmissions. However, for JMA mainly the stretching of the membrane causes a gradually increasing drag force. In

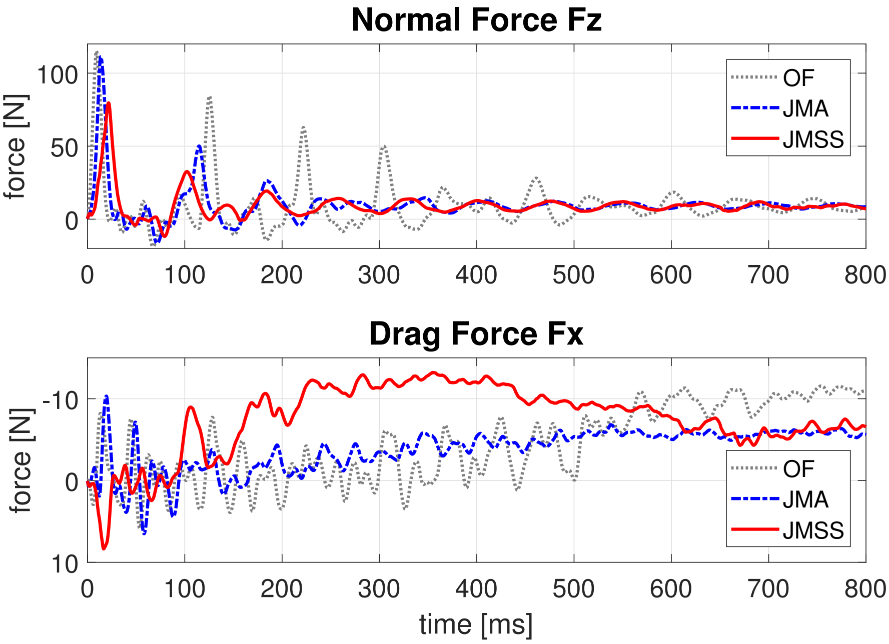

Figure 4.9 – Normal and drag forces of the drop tests of the three tested feet. JMA and JMSS show similar damping properties while OF bounces off the ground several times, delaying the transmission of drag forces. JMSS is able to transmit higher drag forces than OF and JMA, specifically immediately after touchdown.

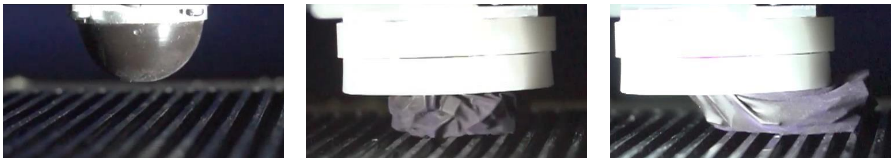

Figure 4.10 – Images extracted from high-speed recordings. Left: OF at 80 ms after touchdown in rebound; Middle: JMSS at 80 ms in hardened state without rebound; Right: JMA at 1.5 s with stretched membrane in steady-state sliding motion.

contrast, JMSS immediately hardens after touchdown and therefore can transmit a higher drag force much faster. Additionally, JMSS also profits from the passive shape adaptation and thus hardens in a terrain-adapted shape. This in combination with the damping ability enables JMSS to apply a drag force approximately one order of magnitude higher than OF and JMA right after touchdown, actively using the structure of the terrain. Fig. 4.10 shows images extracted from the high-speed recording. On the left, OF is shown at approximately 80 ms after the first touchdown where it lost ground contact due to rebound. In the middle, JMSS is shown at the same time instance; it already almost fully damped the impact and switched into the hardened state, starting to transmit drag force. On the right, JMA is shown in steady-state sliding motion (after ≈ 1.5 s); stretching of the membrane results in a reduced drag force.

### 4.4.4 Conclusion of fast state-switching experiments

Ground reaction forces, recorded for drop experiments onto a structured moving ground, indicate that (i) the soft state improves the damping of impact forces compared to previously used feet and enables passive shape adaptation, and (ii) fast state-switching allows a faster transmission of drag forces. This additionally get augmented by profiting from the shape adaptation, both promising aspects for legged locomotion. For an integration into a real robot however, the mechanical design of the evacuation system needs to be revised.

## 4.5 Dynamic jamming: adaptive feet for rough terrain

As the last project in our study of jamming in locomotion, we combined the previous methods to create a mobile, autonomous quadruped robot that dynamically switches between the two states of a jamming membrane. Due to the shape adaptation capabilities, this robot shows its full potential to locomotion for rough terrain. The foot conforms to such terrain while being soft and the switch to the solid state then performs a kind of gripping of the terrain. This section describes the development of a new evacuation system, its local sensory feedback and the implementation into a simple quadruped robot to demonstrate the advantages of jamming membranes as adaptive feet.

### 4.5.1 The MODOK quadruped robot platform

**Main platform:** Research in this and the following chapter required the development of a simple and adaptable quadruped robot that could be equipped with the necessary sensors and modifications needed for a specific set of experiments. Our aim was to create a mechanically simple robot and add a computational unit that is able to gather various sensory information in a centralized place. MODOK embodies a simple quadrupedal morphology with four planar limbs mounted symetrically on a rectangular, wooden plate. Each leg consists of 2 servo motors for hip (Dynamixel RX-28, 18 V) and knee joint (Dynamixel AX-12A, 12 V) that are connected in series such that their movement remains in the sagittal plane. The platform is relatively low-budget by mainly using off-the-shelf components, and is highly customizable and rapidly reconfigurable due to its modular nature. This allows rapid performance of experiments on different morphologies with variable structural and compliance properties. The dimensions of the body are 30 cm x 43 cm, the total height of the robot is 26 cm and the length of each leg (with the foot) is 22.5 cm (Fig. 4.11). In parallel to the hardware, a model in the physics simulator *Webots* was also created, keeping the parameters of the model as close as possible to their physical counterpart.

**Sensors:** A variety of on-board and off-board sensors are integrated in the system, both for measuring locomotion parameters and controlling the robot. On-board are encoders in each servo motor, an IMU (Xsens MTi-3 AHRS) measuring roll, pitch and yaw angles as well as acceleration in x-, y-, and z-direction, and a current sensor (Texas Instruments INA 169)

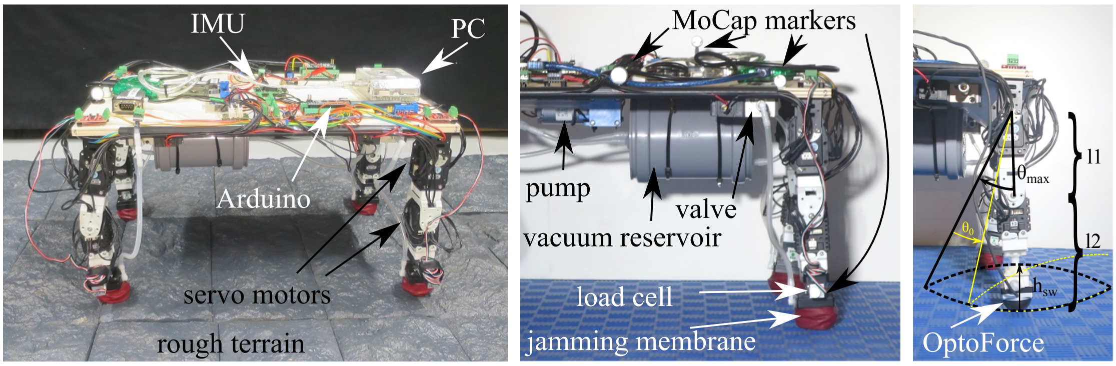

Figure 4.11 – The MODOK platform. Left: The quadruped robot standing on the used rough terrain. A main body frame holds an embedded PC (Odroid), IMU and the separate evacuation control unit. Four legs are fixed on each edge, consisting each of two servo motors in series (hip and knee) and the foot. The total weight of the robot is 30 N. Middle: The pump, vacuum reservoir and valves are fixed underneath the main frame. The evacuation of each foot is triggered by a load cell mounted directly on top of the jamming membrane. Right: Configuration of the leg with an OptoForce sensor as the foot and parameters of the trajectory.

measuring the motor power consumption with an Arduino Nano. The robot can use OptoForce sensors (OMD-30-SE-100N) as feet for force feedback control. However, the experiments in this chapter with the OptoForce sensors are open-loop and serve only as a comparison. Instead, each leg is equipped with a load cell (CZL635 0-5 kg) that - with a separate Arduino Nano - measures the load on each leg (Fig. 4.13 (a)). This information is used by the evacuation controller to distinguish the stance phase from the swing phase of each leg. The Arduino also reads a pressure sensor (Honeywell 030PAAA5) connected to the fore left foot to measure the evacuation speed and the reached vacuum pressure level (Fig. 4.11 middle). Further, a Motion-Capture system (MoCap) system provides off-board position and orientation data of the trunk of the robot as well as the position of the lid of the fore right foot.

All the on-board sensors are connected via USB and the off-board sensors via WiFi to an embedded on-board PC (Odroid-XU4) that controls the servo motors and logs all sensor data. The evacuation system of the feet however is designed to be a standalone control unit that can be switched on and off separately and shares no communication with the main PC besides the logging.

**Open-loop CPG-based control:** The movement of a limb is implemented as a phase-oscillator with coupling terms between them to drive the system response towards a desired limit cycle [152, 73, 34, 33, 74]. Fig. 4.12a shows the network of phase-oscillators, where the time response of each limb $i$ is described by the set of coupled differential equations (Eq. 4.1) given as

$$\dot{\phi}_i = 2\pi f + \sum_j w_{ij} \sin(\phi_j - \phi_i - \psi_{ij}) \tag{4.1}$$

where $\phi$ denotes the phase of an oscillator and $\psi$ is the desired phase difference between two

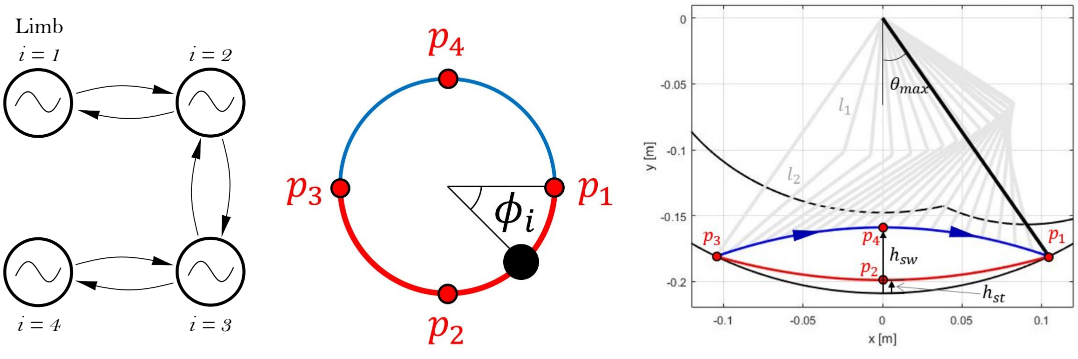

(a) (b) (c)

Figure 4.12 – (a) Network of phase-oscillators with couplings in open-loop CPG and (b) Transformation from limb phase $\phi_i$ to trajectory position in cartesian space . During walking, limb 1 is the right-hind limb (RH), limb 2 is the left-hind limb (LH), 3 is the left-forelimb (LF), and 4 is the right-forelimb (RF). (c) Foot trajectory parametrization: end effector trajectory shown in red for stance phase and in blue for swing phase, limb workspace represented in black, and limb postures during swing presented in gray. The end effector trajectory is parametrized by three parameters and follows the trajectory $p_1 - p_2 - p_3 - p_4$. $h_{st}$ is the distance from position $p_2$ to the limit of the workspace (i.e. comparing to stretched limb) and $h_{sw}$ the distance from the workspace limit to position $p_4$. A trajectory is defined by the maximum amplitude $\theta_{max}$, medium height during swing phase $h_{sw}$, and medium height during stance phase $h_{st}$. Image adapted from [167].

oscillators. The coupling terms adjust the phase update of each oscillator, according to the phase of the neighbors $\phi_j$, to the desired phase shift $\psi_{ij}$ between limbs $i$ and $j$, and to the weight of the coupling $w_{ij}$.

**Foot trajectory:** The high level controller introduced above has as output the phase of each limb ($\phi_i$) at a certain instant. To generate the oscillatory movement of the limb, this phase ($\phi_i$) is then transformed into motor actuations according to a planned trajectory. These trajectories are parametrized in cartesian space and then mapped to the limb phase $\phi_i$, as shown in Fig. 4.12b. Fig. 4.12c describes this trajectory planning within the limb workspace, showing the parameters that define stance and swing phases ($\theta_{max}$, $h_{st}$, $h_{sw}$).

**Parameter selection:** Treating each limb as a phase oscillator with parametrized trajectory following, and therefore coupled motor actuation within each limb, results in a substantial reduction of the search space for finding appropriate locomotion parameters. In the presented case, this allows for fast optimization of the trajectory parameters $\theta_{max}$, $h_{st}$ and $h_{sw}$, along with the desired phase difference $\psi_{ij}$.

The details of the parameter selection can be found in [167] where a combination of Particle Swarm Optimization (PSO) in the physics simulator *Webots* and hardware experiments, optimized for speed and energy efficiency, resulted in a walking trot gait with parameters $\theta_{max} = 0.3$ rad, $h_{st} = 0$ mm and $h_{sw} = 15$ mm with leg lengths $l_1 = 79$ mm and $l_2 = 110$ mm. For the gaits

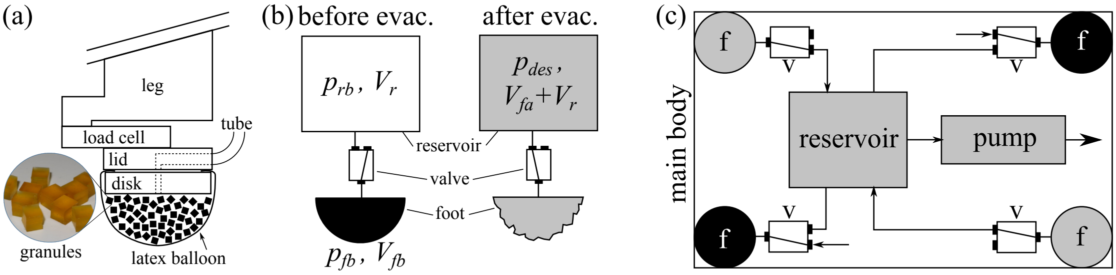

Figure 4.13 – Schematics of the system. (a) A latex balloon is filled with cubic rubber granules and clamped between a disk and a lid to which a tube is connected. A load cell between the foot and the leg measures the vertical load on each leg (front view of the foot). (b) The two systems “reservoir” and “foot”, first separated before evacuation and then in the combined configuration after evacuation. (c) Four feet [f] are each connected to a valve [v] which redirects the airflow to either the outside atmosphere (for a walking trot gait e.g. the bottom left and top right foot) or to the central vacuum reservoir (top left and bottom right foot) in which a vacuum is created by a continuously running pump (view from below).

involving an inclined surface, the trajectory was rotated backwards around the hip joint by $\theta_0 = 0.1$ rad (see Fig. 4.11 right for details) to shift the center of gravity slightly forward to assist the climbing. Due to bandwidth limitations of the servo motors, a gait frequency of 0.5 Hz is selected for all experiments.

### 4.5.2 Improved evacuation mechanism

**Foot design:** The foot design is based on the end effector design in Chapt. 3, consisting of a latex balloon with a diameter of approximately 3.5 cm, filled with the cubic rubber granules. The open end of the balloon is clamped between a disk and a lid to form an airtight seal, where each foot is connected by a tube to the pump-valve-system (Fig. 4.13 (a)).

**Reservoir pump system:** Even though a mechanism for fast evacuation of a single foot based on a closed-air solenoid and syringe system has been shown in the previous section 4.4.1, the system had to be modified because the same mechanism was not scalable for a mobile quadruped. Hence, another system with a reservoir and valves has been developed. A vacuum pump continuously evacuates a single reservoir volume formed by a PVC pipe to which each foot is connected over a separate valve. The valve normally directs the airflow of a foot to atmospheric pressure (soft state). When triggered by a load cell, the valve connects the airflow of a foot to the vacuum reservoir, causing the foot to evacuate to the level of vacuum pressure inside the reservoir (hardened state). These switches are activated depending on the stance and swing phase of each leg individually, described in section 4.5.2.

When dimensioning the pump-valve system, two main aspects were taken into consideration: the required vacuum pressure level and the speed of the evacuation, both defining the performance of the pump, the size of the reservoir and the specifications of the valves. Additionally, the system should be as light as possible to be able to be integrated into a mobile quadruped robot. For the specific requirements, it has been shown in section 4.3 that a pressure difference of -180 mbar in the jamming membrane versus atmospheric pressure produces a significant effect on the locomotion performance, hence the desired pressure difference was around -200 mbar. Further, section 4.4 showed that an evacuation speed of around 60 ms is appropriate to enable the advantages of state-switching. In order to find the performance requirements for the mechatronic components, we define two separate systems, one foot and the reservoir, at two different states - before evacuation and after evacuation - and consider that the pump is switched off in both states (Fig. 4.13 (b)). Since this action only requires the valve to open, it is clear that the total mass of the air during this process stays unchanged, i.e.

$$n_{fb} + n_{rb} = n_{fa} + n_{ra} \tag{4.2}$$

where $n_{fb}$ is the number of moles of air in the foot before evacuation, $n_{fa}$ is the number of moles of air in the foot after evacuation, and similarly for the moles in the reservoir $n_{rb}$ and $n_{ra}$. By considering air as an ideal gas at constant temperature, we can substitute Boyle's law into each component of Eq. 4.2, solve for the unknown pressure inside the reservoir before evacuation and obtain

$$p_{rb} = p_{des} \cdot \frac{V_{fa} + V_r}{V_r} - \frac{p_{fb} \cdot V_{fb}}{V_r} \tag{4.3}$$

where $p_{rb}$ is the required pressure in the reservoir before evacuation in [mbar], $p_{des}$ the desired final vacuum pressure in [mbar], $V_r$ the constant volume of the reservoir in [mL], $p_{fb}$ the pressure in the foot before evacuation in [mbar], $V_{fb}$ the air volume in the foot before evacuation in [mL] and $V_{fa}$ the air volume in the foot after evacuation in [mL]. Eq. 4.3 describes an inversely proportional relationship between the volume of the reservoir and the initial vacuum in the reservoir before evacuation of the foot, i.e. a larger reservoir puts the required initial vacuum pressure closer to the final desired pressure, which in turn reduces the power requirements of the pump. In our case, we define $p_{des} = 800$ mbar, $p_{fb} \approx 1000$ mbar at atmospheric pressure and $V_{fb} \approx 10$ mL. A PVC vacuum reservoir of 500 mL seemed feasible both in size and weight. Since the soft foot deforms under the vacuum, $V_{fa}$ will be only a fraction of $V_{fb}$ and thus around 2 orders of magnitude smaller than $V_r$. In Eq. 4.3, we therefore neglected the contribution of $V_{fa}$ which simplifies the first term to $p_{des}$, resulting in a required pressure of $p_{rb} = 780$ mbar. Next, we need to find a vacuum pump with the appropriate airflow at this vacuum pressure level, i.e. a vacuum pump must be able to evacuate the air volume of the foot within a required time. By again using Boyle's law in Eq. 4.4, we find that the foot volume $V_{fb}$ of 10 mL at $p_{fb} = 1000$ mbar equals a volume $V_{eq}$ of 12.8 mL at $p_{rb} = 780$ mbar by setting

$$V_{eq} = \frac{p_{fb} \cdot V_{fb}}{p_{rb}}. \tag{4.4}$$

This only represents the evacuation volume of one foot. The real robot, with four feet connected to the reservoir (Fig. 4.13 (c)), was designed to have a gait cycle of maximum 1 Hz, meaning that there are at most 4 evacuation events per second. This results in an airflow of $4 \cdot 12.8$ mL/s = 3072 mL/min at 780 mbar. Small-scale diaphragm pumps offer the possibility to reach relatively high levels of vacuum pressure suitable for the present system, hence by taking some performance losses due to e.g. tubing into account, a stronger, relatively lightweight diaphragm pump with the appropriate specifications has been used (Parker D743-21-01, parallel airflow of $\approx$ 3300 mL/min at 780 mbar). The same airflow and pressure requirements also apply to the valves used for each foot (SMC VK332W-6DO-M5-Q). Both pump and valves run on 12 V which is already available on the robotic platform. The pump, valves, reservoir and feet altogether weight roughly 10 N (i.e. one third of the total body mass).

**Jamming membrane state-switch:** The evacuation is controlled by the separate Arduino that processes the data from each load cell in a binary fashion. As soon as a load cell detects the touchdown of a foot, the valve of that foot gets activated, which leads to the evacuation of the foot. Once the leg is determined to be in swing phase, the valve deactivates, resetting the foot reset to atmospheric pressure. It is important to note that this control is local only and acts on each foot individually, regardless of the state of the respective leg or the other legs.

### 4.5.3 Rough terrain

Terrain selection is guided by the hypotheses that (1) the jamming membranes improve friction and damping properties and also influence the overall balance of the robot and (2) the shape adaptation and state-switch of the jamming membranes enables the robot to locomote faster on rough terrain and climb steeper slopes. Hence, flat smooth ground is used to form a baseline, however the majority of the experiments are performed on rough terrain. The terrain consists of a series of bricks fixed on a wooden panel of 0.8 m width and 3 m length. The bricks form a landscape of continuous roughness as well as discrete transitions between the bricks. Fig. 4.11 left shows the roughness of the terrain in comparison to the robot. This terrain is used in the three configurations: flat, inclined by 3 degrees and inclined by 5 degrees.

### 4.5.4 Validation: Evacuation speed 2

#### Experiments

The first experiment was designed to validate the performance of the evacuation system. The robot is initialized to its trot gait and put on flat, smooth ground after the full vacuum in the reservoir has been generated by the pump. The pressure sensor measures the pressure in the fore left foot. The trigger to the valve that evacuates this foot is set to activate as soon as its load cell bears more than 3 N during stance phase, which represents 10 % of the robot's weight. The pressure and load are measured for 7 walking cycles and for each cycle, the time between triggering the stance phase and reaching the maximal vacuum pressure level in the foot is calculated, as well as triggering the swing phase and the time to reset the foot.

### Results

In Fig. 4.14a, the vacuum pressure of the fore left foot is shown for one gait cycle together with the load cell measurement of the foot. Although the system was designed to achieve a pressure difference of around -200 mbar, Fig. 4.14a shows that a pressure difference of around -500 mbar is reached. This can be explained by the slower gait frequency of 0.5 Hz instead of 1 Hz. This effectively halves the required airflow from 3072 mL/min at 780 mbar absolute pressure to around 1500 mL/min, which the pump is still able to deliver at 600 mbar absolute pressure. Considering an overestimation of the foot volume, the airflow likely is even lower, dropping the final pressure to 500 mbar absolute pressure. The larger pressure difference challenges the reported observations of less pressure difference in [60]. However, instead of adjusting the mechatronic components to achieve the weaker -200 mbar difference, we speculated that the qualitative aspects of the state-switch (namely to trade damping and adaptation capabilities for force transmissibility) still hold true, and may even be more pronounced with the higher pressure difference. Nevertheless, the system is potentially over-performing and could be designed with lighter and less power-consuming components, especially a less powerful pump, which is the main reason for the higher pressure difference. Moreover, we did not investigate the optimal pressure difference. Our experiments with this type of membrane and granules however suggest that a wide range of pressure difference is able to create the desired effect of state-switching, potentially with varying characteristics, which may be useful for gait-dependent stiffness adaptation. In any case, even the larger pressure difference is achieved in 61 ± 3.8 ms from the time that the load cell triggers the evacuation, and the evacuation itself takes only 49 ± 4.1 ms. This was considered well within the desired characteristics. Further, even though no active inflation process is implemented, the membrane reset to atmospheric pressure after the trigger takes only 47.7 ± 4.4 ms (where the actual inflation takes 31.9 ± 4.9 ms). Concerning the load, it can be seen that a trigger of 3 N (10 % of the total body mass of 30 N) is appropriate to avoid false triggers due to noise. Further, the leg typically supports 15 N during the stance phase, which is the moment where the total body mass is supported by two legs only, resulting in each leg bearing half of the total load. No significant force peaks due to impacts and dynamical effects are visible.

### 4.5.5 Validation: Altering ground reaction forces 2

### Experiments

After the successful validation of the evacuation system, the altering of ground reaction forces was investigated to test the improvement of friction and damping properties in hypothesis (1). As described earlier, the jamming membrane is thought to act in two stages: it first damps vertical impact forces of the touchdown in its soft state and enables shape adaptation, which is expected to lead to a faster undisturbed contact between the membrane and the terrain. It then transmits horizontal propulsion forces after the state-switch to the hardened state. To exploit the full advantages of this state-switch, it is clear that it should transfer the physical characteristics of the membrane from the best case for damping and shape adaptation to the best case for force transmission. As described earlier, we may not achieve the best force transmission configuration as we only investigate one solid-like state given by the performance of the evacuation system. This only creates a more suitable condition for controlled force transmission but not necessarily represents the best case; more experiments are needed to move towards optimality. However, for the damping and shape adaptation configuration, the best case is when the granules are able to flow under atmospheric pressure. It is shown in [62] and [60] that any negative pressure difference in the membrane changes the spring characteristics and thus bounciness, deteriorating the damping capabilities. Additionally, unconstrained shape adaptation requires the granules to be in their unjammed state which is the case when no pressure difference between the surrounding atmosphere and the inside of the membrane is present. These considerations lead to the rationales that for our experiments, (i) the state-switch is necessary as it is the enabling method to modify the physical characteristics of the foot, which is the basis for our hypotheses; and (ii) the state-switch occurs from atmospheric pressure to the pressure difference given by the evacuation system to produce the maximal modification in these physical characteristics.

Even though it is intuitive that the state-switch should happen as quickly as possible, it could be beneficial to delay the switch, especially not to weaken the damping phase (e.g. the membrane is hard before the impact is fully damped which would prevent the maximal damping effect). Thus, drop tests similar to [61] have been performed with different delays. A jamming membrane with its load cell is fixed on a hinge that restricts the movement to only let the membrane fall vertically onto a horizontally moving force plate from a height of 1.5 cm (maximal height of the stance phase). The foot is weighted such that the steady-state vertical gravitational force corresponds to one quarter of the robot's weight (7.5 N). A treadmill moves the force plate horizontally with 8.3 cm/s (0.3 km/h), which is comparable to the tested maximal speed of the robot with the jamming membrane feet (9.6 cm/s). The membrane is then dropped onto the force plate which records the vertical and horizontal forces in [N] during and after touchdown at 10'000 Hz. Fig. 4.14b shows the setup of the drop test experiments. The drops were also recorded with a high-speed camera at 960 fps. The time between the detection of ground contact by the load cell and the activation of the evacuation valve is varied between 0 ms, 25 ms, 50 ms and 75 ms. For each configuration, 3 trials were recorded and smoothed with a moving average filter with a window size of 10 and equal weights. Then, the mean and standard deviation is calculated with the curves synchronized to the time of the maximal force of the first impact force peak. Additionally, the results are compared to the previously used OptoForce sensors as well as the jamming membrane under only atmospheric pressure (soft state) and full vacuum pressure (hardened state) respectively.

### Results

The force measurements of the drop tests are displayed in Fig. 4.14c. Each graph shows the mean and standard deviation of the 3 trials performed. For each configuration, the motion of the foot undergoes different phases. At first, depending on the damping capabilities, bouncing may occur, as the vertical force recordings show a declining force peak pattern. During this period, the horizontal forces applied to the moving ground are stochastically around zero as no proper ground contact has been formed yet. Only after the foot comes close to a rest in vertical motion is it able to cause a gradual increase in the horizontal forces. All configurations then end in a steady-state sliding motion with comparable forces in both horizontal and vertical directions. The two main criteria for selecting the best foot configuration are the damping behavior and the propulsion delay, where we are aiming at the fastest impact damping and shortest propulsion delay. The top graph in Fig. 4.14c focuses on the damping of the vertical impact (normal) forces. It can be seen that the OptoForce sensor (OF) possesses poor damping capabilities, which is manifested in several bounces after the initial touchdown. This is an undesired effect as it delays the transmission of the horizontal propulsion forces which is expected to reduce the locomotion speed. For the jamming membrane under full vacuum (JMV), the bouncy behavior is less pronounced with three peaks that can be distinguished after the initial touchdown. Additionally, the fully jammed membrane results in the overall stiffest configuration. This is visible in the force peak of the first touchdown which is higher and shorter than in the other configurations, as well in the higher bouncing frequency, indicating inferior damping capabilities. Lastly, the best damping characteristics are shown by the state-switching jamming membranes which display at most two rebounds. For the state-switching jamming membranes with different delays, no significant observation could be made as they all show a similar damping behavior. The influence of the delay is more visible in the bottom graph of Fig. 4.14c where horizontal propulsion forces are visible for the different configurations. OF and JMV are excluded and omitted for visibility reasons and due to their inferior damping characteristics and only the state-switching jamming membrane cases are shown (JMSS). A tendency for later shear force transmission with increasing evacuation delays is visible, e.g. between 100 ms and 250 ms the cases with a shorter delay already transmit higher shear forces. This trend, together with the observation about the similar damping behavior above, led to the selection of the case with the shortest delay possible, i.e. the jamming membrane with 0 ms evacuation delay has been chosen for all following experiments.

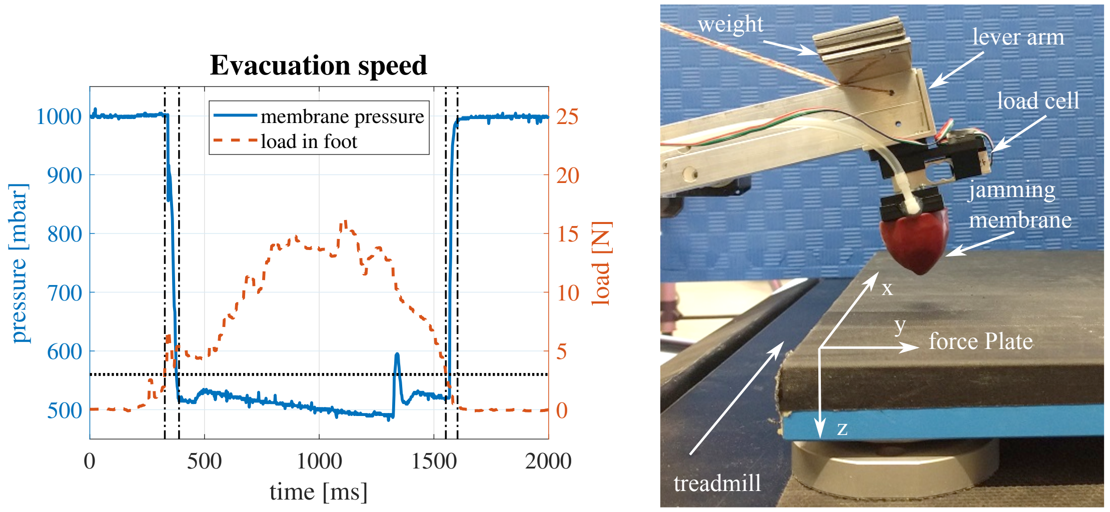

(a) Pressure and load cell measurements of the fore left foot during one gait cycle. After the load cell triggers the evacuation at 3 N (dotted horizontal line), it takes approximately 61 ms for the foot to reach a pressure difference of -500 mbar (black vertical lines on the left). The leg supports up to half of the total body mass during stance phase and triggers the membrane reset to atmospheric pressure again at 3 N; the reset takes approximately 48 ms (black vertical lines on the right).

(b) Setup of the drop test experiments. A hinge drops the attached weighted foot from a height of 1.5 cm onto a horizontally moving force plate which measures vertical and horizontal ground reaction forces. Drops were performed with an OptoForce sensor, jamming membranes with evacuation delays (0, 25, 50 and 75 ms) as well as atmospheric pressure and full vacuum.

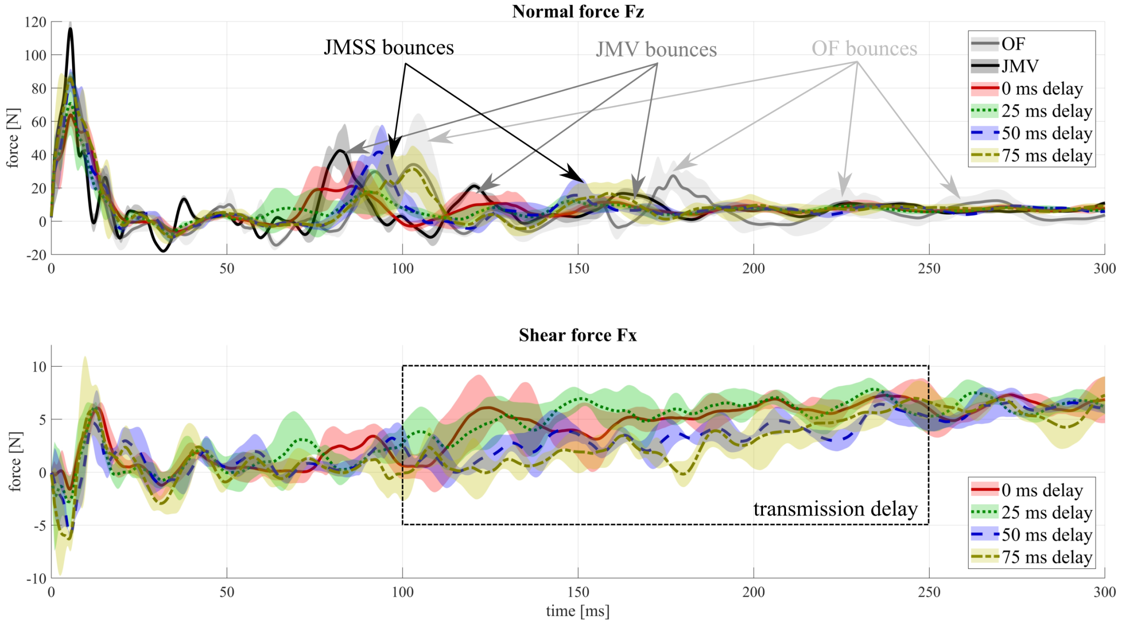

(c) Force measurements of the drop tests. Each graph shows the mean (bold) and standard deviation (shaded area) of 3 trials. Top: Vertical impact forces. OF and JMV bounce off the ground several times, delaying the transmission of horizontal propulsion forces. The jamming membranes possess an improved damping, however different evacuation delays in them do not significantly alter the damping behavior. Bottom: Horizontal propulsion forces (OF and JMF are omitted for clarity). A shorter evacuation delay has a tendency to yield faster shear force transmission (e.g. between 100 ms and 250 ms); the shortest delay of 0 ms has been chosen for the locomotion experiments.

Figure 4.14 – Validation: evacuation speed and impact forces

### 4.5.6 Locomotion on rough terrain

**Experiments**

Lastly, the locomotion performance of the robot with the jamming membranes as feet is analyzed. To test the shape adaptation and locomotion performance in hypothesis (2), locomotion is performed on 4 different terrain layouts: (i) flat, smooth ground, (ii) flat, rough terrain, (iii) rough terrain with an inclination of 3 degrees and (iv) rough terrain with an inclination of 5 degrees. On each of these layouts, the locomotion performance is compared in four different foot configurations: (i) OptoForce sensors (OF), (ii) jamming membranes with state-switch (JMSS, 0 ms delay), (iii) jamming membranes in atmospheric pressure (JMA) and (iv) jamming membranes in their vacuumed state only (JMV). For each run, the robot was first ensured to be in a steady-state locomotion pattern. Then, 10 consecutive walking cycles are recorded which includes IMU data, tracking of the main body frame and tracking of the fore left foot.

**Results**

The collected tracking data is split into two metrics. The tracking of the main body of the robot is converted into a global speed $v$ [cm/s] by calculating the overall difference in forward motion $\Delta x$ in [cm] over the duration of 10 cycles (= 20 seconds), i.e. $v[cm/s] = \frac{\Delta x[cm]}{20[s]}$. The respective speed for each tested configuration is indicated in Tab. 4.4. It can be seen that the OptoForce sensors outperform the other feet on the flat, smooth terrain. All jamming membranes perform roughly similarly, with JMA being the slowest configuration. However, when switching the terrain to the flat, rough case, the speed of the OptoForce sensor feet drastically drops and all jamming membranes locomote faster with the state-switching membrane taking the lead. This tendency grows more pronounced in the inclined terrain cases: the state-switching membrane is considerably faster than any of the other configurations - followed by the full vacuum case - and is even able to climb a 5 degrees inclined terrain where the other foot configurations regularly would get stuck.

The second metric of the tracking data considers the foot tracking and is of a more qualitative nature. Fig. 4.15 shows the trajectory of the fore right foot for each foot configuration. In each subplot, approximately two gait cycles of the foot moving on the flat, smooth surface is shown. Then, 10 gait cycles of the foot on flat, rough terrain are displayed. Each cycle is colored from takeoff (black) to the end of the next stance phase (beige). The differences in the trajectories on the feet give some insight into the speed metric in Tab. 4.4 as the trajectory behavior can vary substantially. In the case of OptoForce, a clean trajectory on smooth terrain can be seen which switches to a rather bouncy and stochastic behavior on rough terrain. The foot placement spacing is not uniform anymore and the robot may even move backward for a short duration, explaining the sudden loss in performance of this foot from smooth to rough terrain. The jamming membrane under full vacuum has a similar difference in the shapes of the trajectories as the OptoForce case, however less significant. Nevertheless, the greater bounciness compared to JMSS and JMA leads to irregularities in the foot placement,

| Terrain | Foot | Speed $v$ [cm/s] |
|---|---|---|
| flat | OptoForce (OF) | 12.1 |
| | JM state-switch (JMSS) | 9.6 |
| | JM atmospheric (JMA) | 8.6 |
| | JM vacuum (JMV) | 10.7 |
| rough | OptoForce (OF) | 4.0 |
| | JM state-switch (JMSS) | 6.7 |
| | JM atmospheric (JMA) | 5.7 |
| | JM vacuum (JMV) | 6.4 |
| inclined 3° | OptoForce (OF) | 3.3 |
| | JM state-switch (JMSS) | 5.2 |
| | JM atmospheric (JMA) | 2.8 |
| | JM vacuum (JMV) | 4.1 |
| inclined 5° | OptoForce (OF) | 1.3 |
| | JM state-switch (JMSS) | 3.4 |
| | JM atmospheric (JMA) | 0.6 |
| | JM vacuum (JMV) | 1.5 |

Table 4.4 – Speed comparison on different terrains. While OF has the fastest locomotion on flat, smooth terrain, the state-switching jamming membrane outperforms all other foot configurations on rough terrain and is even able to climb a 5 degree inclined slope.

reducing the speed. Both JMSS and JMA are able to keep the trajectory consistent on the smooth ground as a result of their superior damping capabilities. Their difference lies in the step length: each step of JMA seems to be slightly shorter than for JMSS due to a “wiggling” around the formed contact area at touchdown and especially at takeoff. The wiggle occurs when part of the motion of the leg is absorbed by the soft compliance instead of generating propulsion, thus slightly reducing the step length. In the case of JMSS, the full propulsion movement of the leg can be used due to the state switch, resulting in JMSS outperforming the other configurations on all the tested cases involving rough terrain.

The specifics of the discussed effects of jamming membranes are highlighted in the supplementary video of the respective publication where slow motion recordings of selected cases are compared. The video includes the drop tests, a close-up of the state-switching membrane during locomotion, the differences in the touchdown behavior and real-time robot locomotion on different terrains. Snapshots of the stance behavior of JMSS are shown in Fig. 4.16.

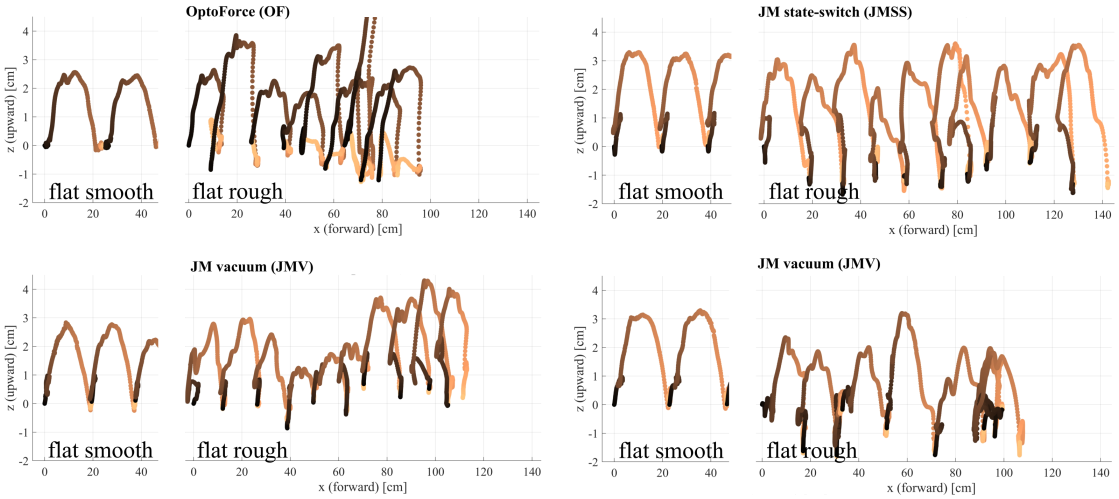

Figure 4.15 – Foot trajectories of the configurations OF, JMSS, JMA and JMV. Each subplot shows approximately 2 gait cycles on flat smooth terrain, followed by 10 gait cycles on flat rough terrain. Each cycle is colored from takeoff (black) to the end of the next stance phase (beige). OF switches to a stochastic, bouncy behavior with non-uniform foot placement when put on rough terrain; a similar transition is visible for JMV, although less pronounced. JMSS and JMA both roughly keep their regular foot placement pattern also on rough terrain due to their superior damping capabilities. A "wiggle" around the contact area formed by the touchdown reduces the average step length of JMA compared to JMSS as part of the leg motion is absorbed by the soft compliance. Due to the state switch, JMSS is able to use the full propulsion movement of the leg, outperforming the other foot configurations in terms of speed in all the experiments involving rough terrain.

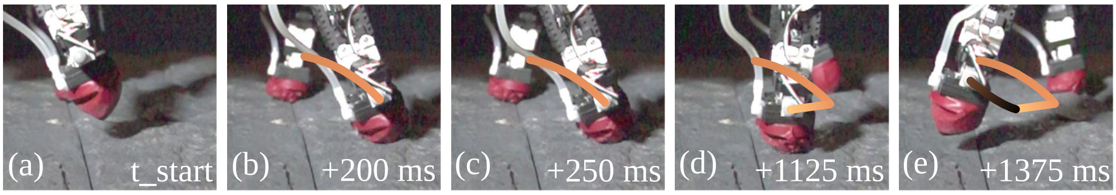

Figure 4.16 – Snapshots of the stance behavior of JMSS. (a) Foot in soft state, approaching touchdown, (b) damping of the impact forces in soft state, (c) state switch to the hard state in 50 ms, (d) foot in support phase, providing propulsion, (e) state switch to soft state after takeoff. The tracking of the foot with the approximate color coding as in Fig. 4.15 is indicated.

## 4.6 Conclusion: jamming membranes as adaptive feet

This chapter presents an experimental study on the usage of compliant universal grippers as feet for legged locomotion. We split the functionalities of a foot during the stance phase into “impact damping” and “force transmission”. Jamming membranes are shown to be well suited as such feet. The soft state can provide a damping mechanism that damps the vertical impact forces at touchdown, enabling a faster undisturbed ground contact. Additionally, the soft state allows a passive shape adaptation of the foot to the ground, which is especially useful when locomoting on rough terrain. The state-switch can then be used to harden the foot in this terrain-adapted shape to transmit the horizontal propulsion forces.

We first investigated the viability of jamming feet on a quadruped robot by measuring generic feet properties of contact friction and impact damping for static jamming. We then more closely inspected alterations in ground reaction forces caused by a dynamic jamming. And lastly, we propose a stand-alone system based on a vacuum pump, a reservoir and valves that is able to quickly and continuously switch the state of jamming membranes as feet. The implementation of the system into a quadruped robotic platform is detailed. The robot consists of a main body and four legs, each formed by two servo motors in series with the jamming membrane as the foot attached. A first validation of the system shows that each foot can separately evacuate to a pressure difference of -500 mbar versus atmospheric pressure in roughly 60 ms, and inflate back to atmospheric pressure in 50 ms. In the used trot gait at 0.5 Hz with a duty factor of 0.5, this corresponds to 6 % and 5 % of the stance and swing duration respectively. Each foot uses the trigger of a local force feedback from a load cell to switch between states independently, regardless of the state of the other legs. A second series of experiments evolved around the optimal delay between the detection of the trigger and the actual evacuation, which was investigated by drop tests of the jamming membranes onto a moving force plate, measuring vertical impact forces and horizontal propulsion forces during and after touchdown. The shortest possible delay was then selected for locomotion experiments both on flat, smooth terrain and flat and inclined rough terrain. It is shown that the superior damping capabilities of the state-switching jamming membrane compared to previously used feet result in a more uniform foot placement pattern even on rough terrain. This enables the robot configuration with state-switching jamming membranes to locomote faster than the other tested configurations on flat rough terrain and even allows the robot to climb steeper inclined terrains with the same open-loop control of the foot trajectory.

Currently used feet in legged robots are often simplistic half-spheres of various materials and rarely possess stiffness variability or shape adaptation capabilities, which could play a key role in the versatility and locomotion performance of animals. In contrast, the unconventional foot design based on the jamming of granular media is a novelty as an attempt to abstract the complex interaction of bones, muscles and tissues often present in animal feet. It is shown that jamming membranes are able to mimic both the compliance and shape adaptation as well as the stiffness variability. Moreover, the transition between these states through the formation of an interlocked system is not unlike the mechanism in humans created by locking and unlocking the tarsal bones.

As this is the first prototype of a mobile quadruped with jamming membranes as feet, there are many possibilities of improvement. For experiments on real outdoor terrains, mechanical modifications are needed especially to increase the durability of the membranes. Over the course of the performed experiments, three membranes had to be replaced due to rupture. A real rough terrain is likely to possess more features that can harm the membrane. Although there has been work on different membrane materials [78, 8], in this study we only explored the often used party latex balloons. Further, transferring the system onto a more powerful robotic platform would give insight into the scalability and limitations of the proposed design. This could include dynamic gaits which are not feasible on the used platform. On such a robot, it could be interesting to have the ability to choose the evacuation vacuum pressure - e.g. based on the gait frequency or ground reaction forces - which would allow a gait-tuned selection of damping and spring characteristics of the foot. In the current system, a foot can only evacuate to a predefined vacuum pressure level in a binary fashion; a more advanced evacuation system would have to be developed. Further, jamming membranes can offer the possibility of multi-functional usage as feet, manipulators/grippers and even sensors, as described in Chapt. 3.

In this chapter, we demonstrated the viability of jamming membranes as feet in legged locomotion and their advantages and basic working principles in a simple system, leaving open many possible directions for further development. We regard the preliminary results in this work as a validation of our approach and see much potential in the method of jamming for the application of legged locomotion.

# Part III

# Mode-switch in control: phase oscillators

# Topic of Part III

## Locomotion with Central Pattern Generators (CPGs)

Locomotion movements under undisturbed conditions seem to follow a periodic rhythm. It has been shown that this rhythm is mainly not controlled by the brain but by the spinal cord, and the brain only gives high-level locomotion signal such as e.g. “start” or “stop”. The spinal cord has the ability to induce rhythmic movement output with a constant input signal, which has famously been demonstrated in the decerebrated cat that walks on a treadmill by only stimulating the brain stem with a constant signal. Interestingly, this resulted in stable locomotion. This indicates that the “blueprint” of locomotion is executed in a feed-forward manner and internal reflex loops in the spinal cord take care of stability concerns.

One way to look at these reflex loops is that they could behave similarly to a compliance, introducing a mechanism that can trade-off adaptability and force transmissibility within a certain dynamic region. This was the concept in [152], a small-scale quadruped with leg compliance. Despite the blindness of the controller, the robot could exhibit robust and energy efficient locomotion. The blueprint of the locomotion is a mathematical abstraction of the rhythmic-output-with-constant-input behavior, described as a Central Pattern Generator (CPG)[73]. In the case of [152], the pattern generating element is a phase oscillator. This is an oscillator whose phase progression $\dot{\phi}$ is described by a function of $\phi$ and other variables $f(\phi, x)$ (Eq. 4.5), i.e.

$$\dot{\phi} = f(\phi, x). \tag{4.5}$$

The phase $\phi$ is used to produce a periodic output $\theta$. As an example, a simple oscillator is given by Eq. 4.6:

$$\theta = A \cos\phi. \tag{4.6}$$

The choice in [152] was to drive a network of such oscillators in a purely open-loop manner where no sensory feedback is acting on $\dot{\phi}$ and let the mechanics of the leg compliance do necessary adjustments for stable locomotion. This was shown to be a successful concept, and because of their simplicity and biological similarity, we use CPG networks for all the locomotion experiments in this part.

## Functionalities in leg movements

The phase progression function $\dot{\phi}$ however is more powerful than driving the system in open-loop only. It gives us an additional degree of freedom that lets us control the velocity of the oscillation. This includes incorporating various feedback terms into $f(\phi, x)$. For legged locomotion, a natural choice for such feedback terms are the ground reaction forces. Each leg in a legged systems is likely to experience a stance phase and a swing phase. By making the phase progression dependent on ground reaction forces, this means that such a feedback term makes the leg move differently in stance and swing.

This is useful if we again draw the correlation to different functionalities, in this case of the leg movement in a locomotion cycle. In the *swing phase*, the movement of the leg has the task of bringing it from the take-off position into touchdown position. This movement is *translating the leg in relation to the body,* and thus its functionality is “displacement of the leg”. In contrast, in the *stance phase*, the movement of the leg has the task of propelling the body. This movement is *translating the body in relation to the leg,* and thus its functionality is “displacement of the body”.

As an example, a newborn kitten is able to move its legs in the air and even somewhat crawl, however it is only after around three weeks where they become strong enough to walk, i.e. when muscles can become stiff enough to counteract gravity. In the air (the swing phase), the leg only has to move itself, whereas in the stance phase it needs to move a portion of the total weight of a body. Under this perspective, it becomes clear that a different set of mechanical properties is required for the two phases, i.e. a mode-switch.

This Part describes how such a mode-switch can be achieved through feedback control of phase oscillators. Its effect can be interpreted as a local computation of trading-off leg displacement and body displacement. We use a clever ground reaction force feedback approach dubbed *tegotae* [83, 117, 118, 116] that switches the phase progression calculation depending on ground reaction forces, and we will detail how this can be interpreted as having a lower joint stiffness in swing and a higher joint stiffness in stance. Chapt. 5 introduces tegotae on a quadruped structure where we analyze its effect on stability and its intriguing property of inducing emergent interlimb coordination. Tegotae is also shown to have beneficial effects for locomotion on rough terrain.

## Control framework for arbitrary legged morphologies

In Chapt. 6, we extend emergent synchronization to the interlimb coordination capabilities of tegotae. Based on previous research, we discuss the prerequisites of multi-legged interlimb coordination. We propose a control framework that aims at creating what we see as the “spinal cord” of a structure, able to execute tasks autonomously as the biological system described in the section above. The goal is to move towards a generic locomotion controller that can generate coordinated locomotion on arbitrary legged morphologies.

Note that the main difference between the legged locomotion in Part II and Part III is that Part II considers a mode-switch method in hardware to create different functionalities of the *foot*, whereas Part III considers a mode-switch method in control to create different functionalities of the *leg*. These methods are not mutually exclusive as they act and perform local computation on different hierarchical levels and could be combined, however the research in this thesis did not get this far and could very well be part of future work on this topic.

# 5 Compliance through tegotae: stabilization and rough terrain locomotion

**Reference publication**

Parts of the text and figures of the following publications have been adapted for this chapter:

- *Mehmet Mutlu,* ***Simon Hauser****, Alexandre Bernardino, and Auke Jan Ijspeert. "Effects of joint compliance in quadrupedal locomotion." The 8th International Symposium on Adaptive Motion of Animals and Machines (AMAM), 2017.*

  **My original contributions**
  - Planning and performing of experiments
  - Data analysis and interpretation
  - Inputs to the manuscript
- *Rui Vasconcelos,* ***Simon Hauser****, Florin Dzeladini, Mehmet Mutlu, Tomislav Horvat, Kamilo Melo, Paulo Oliveira, and Auke Ijspeert. "Active stabilization of a stiff quadruped robot using local feedback." In 2017 IEEE/RSJ International Conference on Intelligent Robots and Systems (IROS), pp. 4903-4910. IEEE, 2017.*

  **My original contributions**
  - Supervision of the master thesis of Rui Vasconcelos
  - Guiding and planning of experiments
  - Performing of experiments
  - Data analysis and interpretation
  - Inputs to the manuscript
- *Mehmet Mutlu,* ***Simon Hauser****, Alexandre Bernardino, and Auke Jan Ijspeert. "Effects of passive and active joint compliance in quadrupedal locomotion." Advanced Robotics 32, no. 15 (2018): 809-824.*

  **My original contributions**
  - Planning and performing of experiments
  - Data analysis and interpretation
  - Preparation of figures for the manuscript
  - Inputs to the manuscript

## 5.1 Inspiration: Compliance in locomotion

Compliance is thought to play a key role in many aspects of locomotion, from safety and gait stabilization to energy efficiency and dynamic gaits (e.g. [6]). It is unclear however which kind of compliance acts on which aspects of locomotion and how to quantify potential benefits. For instance, real animals move in an energy efficient way [40], and according to [54] compliant legs are essential to obtain the basic walking mechanics in bipedal human locomotion.

The following three sections introduce and combine different types of compliance but use the same robotic platform to observe their effects. Section 4.5.1 introduced the MODOK platform. Each of the these sections starts with a brief introduction, followed by a description of how MODOK was adapted for the method used in the section and subsequent experiments and results.

## 5.2 Body compliance: Energy efficiency through joint compliance distribution

A conventional approach to introduce compliance is by adding passive compliance, as demonstrated in [93, 72, 69, 152]. This section briefly explores the MODOK quadruped structure with only passive compliance and where different joint compliance distributions are investigated. This aims at finding the effects of only passive compliance on this structure. A few selected experiments serve as a validation of the platform and sensor gathering methods, and metrics relevant to locomotion are developed and calculated. These later serve as a basis for comparison.

Although this chapter in general focuses on a mode-switch method in control, passive compliance is a mode-switch method in hardware. It is presented here because this brief research ties together with the two following sections, using the same robotic platform. Preliminary results of how joint compliance distribution affects the locomotion performance and variety of other locomotion parameters are described.

### 5.2.1 MODOK configuration

**Compliant modular elements:** Both servo motors in each leg are extended with a series elastic element, called the “compliant element”, that can be easily interchanged. These modular elements are made out of two clamps with a compliant element fixed in between (Fig. 5.1a right). There are three types of elements used in this work: rigid elements out of POM rods (polyoxymethylene) and two types of compliant elements out of super-elastic Nitinol wire. The wires have a diameter of $d = 1.5$ mm (further called “soft”) and 2 mm (further called “hard”) with corresponding flexural stiffnesses 2.3 Nm/rad and 7.3 Nm/rad; torsional stiffnesses 1.75 Nm/rad and 5.54 Nm/rad [170].

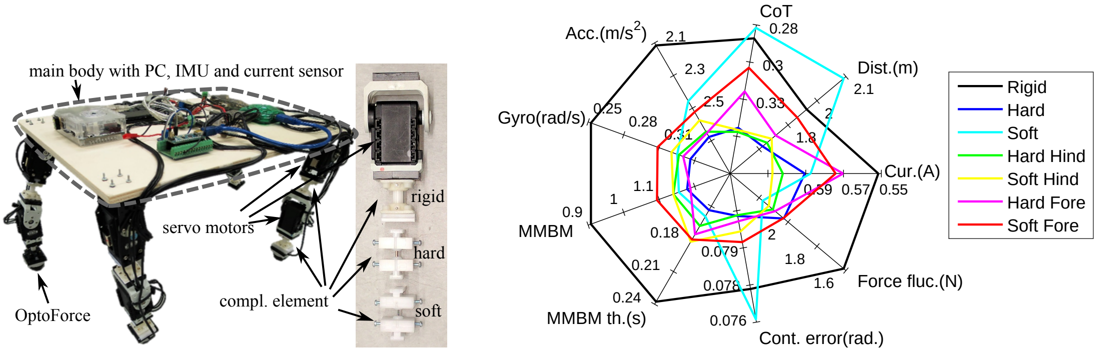

(a) MODOK with compliant elements

(b) Locomotion metrics

Figure 5.1 – Joint compliance distribution experiments. (a) Left: Side view of the robot. It consists of the main body and four limbs, each composed of two servo motors with a compliant element in series. OptoForce sensors are used as feet. Right: one servo motor with the three possible compliant elements. (b) Spider plot of the locomotion metrics with all performed compliance distributions. More desired metrics are positioned further away from the center.

**Sensors:** The robot is equipped with OptoForce sensors as feet. The current sensor measures the total motor power consumption, and the embedded PC reads the position data of the main body from the stream of an external MoCap system and logs all sensor readings with 100 Hz or more (MoCap: 250 Hz, current sensor: 1500 Hz). Thus, all data frames are timestamped with the same clock and they are inherently synchronized.

**Control:** For this preliminary study, a simple open-loop walking trot gait at 0.5 Hz with dutyfactor of 0.5 has been implemented. All the experiments in this study use the same trajectory followed by inverse kinematics by each limb, introduced in 4.5.1.

### 5.2.2 Effects of joint compliance distribution

#### Experiments

Since the control is symmetric and the platform laterally quasi-symmetric, only laterally symmetric compliance distributions have been tested. These are as follows.

**Proximal vs. distal joint compliance:** The compliances closer to the main body (proximal) differ from the compliances further from the main body (distal). It was quickly apparent that the robot only locomotes with rigid proximal compliances; hard and soft proximal compliances did not result in any meaningful behavior. Therefore three experiments were performed: rigid, hard and soft distal compliance with rigid proximal compliance.

**Fore vs. hind leg compliance:** Additionally, four experiments to study fore-hind asymmetries were performed. These are hard and soft distal compliances in the fore and hind legs with rigid proximal elements everywhere else.

#### Results

For each compliance distribution, sensor readings are logged while the robot is walking in steady-state. A concise summary of the results is given in Fig. 5.1b. The most common metrics found in the literature are power consumption, speed and cost of transport (CoT). They are reported as average current (Cur.) drawn by the motors with a constant 18V DC power supply; the distance (Dist.) is taken with the locomotion duration fixed at 20 sec and the ratio of current to distance respectively for the calculation of CoT. The accelerometer (Acc.) and gyro axes show the average euclidean norm of independent x-y-z axes readings. The control error axis is the average position error of the servo motors in all joints while the force fluctuation is the standard deviation of the force sensor readings during the locomotion. Some axes are inverted to position more desired locomotion characteristics further away from the center. Note that the metrics related to “MMBM” involve vision-related metrics that will not be discussed in this thesis; the reader is referred to the original publications [106] and [108].

### 5.2.3 Conclusions of joint compliance distribution experiments

Initial findings indicate that distributions containing hard elements tend to perform worse under the defined metrics, whereas a rigid-proximal/soft-distal distribution even outperforms the distinguished all-rigid distribution in certain metrics, prompting a deeper investigation with more experiments.

## 5.3 Control compliance: Stability through tegotae

In our view, the tegotae feedback emulates joint spring characteristics, introducing compliance into the system. We can use different tegotae parameters to emulate different joint spring characteristics to investigate some of the locomotion aspects mentioned above. This section investigates stability properties due to this form of compliance, using MODOK and applying different forms of morphological changes. In this case, all other forms of compliance are reduced as much as possible to more clearly see the effects of the control compliance.

There are also other ways of achieving control compliance. Using proximal sensors and active control, it is possible to model virtual spring effects and integrate into motor servo control, described as proxy-based sliding mode in [86]. Another use of virtual springs during quadrupedal locomotion is explained in [5]. Impedance control through controlling torque is also widely used to adjust compliance, e.g. [45] shows an implementation on quadrupedal locomotion. Force sensors on the feet can be incorporated to achieve actively compliant locomotion [163] in a morphologically rigid robot. In this thesis, we only considered the tegotae compliance method due to its simplicity and interlimb coordination abilities.

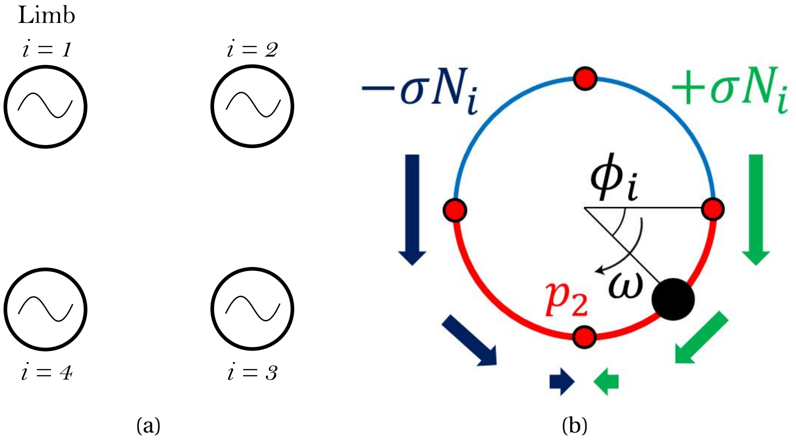

Figure 5.2 – (a) No couplings in closed-loop method based on tegotae and (b) influence of tegotae: Attraction to point $p_2$ proportional to feedback $N_i$ and to $\cos\phi_i$. Image adapted from [167].

### 5.3.1 Tegotae, the rule of good feedback

In tegotae for legged locomotion, each leg movement is generated by a phase oscillator, and the phase, in presence of ground reaction forces during stance, is accelerated towards the stretched stance position of the leg and slowed down thereafter. The interesting aspect of this control architecture is that it is algorithmically completely decoupled. Coupling is only induced by the mechanical connection of the legs through the body.

Whereas in open-loop CPG control coupling terms impose the gait to be performed, tegotae relies on force feedback from the ground and lets the coupling emerge as a dynamic interaction between the brain, body and the environment [83, 118, 117]. It is important to mention that the ground contact forces are felt by each limb separately and the feedback is used locally by affecting only the movement of the corresponding leg. Implemented similarly as in [117], the local reflex mechanism results in an attraction to a stable point $p_2$ (Fig. 5.2b). Thus, the tegotae rule can be considered as a set-point control scheme and it has dampening and exploratory characteristics and imitates a compliant control. The time evolution of each limb's phase ($\phi_i$) is in this case given by the differential equation

$$\dot{\phi}_i = 2\pi f - \sigma\, N_i\, \cos(\phi_i) \tag{5.1}$$

where $N_i$ is the normal ground reaction force and $\sigma$ the attraction coefficient.

During transient, whenever force feedback is felt during a swing phase, the attraction created by the second term of Eq. 5.1 will drive the limb position to the mid-point of stance. All these independent corrections interact through the body dynamics of the robot and drive the system towards a steady state limit cycle where force feedback is experienced only during stance phase, given that the dynamics allow a steady state behavior.

Using this framework we change weight distribution and specific leg lengths, creating symmetrical and asymmetrical body dynamics unknown to the controller. For each configuration, we systematically compare two types of high level controllers: an open-loop CPG-based controller, similar to the one presented in [152], and its closed-loop tegotae-based version similar to the one presented in [117]. Then, experiments with different morphological modifications are described and the results corresponding to the two controllers are compared in terms of stability, symmetry and cycle to cycle correlation.

### 5.3.2 MODOK configuration

For the experiments in this chapter, the MODOK platform is again equipped with four OptoForce sensors to sense ground reaction forces, and the current sensor measures the total motor power consumption. The compliant elements are removed and replaced with rigid elements of the same or different lengths for this section.

### 5.3.3 Emergence of gaits: convergence to walking trot

#### Experiments

Considering the closed-loop decentralized control of each limb, the first series of experiments was intended to examine the capacity of the control to drive the system to steady-state limit cycle locomotion from any initial condition. Three sets of experiments were performed on hardware, starting from different initial gait conditions:

**In-phase limbs:** $\phi_0 = [0, 0, 0, 0]$
**Lateral-sequence (L-S) walk:** $\phi_0 = [3\pi/2, \pi/2, 0, \pi]$
**Diagonal-sequence (D-S) walk:** $\phi_0 = [\pi/2, 3\pi/2, 0, \pi]$

For each of these sets, the transient response was recorded for $\sigma \in [0.05, 0.1, 0.15, 0.2, 0.25]$, until steady-state was reached, where phase differences remained constant. The choice of $\sigma$ is motivated by setting Eq. 5.1 to zero and comparing the first and second term on the right side with $\cos(\phi_i) = 1$. Zero phase progression means that the oscillation is stuck, and so $\sigma$ in Eq. 5.2 should be chosen as to not let a non-maximal force cancel the phase progression completely, i.e.

$$\sigma \approx \frac{2\pi f}{N_{max}} \tag{5.2}$$

#### Results

Gait convergence can be seen in various parameters such as oscillator phases or ground contact forces. Ground contact forces are reported to show the convergence of the gait cycles since they are directly measured with sensors. Fig. 5.3 shows the 3-dimensional ground reaction forces of each foot. In this experiment, the limbs start in-phase ($\phi_i(0) = 0, 1 < i <= 4$)

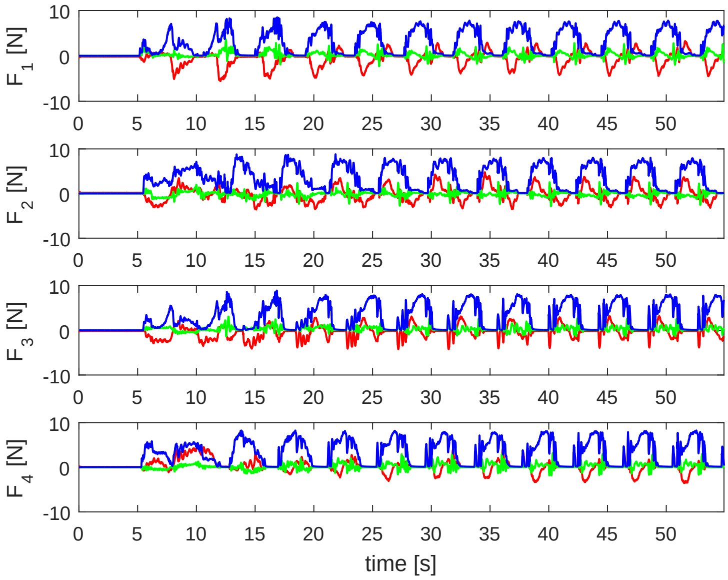

Figure 5.3 – Force measurements of each limb $i$ ($F_{ix}$ in red, $F_{iy}$ in green and $F_{iz}$ in blue) showing convergence to a limit cycle behavior corresponding to trot from in-phase initial condition and $\sigma = 0.1$.

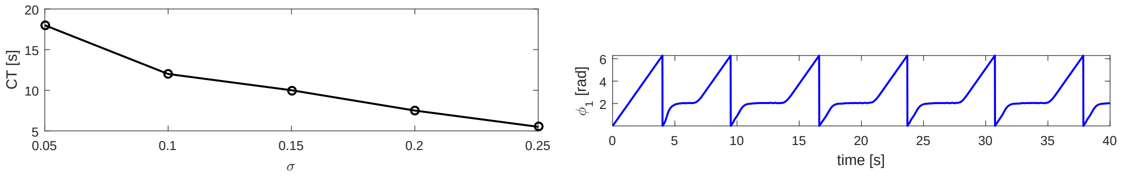

Figure 5.4 – Convergence characteristics. (a) Convergence time (CT) of the gait, from in-phase oscillations to steady-state trot oscillations, with respect to the attraction coefficient $\sigma$. (b) Phase evolution of the first limb in presence of the high attraction coefficient ($\sigma = 0.5$) and low frequency ($f = 0.25$ Hz).

and, with $\sigma = 0.1$, the relatively fast adaptation of the limb phases by physical communication towards a stable periodic trot is visible. Starting from any of the initial conditions given above, the resulting steady-state behavior is a walking-trot.

The time of convergence from in-phase initial condition was found to decrease with increasing $\sigma$, as shown in Fig. 5.4a. The attraction coefficient $\sigma$ should therefore be high enough to allow a fast convergence to the stable limit cycle. However, if this attraction is too high, the phase evolution right after the convergence will be slowed down (Fig. 5.4b), resulting in highly reduced locomotion speed. This is caused by the second term on the right side of Eq. 5.1 counteracting the progressive movement of the first term such that $\dot{\phi}_i$ goes towards zero, resulting in the phase getting stuck in a point attractor.

### 5.3.4 Steady state limit cycle behavior

#### Experiments

Once the effect of local feedback during the transient phase was evaluated, the obtained steady-state behavior was studied. Using the trajectory parameters explained in section 4.5.1, gaits with different attraction coefficients $\sigma$ were analyzed, however the gait was now initialized as trot, based on the previous convergence observation. For different frequencies, a range of $\sigma$ values was tested, where $\sigma = 0$ corresponds to imposing open-loop walking-trot:

**f = 0.25 Hz:** $\sigma = \{0, 0.05, 0.1, 0.15, 0.2, 0.25\}$
**f = 0.50 Hz:** $\sigma = \{0, 0.05, 0.1, 0.15, 0.2, 0.25, 0.3\}$
**f = 0.75 Hz:** $\sigma = \{0, 0.05, 0.1, 0.15, 0.2, 0.25, 0.3, 0.4, 0.5\}$

Throughout these experiments, variables measured comprise: the orientation of the robot, average speed, the DC current used by all the motors, feet contact forces and joint angles.

#### Results

By comparing open-loop cases ($\sigma = 0$) and closed-loop ones with increasing $\sigma$, it is possible to see certain advantages of the latter. The limit cycle response is imposed in open-loop control by the oscillatory couplings. However, the closed-loop control method with tegotae modifies the gait depending on the real-time force feedback, even though the emerging gait was almost always trot. Here, only selected results are presented; a detailed analysis (involving measurements around periodicity and heading) can be found in [167]. Fig. 5.5 highlights some advantages by comparing the open-loop case and a closed-loop one with $\sigma = 0.3$ and $f = 0.75$ Hz. After performing both experiments, five consecutive cycles were selected and their inertial responses presented first in terms of roll versus pitch. This represents an inverted pendulum behavior of the robot's body. Each cycle is colored from blue at the cycle's beginning to yellow at its end. Then, the time evolution of the yaw angles is shown. In this representation, two main advantages are observable. First, in the open-loop case, the orientation suffers from rough changes as can be seen in the peaks of roll × pitch which derive from certain foot collisions with the ground, generating slippage or bouncing. This is correlated with the drift seen in yaw for the open-loop case (Fig. 5.5c). Second, the decentralized closed-loop approach makes the limit cycle more smooth, reducing limping and allowing therefore a more straight locomotion pattern.

### 5.3.5 Gait adaptation to morphological modifications

#### Experiments

Taking advantage of the versatility of the robotic platform, a final series of experiments was performed, applying certain morphological changes. Two types of morphological adjustments were made: (i) variation of mass distribution by a 10% body weight increase (225 g) distinctly positioned and (ii) modification of limb length ($l_1$, $l_2$ or both). The set of experiments per-

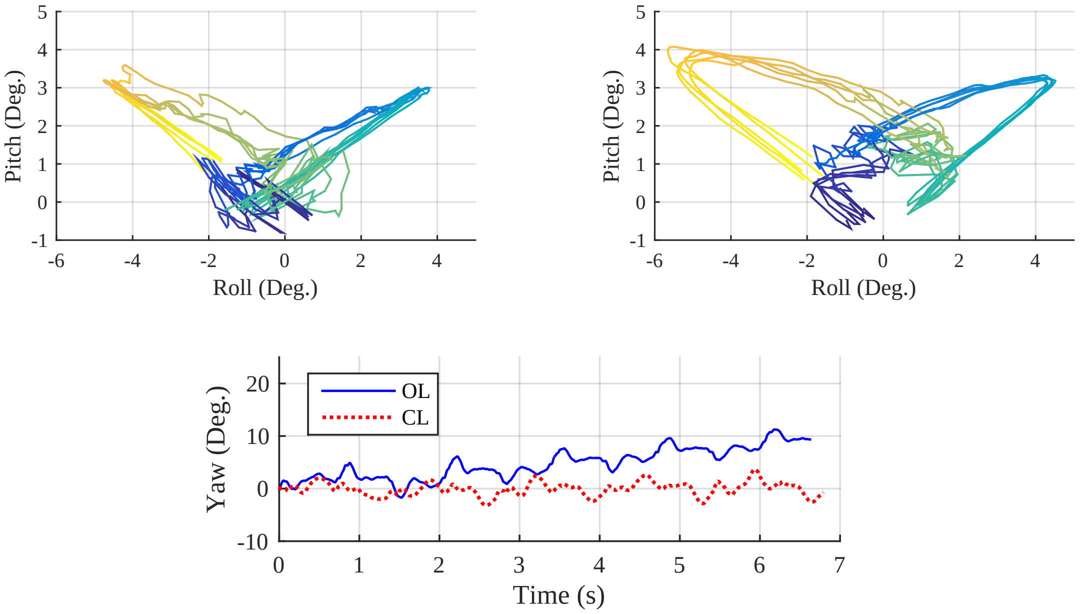

Figure 5.5 – Initial Morphology (Symmetric): (a) Open- and (b) closed-loop pendular behaviors observed in roll (Φ) vs. pitch (Θ). (c) Yaw angle drift in time for both control methods.

formed is described in Tab. 5.1 and can be divided into two groups of changes: symmetrical or asymmetrical in terms of left-right body symmetry. Experiment 0 refers to the initial state presented above, experiments 1 to 3 are induced asymmetries to the robot, whereas the last two represent morphological changes of having shorter hind limbs (Exp. 4) and shortened fore limbs (Exp. 5). All the experiments of this section were performed with $f = 0.75$ Hz. For the open-loop cases, trot is imposed, while in the closed-loop case $\sigma = 0.3$ is chosen as it displayed the best trade-off between time of convergence and locomotion speed (see [167] for details).

| Exp. | Type of perturbation | location |
|---|---|---|
| 0 | none | |
| 1 | + 5 mm in $l_2$ | limb 4 |
| 2 | 10% of added weight | between limbs 1 and 4 |
| 3 | | above limb 3 |
| 4 | -25 mm in $l_1$ and $l_2$ | hind limbs (3 and 4) |
| 5 | | forelimbs (1 and 2) |

Table 5.1 – Gait adaptation analysis

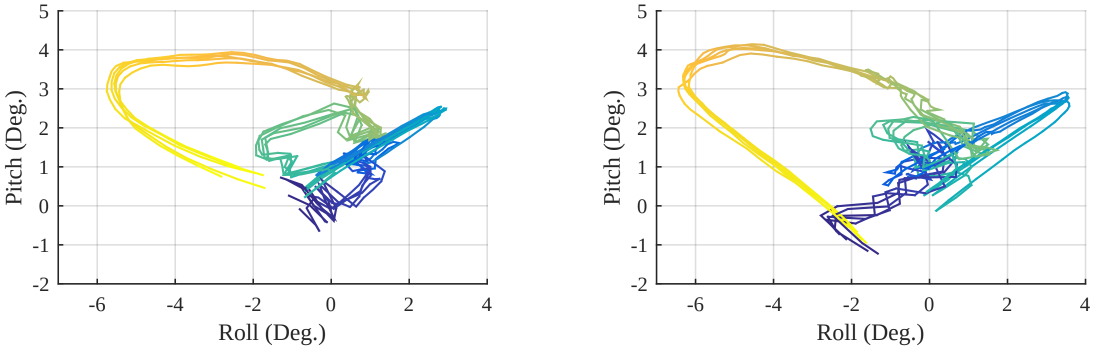

Figure 5.6 – Exp. 1 (small asymmetry): (a) Open- and (b) closed-loop pendular behaviors observed in roll (Φ) *versus* pitch (Θ).

### Results

The pendular behavior for Exp. 1 is shown in Fig. 5.6. Comparing again the open-loop and local feedback cases, and with the symmetric case in mind (Fig. 5.5), it can be inferred that the closed-loop technique approximates the dynamical response towards the non-perturbed system. The result of Exp. 2 is presented in Fig. 5.7, where it is seen that the closed-loop limit cycle is in this case much less periodic. This effect is due to the hard corrections being constantly performed to counter the effect of the asymmetric weight distribution, and the turning caused by the additional weight is considerably removed. In addition, the limit cycle of the closed-loop control resembles the limit cycles of the symmetric structure (Fig. 5.5).

Exp. 3, in which the extra weight is placed on the left forelimb, results in a significantly different gait which has periodicity over two cycles: odd numbered gait cycles are quasi periodic among the other odd numbered cycles, and the even numbered gait cycles are periodic among the even ones. The main reason is the mass concentrated in the corner of the robot: the momentum of the extra mass during one cycle affects the second one, yet, that effect is reversed in the third cycle. The changed gait was not analyzed in terms of stability, however it is important to notice that it emerged autonomously based on the changed morphology, meaning that the tegotae control can be suitable for moving a gait generator from a computationally expensive operation into a much lighter, self-organizing framework.

The effects of having smaller hind or fore limbs is explored in Exp. 4 and 5 respectively. The results of Exp. 4 are presented in Fig. 5.8 where a new gait (D-S) appears. Again, instead of treating the morphological change as a perturbation and pushing the locomotion pattern in the direction of trot, a different symmetrical behavior emerges. In the case of open-loop, despite the left-right symmetry of the new configuration, the imposed trot gait results in a periodic but asymmetric limit cycle. On the other hand, the local feedback actively adjusts the phases to allow a symmetrically oscillating body motion. The limb phase oscillations are shown in Fig. 5.8c, where the limbs are reordered into $[\phi_3, \phi_1, \phi_2, \phi_4]$ to favor the comparison between diagonal limbs. While in the first diagonal ($\phi_3 - \phi_1$) hardly any change occurs from the initial trot condition to the steady state one, in the second one ($\phi_2 - \phi_4$) a dephasing occurs during a transient and is kept throughout the steady state oscillation. The phase shift between diagonals is also adapted, pushing the footfall pattern towards a diagonal-sequence walk. This gait interestingly is observed in primates [172, 67] where the walking posture includes a positively tilted torso, like the robot's morphology in Exp. 4. Ground contact forces are also more evenly distributed through all the limbs in the case of closed-loop control.

In the final case of having shorter forelimbs (Exp. 5), gait adaptation was also observed, however without significant drifts from the trot gait.

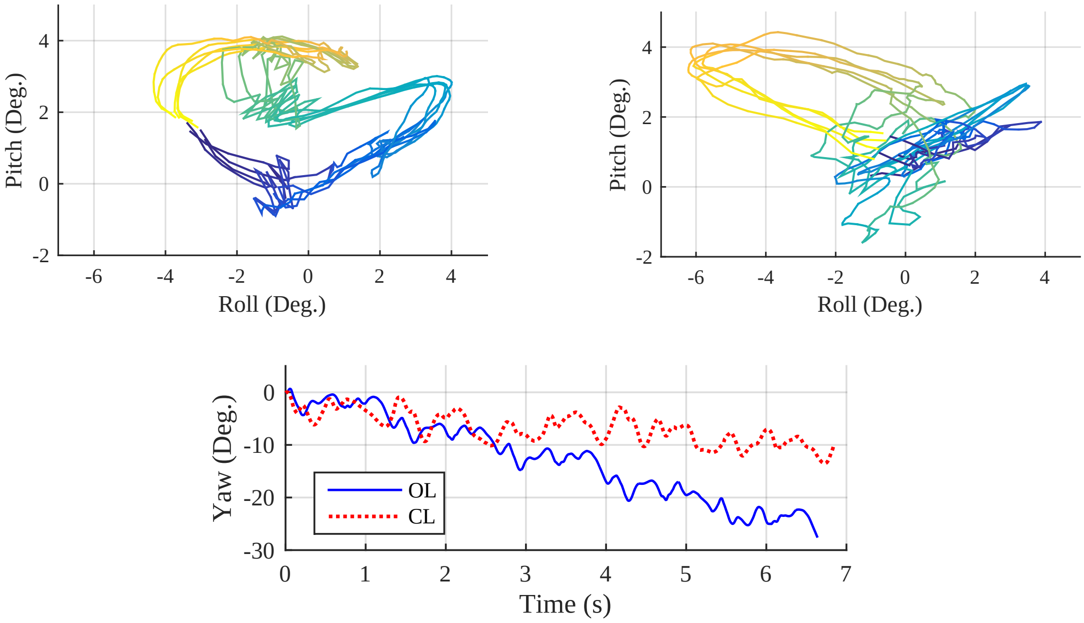

Figure 5.7 – Exp. 2 (distinct asymmetry): (a) Open- and (b) closed-loop pendular behaviors observed in roll (Φ) *versus* pitch (Θ). (c) Yaw angle drift in time for both control methods.

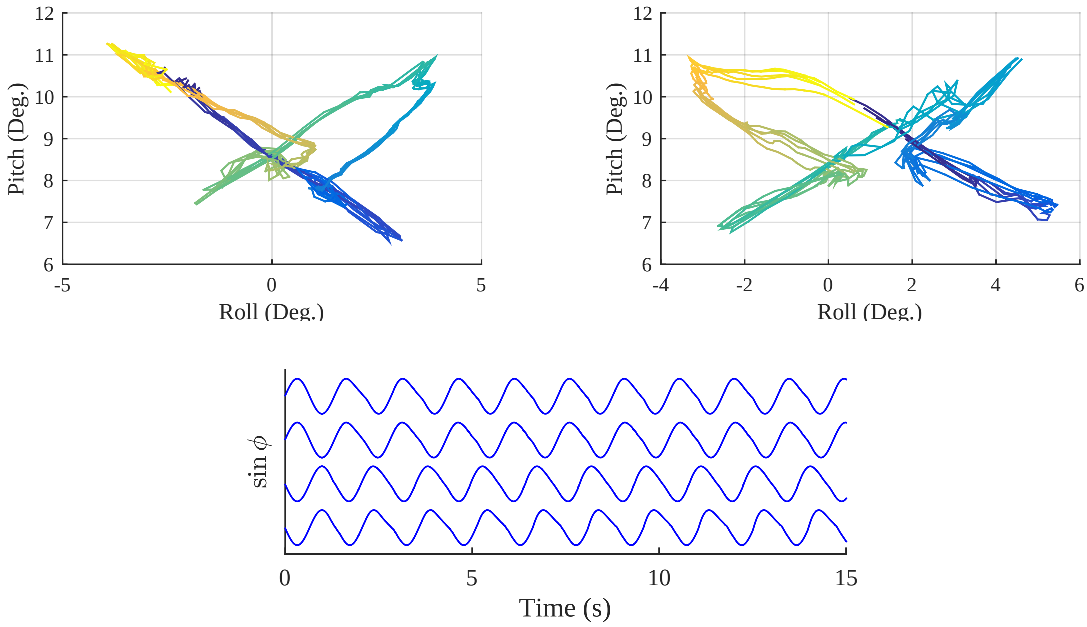

Figure 5.8 – Exp. 4 (small hind limbs): (a) Open- and (b) closed-loop pendular behaviors observed in roll (Φ) *versus* pitch (Θ). (c) Limb phase oscillations during closed-loop gait - convergence towards diagonal-sequence (D-S) walk - oscillations from top to bottom are $\phi_3$, $\phi_1$, $\phi_2$ and $\phi_4$.

### 5.3.6 Conclusions of stability through tegotae

The results show several interesting properties of the controller. First, regarding the open-loop controller, the results suggest that the lack of compliance in the leg does not prevent the body from synchronizing with the controller, although the observed gaits are less smooth. Second and more interestingly, the tegotae-based control not only increases the symmetry of the generated gaits when compared to the open-loop controller but also exhibits autonomous gait transition induced by morphological changes. Another remarkable feature is its ability to stabilize symmetric gaits in the presence of real world noise and even in case of asymmetric morphological changes, leading to straighter directional heading (implicitly desired by the symmetric gait).

## 5.4 Stability on rough terrain: Tegotae and joint compliance

The robots that use the tegotae-based control scheme (active compliance) have usually been reported to have series elastic elements (passive compliance) in the legs [115]. The tegotae scheme can clearly generate different gaits (trot, bound, gallop etc.) and the passive compliance of the leg has a modulating role. [49] declares that a lower level of active stiffness results in less tegotae (good/useful feedback) in robot-environment interaction and steady-state locomotion may be severely degraded for very low stiffness values.

Despite all previous work emphasizing the importance of compliant legs, they cover only limited aspects. In particular, they lack the analysis of compliant locomotion on rough terrain. Moreover, there are limited previous studies on the combined effect of passive and active compliance on locomotion performance.

Here, the two strageties of the two previous sections are now combined: passive compliance in the joints and active compliance in the control. The goal of this work is to understand how these mechanisms can work together to improve the locomotion performance, specifically cost of transport and stability properties, and test them on rough terrain. We present various locomotion metrics together with observations on potentially advantageous and disadvantageous compliance, both of hardware and control.

### 5.4.1 MODOK configuration

**Morphology and control:** The overall structure of the robot can be seen in Fig. 5.9a. In section 5.2, it is shown that the proximal parts of the limb should have lower compliance compared to the distal parts, hence the proximal hip part of the leg is directly connected to the lower (distal) leg without any compliant elements in between. The lengths of the upper leg (L1) and the lower leg (L2) are updated to 79 mm and 110 mm respectively. This changes the inverse kinematics model and slightly alters the foot trajectory by using the same trajectory parameters $\theta_{max}$, $h_{st}$ and $h_{sw}$ (Fig. 5.9b). For locomotion on inclined surfaces, the trajectory

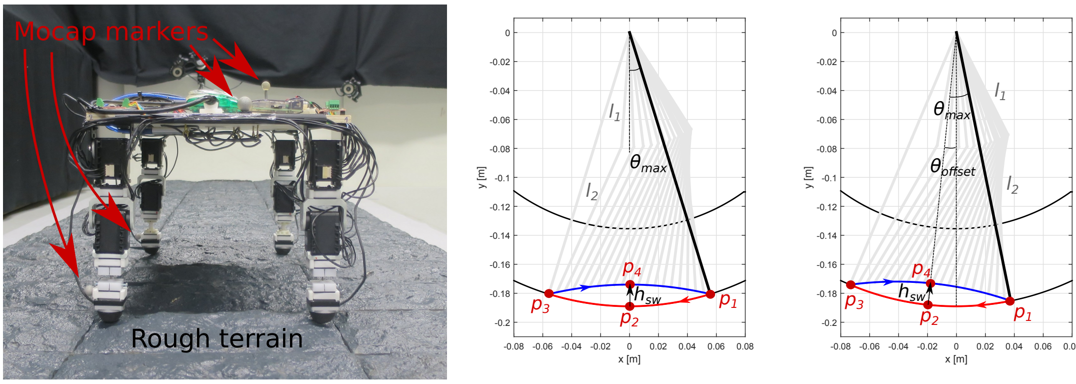

(a) (b) (c)

Figure 5.9 – MODOK configuration for the combined mechanisms experiments. (a) MoCap markers on the main body and front and hind foot on the right side. The proximal compliance is removed and the two servo motors screwed together; the distal compliance can still be changed to rigid, hard and soft. (b) Updated inverse kinematics of the foot trajectory. Blue elliptic arc shows the swing phase and the red one shows the stance phase. Limits of the workspace is shown with black arcs. Parameters defining the gait are hip angle maximum extension ($\theta_{max} = 0.3$ rad), height difference from swing phase mid point to fully stretched leg ($h_{sw} = 15mm$) and height difference from stance phase mid point to fully stretched leg ($h_{st} = 0$ mm). (c) As an inclination compensation, an offset angle ($\theta_{offset} = 0.1$ rad) is added to the hip angle to shift the center of mass slightly forward.

was offset by the angle $\theta_{offset} = 0.1$ rad around the hip (Fig. 5.9c). The same trot gait as above was used.

**Passive compliance distributions:** The passive elements tested in this study are the same as the ones used in section 5.2. The rigid element sets a baseline for the other compliant elements. It is important to note that the robot itself has an intrinsic compliance arising from body elasticities, motor and connector backlashes and low level servo control errors. Hence, even the case with the rigid elements has a hard-to-model parasitic (non-zero) compliance. The other elements introduce significant compliance on the lower limb only.

The selection of compliance distribution is empirical. The main aim is to observe effects of relative compliance. There exists $3^4 = 81$ different distributions using only 3 compliance levels on 4 limbs. Left-right of the robot is always kept symmetric as in most healthy quadrupedal animals. When the left/right symmetry is considered, the number of possible compliance distributions reduces to $3^2 = 9$. Most quadrupedal animals also have stronger and larger hind limbs then fore limbs. Thus, the distributions where hind limbs are softer than fore limbs (3 cases) are discarded. In this study 5 different compliant element distributions are tested: (i) “all limbs rigid” (practically no bending), (ii) “all limbs hard” (low to moderate bending), (iii) “all limbs soft” (moderate to high bending), (iv) “fore limbs hard / hind limbs rigid, (v) “fore limbs soft / hind limbs rigid”. The “fore limbs soft / hind limbs hard” distribution is intentionally left out because the “fore limbs complaint / hind limbs rigid” cases ($4^{th}$ and $5^{th}$ distributions) are expected to give a similar trend as the excluded case. Moreover, initial tests revealed that the robot has more trouble with soft leg compliances compared to harder/moderate distributions. Hence one of the visually not very promising distributions is not selected for further experiments to reduce the total number of runs.

**Tegotae-based active compliance:** It may not be a perfectly matching condition to compare open-loop and tegotae control since tegotae may not always stay in trot mode, especially in rough terrain. To keep the comparison to the open-loop case fair, we have initialized the gaits controlled by tegotae in trot. We also set a single value of the tegotae attraction coefficient ($\sigma = 0.3$) which is experimentally checked to converge to trotting gait at steady-state when locomoting on flat surface. Due to its randomness, it is not possible to guarantee steady-state trot convergence on the rough terrain. However, the various response characteristic possibilities of the tegotae control make it even more interesting and worthy to study as an active compliance source.

### 5.4.2 Performance metrics

This section presents the analysis of the data collected during the experiments as well as our observations and comments on the data. Quantifying the locomotion performance is done by introducing various metrics calculated using logged data. Furthermore, qualitative gait symmetry analysis is presented to illustrate locomotion modes emerging from different leg compliance levels as well as the tegotae-based rule. Finally, more insights are given about the tegotae-based control on various surfaces.

Quantifying performance of locomotion is a challenging task as there are ways to view the same data, and some of those approaches can be biased or not as important as others. In order to be as fair and rigorous as possible, many different performance metrics have been proposed. They can be grouped into two subgroups: (i) conventional metrics such as speed, cost of transport, power consumption etc., and (ii) stability of locomotion metrics to evaluate how much the body oscillated during the locomotion, i.e. how much it deviates from the horizontal plane.

**Stride length ($l_s$):** The foot trajectory is the same for all of the experiments. However, the stride length is expected to change for different configurations because of slippage and the robot getting stuck. Having long strides without getting stuck is a desired locomotion criteria. This metric is calculated as

$$l_s = d_t / N_s \tag{5.3}$$

where $d_t$ is the total distance taken in 10 steps and $N_s$ is the number of steps (fixed to 10 in this study).

**Experiment time for 10 steps ($t_e$):** By the definition of tegotae, it has power to suppress or advance the gait phase. So, taking 10 steps always takes the same amount of time in open-loop locomotion whereas the actual time needed to perform 10 steps with the tegotae control varies around the gait period ($1/f$). Hence, we report the time tegotae-based control needs to take 10 steps. This metric is reported for completeness and further used to calculate average speed. It is important to note that taking 10 steps within less time does not necessarily mean faster locomotion since actual stride length can change due to foot slipping or getting stuck, even though the desired foot trajectory is the same for all experiments.

**Average speed ($v_a$):** Although the stride length $l_s$ is correlated with the average speed $v_a$, there can be differences since the experiment time for the tegotae control is not fixed, i.e.:

$$v_a = d_t / t_e \tag{5.4}$$

Average speed is one of the most reported locomotion metrics in the literature since many researchers are trying to make faster robots.

**Average power consumption ($P_a$):** The current demand for the locomotion is among the logged measurements. Motors are powered using a fixed DC voltage source. Hence the total power consumption for the experiment is

$$P_a = \frac{V_{DC}}{t_e} \cdot \int_0^{t_e} I(t)dt \tag{5.5}$$

where $V_{DC}$ = 18 V. Power consumption is a widely used metric in robotics because it has implications for the battery size and operation time of a robot.

**Cost of transport ($CoT$):** The cost of transport evaluates the power efficiency of the locomotion and is calculated as

$$CoT = \frac{P_a}{m \cdot g \cdot v_a} \tag{5.6}$$

where m is the mass of the robot ($m = 2.25$ kg) and g is the gravitational constant. $CoT$ is also one of the most common locomotion metrics in the literature and it gives the operation cost of the robot to move from point A to B.

**Control tracking error ($e$):** We log the actual motor angles read from the encoders and desired joint angles. The control error $e$ is simply the mean (per actuator) of the absolute value of the difference of the setpoint and the actual motor angle. Setpoint tracking capability is a feature of the local controller, hence expected to be invariant throughout experiments since the weight does not change. However, when the high level control input is very high or when motors are blocked, actuators may have a higher setpoint tracking error. Lower local control errors indicate that the robot is at least moving in a desired way and not getting stuck.

**Average acceleration ($a_a$):** This metric and the following ones are related to the smoothness (oscillation amount) of the body motion during locomotion. A more oscillating locomotion may not necessarily be less stable than a more flat one. However, it is an indicator of the energy efficiency. We consider lower accelerations to be potentially better gaits. The average acceleration is simply the mean value of all acceleration vectors' Euclidean norms logged during the locomotion.

**Average rotational velocity ($\omega_a$):** The IMU gives rotational velocity with respect to each axis in 3D. Total rotational velocity $\omega_a$ is calculated the same way as the acceleration and it relates to the stability of the body too.

**Force fluctuations ($\sigma_f$):** The axial force fluctuation is calculated as

$$\sigma_f = \sum_{i=1}^{4} \sigma_i \tag{5.7}$$

where $\sigma_i$ is the standard deviation of the norm of (3D) data collected by the OptoForce sensors during the experiment. This metric is correlated with the amplitude of foot touchdown impacts. Higher impacts will usually result in higher $\sigma_f$ values. High impacts can also deteriorate sensor readings and usually they are undesired in robotics, unless high impacts are needed for a specific task.

**Motion blur metrics ($\mu_a$ and $\mu_{\%}$):** The Motion-based Motion Blur Metrics (MMBM $\mu_a$ and $\mu_{\%}$) are vision-related metrics and will not be discussed here; the reader is referred to [108].

### 5.4.3 Locomotion on flat surface, rough surface and rough inclination

#### Experiments

Experiments involve analyzing various hardware configurations using open- and closed-loop controllers on different surface conditions and center around the following hypothesis:

> *Tegotae-based control will improve rough terrain locomotion performance thanks to its exploratory nature.*

Our approach is an exhaustive systematic search where only one parameter is changed at a time. At each different scenario, the robot runs more than 10 steps in steady-state and the last 10 steps of each run are taken for analysis. Since tegotae control is fundamentally based on the robot-environment interaction, different surface conditions are included in the study.

**Flat surface, no inclination:** The flat surface with no inclination constitutes the baseline for the different surface types, because gait cycles are consistently repetitive and it is easier to observe steady state behavior particularly for the tegotae control. This surface type is the most commonly used one for the tegotae experiments. Hence, it can be used as a bridge between other studies and our study.

**Rough surface, no inclination:** A rough surface of 3 m x 1 m size is made out of house decoration tiles. The tiles are painted with spray paint to obtain the surface seen in Fig. 5.9a because the original white color was too reflective under the motion capture system. The roughness consists of valleys and peaks having approximately 1 cm and maximum 2 cm height difference. Such roughness introduces stochastic perturbations to the robot's locomotion in the form of slippage or getting stuck. Robust locomotion is expected to perform well on the rough terrain.

**Rough surface, 3° uphill inclination:** The final experiment surface is the 3° inclined version of the same rough terrain. The robot walked uphill during the tests. Uphill conditions are even more challenging since the gravity is against the locomotion direction.

In summary, we exhaustively tested all different conditions. Therefore, the experiment set consists of 5 (compliant element distribution) * 2 (open- and closed-loop control) * 3 (surface types) = 30 runs.

### Results

**Overall locomotion performance:** The performance metrics explained in the previous subsection are calculated for all of the experimental data and the results are presented in Fig. 5.10. The axes in the spider plots have been reversed in necessary cases such that outer (from center) values indicate better locomotion performance in accordance with the defined metrics. Furthermore, all of the axes have the same range across different plots and their range is scaled and normalized such that the minimum metric value is always very close to the center and the maximum metric value is at the outer limits of the spider plot. Therefore, the area of each spider plot gives an idea about how good the performance is. However, it is important to note that under real conditions, different axes have different importances, thus the area of the spider plot is not an absolute classification criteria for any locomotion task. It is rather up to the reader's interests and intentions to choose and weight desired metrics for a performance evaluation. It is also important to note that very small metric value differences between different experiments may not be an absolute indicator. The experiment time was limited to 10 gait cycles and especially on rough surface, error margins are expected to be higher due to the randomness of the contact points.

The flat and rough terrain results show two major differences between open-loop and tegotae control: (i) tegotae control takes longer $t_e$ (experiment time for 10 steps) than the open-loop control, but (ii) the tracking error $e$ resulting from the tegotae control is less than the open-loop $e$. Similar observations also hold for $e$ on inclined surface locomotion, but the difference of $e$ between open-loop and tegotae control is less pronounced. An interesting observation is that $t_e$ in tegotae control is less than the open-loop case on the inclined surface. The shortest $t_e$ case occurs with the soft fore / rigid hind limb compliance on the inclined surface. The reason is that the force on the z axis of the force sensor is changing direction. Fig. 5.11 shows the right fore leg, the ground reaction forces, force sensor orientation and the sensor tip point during the mid-stance instance in rigid and soft fore / rigid hind compliance configurations. The leg is bent beyond the natural range when the compliance is too soft.

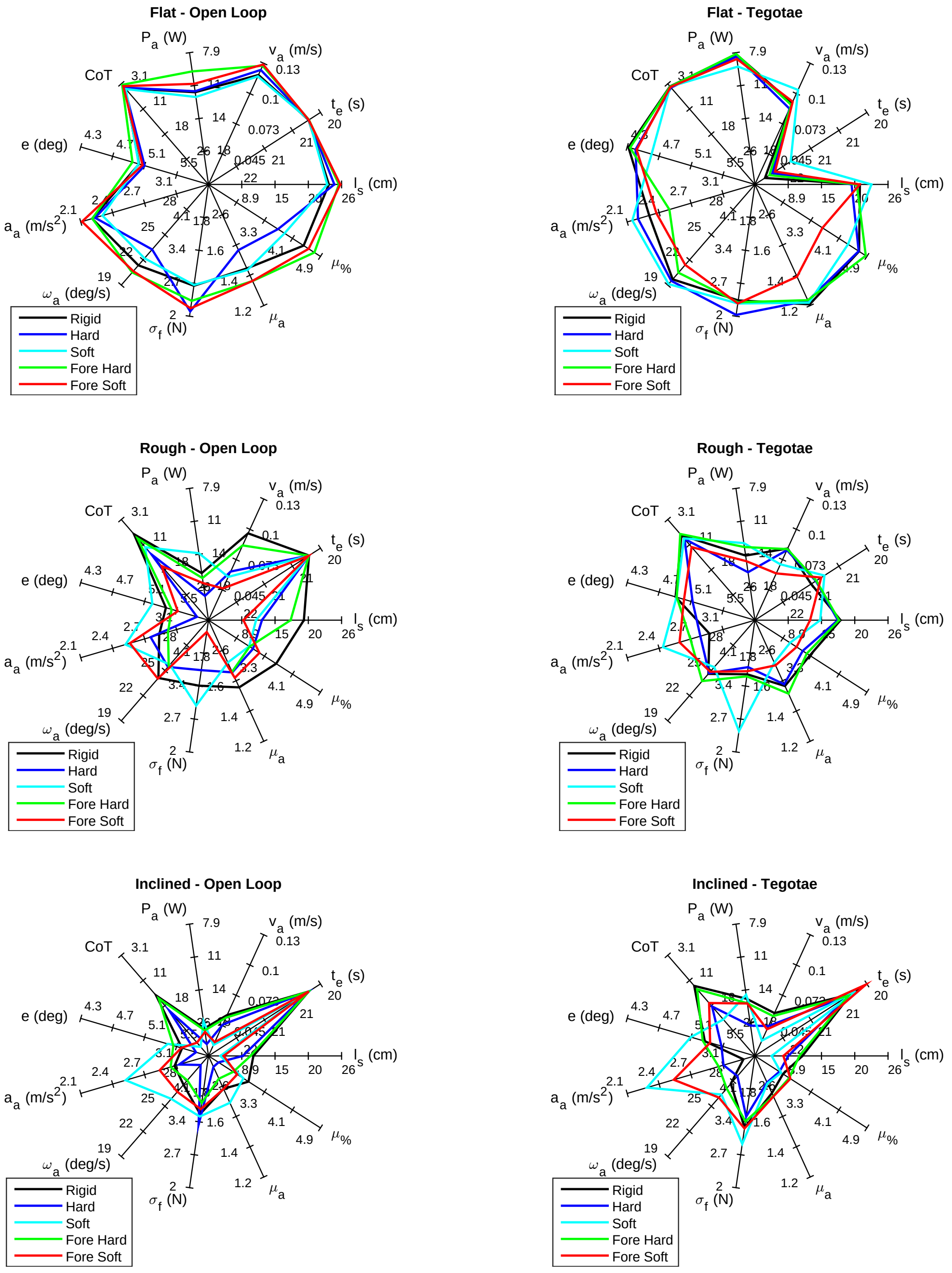

Figure 5.10 – Evaluation of the proposed metrics for all of the experiments. The data is divided into 6 spider plots illustrating (a) flat terrain / open-loop control, (b) flat terrain / tegotae control, (c) rough terrain / open-loop control, (d) rough terrain / tegotae control, (e) inclined rough terrain / open-loop control, (f) inclined rough terrain / tegotae control. Each plot shows all of the tested compliance distributions: (i) all rigid elements (practically no bending), (ii) all hard elements (low to moderate bending), (iii) all soft elements (moderate to high bending), (iv) fore limbs hard / hind limbs rigid elements, and (v) fore limbs soft / hind limbs rigid elements.

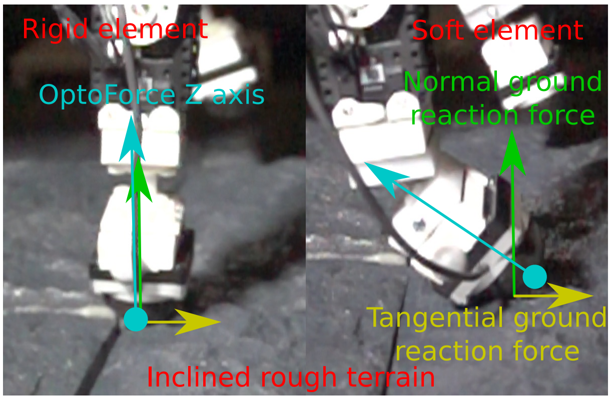

Figure 5.11 – The ground reaction force and the orientation of the force sensor mounted on the foot. When the compliance is very low the bending can reach quite high and unnatural looking levels.

Another interesting observation is that the tegotae control seems to have multiple benefits on both rough 0 deg and 3 deg inclined terrains. First of all, it has a tendency to decrease the cost of transport. Additionally, the metrics related to the stability of the robot ($a_a$, $\omega_a$, $e$, $\mu_a$ etc.) indicate a performance increase. Finally, the whole area that is covered by the spider plots also increase from open-loop gaits to tegotae control. That is a significant outcome, indicating the tegotae rule can boost locomotion performance on rough terrain, thus our hypothesis is validated. It can also be concluded that introducing passive compliance to a robot having tegotae-based control improves locomotion performance as long as compliance is within favorable range.

In terms of the compliance distribution, there is no single outstanding observation dominating for all runs, but some of the distributions perform better under specific conditions. This is an expected result since this work tries to answer a broad range of questions. As there is no single algorithm to solve all problems, there is no perfect compliance distribution to satisfy different goals. It is still possible to infer that fore hard / hind rigid case has better performance over all hard distribution, which points out that asymmetric fore and hind limb compliance has potential to improve locomotion performance.

**Feet trajectories:** During the trot, two legs should be in the stance phase while the other two should be in the swing phase. However, our robot does not have active feet controlled from the ankle and only has passive spherical feet. As a result, the robot has only two points, rather than two surfaces as in real quadrupedal animals, touching the ground most of the time. Thus, the robot dynamics exhibit unstable, inverted-pendulum-like behavior, and one of the swing phase legs sometimes prematurely touches the ground to form a dynamically stable tripod (unnatural for animals). Even though the center of mass is approximately at the geometric center of the robot, the tripod is formed by two hind limbs and a fore limb for all of the open-loop gaits. Even when one of the swing phase legs touches the ground, the majority of the weight is still carried by the stance phase legs. In order to capture such behaviors, right feet trajectories are recorded during flat terrain experiments. Fig. 5.12 gives the fore and hind limb trajectories for all uniform compliance distributions when locomoting on the flat surface. It is clear that the hind leg is always dragging as it barely lifts off the ground in the open-loop cases. However, tegotae control is trying to balance that instability and to bring the system to more uniform swing/stance phases. Previously, it was reported in [167] that tegotae can fight against introduced morphological asymmetries and tries to bring the locomotion to a more symmetrical regime. Similarly, we re-validate that tegotae tries to overcome locomotion asymmetries. Furthermore, we observe cues to extend that hypothesis to include asymmetries arising from the locomotion surface.

**Phase vs compliance in tegotae-based control:** The time evolution of the phase gives important clues about the locomotion in tegotae control. The phase of the limb oscillators when the robot is controlled with tegotae is given in Fig. 5.13. The figure displays three different runs with different uniform compliant elements. For each run, both right (fore and hind) limbs' phases are plotted. More stiff legs can have higher interaction forces and we observe that phase delay is increased. This observation is also consistent with the literature.

**Emerging gaits from tegotae-based control:** Open-loop runs were always forced to be trot. However, tegotae control does not have any direct coupling between phase oscillators of limbs. Nevertheless, on flat surface tegotae always converges to trot (for our selected $s = 0.3$) no matter which compliant element is used. However, the rough surface has peaks and valleys resulting in unexpected touchdown moments. Even on the rough terrain, the gait mostly remains a trot while in some cases deviations from trot have been observed. We believe those deviations towards different gait modes help the robot to move more efficiently on the rough terrain. Hence we associate the decrease on the cost of transport (under aforementioned scenarios) to the gait adaptation capability of tegotae. Indeed, open-loop control can sometimes get stuck (repeating same steps blindly with no actual forward motion) on some unfavorable spots on the rough terrain whereas tegotae control explores different locomotion modes on the same spots and has higher likelihood of passing those points.

**Limitations of the platform:** The platform has inherent and uncontrolled compliance stemming from the construction materials. Hence, even the rigid case is not completely rigid. Even though it is an animal-like quadruped structure, unlike real animals, the mass is centered more on the legs rather than the body. Moreover, the sticktion of force sensors at feet causes energy accumulation in compliant elements during the locomotion. At takeoff, the compliant leg can start oscillating because of the lack of damping. Such oscillations become significant distortions when the leg mass is relatively high compared to the body mass and can be noticed especially in stability related metrics.

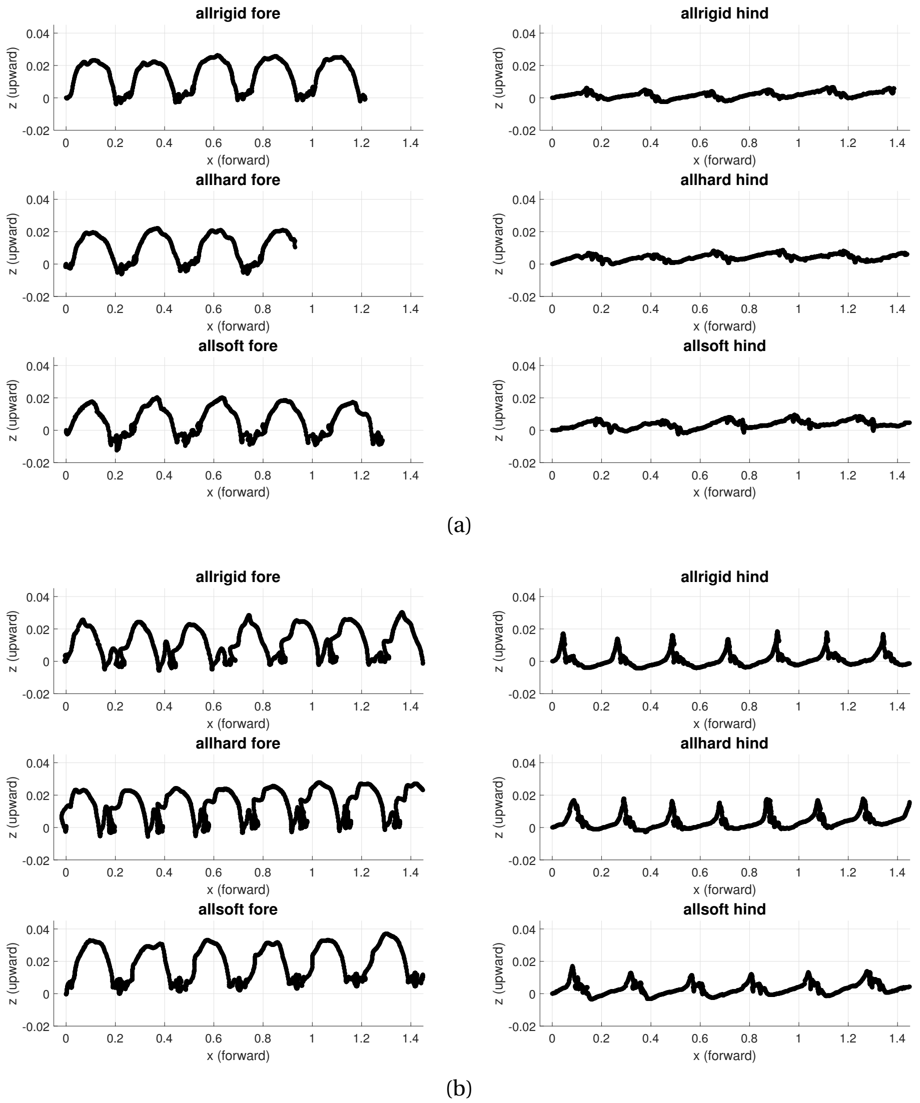

(a)

(b)

Figure 5.12 – Foot trajectories during locomotion on the flat surface, using different uniform compliance when the robot is controlled with (a) open-loop or (b) tegotae based controllers.

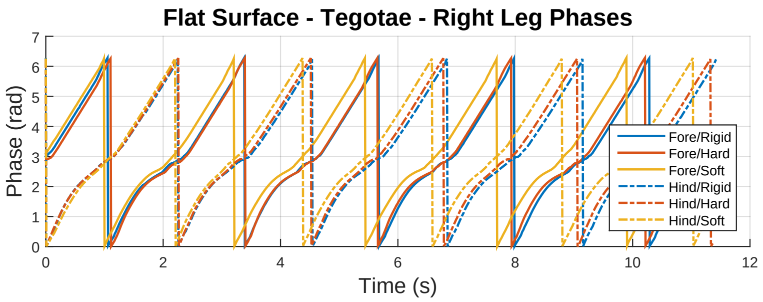

Figure 5.13 – Phase evaluation of fore and hind right limbs when the robot is locomoting on flat surface with tegotae control. Three different uniform compliance tested. When the limbs are more stiff, the robot-environment interaction is higher and phases get longer delay.

## 5.5 Conclusions of tegotae for rough terrain locomotion and Future Work

This chapter tackles the complex problem of compliance in locomotion with a variety of systematic hardware experiments and the analysis of a rich set of locomotion metrics. First, joint compliance distribution in a quadruped robot is studied, finding that there are more and less favorable distributions considering energy efficiency. Then, the compliant control *tegotae* on a stiff robot configuration is studied, showing that this control has the ability to stabilize the locomotion against real world noise and even morphological modifications. Lastly, both approaches have been combined, which resulted in a remarkable ability of the quadruped robot to improve locomotion on rough terrain.

However, the problem has many dimensions to consider and there is no single compliance distribution and control combination outperforming all the others. Rather there appears to be some favorable combinations for certain criteria in specific scenarios. The relation of compliance to the gait is highly nonlinear and is affected by many parameters; readers with various different applications in mind can select a subset of findings presented in this chapter to guide their compliant robot and controller designs.

Tegotae based control presents a great value as an active compliance source. In this study only one level of tegotae attraction coefficient $\sigma$ is tested and is set to a fixed value which has the tendency to converge to trot in all test cases. When the limbs are physically more stiff, the effects of Tegotae are more pronounced. One of the most prominent effects of tegotae is observed to be reducing the cost of transport for locomotion on rough terrain. The most likely reason for such performance increase is the adaptation capability of the tegotae control. By exploring slight gait changes around trot, it overcomes certain local minima where open-loop gaits can exhibit significant performance drops. A closer investigation with a more capable robotic platform could lead to better insights in the limitations of the presented approach.

Overall, the mode-switch method of phase oscillators - the underlying mathematics of tegotae - to induce the leg movement functionalities “displacement of the leg” and “displacement of the body” is shown to be viable, however the parameters of it are relatively sensitive. Unlike in Chapt. 4 where a mode-switch of the foot improved locomotion on rough terrain as long as the foot switched to a hard-enough state, the sensitivity resembles more that of the climbing system in Chapt. 3, requiring a finer tuning of mode-switch parameters. This might be due to the actual differences in the functionalities. In the case of the foot, damping and shape adaptation is very different from force transmission. In the case of the leg, leg movement and body movement arguably are still similar functionalities, and thus the transition between them is more subtle.

# 6 Learning to move in arbitrary morphologies

The previous chapter focused on the control mode-switch method of phase oscillators, using *tegotae* as a way to introduce compliance into a legged structure. In this chapter, we go deeper into the other interesting property of tegotae to create emergent interlimb coordination. Even though such coordination was also shown on MODOK, the arguably fixed morphology did not show the limitations of this property. Here, we want to fully utilize modular robots to create a generic locomotion controller which can induce coordinated locomotion behavior on "arbitrary" legged morphologies.

**Reference publication**

This chapter is partly based on ***Simon Hauser**, Matthieu Dujany, Martijn van der Saar, Mehmet Mutlu, and Auke Ijspeert. "Learning to walk in arbitrary morphologies." Submitted to The 9th International Symposium on Adaptive Motion of Animals and Machines (AMAM), 2019.*. Parts of the text and figures have been reorganized in this chapter.

**My original contributions**

- Development of concept
- Development of robot hardware
- Planning of experiments
- Interpretation of results
- Writing of manuscript

**Work in progress**

The research in this chapter is incomplete and currently being worked on. We explain the overall concept and present preliminary results from first validation experiments, however some details in the explanation are missing at the current state of the research.

## 6.1 Inspiration: Locomotion adaptation in animals

### 6.1.1 Recovery of locomotion ability

A common strategy to develop a locomotion controller for a legged robot is to create a model of a robot in simulation, define joint movement parameters and use an optimization method to find a suitable locomotion strategy. However, usually a controller found with this method is tied to the morphology it was optimized for; if the morphology undergoes modifications, the controller has to be re-optimized to incorporate these modifications. It is only in rare cases that a controller is transferable between different morphologies. Especially if the controller acts in an open-loop manner, it might simply be a matter of luck. A closed-loop controller that takes feedback from certain run-time variables of locomotion into account (e.g. ground reaction forces) can improve the chances of a successful control transfer, however it is unclear, which feedback variables could be useful and how to actually use them. Moreover, it is likely that a re-optimization of closed-loop variables such as feedback gains is still required.

Morphological modifications can occur during all stages of an animal. First and foremost, animals undergo growing, changing their body proportions and weight in the process. While these are not drastic changes in a small time frame, a controller still needs to take them into account, given that most of nature's optimization is centered around energy efficiency. Also drastic changes are a real possibility: attacks of predators or other accidents can reduce the functionality of a limb, or an animal can even lose an entire leg. From the perspective of the controller, these are challenging situations as the animal needs to adapt and recover its locomotion ability as quickly as possible to not become easy prey. So in such an extreme case, how fast is this recovery?

Observations on animals suggest that the recovery is basically instantaneous, at least a partial recovery of the functionality; a full recovery might include an adaptation phase, fine-tuning control parameters. Moreover, the severity of the morphological modification, the redundancy and the potential change in the dynamics of the system certainly have to be considered. A spider losing one of its eight legs intuitively will very quickly be able to locomote similarly with seven legs (static locomotion with eight legs to static locomotion with seven legs), while it arguably will take more time for a dog to learn how to walk only on its hind legs in case the front legs are unavailable (static locomotion with four legs to dynamic locomotion with two legs). Nevertheless, the adaptation capabilities are impressive, and seemingly do not require a lengthy re-optimization as described above.

### 6.1.2 Approaches in robotics

Examples in literature that try to replicate these adaptation capabilities in robotics are sparse. Although the authors in [36] explicitly state that 'natural animals do not use the specific algorithm' presented in their work, they describe an "animal-like" trial-and-error strategy that involves the creation of an enormous database of simulating millions of locomotion behaviors of a hexapod robot. The robot then is able to regain its locomotion performance by testing a sample of different simulation models in an efficient manner once it detects a performance drop due to injury or malfunction. A similar strategy is presented in [21] where a set of simulation models are generated during run-time. After a morphological change, a quadruped robot synthesizes self-models of its own morphology through self-directed exploration (arbitrary motor actions); it then simulates the best found model to generate a locomotion behavior that results in the desired forward motion and applies it on its hardware. The research mentions that 'it is unlikely that organisms maintain explicit models' but notes that directed exploration for the acquisition of predictive self-models could play a critical role, which corresponds well with the approach presented in this chapter.

Other strategies are developed in the field of *evolutionary robotics* [22, 20] where offspring-robots are created through inheriting genome traits from their parents, using nature-inspired mechanisms such as genome recombination and mutation to generate diverse phenotypes. A selection method then drives the evolutionary process towards an optimized solution, whose tasks could be locomotion. In [24], the locomotion controllers are open-loop, and an offspring robot receives its controller from a combination of its parents' controllers, thus involving the element of luck for its suitability. In [173], offspring robots inherit a prototype controller from their parents which then undergoes an "infancy" stage where the controller adapts parameters of the prototype controller to the morphology of the offspring. This is not unlike the re-optimization strategy, requiring a significant amount of time.

The most interesting research in terms of run-time adaptation of control parameters is presented in [115] where tegotae and phase oscillators are used to actuate a hexapod robot. An extension of tegotae is developed, where each leg modulates its movement not only based on its own force feedback but also takes the force feedback of neighboring legs into account. The robot with this controller converges to a tetrapod-gait - the ipsilateral legs are coordinated and move in the order of hind, middle and fore legs - with six legs. The robot then has its two middle legs amputated during run-time, upon which it not only continues walking but adapts its gait to an LS-gait with the remaining four legs. Although it is unclear at the moment, how generalizable and scalable this approach is with other multi-legged structures, it is currently the most promising, both in terms of the results already produced with the hexapod robot and the simplicity of the controller.

### 6.1.3 Application of tegotae in arbitrary morphologies

The research in [115] indicates that the extension of tegotae to consider the state of neighboring legs is a necessity to obtain a coordinated gait pattern with six legs. This means that in general, interlimb coordination is likely not entirely morphology agnostic. The controller needs to be provided with certain information about the morphology it is acting on to react intelligently (some form of embodied intelligence [122]), although the exact kind of information necessary is unclear. While considering the forces in neighboring legs was shown to be sufficient as presented in [115], the approach seems to stem from an educated guess rather than from a systematic derivation. The question becomes now if we can come up with a generic strategy that contains the necessary morphological information for interlimb coordination on arbitrary legged morphologies?

In this work, we propose the introduction of a generic, bio-inspired learning procedure with the goal of gathering basic knowledge of the kinematic properties of an arbitrary structure. We hypothesize that this knowledge can be used to inform a network of phase oscillators to generate locomotion. Tegotae is used as the interlimb coordination mechanism for robots with legged morphologies, and thus the robotic structure is assumed to consist out of motors and sensors. In this case, basic kinematics could be how motors are connected to each other, and to measure their influence on the sensors. A controller with this knowledge could act similarly to the spinal cord: upon receiving a high-level locomotion command from the brain, the spinal cord autonomously coordinates leg muscles into a locomotion pattern that matches the intention of the brain. Our goal is to create the “spinal cord” of any arbitrary legged morphology.

To achieve this, we explore the combination of the biological phenomena of “Spontaneous Motor Activities” (SMA) - a specific movement pattern observed during the REM-sleep of mammals - with Hebbian learning as a method to create an internal kinematic model of such structures. These processes and the used modular robot hardware are explained in the following sections, accompanied by preliminary experiments and results available at the time of writing this thesis.

### 6.1.4 Prerequisites for multi-legged tegotae

The formulas used in [115] for interlimb coordination of a hexapod robot assign a phase oscillator with output $\theta$ of the form

$$\theta_i = A \cos\phi_i \tag{6.1}$$

with a phase $\phi$ and amplitude $A$ to each limb $i$. The phase progression $\dot{\phi}_i$ is given by

$$\dot{\phi}_i = \omega - \sigma_1 N_i^V \cos\phi_i + \sigma_2 \left( \frac{1}{n_L} \sum_{j \in L(i)}^{n_L} k_j N_j^V \right) \cos\phi_i. \tag{6.2}$$

In Eq. 6.1, assigning an oscillator to a limb requires us to define *limbs*, the first prerequisite (P1). While this usually is obvious in the case of a standard controller development of a legged robot, it is important to remember that we want to find a generic controller that does not know its morphology *a priori* and has to derive an internal model from clever internal observations. In Eq. 6.2, $\omega$ is the intrinsic frequency of the oscillation. The second term is the standard tegotae term where the normal force at the foot modifies the speed of the oscillation of a limb; the minus in front of $\sigma_1$ drives the limb towards *mid-stance*. This brings us to the second prerequisite (P2): each limb must contain at least one force sensor capable of measuring normal forces (it could however also contain multiple force sensors). The third term describes the neighboring relationship $L(i)$. The middle leg on each side of a hexapod has 3 neighbors (front, back and side, $n_L = 3$) whereas all the other legs only have two neighbors (side and either front or back, $n_L = 2$), and the average of the neighboring normal forces also contribute to the phase progression of a limb. $k_j$ are gains to tune the influence of neighboring normal forces according to their geometric arrangement to the limb in question where a neighbor can be either anterior, posterior or contralateral. It is important to note that the sign before $\sigma_2$ is flipped in comparison to $\sigma_1$. This means that neighboring limbs have the *opposite* effect on the limb in question: the positive contribution of the neighboring limb drives a limb towards *mid-swing*, a property that we will encounter again later. As the third prerequisite (P3), the controller needs to know which are his neighboring limbs and how they are spacially arranged. Even then, the positive constants $\sigma_1$ and $\sigma_2$ need to be found for the system to achieve stable locomotion, and the question of how to find this also needs to be addressed.

## 6.2 The ARBITER robotic platform

### 6.2.1 Modular motors and modular sensors

The robotic platform used in this work is a customized version of the Bioloid-Kit [134]. The main components are 1 DoF (Degree of Freedom) hinged servo motors (Dynamixel AX-12+) and structural passive parts. Both components are equipped with custom designed male-female-male connectors that allow a fast assembly of almost arbitrary shape. The servo motors are controlled with a microcontroller (Robotis OpenCM9.04) and powered by a battery (Conrad energy BEC 11.1 V 1300 mAh 12 C). 3-axis loadcells (LCT LAN-X1) measure linear forces ($x$, $y$, $z$ in the loadcell coordinate frame). The modular design allows the loadcells to be placed in between any two elements. Because of the reliance of the control method on ground reaction forces, the loadcells are mostly placed as close as possible to the ground which interacts with a semi-spherically shaped rubber foot. An accelerometer (ADXL345) measures linear accelerations ($x$, $y$, $z$), and a gyroscope (ITG-3200, both integrated in the Sparkfun Razor IMU M0) measures the angular velocity in roll, pitch and yaw in the IMU coordinate frame. All data is collected by the microcontroller; in the future, data processing on the microcontroller will also be implemented, however at the moment all the data is processed externally in MATLAB. The mechanics and electronics of the ARBITER platform are completely modular: a structure can contain as many servo motors and loadcells as desired and their location can be freely chosen; microcontroller, battery and IMU are bundled together as the “spinal cord” and must only be placed once into a structure. This element also contains a bluetooth module that receives high-level commands from an external source (“brain”). As the control framework is designed to work with legged structures, we assume that an “arbitrary legged morphology” consists of *body segments* to which *limbs* are attached, however we do not specify these elements further. An example of a quadruped robot with the main components and the connectors can be seen in Fig. 6.1; the robot weights approximately 16.8 N.

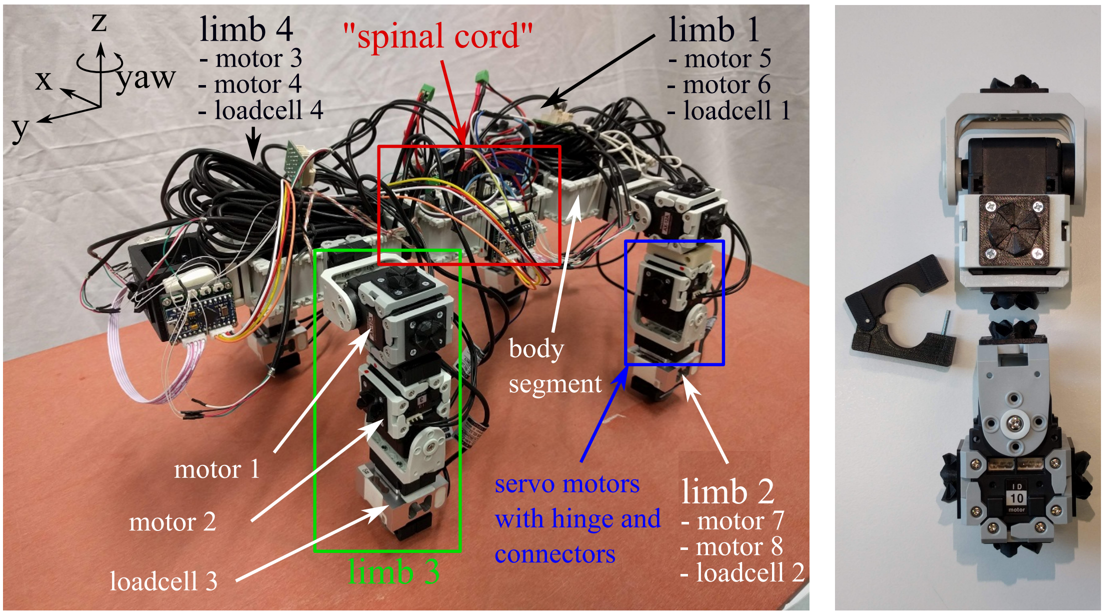
z
x
yaw
y
limb 4
- motor 3
- motor 4
- loadcell 4
"spinal cord"
limb 1
- motor 5
- motor 6
- loadcell 1
body
segment
motor 1
motor 2
loadcell 3
limb 3
servo motors
with hinge and
connectors
limb 2
- motor 7
- motor 8
- loadcell 2
10

(a) (b)

Figure 6.1 – (a) Quadruped prototype with the ARBITER platform. (b) Close-up of the connector: two “crowns” (in black) interlock in 90 degree increments; a “cuff” wraps and is tightened around the combined crowns, preventing them from disconnecting.

### 6.2.2 Costs

ARBITER is designed to be a low-cost platform with easy programming such that controllers can quickly be tried out. Moreover, the modular sensor integration allows the design and testing of closed-loop controllers, based on sensory feedback, on a largely open morphology space. In Tab. 6.1, we listed the costs of the main components and sum the total costs for the quadruped morphology in Fig. 6.1a with 8 motors as well as a large structure with 34 motors (“centipede”; 10 limbs with 3 DoF each, 5 main body segments with 4 segment actuations in between). We regard the total costs acceptable in light of the flexibility of the platform and the sensorization capabilities.

## 6.3 Controller strategy: twitching, learning and tegotae

### 6.3.1 Full process: building to walking

To get an overview from building a legged morphology with ARBITER to making it locomote, we briefly list the separate processes. First, the hardware has to be built. Motors and sensors can be combined to form a structure with the following design rules: (i) a morphology must contain the “spinal cord” unit, (ii) there should be a “main body” to which “limbs” are attached, (iii) the main body can consist of several body segments, (iv) actuation between body segments

| component | cost (USD) | # in quadruped | # in centipede |
|---|---|---|---|
| motor module | 60.85 | 8 | 34 |
| loadcell module | 186.9 | 4 | 14 |
| body segment | 16 | 3 | 9 |
| foot | 3 | 4 | 10 |
| “spinal cord” | 88.8 | 1 | 1 |
| combiner | 4.2 | 20 | 60 |
| total costs quadruped (USD) | 1468 | | |
| total costs centipede (USD) | 5200 | | |

Table 6.1 – Cost of ARBITER

is allowed (i.e. spine movement), however only with placing a loadcell at the actuated joint, (v) each limb must contain at least one loadcell, and (vi) the limbs kinematically should be able to experience a *swing* and *stance* phase during a limb oscillation cycle. After building and wiring the components, the structure undergoes a learning process, during which it activates each motor individually (Spontaneous Motor Activity) and measures all available sensory information (motor positions, forces, accelerations, angular velocities). The motor activations and sensory responses then are used to build a correlation map (Hebbian learning) to create a basic internal model of the robot. This includes the finding of how many limbs are in the structure, which motors does each limb contain, which are the neighboring limbs, and if there are actuated body segments in the structure. Additionally, the kinematic model is extracted that defines the global effect of each motor movement on the structure. All these information then is used to assign a phase oscillator to each limb. Upon receiving a high-level movement command from the bluetooth module, the control framework then initiates each limb oscillator to globally match the intention of the command and employs tegotae to achieve interlimb coordination for creating an appropriate gait pattern.

### 6.3.2 Model simplifications at the current stage of the project

To simplify the development of some of the processes described above, we currently work on the quadruped structure seen in Fig. 6.1a. Additionally to the design rules mentioned above, this structure contains no actuation between body segments and exactly one loadcell per limb which are all mounted in the same orientation, however this is in general unknown to the controller but allows us to skip certain processes. The results of the application of each process to this quadruped structure are presented directly in the subsection for an easier understanding. The additional considerations for the application of the full procedure on structures without these additional rules are also briefly pointed out in the corresponding sections but will not be discussed in extensive detail.

### 6.3.3 Spontaneous Motor Activity

*Spontaneous Motor Activity (SMA)*, or *twitching*, occurs during REM-sleep of mammals [14]. It consists of single muscle burst activation against a background of muscle atonia. SMA is thought to help the self-organization of motor synergies. The idea is that the activation of a single muscle with all other muscles in a relaxed state induces movement in the body which can be perceived by the relaxed muscles. This "cause-and-effect"-correlation can be decoded into a map that is thought to contain information about how the musculoskeletal system is interconnected. Since REM-sleep occurs multiple times in every sleep period during the life of a mammal, this concept could be used to explain lifetime learning processes, e.g. the muscle activation adaptation for a growing body (i.e. morphological changes as in [19]). The method in general bears a striking similarity to the well-known impulse response characterization used for system identification purposes of dynamical systems [121]. The impulse response indicates the stability of a dynamical system with feedback and provides information on key system-characteristics such as damping, dominating time constant, and time delay. For Linear Time-Invariant (LTI) systems, the impulse response fully characterizes the system and can be used to model the output of any input signals. An arbitrary legged morphology arguably contains many non-linearities where forming a full internal model might not be achievable with a characterization of such an impulse response only. However, we regard SMA as a method to perform an impulse response characterization on a specific operation point (the current position around which the twitches occur), thus characterizing a *linearized* version of the system. We hypothesize that this characterization contains enough information to let us predict the behavior of the full system. It will be the research of future work to analyze the limitations of this assumption and to create conditions for its applicability.

In Fig. 6.2 on the left, a twitch of one motor in a limb is shown, together with examples of all sensory response types. The motor twitches first in one direction, resets to initial position, then twitches in the other direction and resets again. The robot is initialized in the position seen in Fig. 6.1 and the twitch amplitudes are approximately 7.5 degrees and take 500 ms to complete. During the twitching time, all sensory data is sampled at 50 Hz. Resets are faster because they use the full speed of the servo, however an actual twitch with the same speed would not produce enough data points for the correlation process and is thus slowed down.

### 6.3.4 Number of limbs

The first goal is to define the number of limbs in the system. Due to the simplifications above, the controller knows that there are as many limbs as loadcells in the robot. Thus the structure in Fig. 6.1 has four limbs, crucial information to fulfill the first prerequisite (P1). In general, we suggest that limbs can be detected by analyzing the static value of the loadcells. Loadcells in the limbs would bear a portion of the robot's weight, whereas loadcells in the spine could show a different characteristic. Detecting limbs in a generic manner however will require more research.

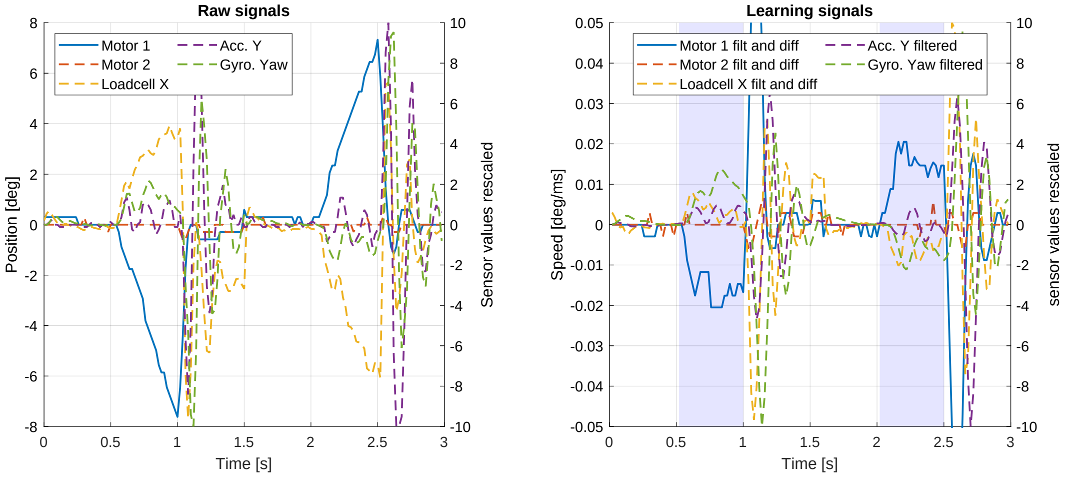

Figure 6.2 – Raw sensory responses (left) and their processed form for the correlation stage (right; blue shaded region is where the correlation is formed)

### 6.3.5 Motor-sensor correlations

#### Hebbian learning

One of the available methods to build an aforementioned correlation map that is based on causally related effects is the bio-inspired *Hebbian learning* [63]. The principle of “fire together, wire together” in this case is used to modify weights of a correlation matrix between effect-causing elements and effect-recording elements (i.e. muscles and muscle sensors). Connection weights between an induced movement and high sensory response are strengthened, while connection weights to low sensory response are weakened during a learning period. Modifications of the weights during this period is governed by a repeated application of an update rule that incrementally adapts the weights until the increment becomes insignificant, i.e. the weights are converged. The most common rule with the additional property of normalizing weights - preventing unbounded growth - is Oja’s rule (Eq. 6.3)

$$\Delta w_{i,j}^{k} = \eta\, s_i^k\, (s_j^k - s_i^k\, w_{i,j}^k) \tag{6.3}$$

$$w_{i,j}^{k+1} = w_{i,j}^k + \Delta w_{i,j}^k \tag{6.4}$$

where $s_i^k$ and $s_j^k$ are two signals to be correlated, $w_{i,j}^k$ is the connection weight from signal $j$ to signal $i$, and $\eta$ is a hand-tuned learning rate. $k$ is a discrete time index, and Eq. 6.4 shows the incremented update of the weight $w_{i,j}^k$ to $w_{i,j}^{k+1}$. In the biological example above [100], $s_i^k$ is the activation signal of muscle $i$, $s_j^k$ is the sensory response of muscle sensor $j$, and $w_{i,j}^k$ is the connection from muscle sensor $j$ to muscle $i$. In our case, $s_i^k$ is a motor movement and $s_j^k$ is a response in one of the implemented sensors.

### Differential hebbian learning

We use a variant of hebbian learning, the *differential* hebbian learning [89] to form the correlation matrix, which uses the derivatives of signals for the update step in Eq. 6.3 instead of directly the measured values. This is shown to have several advantages over the classic rule, most notably the switch to increase the connection strength in the case of "simultaneous change" instead of "simultaneous activation". Consider the following example, interpreting both a motor signal (e.g. $s_1^k = s_m^k$) and a measured force (e.g. $s_2^k = s_F^k$) as firing rates of neurons (the original concept of Hebb) that by definition cannot be negative. Let's start with the case where the motor signal is zero, but a non-zero steady force is present. If by the activation of the motor the force drops to a lower value, Hebb's definition requires the connection strength to be weakened since there is clearly no simultaneous increase of the firing rates of both signals, the condition to be wired together. Yet, the update rule in Eq. 6.3 would still result in a positive weight increment, contradicting the core of the concept. If we now perform the same example with the derivatives of the signals, the motor change is still positive, however it now correlates to a *negative* force change. The weight increment now becomes negative, and so does the weight itself. In a true Hebbian interpretation, this would mean that the signals are anti-causally related. We adopt a more intuitive interpretation where signals simply can be positively related, negatively related, or not related at all.

### Differential hebbian learning in ARBITER

As described in the previous section, the differential hebbian learning rule was developed with non-negative firing rates of neurons in mind, and it allows negative correlation due to the differentiation of signals (which very well can be negative, even in strictly positive signals). At the same time, differential hebbian learning generalizes the raw input signals such that also a "negative firing rate" (simply a negative signal) is allowed since the weight update explicitly acts on the "change" of the signal, as long as the signal is differentiable. This means that we can use both the motor position of the servos and the force measurements of the loadcells in their raw measurement form, to be processed into their differentiated form in the update rule. In the case of the IMU however, it is important to note that accelerations and angular velocity are already measured as "rate of change" measurements, hence signals from the IMU are not differentiated for the update rule (one could make the argument that acceleration as the second derivative of position actually needs to be *integrated* to achieve the same response characteristics; this will be subject of future research). The signals used for the learning can be seen in Fig. 6.2 on the right with the learning period shaded in blue. We apply a moving average filtering with 5 samples and equal weights on the raw signals for a slight signal smoothing. For calculating the weights, we define the update rules as follows:

$$\Delta w_{i,j}^{k} = \begin{cases} \eta_m \, \dot{m_i}^k \, (\dot{m_j}^k - \dot{m_i}^k \, w_{i,j}^k), & \text{for } m_j \text{ position measurements of servo motors} \\ \eta_f \, \dot{m_i}^k \, (\dot{f_j}^k - \dot{m_i}^k \, w_{i,j}^k), & \text{for } f_j \text{ force measurements of loadcells} \\ \eta_a \, \dot{m_i}^k \, (a_j^k - \dot{m_i}^k \, w_{i,j}^k), & \text{for } a_j \text{ acceleration measurements of the IMU} \\ \eta_r \, \dot{m_i}^k \, (r_j^k - \dot{m_i}^k \, w_{i,j}^k), & \text{for } r_j \text{ angular velocity measurements of the IMU} \end{cases} \tag{6.5}$$

where $w_{i,j}$ is the connection between the servo motor $i$ and sensor $j$, $m_i$ is a servo motor position, $f_j$ is a force measurement, $a_j$ is an acceleration measurement, $r_j$ is an angular velocity measurement, and $\eta_{m,f,a,r}$ are the learning rates set to $\eta_{m,f,a,r} = 10$ in our system. The weight increment is the same as in Eq. 6.4. With $n_m$ as the number of servo motors in a morphology, $n_l$ as the number of loadcells and $n_{IMU} = 1$ as the single IMU, this results in a matrix with $(n_m + 3 \cdot n_l + 3 + 3)$ rows with sensory information and $(n_m \cdot 2)$ columns with motor movements; each loadcell measures forces in 3 directions, the IMU measures acceleration in 3 directions and 3 rotations, and each servo motor twitches in 2 directions (the servo position measurement itself is single-channel). Fig. 6.3a shows examples of the weight convergence with the update rule in Eq. 6.5 and increment rule in Eq. 6.4. A low iteration number is desired, and the current learning rates show converged behavior after only 5 iterations. To keep the overview, in Fig. 6.3b a hinton diagram for a single limb is shown, with the area of the squares corresponding to the final converged weight. Note that in both of these figures, the sensory responses are scaled to an interval of [-1,1] within each sensor type (motor, loadcell, linear accelerations, angular velocity) for visualization and post-processing purposes. Further, in most of the cases the sign of the weights for twitching in both directions stays the same, i.e. if a twitch in one direction induces a certain response, a twitch in the opposite direction in most cases induces the opposite response, and so the correlation is the same for both. We manually flip the sign of the weights for one twitch direction to aid the understanding. The full correlation matrix is shown in Fig. B.1.

### 6.3.6 Internal kinematic model

#### Limb segregation

The output after the learning period of weight convergence is a correlation matrix that contains data on how motors are connected together (motor-motor map), how their movement affects the force feedback (motor-loadcell map), the displacement (motor-acceleration map) and the orientation (motor-gyro map) of the entire structure and can be split into these four separate block matrices.

We can now assign motors to limbs to know which limb consists of which motors by analyzing the loadcell data (motor-loadcell map). Under the assumption that a motor movement provokes a higher response in sensors closer in proximity to the motor than in sensors further away, we simply assign a motor to the limb with the highest loadcell response. To do this, we

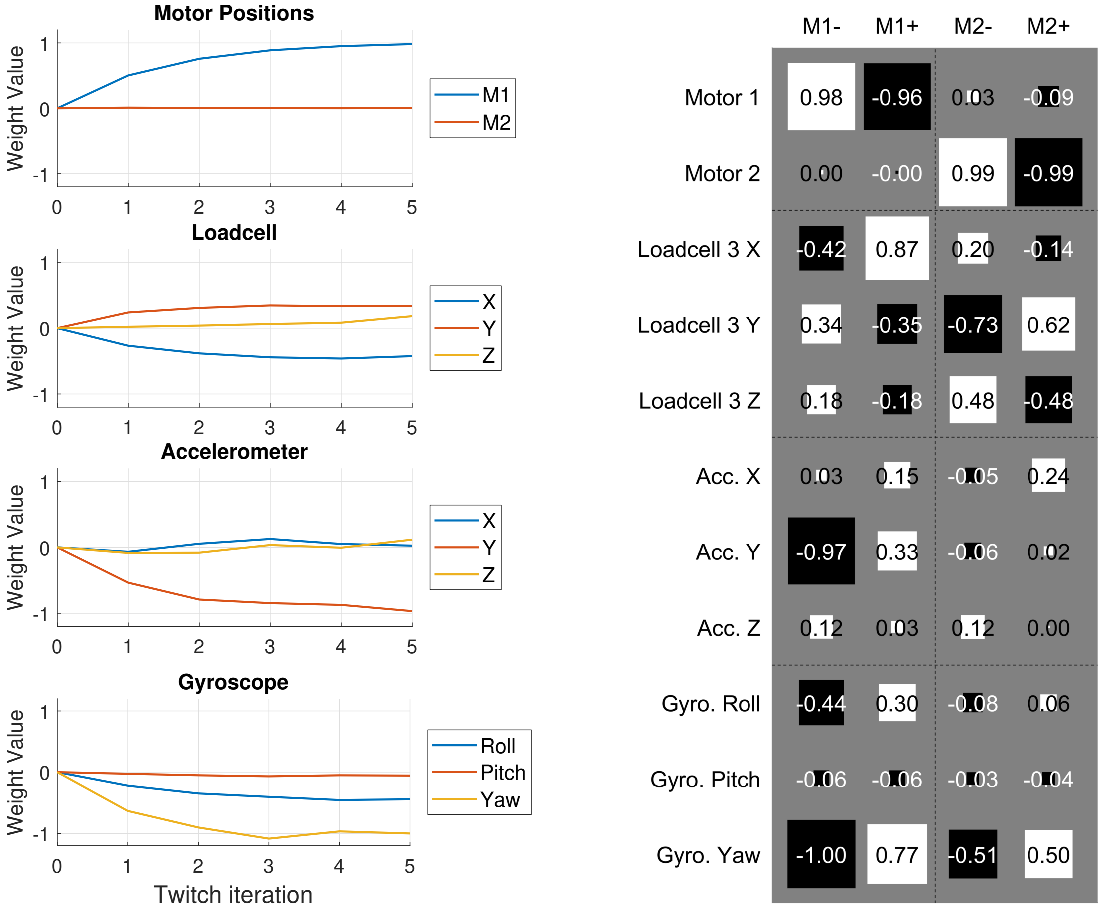

(a) Convergence of the weights

(b) Hinton plot of the weights

Figure 6.3 – Weight convergence (left) and Hinton map (right).

first form the average of the absolute values of all the responses that a motor causes in a given loadcell in both motor directions and all loadcell directions to get an “overall effect” of a motor to a loadcell. We then check the maximal value for a motor in each loadcell and assign the motor to the corresponding limb (Fig. 6.4 with the numeric values of the absolute summed weights and Tab. 6.2 for the assignment). In this example, the value of e.g. 0.39 between Motor 1 and loadcell 3 (LC3) in Fig. 6.4 is formed by the average of the absolute values of M1- and M1+ to Loadcell 3 X, Y and Z ($(0.42+0.87+0.34+0.35+0.18+0.18)/6 = 0.39$). The limb assignment completes the first prerequisite (P1). Note that at this stage the order of the motors within a limb is irrelevant; their actual kinematic effect will be analyzed in a later stage.

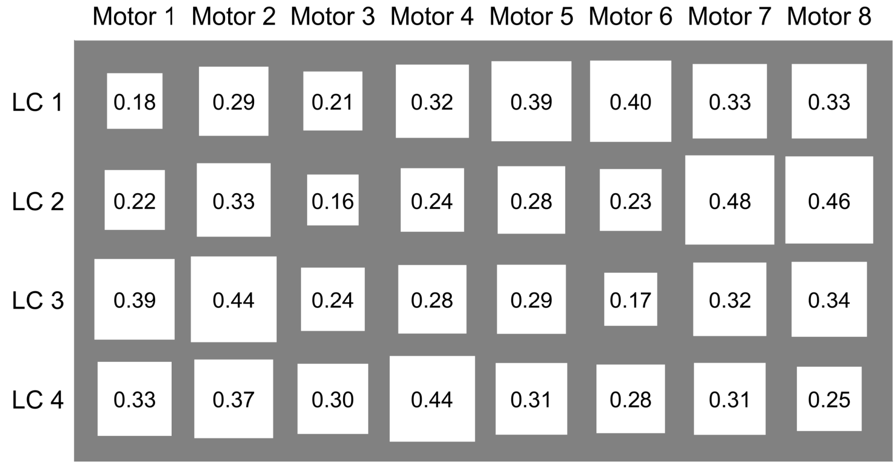

| | Motor 1 | Motor 2 | Motor 3 | Motor 4 | Motor 5 | Motor 6 | Motor 7 | Motor 8 |
|---|---|---|---|---|---|---|---|---|
| LC 1 | 0.18 | 0.29 | 0.21 | 0.32 | 0.39 | 0.40 | 0.33 | 0.33 |
| LC 2 | 0.22 | 0.33 | 0.16 | 0.24 | 0.28 | 0.23 | 0.48 | 0.46 |
| LC 3 | 0.39 | 0.44 | 0.24 | 0.28 | 0.29 | 0.17 | 0.32 | 0.34 |
| LC 4 | 0.33 | 0.37 | 0.30 | 0.44 | 0.31 | 0.28 | 0.31 | 0.25 |

Figure 6.4 – Overall effect of a motor to each loadcell.

| motor | 1 | 2 | 3 | 4 | 5 | 6 | 7 | 8 |
|---|---|---|---|---|---|---|---|---|
| limb | 3 | 3 | 4 | 4 | 1 | 1 | 2 | 2 |

Table 6.2 – Limb assignment.

### The neighboring function

The output of the limb segregation defines which motors form separate limbs, but it does not contain the exact information concerning the geometric arrangement of the limbs, i.e. which are the neighboring limbs. The solution to this problem is a “map-inversion” of the “direct” *limb-loadcell map*, such that it can be used as as the “inverted” *loadcell-limb map*. This is because during runtime of the robot, the controller measures forces from the loadcells and - per tegotae - generates limb movements based on these measurements, inverting the information flow from loadcells to limbs (loadcell-limb map).

Since tegotae relies on the feedback of the vertical ground reaction forces, due to the simplifications we only have to analyze the z-direction of the loadcells. Thus, the first thing to do is to form a matrix with the averaged loadcell effects in z-direction for each motor, grouped into limbs (Fig. 6.5). Ideally, it should be visible in this map, which motors are more suitable to load and unload a leg, e.g. M5 (a “hip” motor in limb 1) has a higher effect on LC1Z than M6 (a “knee” motor in limb 1). These motors would potentially be more suitable to induce swing- and stance-phase, and the other motor in the limb would then be used for propulsion. The presented example currently does not hold for all the limbs, requiring a closer investigation. For now, we use a human observer to pick the correct values out of Fig. 6.5 to form the square “direct” map $\boldsymbol{S}_{LCz}$ in Fig. 6.6a. Some of the signs in $\boldsymbol{S}_{LCz}$ change in comparison to the matrix in Fig. 6.5 because the feedback from the own limb has to be negative, inverting the signs of the entire column. To form the map inversion, we simply transpose $\boldsymbol{S}_{LCz}$ and normalize by the highest value. This creates the matrix $|\boldsymbol{S}_{LCz}^{\top}|$ in Fig. 6.6b, mapping the the influence of the vertical ground reaction forces of each loadcell to each limb.

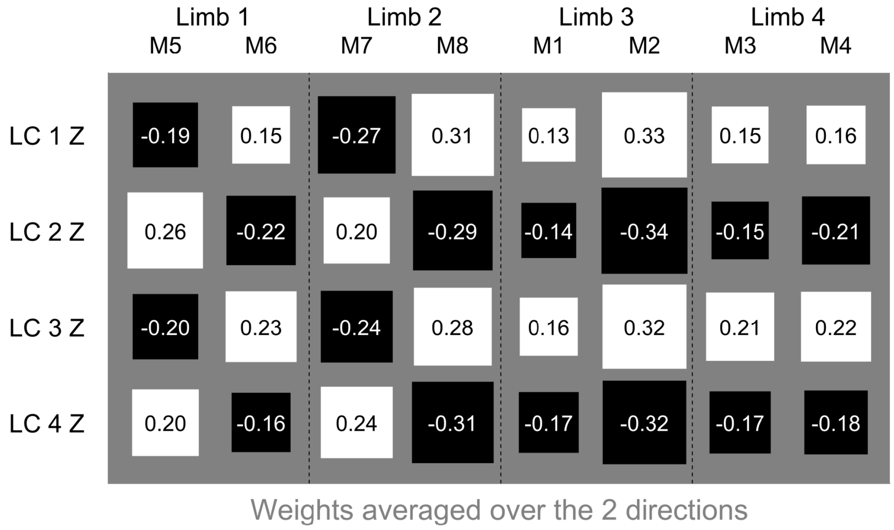

| | Limb 1 | | Limb 2 | | Limb 3 | | Limb 4 | |
|---|---|---|---|---|---|---|---|---|
| | M5 | M6 | M7 | M8 | M1 | M2 | M3 | M4 |
| LC 1 Z | -0.19 | 0.15 | -0.27 | 0.31 | 0.13 | 0.33 | 0.15 | 0.16 |
| LC 2 Z | 0.26 | -0.22 | 0.20 | -0.29 | -0.14 | -0.34 | -0.15 | -0.21 |
| LC 3 Z | -0.20 | 0.23 | -0.24 | 0.28 | 0.16 | 0.32 | 0.21 | 0.22 |
| LC 4 Z | 0.20 | -0.16 | 0.24 | -0.31 | -0.17 | -0.32 | -0.17 | -0.18 |

Weights averaged over the 2 directions

Figure 6.5 – Effect of a motor on the z-direction of each loadcell.

The inherent scaling could mean that instead of empirically finding different $\sigma_i$ feedback and $k_j$ scaling gains according to the neighboring relationship, only one single $\sigma$ to scale the complete inversion map will be needed; it also remains to be seen if only the immediate neighbors are required or if the full matrix can be used. However, our preliminary proposition is a new phase progression equation. By interpreting the second and third term in Eq. 6.2 as a limb-specific *weighted average* of the normal forces of all limbs, which is essentially the same information as encoded in the inversion map, we can rewrite the phase progression $\dot{\boldsymbol{\phi}} = \dot{\phi}_i \; \forall \; i$ of all oscillators as

$$\dot{\boldsymbol{\phi}} = \boldsymbol{\omega} + \sigma \, \boldsymbol{I} \cos\boldsymbol{\phi} |\boldsymbol{S}^{\top}_{LCz}| \, \boldsymbol{N} \tag{6.6}$$

with $\sigma$ as a single *scalar* gain and $|\boldsymbol{S}^{\top}_{LC}|$ the matrix with the entries from the loadcell-motor map inversion. In Eq. 6.6, $\dot{\phi}$ is a column vector ($\dot{\phi} = [\dot{\phi}_1, \dot{\phi}_2, \ldots, \dot{\phi}_n]^{\top}$), $\boldsymbol{\omega}$ is a column vector with same entries of $\omega$ (i.e. $\boldsymbol{\omega} = \omega \cdot [1, 1, \ldots, 1]^{\top}$), $\boldsymbol{I}$ is the identity matrix, $\cos\boldsymbol{\phi}$ is a column vector ($\cos\boldsymbol{\phi} = [\cos\phi_1, \cos\phi_2, \ldots, \cos\phi_n]^{\top}$), and $\boldsymbol{N}$ a column vector ($\boldsymbol{N} = [N_1, N_2, \ldots, N_n]^{\top}$). The future research on this project will show if Eq. 6.6 is applicable as proposed. However, it already shows interesting properties such as the neighbor opposition effect described in section 6.1.4. If we look at e.g. limb 3, we can see in $|\boldsymbol{S}^{\top}_{LC}|$ that the loadcell measurements LC2 and LC4 (0.506 and 0.603) of its immediate neighboring limbs will affect the phase progression $\dot{\phi}_3$ *opposite* to its own effect (-0.566). This corresponds to the sign inversion indicated in Eq. 6.2.

Note that in case a limb contains more than one loadcell, the limb-loadcell map $\boldsymbol{S}_{LC}$ in Fig. 6.6a is not square, however the normalized tranpose can still be formed. Further, it could be useful to split the ground reaction force directions and form separate map inversions such that the feedback of loadcell directions is treated differently in tegotae. This is proposed in

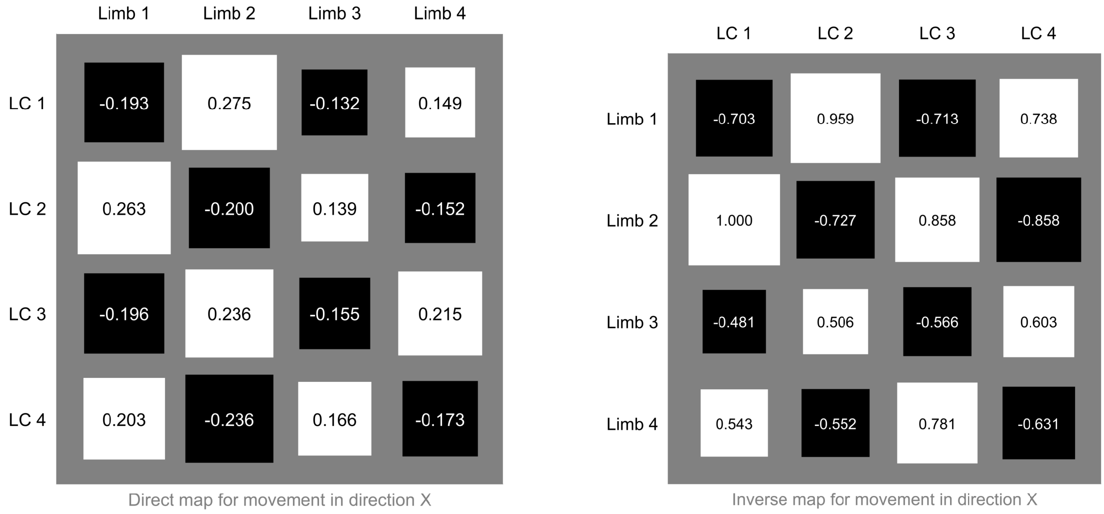

(a) $\boldsymbol{S}_{LCz}$ (b) $|\boldsymbol{S}^{\mathsf{T}}_{LCz}|$

Figure 6.6 – Loadcell-limb map inversion. (a) "Direct" limb-loadcell correlation matrix $\boldsymbol{S}_{LCz}$ (limb-loadcell map). (b) "Inverted" and normalized loadcell-limb matrix $|\boldsymbol{S}^{T}_{LCz}|$ (loadcell-limb map).

[50] where the normal force is used for standard tegotae to incorporate body support and the vertical friction force is used for another tegotae term to incorporate propulsion. We can imagine forming similar, directional loadcell map-inversions $|\boldsymbol{S}^{\mathsf{T}}_{LCx}|$ and $|\boldsymbol{S}^{\mathsf{T}}_{LCy}|$ for the other force directions. These maps could be used for including other or more sensory feedback terms in the phase progression equation Eq. 6.6. Likewise, such maps could also be formed for other sensory feedback caused by a limb, e.g. $\boldsymbol{S}_{ax}$ and $|\boldsymbol{S}^{\mathsf{T}}_{ax}|$ for the accelerations in $x$-direction. We thus call $\boldsymbol{S}$ the set of all limb-*sensor* maps.

### 6.3.7 Accelerations

With the limbs separated, the next step before limb movement can be tackled is to understand the local kinematic effect of each motor within a limb to the IMU. It is clear that servo motors have different functions in a limb. A twitch could cause a limb to lift off the ground; this motor could have the function of inducing stance and swing phase of its limb. A twitch in another motor could result in the increase of horizontal ground reaction forces, that at the same time are measured by the IMU as e.g. an acceleration in the global $x$-direction; this motor could have the function of propulsion. The goal of the internal kinematic model is to use it as the basis to generate a trajectory for each limb that - based on this information - performs an elliptical movement, with one axis in the global $z$-coordinate to induce stance and swing, and the other axis in either global $x$- or $y$-coordinate, depending on the desired locomotion direction, to induce propulsion. The idea is that if this trajectory can be successfully generated for each limb individually, i.e. an *intralimb coordination* can be defined, a proper *interlimb coordination* can take place on top, which then results in a global locomotion pattern.

Forming the internal kinematic model follows a set of rules. Each force weight matrix is correlated to the acceleration weight and gyro weights to categorize its local effect, creating a limb-specific transformation map between forces, accelerations and rotations. Due to the current simplification in the quadruped that all loadcells are mounted in the same orientation, we can form these maps manually, however the research has not progressed this far yet.

We are aware that the local effect only defines a single point on a complete limb trajectory. It is by no means guaranteed that this could result in a successful trajectory execution, however there are certainly conditions under which the approach is valid, and we plan to investigate these limitations.

### 6.3.8 Assignment of oscillator parameters

Now everything is ready for assigning oscillatory movements to each motor, depending on the desired overall direction of heading. Similar to the biological systems of brain and spinal cord, the brain only sends high-level commands to the spinal cord which takes care of the low-level coordination to match the desired command. In our case, the high-level command is a requirement to the IMU. As an example, let us assume the robot is standing still and we demand the IMU to experience an acceleration in global $x$-direction such that the robot starts to translate itself forward. The controller detects the mismatch of the current and desired state of the IMU. The internal kinematic model from the correlation map (spinal cord) at this stage has the ability to inform the controller of how the motors need to be moved to match the demand of the IMU. The controller now assigns the oscillatory trajectory to each limb such that it instantaneously corresponds to the servo movement requirements defined by the kinematic model.

There are three major conditions that need to be fulfilled for the robot to obtain limb oscillations suitable for locomotion: (i) the actual full kinematics of the robot must permit all the limb trajectories, (ii) the full trajectory of each limb has the same global effect on the IMU as the local twitch, and (iii) the full trajectory must also contain a stance and a swing phase for each limb.

Although we cannot provide a fool-proof strategy to fulfill these conditions at this stage of the project, we can make certain predictions on when the conditions are more likely to be met. All of them depend on how a designer (a human or an algorithm) creates a legged structure. By e.g. creating enough space between limbs, one can ensure that the full limb movements do not collide with any other element of the robot. Orthogonal motor movements reduce the complexity of trajectories, which is beneficial to the global kinematic effect of the trajectory. At last, a limb having the possibility of a stance and swing phase also largely depends on the initial robot design and around which operation point the robot is initiated.

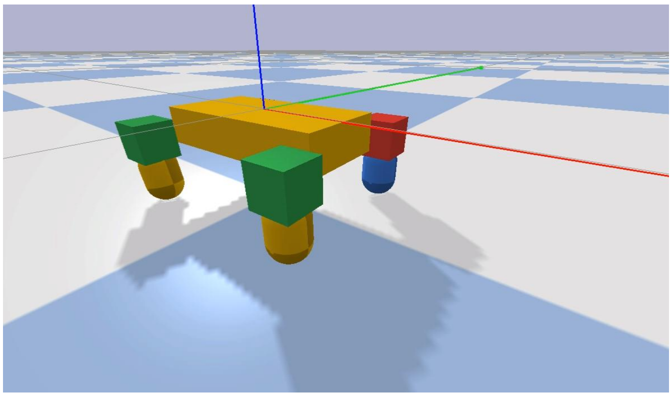

Figure 6.7 – Simulation of the ARBITER quadruped.

### 6.3.9 Simulation

A simulation is currently being developed. At the moment, it contains a model of the quadruped with dimensions and weight distribution taken from the real hardware (Fig. 6.7). Only the twitching process is implemented, however several simulation parameters still need to be tuned (e.g. ground friction properties and joint damping properties) to result in a stable process. The work on the simulation will be done in parallel to the hardware experiments.

## 6.4 Conclusion and Future work

This chapter presents the first steps towards a generic locomotion controller for arbitrary legged morphologies. We developed ARBITER, a low-cost modular robot platform that allows the fast creation of such morphologies consisting of 1 DoF servo motors, 3-axis loadcells, an IMU, bluetooth module and microcontroller, all powered by an on-board battery. We propose a control framework that involves the generation of an internal model estimation with the use of Spontaneous Motor Activities (SMA) and differential Hebbian learning. The output of these processes is a map that we see as the "spinal cord" of the legged structure: it contains information on how many limbs the structure has, which motors belong to which limbs, how the measurements in one limb are influenced by other limbs, and the local kinematic effect of each motor movement. This information then is used to assign phase oscillators to each limb, creating elliptical feet trajectories that are suitable for locomotion (intralimb coordination). The interlimb coordination is achieved by a generalized version of multi-legged tetogae, a force-feedback method to modulate the phase progression. This method requires a limb neighboring function, for which we propose a new, systematically derived mapping method resulting in the required function with the additional feature of inherent scaling.

The "spinal cord"-approach can be seen as forming an internal model based on specific motor exploration. This bears many similarities to [21] to which we will compare our results once the concept is fully developed.

As this work is currently in progress, we performed validating experiments on a quadrupedal morphology and present preliminary data such as data collection (on-board), off-board data processing, limb segregation, the correlation matrix based on differential hebbian learning, motor-limb assignment and a limb-loadcell map inversion to create the neighboring function. In parallel, we started the development of a simulation to validate the approach also in simulated physics. Such a simulation potentially could then be used in optimization algorithms (e.g. evolutionary algorithms).

The next steps are to assign the phase oscillators to the limbs based on the formed internal model and apply the multi-legged tegotae to achieve interlimb coordination. Some of the processes involved in creating the locomotion controller still need further detailing as the current controller derivation is based on simplifications that helped the development of the different stages. Moving towards genericness requires a careful re-analysis of all processes, however we expect that having both hardware and simulation in hand should enable us to perform the necessary tests to progress.

# Conclusion and Future Work

This thesis investigates mode-switch methods in hardware and control for legged locomotion of robots on smooth and especially rough terrain, the primary environment of animals. In our research, we take inspiration from animals to build robots, and in return we aim to advance the understanding of animal locomotion with these robotic tools. The underlying intuition is that the effort and work needed to make a robot locomote on smooth terrain usually is already significant; the comparatively "minor" change to rough terrain seems negligible, yet the locomotion performance of robots often deteriorates or they can fail completely due to perturbations caused by the rough terrain. In contrast, animals display impressive locomotion capabilities on all kinds of terrains.

We hypothesize that it is not the main control unit that needs to take such perturbations into account. By isolating different instances in a locomotion cycle, we suggest that some sub-systems need to perform different tasks at different times, and thus locally change their *functionality*. The key characteristic is that these systems modify their dynamical response, which we call a *mode-switch*. These mode-switches perform a local computation that locally trades-off characteristics of soft and hard materials, e.g. adaptability and force transmissibility, and these local effects are shown to have a global influence on the locomotion of a robot.

We present one mode-switch method in hardware and one approach in control that - if designed appropriately - deal with perturbations in legged locomotion, especially caused by rough terrain. The goal of mode-switches is to simplify the control, thus reducing the need for developing complex interaction models and computationally expensive algorithms. The presented mode-switch methods act on different hierarchical levels in locomotion (foot and leg), making them independent form each other. This separation allows them to be combined in future research.

Local mode-switch methods ideally should be morphology agnostic such that they could be applied to any legged structure. As robotic hardware that reflects this flexibility, we selected reconfigurable modular robots that can be configured into various morphologies. For most of the research, we use a customized version of the commercially available modular robotic system Bioloid-Kit. Additionally, we explore the aspect of autonomous reconfiguration of such a system. For this, we use the self-reconfigurable modular robot (SRMR) system Roombots. A proof-of-concept hardware version of this platform has been developed in the Biorobotics

Laboratory over the last ten years, however further development was needed to improve the self-reconfiguring aspects.

## Roombots as a self-reconfigurable modular robot platform

### Summary and outcomes

The long-term vision of our self-reconfigurable modular robot system *Roombots* is to use them as adaptive and assistive furniture in our living space, where tens of modules act together to form dynamic, furniture-like structures. To take a step towards this vision, Roombots had to be brought from a proof-of-concept hardware project to a proof-of-concept application project. Part I of this thesis focused on the required improvements of Roombots, both in hardware and control. The main challenges were to on the one hand increase the precision of a single module and on the other hand develop strategies to deal with real world effects, namely alignment issues, that occur especially in scenarios with multiple, collaborating modules as imagined in our vision.

We motivated the choice of using stronger materials for the mechanics of Roombots and detail the addition of sensors to enable feedback control for docking sequences. Both these improvements significantly increased the reliability of a single module, and 11 new functional modules were built with this hardware and control iteration. This larger number of modules enabled us to perform a variety of new demonstrations that were not possible before, among which we show a large-scale reconfiguration sequence with 12 modules (36 DoF) resulting in a chair structure. This puts Roombots among a few selected 3D SRMR systems that are able to perform such complex self-reconfiguration sequences. Moreover, to the best of our knowledge it is the only self-reconfiguration at this scale where all the modules are initialized completely separate (detached).

We explore further applications of Roombots as adaptive and assistive furniture and perform various demonstrations around this vision. These include a chair following and evading a user, mobile furniture that can adapt to the environment and overcome obstacles, manipulation tasks such as picking up a pen and opening a PET bottle, and the development of a user interface to easily control Roombots. Some of these tasks required object manipulation capabilities. We developed a mobile version of a “Universal Gripper” [26] that uses the concept of *jamming of granular media* to grip a variety of everyday objects, and we detail its integration into Roombots modules.

We showcase the *versatility* aspect advertised in modular robots (explained in the topic introduction of Part I) by solving a variety of tasks with the same modules, configured differently according to these tasks. Concerning the *robustness*, we significantly improved the reliability (i.e. system robustness) of one module such as command execution, control precision and docking. However, even though we improved the strength of mechanical subsystems such as gearboxes, the overall mechanical robustness could still be considered fragile: the chair built with 12 modules is not able to support the weight of a user and modules would start to break. This is related to the third point of the list, *low-cost.* Due to the high mechanical complexity of a module, most of the hardware is custom, making the system in general susceptible to mechanical failure while also drastically increasing the production costs at the same time. Mass-producing parts eventually would help to drive down the costs, however mechanical simplicity is certainly a requirement for low-cost modules.

### Future Work

The platform in its current state can be used for further research in self-reconfiguration as well as finding potential applications in general for SRMRs. Several research directions could be explored with Roombots, including vision capabilities and new collaboration algorithms that could deal with the integration of passive parts to create larger formations. It should however also be mentioned that the demonstrations performed in this thesis operate at the limitations of the platform in terms of number of modules, duration and complexity of experiments, and available module power (i.e. one module can only lift one other module), hence one has to consider developing a new platform for new research.

Even though SRMRs are thought to be “universal”, a concrete application should still be kept in mind. My experience is that a usual reaction to Roombots is the question “Can you make it smaller?”, and this question seems to have been driving many similar researches, ultimately all dealing with space constraints within a module and power density considerations. To me, the answer to this question is “What will the system be used for?” This question also challenges Roombots themselves: in the application of adaptive furniture, the smallest furniture “unit” seems to be in the order of a stool rather than in the order of a leg of a stool. On the flip side, in the application of multi-degree object manipulation, which forms a substantial part in the demonstrations presented in Part I, the size of one module seems more appropriate.

It is thus vital to consider the application first, which then can be used to guide the development of new hardware and control, potentially with new future technologies.

## Local computation in locomotion

### Summary and outcomes

Part II and Part III of the thesis investigated legged locomotion in combination with methods in hardware and control that result in mode-switches, i.e. methods that can gradually or rapidly modify the local dynamic response, resulting in the effect of a local computation. Altering the dynamical response can be interpreted as changing mechanical properties, which in turn is described as a change in *functionality.* The presented methods were developed with genericness in mind such that they could be applied to any legged system. As the robotic hardware, the modular robot platform *Bioloid-Kit* [134] is used in these Parts.

### Mode-switch methods in hardware and control

Part II introduces the hardware mode-switch method *jamming of granular media* [96]. Using cubically shaped compliant rubber granules, a flexible membrane and vacuum, one can achieve a practically linear transition between a "soft" state (fluid state) with shape adaptation and strong damping abilities and a "hard" state (jammed state) with high stiffness properties through jamming. Downsizing the involved mechatronic components of such a system resulted in a wearable joint support device that can be used to stiffen or block the movements of various human joints (ellbow, shoulder, knee, ankle), transitioning between the functionalities "free movement" and "freeze movement".

We then used the concept to create jamming membranes as end effectors, creating a robot that can climb a variety of specifically shaped terrain due to the state transition. In this case, the end effectors switch between the functionalities "shape adaptation" and "force transmission".

Going deeper into the subject of jamming end effectors, we analyzed the role of the *foot* in locomotion and isolated two different functionalities of the foot in a locomotion cycle: at touchdown, it creates a contact area and must damp the impact forces to avoid bouncing, and in stance, it must transmit propulsion forces generated by the body over the contact area to the ground. The functionalities are thus "impact damping" and "propulsion force transmission", with the additional "side-effect" functionality of "shape adaptation" playing a crucial role in locomotion on rough terrain. Jamming end effectors are shown to be well suited to fulfill these tasks. Moreover, a comparison to human feet revealed that a group of bones known as the *tarsal bones* could perform a very similar state transition from a compliant system to an interlocked system [13], shedding light on how a biological system potentially uses a mode-switch for legged locomotion.

In Part III, we introduce the control mode-switch method *tegotae* [116], a force feedback strategy that was shown can be interpreted as temporarily increasing the "spring stiffness of movements", i.e. it accelerates or slows down oscillatory movements - governed by phase oscillators - with characteristics similar to a spring. This method focuses on a functionality change in the *leg*: in our view, the leg movement in swing phase has the functionality of "displacing the leg", whereas in stance phase it has the functionality of "displacing the body". Tegotae is able to accommodate this switch, and we show that this control method has the ability to improve the locomotion stability of a quadruped robot. Additionally, it is also shown that the energy efficiency in rough terrain locomotion is improved due to the method's ability to locally trade off between body stabilization and body propulsion.

In the last chapter, we explore the interesting property of tegotae of emergent interlimb coordination. In previous research, it was shown that tegotae could autonomously create a locomotion pattern in a hexapod robot [115]. We discuss the prerequisites for this phenomena to occur and started to develop a generic control framework that is able to induce coordinated locomotion behavior in arbitrary legged structures. We speculate that this controller could function similarly to the spinal cord and plan to test its capabilities on various morphologies, fully utilizing the properties of modular robots to quickly create such morphologies. As this work is currently in progress, we introduce the overall concept and present preliminary results of validation experiments.

### Can locomotion control be simplified?

Let us put these investigations in perspective to my research question "Can local computation through mode-switches be beneficial for locomotion in general and specifically for legged locomotion on rough terrain, and if so, what are the effects of them and how do they improve locomotion?"

The answer to the first part of my research question, I would say that our results report locomotion improvements. Most of the experiments with the quadrupedal robot use the same high-level movement controller, yet locomotion metrics improve when mode-switches are implemented. We can draw the analogy that mode-switching performs a certain kind of local computation that has a beneficial global effect. If the mode-switch method is in hardware, this might be equivalent to the definition of *variable morphological computation* [140] (changing the intrinsic mechanical dynamics of its hardware). However, in this thesis we also discuss locomotion performance increases by a mode-switch method in control that also changes the dynamical response, which would not fall under this category. I see the computational effort of mode-switch methods in the general ability of the method to locally modify the dynamical response to perturbations, which can also be achieved by a control strategy. The *effect* of changing dynamical responses is that perturbations are dealt with differently at different instances: due to noise and other disturbances, sometimes a perturbation needs to be absorbed a little bit more than usual (e.g. adaptation in "soft" mode), whereas sometimes a bit more resistance to a perturbation is required (e.g. force transmission in "hard" mode).

In this thesis, the reasons why modifying dynamical responses is needed are either (i) effects of real world physics that are extremely difficult to model or (ii) to introduce a dynamic coupling between elements such that information can be exchanged over physical links. It seems that hardware mode-switches rather tackles the former problem, e.g. the complex interparticle interaction in jamming systems results in a highly complicated spring-damper system that can be used to deal with friction interaction between the ground and a foot contact area, a phenomena which would be extremely difficult to accurately model. On the other hand, the presented control switch-method seems to affect the locomotion more globally. It acts on movement adjusting parameters by dynamically coupling them to the environment via feedback, allowing the dynamics of the locomotion to exchange information with the environment in this process. This in part answers the second part of my research question on what the effects of the mechanisms are, although a mathematically more rigorous analysis of contact interaction forces and limit cycle behavior could provide more insight in e.g. the exchange or loss of energy caused by altering the dynamic response.

For answering the third part of my research question on how the mode-switches improve locomotion, the reported results in the chapters provide clues for the individual working principles of the methods. Jamming in an end-effector allows it to switch between a shape-adapting damping element and a shape-adapted, force-transmitting spring element. In rough terrain locomotion, it can adapt to the terrain shape and simultaneously damp vertical impact forces and horizontal forces caused by an imprecise coordination between touchdown and maximal horizontal foot trajectory. This causes less bounces, letting propulsion forces act earlier and more consistent on the formed ground contact area. This in turn makes the step lengths more uniform, resulting in an overall faster and more stable locomotion. In tegotae, the slight accelerations and decelerations that the oscillation of each limb can experience promote a limb towards its optimal state for weight bearing. This induces a globally coordinated behavior through information exchange of the intrinsic dynamics: the locomotion controller recognizes the stability brought by limbs that bear weight and rather focuses on moving the ones that do not, gaining some form of embodied intelligence [122]. Especially on rough terrain where transitions between stance and swing happen more inconsistently due to the terrain irregularity, this creates a better match between the intention of the controller and the physical state of the system.

And lastly, we have to look at the aim of mode-switching to simplify locomotion control. Here again, the fact that the same high-level locomotion controller on the quadruped resulted in locomotion improvement if used in combination with mode-switching methods seems to confirm this hypothesis. We assume that we could create the same beneficial effects with complex control strategies and high-performing hardware, accounting for a certain computational effort. This effort corresponds to the local computation carried out by the mode-switch, which in the high-level controller now is available for other tasks.

## Future Work

It is important to note that the mode-switch methods of jamming and tegotae act on different functionalities in locomotion and are not mutually exclusive and in fact could easily be combined. I would argue that more such functionality changes by altering the dynamical response of a component can be identified, potentially also in other tasks besides locomotion, and individual strategies of local computation through mode-switching could be developed. Ideally, this could lead to a library of such methods with different effects, and one could pick the methods with the desired features and combine them.

Local computation through mode-switching might very well be task specific, however it is supposed to work in a generic manner, more or less independent of the robot morphology it is applied to. Thus the application of such methods - the ones presented in this thesis as well as potential methods in future research - to different morphologies and even different robotic platforms would provide valuable information about their generality. In the end, if this research could be transferable to advance the understanding of animal locomotion, then the aim of this thesis was reached.

# A Further applications with Roombots

This chapter briefly summarizes further projects with Roombots that are not the main focus of this thesis but carried out alongside the development of Roombots.

## A.1 Application: Playdough to Roombots

**Reference publication**

Parts of the text and figures of *Mehmet Mutlu, **Simon Hauser**, Alexandre Bernardino and Auke Ijspeert. "Playdough to Roombots: Towards a novel tangible user interface for self-reconfigurable modular robots." In 2018 IEEE International Conference on Robotics and Automation (ICRA), pp. 1970-1977. IEEE, 2018.* have been reorganized in this section.

**My original contributions**

- Writing of the Introduction
- Help in the supplementary video, particularly in the hardware experiments
- Inputs to the manuscript

### A.1.1 Purpose

A modular robot system can have the ability to represent every shape more or less accurately. It is however a challenge to bring the imagination of a user into a form such that the system is able to assume this form as closely as possible. This work describes the method of a tangible user interface (TUI), involving modeling clay and 3D-scanning, to quickly transform a users inspiration into an abstract representation that can be understood by a modular system, such that further processes are able to bring this inspiration to life by recreating it with the robotic system.

### A.1.2 Summary of the work

#### Overview

One of the grand challenges for the intended usage of structures built with SRMR is the method of how the inspiration for a structure by a user is translated into an real world representation with SRMR [181]. This process is illustrated in Fig. A.1. We formally split the full process into five subprocesses: (i) expression, where an idea of a user takes shape in the real world, (ii) digitization, where this idea gets digitized and put into a PC, (iii) abstraction, where the raw digital representation is post-processed into a representation that can be used by an SRMR system, (iv) planning where algorithms produce an instruction plan that creates the desired shape in the form of a building sequence and finally (v) formation, where the SRMR form into the initial inspiration in the real world by following the building plan provided by the planning step. It is important to notice that only the first and the last processes take place in the real world and only they are usually able to provide any other than visual feedback (e.g. haptic feedback) which is the primary type of feedback in the digital representation.

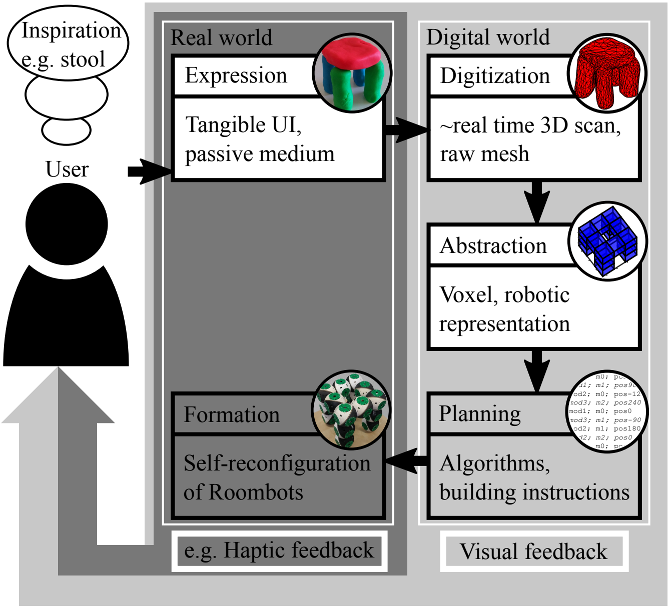
Inspiration
e.g. stool
User
Real world
Expression
Tangible UI,
passive medium
Formation
Self-reconfiguration
of Roombots
e.g. Haptic feedback
Digital world
Digitization
~real time 3D scan,
raw mesh
Abstraction
Voxel, robotic
representation
Planning
Algorithms,
building instructions
Visual feedback

Figure A.1 – The cycle from an inspiration to the final Roombots shape. The inspiration first is expressed in the real world. A digitization step transforms it into the digital world where the processing steps abstraction and planning can take place. At last, the inspiration takes shape with the SRMR by the formation.

This work focuses on the three aspects expression, digitization and abstraction as a whole. In particular, we seek a method that is able to rapidly produce the abstracted representation of an idea; as one of the main strengths of SRMR is their ability to shape-shift and create (almost) arbitrary structures, a fast abstraction of the inspiration is necessary to allow a purposeful interaction with an SRMR-system. We present a method that combines the relatively novel technology of 3D-scanning with an existing algorithmic approach (DFS) with adjustments to autonomously generate the building instructions for Roombots, bringing us one step closer to the vision of Roombots to be used as "fast-protyping" user-created furniture. The planning and formation (self-reconfiguration) steps are described in other works (e.g. [84]) and will not be further discussed here.

### Process methods

**Expression - Modeling clay:** The Roombots is a complex robotic system. In order to simplify the interaction, we inclined for a passive medium which can be anything (LEGO® blocks, wood pieces etc.) that allows creation of structures that can be replicated with Roombots. Modeling clays are widely used for 3D shape modeling in games, e.g. Cranium® and Cluzzle®, or professional activities like architecture or art. Play-Doh® or similar modeling clays are very easy to shape and made for kids to create 3D shapes. Modeling clay is also one of the most studied tangible user interface (TUI) material used in the literature [127, 75, 81, 51].

**Digitization - 3D scanning:** Having a passive interaction medium requires an additional step to digitize the shape information that is formed by the playdough (note that if the inspiration is directly digitized e.g. by modeling a structure in a PC, the expression step can be skipped). In this regard, we rely on commercial scanning solutions - which are becoming widely available and cheaper - to convert the real object to the digital data. The result of the 3D-scanning process is a mesh grid that approximates the shape of an object with surface triangles.

**Abstraction - Voxels and Roombots:** For representing the 3D information, we use a voxel representation. Voxels are commonly used to represent SRMRs, particularly lattice types like Roombots. Example usage of cubic SRMR representation can be seen in [155, 157] and [138].

### From playdough to Roombots

The construction of structures with a shape given by the playdough is a multi stage process that is almost completely autonomous. Once the user shapes the playdough, the following stages are (i) 3D scanning (scanning the playdough structure with a handheld 3D scanner), (ii) mesh pre-processing (verification of the surface mesh produced by the 3D scanning process), (iii) voxelization (approximating the surface mesh with small voxels to obtain a volumetric representation), (iv) initial module placement (important for the start of the search algorithms),(v) construction search (creating a low resolution voxel representation with Depth First Seach (DFS)) and (vi) the user feedback (manual pruning and removing of superfluous voxels).

### Conclusion and limitations of the proposed solution

Our demonstrated system has three major limitations: (i) 3D scanning is not real time, thus we only demonstrate the proof-of-concept, (ii) it does not use the full potential of Roombots and

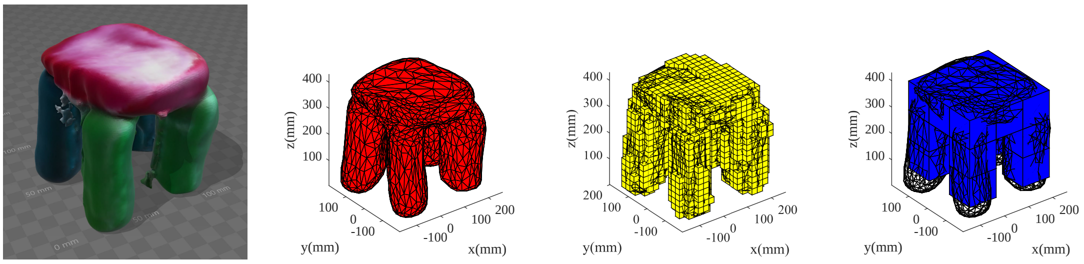

(a) initial view of the 3D scan (b) mesh pre-processing (c) high resolution voxelization (d) low resolution voxelization

Figure A.2 – Stages of playdough-to-Roombots. The initial 3D scan is processed into a mesh which then is filled with small voxels to obtain a high resolution model. This is then converted into a low resolution model with the DFS search algorithm, involving careful seed-module placement, pruning methods and user feedback to create the final Roombots structure (blue voxels).

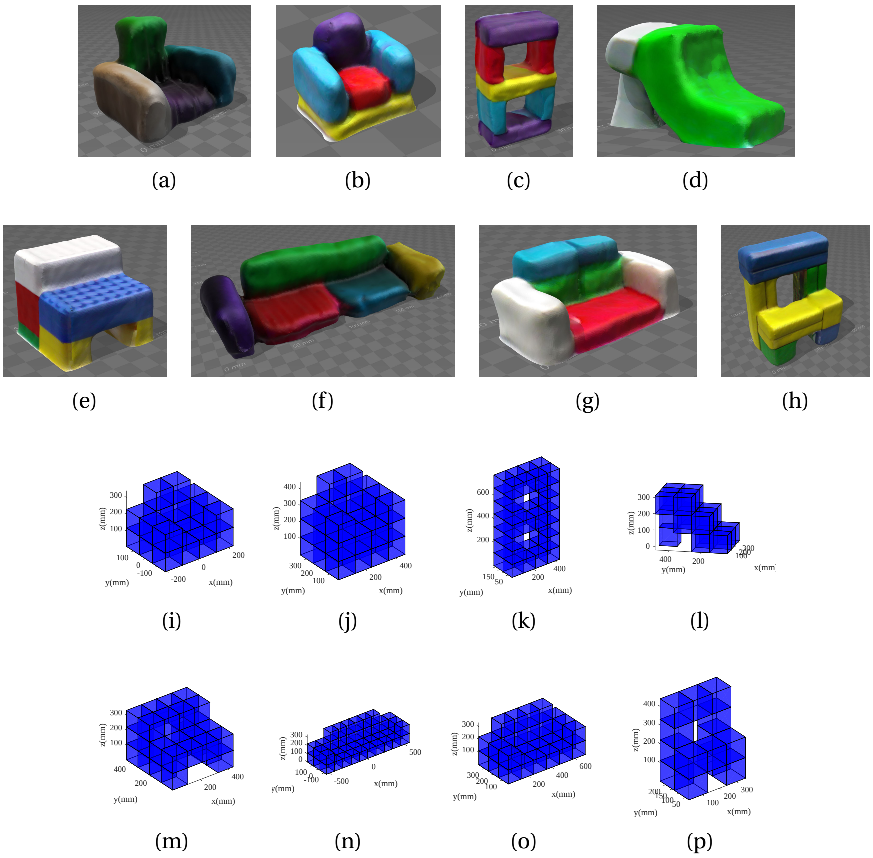

Figure A.3 – Benchmarking objects for playdough-to-Roombots and the corresponding found Roombots structures.

assumes them as uniform construction bricks, and (iii) scaling up the size of desired structures leads to exponential computation time. The suggested DFS with history and the pruning check can solve a reasonably sized search space in real time for our 13 Roombots modules. However, scaling up to more than 40-module-structures starts suffering from computation time. For larger structures, additional strategies are needed.

## A.2 Application: natural user interface

**Reference publication**

Parts of the text and figures of *Mehmet Mutlu, Stéphane Boardi, Massimo Vespignani, **Simon Hauser**, Alexandre Bernardino and Auke Ijspeert. "Natural user interface for lighting control: Case study on desktop lighting using modular robots." In 2016 25th IEEE International Symposium on Robot and Human Interactive Communication (RO-MAN), pp. 288-293. IEEE, 2016.* have been reorganized in this section.

**My original contributions**

- Help in the supplementary video, particularly in the hardware experiments
- Inputs to the manuscript

### A.2.1 Purpose

The Roombots modules can be configured not only into static pieces of furniture but also into dynamic, assistive pieces that can be coupled with various input devices. As one of such an device, a Kinect has been used in the past in combination with Roombots to create a natural user interface to position single Roombots modules. In this work, we show another use of the Kinect to naturally and dynamically control an overhead spotlight formed by a Roombots metamodule.

### A.2.2 Summary of the work

A Kinect depth camera is recording a top view of a desk workspace and detects a user's arm hold on a specific height. The position of the hand is extracted from this information with image processing and converted into global $x$- and $y$-coordinates. These coordinates then are passed to an inverse kinematics model that calculates the motor angles of the meta-module, moving the attached spotlight to the desired location. A similar procedure is used to control the brightness of the spotlight for which a different specific height of the arm is reserved. The control-loop of the illumination can be closed by comparing the position of the hand and the actual position of the spotlight and using the inverse kinematics model to correct the deviations. The results present an intuitive user interface for a spotlight illumination control.

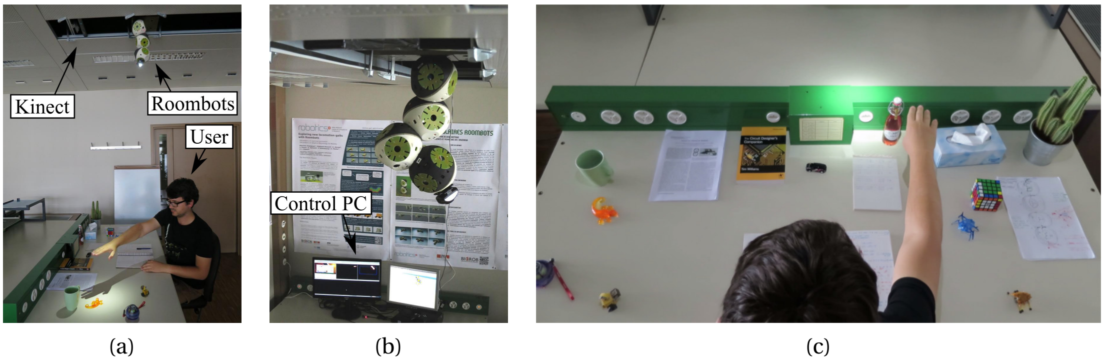

(a) (b) (c)

Figure A.4 – Setup of the spotlight user interface consisting of (a) a Roombots metamodule and Kinect and (b) a control PC. In (c), a user directing the spotlight with his hand can be seen.

## A.3 Application: virtual reality for reconfigurable rooms

**Reference publication**

Parts of the text and figures of *Valentin Nigolian, Mehmet Mutlu,* ***Simon Hauser****, Alexandre Bernardino and Auke Ijspeert. "Self-reconfigurable modular robot interface using virtual reality: Arrangement of furniture made out of roombots modules." In 2017 26th IEEE International Symposium on Robot and Human Interactive Communication (RO-MAN), pp. 772-778. IEEE, 2017.* have been reorganized in this section.

**My original contributions**

- Co-supervision of Valentin Nigolian
- Preparation of figures for the manuscript
- Inputs to the manuscript

### A.3.1 Purpose

A key question when working with a modular robot system is how to interact with such a bulk of robots, e.g. how to design a user defined shape to execute a specific task, as such systems get complex very quickly, especially when the kinematics of a module are particular as in Roombots. As an attempt to familiarize oneself with the Roombots platform and capabilities, this work uses Virtual Reality to design furniture based on Roombots modules and lets a user virtually arrange the created pieces of furniture in a virtual living room.

### A.3.2 Summary of the work

This work describes the development of a Virtual Reality environment to virtually assemble Roombots structures such as furniture in a "workshop" and afterwards arrange these and premade structures in a "living room". The Oculus Rift was used as a head-mounted-display

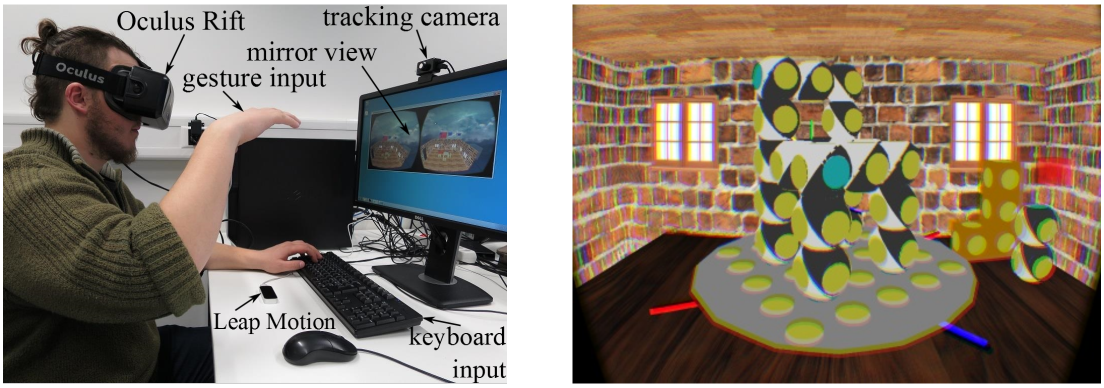

(a) (b)

Figure A.5 – Virtual Reality setup. (a) The complete set-up required by the system during a user test. (b) Main components of the GUI in the Workshop. On the right, RB modules and L-shapes can be grabbed and manipulated (the red cube represents the hand-controlled pointer). The cube turns white when holding a handle, to give the user feed-back that he or she pinched it. At the bottom, the "turntable" and its handles. In the center, the structure being currently assembled.

(HMD) and the Leapmotion provides gesture inputs, i.e. pinching and hand movement, to assemble modules. The interface was generally well received by the testers as a way to "play" and get into the complex movement capabilities of Roombots, however a comprehensive user study is needed to clarify the benefits of the virtual assembly.

# B Correlation maps

The full hinton matrix of section 6.3.5 is shown on the next page.

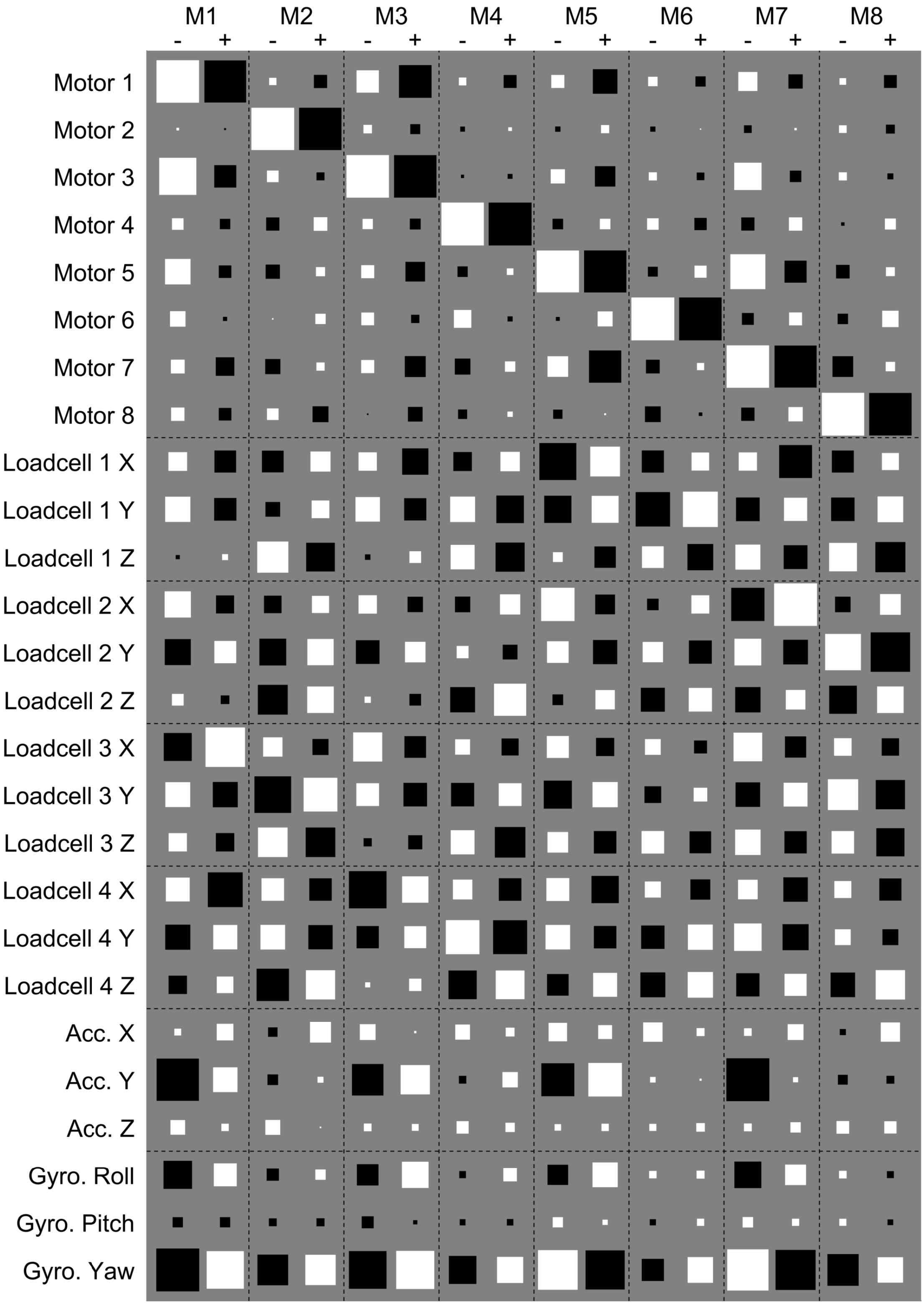

Figure B.1 – Full hinton diagram.

# Bibliography

[1] Abad, S. A., Sornkarn, N., and Nanayakkara, T. The role of morphological computation of the goat hoof in slip reduction. In *2016 IEEE/RSJ International Conference on Intelligent Robots and Systems (IROS)* (Oct. 2016), pp. 5599–5605.

[2] Ahmadzadeh, H., and Masehian, E. Modular robotic systems: Methods and algorithms for abstraction, planning, control, and synchronization. *Artificial Intelligence 223* (June 2015), 27–64.

[3] Ahmadzadeh, H., Masehian, E., and Asadpour, M. Modular Robotic Systems: Characteristics and Applications. *Journal of Intelligent & Robotic Systems* (June 2015), 1–41.

[4] Ajallooeian, M. *Pattern Generation for Rough Terrain Locomotion with Quadrupedal Robots.* PhD thesis, EPFL, 2015.

[5] Ajallooeian, M., Pouya, S., Sproewitz, A., and Ijspeert, A. J. Central Pattern Generators augmented with virtual model control for quadruped rough terrain locomotion. In *2013 IEEE International Conference on Robotics and Automation* (May 2013), pp. 3321–3328.

[6] Alexander, R. M. Elastic Energy Stores in Running Vertebrates. *American Zoologist 24*, 1 (1984), 85–94.

[7] Amend, J., Brown, E., Rodenberg, N., Jaeger, H., and Lipson, H. A Positive Pressure Universal Gripper Based on the Jamming of Granular Material. *IEEE Transactions on Robotics 28*, 2 (Apr. 2012), 341–350.

[8] Amend, J., Cheng, N., Fakhouri, S., and Culley, B. Soft Robotics Commercialization: Jamming Grippers from Research to Product. *Soft Robotics 3*, 4 (Dec. 2016), 213–222.

[9] Asfour, T., Vahrenkamp, N., Schiebener, D., Do, M., Przybylski, M., Welke, K., Schill, J., and Dillmann, R. ARMAR-III: Advances in Humanoid Grasping and Manipulation. *Journal of the Robotics Society of Japan 31*, 4 (2013), 341–346.

[10] Bajkowski, J. M., Dyniewicz, B., and Bajer, C. I. Damping properties of a beam with vacuum-packed granular damper. *Journal of Sound and Vibration 341* (Apr. 2015), 74–85.

[11] Bartsch, S., and Planthaber, S. Scarabaeus: A Walking Robot Applicable to Sample Return Missions. In *Research and Education in Robotics — EUROBOT 2008* (May 2008), Communications in Computer and Information Science, Springer, Berlin, Heidelberg, pp. 128–133.

[12] Beetz, M., Jain, D., Mosenlechner, L., Tenorth, M., Kunze, L., Blodow, N., and Pangercic, D. Cognition-Enabled Autonomous Robot Control for the Realization of Home Chore Task Intelligence. *Proceedings of the IEEE 100*, 8 (Aug. 2012), 2454–2471.

[13] Blackwood, C. B., Yuen, T. J., Sangeorzan, B. J., and Ledoux, W. R. The Midtarsal Joint Locking Mechanism. *Foot & Ankle International 26*, 12 (Dec. 2005), 1074–1080.

[14] Blumberg, M. S., Coleman, C. M., Gerth, A. I., and McMurray, B. Spatiotemporal Structure of REM Sleep Twitching Reveals Developmental Origins of Motor Synergies. *Current Biology 23*, 21 (Nov. 2013), 2100–2109.

[15] Bonardi, S., Blatter, J., Fink, J., Moeckel, R., Jermann, P., Dillenbourg, P., and Ijspeert, A. Design and evaluation of a graphical iPad application for arranging adaptive furniture. In *2012 IEEE RO-MAN* (Sept. 2012), pp. 290–297.

[16] Bonardi, S., Moeckel, R., Sproewitz, A., Vespignani, M., and Ijspeert, A. J. Locomotion through Reconfiguration based on Motor Primitives for Roombots Self-Reconfigurable Modular Robots. In *Robotics; Proceedings of ROBOTIK 2012; 7th German Conference on* (2012), VDE, pp. 1–6.

[17] Bonardi, S., Vespignani, M., Moeckel, R., and Ijspeert, A. J. Collaborative manipulation and transport of passive pieces using the self-reconfigurable modular robots roombots. In *Intelligent Robots and Systems (IROS), 2013 IEEE/RSJ International Conference on* (2013), Ieee, pp. 2406–2412.

[18] Bonardi, S., Vespignani, M., Moeckel, R., Van den Kieboom, J., Pouya, S., Sproewitz, A., and Ijspeert, A. Automatic generation of reduced CPG control networks for locomotion of arbitrary modular robot structures. In *Proceedings of Robotics: Science and Systems* (2014).

[19] Bongard, J. Morphological change in machines accelerates the evolution of robust behavior. *Proceedings of the National Academy of Sciences 108*, 4 (Jan. 2011), 1234–1239.

[20] Bongard, J. The 'What', 'How' and the 'Why' of Evolutionary Robotics. In *New Horizons in Evolutionary Robotics* (2011), S. Doncieux, N. Bredèche, and J.-B. Mouret, Eds., Studies in Computational Intelligence, Springer Berlin Heidelberg, pp. 29–35.

[21] Bongard, J., Zykov, V., and Lipson, H. Resilient Machines Through Continuous Self-Modeling. *Science 314*, 5802 (Nov. 2006), 1118–1121.

[22] Bongard, J. C. Evolutionary robotics. *Communications of the ACM 56*, 8 (2013), 74–83.

[23] BRANDT, D., CHRISTENSEN, D. J., AND LUND, H. H. ATRON Robots: Versatility from Self-Reconfigurable Modules. In *2007 International Conference on Mechatronics and Automation* (Aug. 2007), pp. 26–32.

[24] BRODBECK, L., HAUSER, S., AND IIDA, F. Morphological Evolution of Physical Robots through Model-Free Phenotype Development. *PLoS ONE 10*, 6 (June 2015), e0128444.

[25] BROEKENS, J., HEERINK, M., AND ROSENDAL, H. Assistive social robots in elderly care: a review. *Gerontechnology 8*, 2 (Apr. 2009).

[26] BROWN, E., RODENBERG, N., AMEND, J., MOZEIKA, A., STELTZ, E., ZAKIN, M. R., LIPSON, H., AND JAEGER, H. M. Universal robotic gripper based on the jamming of granular material. *Proceedings of the National Academy of Sciences 107*, 44 (2010), 18809–18814.

[27] CAMPLANI, M., PAIEMENT, A., MIRMEHDI, M., DAMEN, D., HANNUNA, S., BURGHARDT, T., AND TAO, L. Multiple human tracking in rgb-depth data: a survey. *IET Computer Vision 11* (June 2017), 265–285(20).

[28] CANIO, G. D., STOYANOV, S., LARSEN, J. C., HALLAM, J., KOVALEV, A., KLEINTEICH, T., GORB, S. N., AND MANOONPONG, P. A robot leg with compliant tarsus and its neural control for efficient and adaptive locomotion on complex terrains. *Artificial Life and Robotics 21*, 3 (Sept. 2016), 274–281.

[29] CARLSON, T., AND DEMIRIS, Y. Collaborative Control for a Robotic Wheelchair: Evaluation of Performance, Attention, and Workload. *IEEE Transactions on Systems, Man, and Cybernetics, Part B (Cybernetics) 42*, 3 (June 2012), 876–888.

[30] CATES, M. E., WITTMER, J. P., BOUCHAUD, J.-P., AND CLAUDIN, P. Jamming, force chains, and fragile matter. *Physical review letters 81*, 9 (1998), 1841.

[31] CHU, B., JUNG, K., HAN, C.-S., AND HONG, D. A survey of climbing robots: Locomotion and adhesion. *International Journal of Precision Engineering and Manufacturing 11*, 4 (Aug. 2010), 633–647.

[32] CLUB, K. The Kennel Club, Dec. 2017.

[33] COHEN, A. H., HOLMES, P. J., AND RAND, R. H. The nature of the coupling between segmental oscillators of the lamprey spinal generator for locomotion: A mathematical model. *Journal of Mathematical Biology 13*, 3 (Jan. 1982), 345–369.

[34] COLLINS, J. J., AND STEWART, I. N. Coupled nonlinear oscillators and the symmetries of animal gaits. *Journal of Nonlinear Science 3*, 1 (Dec. 1993), 349–392.

[35] CUI, X., ZHAO, J., ZHU, Y., AND TANG, S. UBot: a new reconfigurable modular robotic system with multimode locomotion ability. *Industrial Robot: the international journal of robotics research and application 39*, 2 (Mar. 2012), 178–190.

[36] CULLY, A., CLUNE, J., TARAPORE, D., AND MOURET, J.-B. Robots that can adapt like animals. *Nature 521*, 7553 (May 2015), 503–507.

[37] DAUDELIN, J., JING, G., TOSUN, T., YIM, M., KRESS-GAZIT, H., AND CAMPBELL, M. An integrated system for perception-driven autonomy with modular robots. *Science Robotics 3*, 23 (2018).

[38] DAVEY, J., KWOK, N., AND YIM, M. Emulating self-reconfigurable robots - design of the SMORES system. In *2012 IEEE/RSJ International Conference on Intelligent Robots and Systems (IROS)* (2012), pp. 4464–4469.

[39] DEMIRIS, Y. Knowing when to assist: Developmental issues in lifelong assistive robotics. In *2009 Annual International Conference of the IEEE Engineering in Medicine and Biology Society* (Sept. 2009), pp. 3357–3360.

[40] DICKINSON, M. H., FARLEY, C. T., FULL, R. J., KOEHL, M. A. R., KRAM, R., AND LEHMAN, S. How Animals Move: An Integrative View. *Science 288*, 5463 (Apr. 2000), 100–106.

[41] DONATELLI, R. Normal Biomechanics of the Foot and Ankle. *Journal of Orthopaedic & Sports Physical Therapy* (Nov. 1985).

[42] ECKERT, P., SPRÖWITZ, A., WITTE, H., AND IJSPEERT, A. J. Comparing the effect of different spine and leg designs for a small bounding quadruped robot. In *2015 IEEE International Conference on Robotics and Automation (ICRA)* (May 2015), pp. 3128–3133.

[43] FÜCHSLIN, R. M., DZYAKANCHUK, A., FLUMINI, D., HAUSER, H., HUNT, K. J., LUCHSINGER, R. H., RELLER, B., SCHEIDEGGER, S., AND WALKER, R. Morphological Computation and Morphological Control: Steps Toward a Formal Theory and Applications. *Artificial Life 19*, 1 (Jan. 2013), 9–34.

[44] FIROUZEH, A., SALERNO, M., AND PAIK, J. Soft pneumatic actuator with adjustable stiffness layers for multi-dof actuation. In *2015 IEEE/RSJ International Conference on Intelligent Robots and Systems (IROS)* (2015), IEEE, pp. 1117–1124.

[45] FOCCHI, M., BOAVENTURA, T., SEMINI, C., FRIGERIO, M., BUCHLI, J., AND CALDWELL, D. G. Torque-control based compliant actuation of a quadruped robot. In *2012 12th IEEE International Workshop on Advanced Motion Control (AMC)* (Mar. 2012), pp. 1–6.

[46] FONDAHL, K., KUEHN, D., BEINERSDORF, F., BERNHARD, F., GRIMMINGER, F., SCHILLING, M., STARK, T., AND KIRCHNER, F. An adaptive sensor foot for a bipedal and quadrupedal robot. In *2012 4th IEEE RAS EMBS International Conference on Biomedical Robotics and Biomechatronics (BioRob)* (June 2012), pp. 270–275.

[47] FORLIZZI, J., AND DISALVO, C. Service robots in the domestic environment: A study of the roomba vacuum in the home. In *Proceedings of the 1st ACM SIGCHI/SIGART Conference on Human-robot Interaction* (New York, NY, USA, 2006), HRI '06, ACM, pp. 258–265.

[48] FUKUDA, T., NAKAGAWA, S., KAWAUCHI, Y., AND BUSS, M. Self Organizing Robots Based on Cell Structures - CEBOT. In *IEEE International Workshop on Intelligent Robots* (Oct. 1988), pp. 145–150.

[49] FUKUHARA, A., OWAKI, D., KANO, T., AND ISHIGURO, A. Leg Stiffness Control Based on “TEGOTAE” for Quadruped Locomotion. In *Biomimetic and Biohybrid Systems* (July 2016), Lecture Notes in Computer Science, Springer, Cham, pp. 79–84.

[50] FUKUHARA, A., OWAKI, D., KANO, T., KOBAYASHI, R., AND ISHIGURO, A. Spontaneous gait transition to high-speed galloping by reconciliation between body support and propulsion. *Advanced Robotics 32*, 15 (Aug. 2018), 794–808.

[51] GAO, W., ZHANG, Y., NAZZETTA, D. C., RAMANI, K., AND CIPRA, R. J. RevoMaker: Enabling Multi-directional and Functionally-embedded 3d Printing Using a Rotational Cuboidal Platform. In *Proceedings of the 28th Annual ACM Symposium on User Interface Software & Technology* (New York, NY, USA, 2015), UIST ’15, ACM, pp. 437–446.

[52] GEORGOULAS, C., LINNER, T., AND BOCK, T. Towards a vision controlled robotic home environment. *Automation in Construction 39* (2014), 106 – 116.

[53] GERMANN, J., DOMMER, M., PERICET-CAMARA, R., AND FLOREANO, D. Active Connection Mechanism for Soft Modular Robots. *Advanced Robotics 26*, 7 (Jan. 2012), 785–798.

[54] GEYER, H., SEYFARTH, A., AND BLICKHAN, R. Compliant leg behaviour explains basic dynamics of walking and running. *Proceedings of the Royal Society of London B: Biological Sciences 273*, 1603 (Nov. 2006), 2861–2867.

[55] GROSS, M. D., AND GREEN, K. E. Architectural robotics, inevitably. *interactions 19*, 1 (Jan. 2012), 28–33.

[56] GROSS, R., TUCI, E., DORIGO, M., BONANI, M., AND MONDADA, F. Object transport by modular robots that self-assemble. In *Proceedings 2006 IEEE International Conference on Robotics and Automation, 2006. ICRA 2006.* (May 2006), pp. 2558–2564.

[57] GUO, D., AND HU, H. Nonlinear stiffness of a magneto-rheological damper. *Nonlinear Dynamics 40*, 3 (2005), 241–249.

[58] HAM, R., SUGAR, T., VANDERBORGHT, B., HOLLANDER, K., AND LEFEBER, D. Compliant actuator designs. *IEEE Robotics & Automation Magazine 16*, 3 (Sept. 2009), 81–94.

[59] HAN, J., PAUWELS, E. J., DE ZEEUW, P. M., AND DE WITH, P. H. N. Employing a rgb-d sensor for real-time tracking of humans across multiple re-entries in a smart environment. *IEEE Transactions on Consumer Electronics 58*, 2 (May 2012), 255–263.

[60] HAUSER, S., ECKERT, P., TULEU, A., AND IJSPEERT, A. Friction and damping of a compliant foot based on granular jamming for legged robots. In *2016 6th IEEE International*

*Conference on Biomedical Robotics and Biomechatronics (BioRob)* (2016), IEEE, pp. 1160–1165.

[61] HAUSER, S., MELO, K., MUTLU, M., AND IJSPEERT, A. J. Fast state-switching of a jamming-based foot.

[62] HAUSER, S., MUTLU, M., FREUNDLER, F., AND IJSPEERT, A. Stiffness variability in jamming of compliant granules and a case study application in climbing vertical shafts. IEEE, p. in press.

[63] HEBB, D. O. *The organization of behavior; a neuropsychological theory.* The organization of behavior; a neuropsychological theory. John Wiley & Sons Inc, Oxford, England, 1949.

[64] HILDEBRAND, M. The Quadrupedal Gaits of Vertebrates. *BioScience 39*, 11 (Dec. 1989), 766–775.

[65] HONG, Y. S., YI, S. Y., RYU, S. B., AND LEE, C. W. Design and experimental test of a new robot foot for a quadrupedal jointed-leg type walking robot. In *, 5th IEEE International Workshop on Robot and Human Communication, 1996* (Nov. 1996), pp. 317–322.

[66] HU, M., MU, Q.-S., LUO, N., LI, G., AND PENG, N.-B. Behavior of hollow balls containing granules bouncing repeatedly off the ground. *EPL (Europhysics Letters) 103*, 1 (July 2013), 14003.

[67] HUNT, K. D., CANT, J. G. H., GEBO, D. L., ROSE, M. D., WALKER, S. E., AND YOULATOS, D. Standardized descriptions of primate locomotor and postural modes. *Primates 37*, 4 (Oct. 1996), 363–387.

[68] HUTTER, M., GEHRING, C., JUD, D., LAUBER, A., BELLICOSO, C. D., TSOUNIS, V., HWANGBO, J., BODIE, K., FANKHAUSER, P., BLOESCH, M., DIETHELM, R., BACHMANN, S., MELZER, A., AND HOEPFLINGER, M. ANYmal - a highly mobile and dynamic quadrupedal robot. In *2016 IEEE/RSJ International Conference on Intelligent Robots and Systems (IROS)* (Oct. 2016), pp. 38–44.

[69] HUTTER, M., REMY, C. D., HOEPFLINGER, M. A., AND SIEGWART, R. Efficient and Versatile Locomotion With Highly Compliant Legs. *IEEE/ASME Transactions on Mechatronics 18*, 2 (Apr. 2013), 449–458.

[70] IIDA, F., GOMEZ, G., AND PFEIFER, R. Exploiting body dynamics for controlling a running quadruped robot. In *ICAR '05. Proceedings., 12th International Conference on Advanced Robotics, 2005.* (July 2005), pp. 229–235.

[71] IIDA, F., AND PFEIFER, R. Cheap rapid locomotion of a quadruped robot: Self-stabilization of bounding gait. In *In: Proceedings of the International Conference on Intelligent Autonomous Systems* (2004), vol. 8, pp. 642–649.

[72] Iida, F., Rummel, J., and Seyfarth, A. Bipedal Walking and Running with Compliant Legs. In *Proceedings 2007 IEEE International Conference on Robotics and Automation* (Apr. 2007), pp. 3970–3975.

[73] Ijspeert, A. J. Central pattern generators for locomotion control in animals and robots: A review. *Neural Networks 21*, 4 (May 2008), 642–653.

[74] Ijspeert, A. J., Crespi, A., Ryczko, D., and Cabelguen, J.-M. From Swimming to Walking with a Salamander Robot Driven by a Spinal Cord Model. *Science 315*, 5817 (Mar. 2007), 1416–1420.

[75] Ishii, H., Ratti, C., Piper, B., Wang, Y., Biderman, A., and Ben-Joseph, E. Bringing Clay and Sand into Digital Design — Continuous Tangible user Interfaces. *BT Technology Journal 22*, 4 (Oct. 2004), 287–299.

[76] Jakobi, N., Husbands, P., and Harvey, I. Noise and the reality gap: The use of simulation in evolutionary robotics. In *Advances in Artificial Life*, vol. 929. Springer Berlin Heidelberg, Berlin, Heidelberg, 1995, pp. 704–720.

[77] Jiang, A., Ataollahi, A., Althoefer, K., Dasgupta, P., and Nanayakkara, T. A variable stiffness joint by granular jamming. In *ASME 2012 International Design Engineering Technical Conferences and Computers and Information in Engineering Conference* (2012), American Society of Mechanical Engineers, pp. 267–275.

[78] Jiang, A., Ranzani, T., Gerboni, G., Lekstutyte, L., Althoefer, K., Dasgupta, P., and Nanayakkara, T. Robotic Granular Jamming: Does the Membrane Matter? *Soft Robotics 1*, 3 (2014), 192–201.

[79] Jiang, A., Xynogalas, G., Dasgupta, P., Althoefer, K., and Nanayakkara, T. Design of a variable stiffness flexible manipulator with composite granular jamming and membrane coupling. In *2012 IEEE/RSJ International Conference on Intelligent Robots and Systems (IROS)* (Oct. 2012), IEEE, pp. 2922–2927.

[80] Jing, G., Tosun, T., Yim, M., and Kress-Gazit, H. An end-to-end system for accomplishing tasks with modular robots. In *Robotics: Science and Systems* (2016).

[81] Johnson, S., and Thomas, A. P. Squishy Circuits: A Tangible Medium for Electronics Education. In *CHI '10 Extended Abstracts on Human Factors in Computing Systems* (New York, NY, USA, 2010), CHI EA '10, ACM, pp. 4099–4104.

[82] Kang, H. j., Hashimoto, K., Kondo, H., Hattori, K., Nishikawa, K., Hama, Y., Lim, H. o., Takanishi, A., Suga, K., and Kato, K. Realization of biped walking on uneven terrain by new foot mechanism capable of detecting ground surface. In *2010 IEEE International Conference on Robotics and Automation* (May 2010), pp. 5167–5172.

[83] Kano, T., Nagasawa, K., Owaki, D., Tero, A., and Ishiguro, A. A CPG-based decentralized control of a quadruped robot inspired by true slime mold. In *2010 IEEE/RSJ International Conference on Intelligent Robots and Systems* (Oct. 2010), pp. 4928–4933.

[84] KHODR, H., MUTLU, M., HAUSER, S., BERNARDINO, A., AND IJSPEERT, A. An optimal planning framework to deploy self-reconfigurable modular robots. In *2019 IEEE/RSJ International Conference on Intelligent Robots and Systems (IROS)* (2019), p. (Submitted).

[85] KHORAMSHAHI, M., SPROWITZ, A., TULEU, A., AHMADABADI, M. N., AND IJSPEERT, A. Benefits of an Active Spine Supported Bounding Locomotion With a Small Compliant Quadruped Robot. *Proceedings of 2013 IEEE International Conference on Robotics and Automation* (2013).

[86] KIKUUWE, R., YASUKOUCHI, S., FUJIMOTO, H., AND YAMAMOTO, M. Proxy-Based Sliding Mode Control: A Safer Extension of PID Position Control. *IEEE Transactions on Robotics 26*, 4 (Aug. 2010), 670–683.

[87] KIM, S., LASCHI, C., AND TRIMMER, B. Soft robotics: a bioinspired evolution in robotics. *Trends in Biotechnology 31*, 5 (May 2013), 287–294.

[88] KOPPULA, H. S., GUPTA, R., AND SAXENA, A. Learning human activities and object affordances from rgb-d videos. *The International Journal of Robotics Research 32*, 8 (2013), 951–970.

[89] KOSKO, B. Differential Hebbian learning. *AIP Conference Proceedings 151*, 1 (Aug. 1986), 277–282.

[90] KRUPKE, D., LI, G., ZHANG, J., ZHANG, H., AND HILDRE, H. P. Flexible modular robotic simulation environment for research and education. In *European Conference on Modelling and Simulation (ECMS)* (2012), pp. 243–249.

[91] KUROKAWA, H., TOMITA, K., KAMIMURA, A., KOKAJI, S., HASUO, T., AND MURATA, S. Distributed Self-Reconfiguration of M-TRAN III Modular Robotic System. *The International Journal of Robotics Research 27*, 3-4 (Mar. 2008), 373–386.

[92] KUROKAWA, H., TOMITA, K., YOSHIDA, E., MURATA, S., AND KOKAJI, S. Motion simulation of a modular robotic system. In *2000 26th Annual Conference of the IEEE Industrial Electronics Society. IECON 2000. 2000 IEEE International Conference on Industrial Electronics, Control and Instrumentation. 21st Century Technologies* (Oct 2000), vol. 4, pp. 2473–2478 vol.4.

[93] LASA, M. D., AND BUEHLER, M. Dynamic compliant quadruped walking. In *Proceedings 2001 ICRA. IEEE International Conference on Robotics and Automation (Cat. No.01CH37164)* (2001), vol. 3, pp. 3153–3158 vol.3.

[94] LASCHI, C., ROSSITER, J., IIDA, F., CIANCHETTI, M., AND MARGHERI, L. *Soft robotics: trends, applications and challenges.* Springer Berlin Heidelberg, New York, NY, 2016.

[95] LIEDKE, J., MATTHIAS, R., WINKLER, L., AND WÖRN, H. The Collective Self-reconfigurable Modular Organism (CoSMO). In *2013 IEEE/ASME International Conference on Advanced Intelligent Mechatronics* (July 2013), pp. 1–6.

[96] LIU, A. J., AND NAGEL, S. R. Nonlinear dynamics: Jamming is not just cool any more. *Nature 396*, 6706 (1998), 21–22.

[97] LIU, J., LIU, Y., ZHANG, G., ZHU, P., AND CHEN, Y. Q. Detecting and tracking people in real time with rgb-d camera. *Pattern Recognition Letters 53* (2015), 16 – 23.

[98] MAGNÚSSON, A., PACHECO, M., MOGHADAM, M., LUND, H. H., AND CHRISTENSEN, D. J. Fable: Socially Interactive Modular Robot. *The Eighteenth International Symposium on Artificial Life and Robotics* (2013), 9.

[99] MAITIN-SHEPARD, J., CUSUMANO-TOWNER, M., LEI, J., AND ABBEEL, P. Cloth grasp point detection based on multiple-view geometric cues with application to robotic towel folding. In *2010 IEEE International Conference on Robotics and Automation* (May 2010), pp. 2308–2315.

[100] MARQUES, H. G., IMTIAZ, F., IIDA, F., AND PFEIFER, R. Self-organization of reflexive behavior from spontaneous motor activity. *Biological Cybernetics 107*, 1 (Feb. 2013), 25–37.

[101] MARTIN, S., KELLY, G., KERNOHAN, W. G., MCCREIGHT, B., AND NUGENT, C. Smart home technologies for health and social care support. *Cochrane Database of Systematic Reviews 2008 4*, 2 (2009), 13.

[102] MELO, K., GARABINI, M., GRIOLI, G., CATALANO, M., MALAGIA, L., AND BICCHI, A. Open Source VSA-CubeBots for Rapid Soft Robot Prototyping. In *Robot Makers-Workshop in conjunction with 2014 Robotics Science and Systems Conference* (2014), pp. 1–5.

[103] METHTHANANDA, I. M., PARKER, S., PATEL, M. P., AND BRADEN, M. The relationship between Shore hardness of elastomeric dental materials and Young's modulus. *Dental Materials 25*, 8 (Aug. 2009), 956–959.

[104] MONDADA, F., GAMBARDELLA, L. M., FLOREANO, D., NOLFI, S., DENEUBORG, J. ., AND DORIGO, M. The cooperation of swarm-bots: physical interactions in collective robotics. *IEEE Robotics Automation Magazine 12*, 2 (June 2005), 21–28.

[105] MUTLU, M., BONARDI, S., VESPIGNANI, M., HAUSER, S., BERNARDINO, A., AND IJSPEERT, A. J. Natural user interface for lighting control: Case study on desktop lighting using modular robots. In *2016 25th IEEE International Symposium on Robot and Human Interactive Communication (RO-MAN)* (Aug. 2016), pp. 288–293.

[106] MUTLU, M., HAUSER, S., BERNARDINO, A., AND IJSPEERT, A. Effects of joint compliance in quadrupedal locomotion. p. 2.

[107] MUTLU, M., HAUSER, S., BERNARDINO, A., AND IJSPEERT, A. Playdough to Roombots: Towards a novel tangible user interface for self-reconfigurable modular robots. IEEE, p. in press.

[108] MUTLU, M., SARANLI, A., AND SARANLI, U. A real-time inertial motion blur metric: Application to frame triggering based motion blur minimization. In *2014 IEEE International Conference on Robotics and Automation (ICRA)* (May 2014), pp. 671–676.

[109] NARIOKA, K., HOMMA, T., AND HOSODA, K. Humanlike ankle-foot complex for a biped robot. In *2012 12th IEEE-RAS International Conference on Humanoid Robots (Humanoids 2012)* (Nov. 2012), pp. 15–20.

[110] NEUBAUER, W. Locomotion with articulated legs in pipes or ducts. *Robotics and Autonomous Systems 11*, 3-4 (1993), 163–169.

[111] NEUBERT, J., AND LIPSON, H. Soldercubes: a self-soldering self-reconfiguring modular robot system. *Autonomous Robots* (July 2015).

[112] NIGOLIAN, V., MUTLU, M., HAUSER, S., BERNARDINO, A., AND IJSPEERT, A. Self-reconfigurable modular robot interface using virtual reality: Arrangement of furniture made out of roombots modules. In *2017 26th IEEE International Symposium on Robot and Human Interactive Communication (RO-MAN)* (Aug. 2017), pp. 772–778.

[113] OHTSUKA, S., ENDO, G., FUKUSHIMA, E. F., AND HIROSE, S. Development of terrain adaptive sole for multi-legged walking robot. In *2010 IEEE/RSJ International Conference on Intelligent Robots and Systems* (Oct. 2010), pp. 5354–5359.

[114] ORILIVING. Robotic wardrobes, 2019.

[115] OWAKI, D., GODA, M., MIYAZAWA, S., AND ISHIGURO, A. A Minimal Model Describing Hexapedal Interlimb Coordination: The Tegotae-Based Approach. *Frontiers in Neurorobotics 11* (2017).

[116] OWAKI, D., KANO, T., NAGASAWA, K., TERO, A., AND ISHIGURO, A. Simple robot suggests physical interlimb communication is essential for quadruped walking. *Journal of The Royal Society Interface* (Oct. 2012), rsif20120669.

[117] OWAKI, D., MORIKAWA, L., AND ISHIGURO, A. Listen to body's message: Quadruped robot that fully exploits physical interaction between legs. In *2012 IEEE/RSJ International Conference on Intelligent Robots and Systems* (Oct. 2012), pp. 1950–1955.

[118] OWAKI, D., MORIKAWA, L., AND ISHIGURO, A. Why do quadrupeds exhibit exclusively either trot or pace gaits. *Proc. of Dynamic Walking 2013* (2013).

[119] OZGUR, A., BONARDI, S., VESPIGNANI, M., MOCKEL, R., AND IJSPEERT, A. J. Natural user interface for Roombots. In *Robot and Human Interactive Communication, 2014 RO-MAN: The 23rd IEEE International Symposium on* (2014), IEEE, pp. 12–17.

[120] PACHECO-VÁZQUEZ, F., AND DORBOLO, S. Rebound of a confined granular material: combination of a bouncing ball and a granular damper. *Scientific Reports 3* (July 2013).

[121] PETERSSON, P., WALDENSTRÖM, A., FÅHRAEUS, C., AND SCHOUENBORG, J. Spontaneous muscle twitches during sleep guide spinal self-organization. *Nature 424*, 6944 (July 2003), 72–75.

[122] PFEIFER, R., AND BONGARD, J. *How the Body Shapes the Way We Think: A New View of Intelligence*. MIT Press, Oct. 2006. Google-Books-ID: EHPMv9MfgWwC.

[123] PFEIFER, R., AND GÓMEZ, G. Morphological Computation – Connecting Brain, Body, and Environment. In *Creating Brain-Like Intelligence: From Basic Principles to Complex Intelligent Systems*, B. Sendhoff, E. Körner, O. Sporns, H. Ritter, and K. Doya, Eds., Lecture Notes in Computer Science. Springer Berlin Heidelberg, Berlin, Heidelberg, 2009, pp. 66–83.

[124] PFEIFER, R., IIDA, F., AND GÓMEZ, G. Morphological computation for adaptive behavior and cognition. *International Congress Series 1291* (June 2006), 22–29.

[125] PFEIFER, R., LUNGARELLA, M., AND IIDA, F. Self-Organization, Embodiment, and Biologically Inspired Robotics. *Science 318*, 5853 (Nov. 2007), 1088–1093.

[126] PIAZZA, C., SANTINA, C. D., GASPARRI, G. M., CATALANO, M. G., GRIOLI, G., GARABINI, M., AND BICCHI, A. Toward an adaptive foot for natural walking. In *2016 IEEE-RAS 16th International Conference on Humanoid Robots (Humanoids)* (Nov. 2016), pp. 1204–1210.

[127] PIPER, B., RATTI, C., AND ISHII, H. Illuminating Clay: A 3-D Tangible Interface for Landscape Analysis. In *Proceedings of the SIGCHI Conference on Human Factors in Computing Systems* (New York, NY, USA, 2002), CHI '02, ACM, pp. 355–362.

[128] POULAKAKIS, I., SMITH, J. A., AND BUEHLER, M. Modeling and Experiments of Untethered Quadrupedal Running with a Bounding Gait: The Scout II Robot , Modeling and Experiments of Untethered Quadrupedal Running with a Bounding Gait: The Scout II Robot. *The International Journal of Robotics Research 24*, 4 (Apr. 2005), 239–256.

[129] RAIBERT, M., BLANKESPOOR, K., NELSON, G., AND PLAYTER, R. BigDog, the Rough-Terrain Quadruped Robot. *IFAC Proceedings Volumes 41*, 2 (Jan. 2008), 10822–10825.

[130] RAIBERT, M., CHEPPONIS, M., AND BROWN, H. Running on four legs as though they were one. *IEEE Journal on Robotics and Automation 2*, 2 (June 1986), 70–82.

[131] RAMEY, A., GONZALEZ-PACHECO, V., AND SALICHS, M. A. Integration of a low-cost rgb-d sensor in a social robot for gesture recognition. In *2011 6th ACM/IEEE International Conference on Human-Robot Interaction (HRI)* (March 2011), pp. 229–230.

[132] ROBERTSON, M. A., SADEGHI, H., FLOREZ, J. M., AND PAIK, J. Soft Pneumatic Actuator Fascicles for High Force and Reliability. *Soft Robotics* (Oct. 2016).

[133] ROBINSON, G., AND DAVIES, J. B. C. Continuum robots-a state of the art. In *Robotics and Automation, 1999. Proceedings. 1999 IEEE International Conference on* (1999), vol. 4, IEEE, pp. 2849–2854.

[134] ROBOTIS. Bioloid comprehensive kit, July 2018.

[135] ROH, S., AND CHOI, H. R. Differential-drive in-pipe robot for moving inside urban gas pipelines. *IEEE Transactions on Robotics 21*, 1 (Feb. 2005), 1–17.

[136] ROLLINSON, D., BILGEN, Y., BROWN, B., ENNER, F., FORD, S., LAYTON, C., REMBISZ, J., SCHWERIN, M., WILLIG, A., VELAGAPUDI, P., AND CHOSET, H. Design and architecture of a series elastic snake robot. In *2014 IEEE/RSJ International Conference on Intelligent Robots and Systems (IROS)* (2014), IEEE, pp. 4630–4636.

[137] ROMANISHIN, J. W., GILPIN, K., CLAICI, S., AND RUS, D. 3d M-Blocks: Self-Reconfiguring robots capable of locomotion via pivoting in three dimensions. In *Robotics and Automation (ICRA), 2015 IEEE International Conference on* (2015), IEEE, pp. 1925–1932.

[138] ROMANISHIN, J. W., GILPIN, K., AND RUS, D. M-blocks: Momentum-driven, magnetic modular robots. In *2013 IEEE/RSJ International Conference on Intelligent Robots and Systems* (Nov. 2013), pp. 4288–4295.

[139] ROSSET, S., GEBBERS, P., O'BRIEN, B. M., AND SHEA, H. R. The need for speed. Y. Bar-Cohen, Ed., p. 834004.

[140] RYU, H., NAKATA, Y., NAKAMURA, Y., AND ISHIGURO, H. Adaptive Whole-Body Dynamics: An Actuator Network System for Orchestrating Multijoint Movements. *IEEE Robotics & Automation Magazine 23*, 3 (Sept. 2016), 85–92.

[141] SALEMI, B., MOLL, M., AND SHEN, W.-M. SUPERBOT: A deployable, multi-functional, and modular self-reconfigurable robotic system. In *Intelligent Robots and Systems, 2006 IEEE/RSJ International Conference on* (2006), IEEE, pp. 3636–3641.

[142] SEMINI, C., TSAGARAKIS, N. G., GUGLIELMINO, E., FOCCHI, M., CANNELLA, F., AND CALDWELL, D. G. Design of HyQ – a hydraulically and electrically actuated quadruped robot. *Proceedings of the Institution of Mechanical Engineers, Part I: Journal of Systems and Control Engineering 225*, 6 (Sept. 2011), 831–849.

[143] SEO, J. T., AND YI, B. J. Modeling and analysis of a biomimetic foot mechanism. In *2009 IEEE/RSJ International Conference on Intelligent Robots and Systems* (Oct. 2009), pp. 1472–1477.

[144] SHANG, J., NOONAN, D. P., PAYNE, C., CLARK, J., SODERGREN, M. H., DARZI, A., AND YANG, G.-Z. An articulated universal joint based flexible access robot for minimally invasive surgery. In *Robotics and Automation (ICRA), 2011 IEEE International Conference on* (2011), IEEE, pp. 1147–1152.

[145] SIRKIN, D., MOK, B., YANG, S., AND JU, W. Mechanical ottoman: How robotic furniture offers and withdraws support. In *Proceedings of the Tenth Annual ACM/IEEE International Conference on Human-Robot Interaction* (New York, NY, USA, 2015), HRI '15, ACM, pp. 11–18.

[146] SÁNCHEZ, M., ROSENTHAL, G., AND PUGNALONI, L. A. Universal response of optimal granular damping devices. *Journal of Sound and Vibration 331*, 20 (2012), 4389–4394.

[147] SPROEWITZ, A. *Roombots: Design and Implementation of a Modular Robot for Reconfiguration and Locomotion.* PhD thesis, EPFL, 2010.

[148] SPROEWITZ, A., BILLARD, A., DILLENBOURG, P., AND IJSPEERT, A. Roombots-mechanical design of self-reconfiguring modular robots for adaptive furniture. In *IEEE International Conference on Robotics and Automation, 2009. ICRA '09* (May 2009), pp. 4259–4264.

[149] SPROEWITZ, A., LAPRADE, P., BONARDI, S., MAYER, M., MOECKEL, R., MUDRY, P.-A., AND IJSPEERT, A. J. Roombots - Towards decentralized reconfiguration with self-reconfiguring modular robotic metamodules. In *2010 IEEE/RSJ International Conference on Intelligent Robots and Systems* (Taipei, Oct. 2010), IEEE, pp. 1126–1132.

[150] SPROEWITZ, A., MOECKEL, R., MAYE, J., AND IJSPEERT, A. J. Learning to Move in Modular Robots using Central Pattern Generators and Online Optimization. *The International Journal of Robotics Research 27*, 3-4 (Mar. 2008), 423–443.

[151] SPROWITZ, A., POUYA, S., BONARDI, S., KIEBOOM, J. V. D., MOCKEL, R., BILLARD, A., DILLENBOURG, P., AND IJSPEERT, A. J. Roombots: Reconfigurable Robots for Adaptive Furniture. *IEEE Computational Intelligence Magazine 5*, 3 (Aug. 2010), 20–32.

[152] SPROWITZ, A., TULEU, A., VESPIGNANI, M., AJALLOOEIAN, M., BADRI, E., AND IJSPEERT, A. J. Towards dynamic trot gait locomotion: Design, control, and experiments with Cheetah-cub, a compliant quadruped robot. *The International Journal of Robotics Research 32*, 8 (July 2013), 932–950.

[153] SPRÖWITZ, A., MOECKEL, R., VESPIGNANI, M., BONARDI, S., AND IJSPEERT, A. Roombots: A hardware perspective on 3d self-reconfiguration and locomotion with a homogeneous modular robot. *Robotics and Autonomous Systems 62*, 7 (July 2014), 1016–1033.

[154] SRINIVASA, S. S., BERENSON, D., CAKMAK, M., COLLET, A., DOGAR, M. R., DRAGAN, A. D., KNEPPER, R. A., NIEMUELLER, T., STRABALA, K., WEGHE, M. V., AND ZIEGLER, J. Herb 2.0: Lessons Learned From Developing a Mobile Manipulator for the Home. *Proceedings of the IEEE 100*, 8 (Aug. 2012), 2410–2428.

[155] STOY, K. Using cellular automata and gradients to control self-reconfiguration. *Robotics and Autonomous Systems 54*, 2 (Feb. 2006), 135–141.

[156] STOY, K., BRANDT, D., AND CHRISTENSEN, D. J. *Self-reconfigurable robots: an introduction.* Intelligent robotics and autonomous agents. MIT Press, Cambridge, Mass, 2010.

[157] STOY, K., AND NAGPAL, R. Self-repair through scale independent self-reconfiguration. In *2004 IEEE/RSJ International Conference on Intelligent Robots and Systems (IROS) (IEEE Cat. No.04CH37566)* (Sept. 2004), vol. 2, pp. 2062–2067 vol.2.

[158] Sugahara, Y., Hosobata, T., Mikuriya, Y., Sunazuka, H., Lim, H.-o., and Takanishi, A. Realization of dynamic human-carrying walking by a biped locomotor. In *IEEE International Conference on Robotics and Automation, 2004. Proceedings. ICRA '04. 2004* (Apr. 2004), vol. 3, pp. 3055–3060 Vol.3.

[159] Takuma, T., Ikeda, M., and Masuda, T. Facilitating multi-modal locomotion in a quadruped robot utilizing passive oscillation of the spine structure. In *2010 IEEE/RSJ International Conference on Intelligent Robots and Systems* (Oct. 2010), pp. 4940–4945.

[160] Terada, Y., and Murata, S. Automatic Modular Assembly System and its Distributed Control. *The International Journal of Robotics Research 27*, 3-4 (Mar. 2008), 445–462.

[161] Tordesillas, A., Lin, Q., Zhang, J., Behringer, R., and Shi, J. Structural stability and jamming of self-organized cluster conformations in dense granular materials. *Journal of the Mechanics and Physics of Solids 59*, 2 (Feb. 2011), 265–296.

[162] Tosun, T., Daudelin, J., Jing, G., Kress-Gazit, H., Campbell, M., and Yim, M. Perception-informed autonomous environment augmentation with modular robots. In *2018 IEEE International Conference on Robotics and Automation (ICRA)* (May 2018), pp. 6818–6824.

[163] Ugurlu, B., Kotaka, K., and Narikiyo, T. Actively-compliant locomotion control on rough terrain: Cyclic jumping and trotting experiments on a stiff-by-nature quadruped. In *2013 IEEE International Conference on Robotics and Automation* (May 2013), pp. 3313–3320.

[164] Çulha, U., and Iida, F. Enhancement of finger motion range with compliant anthropomorphic joint design. *Bioinspiration & Biomimetics 11*, 2 (Feb. 2016), 026001.

[165] van den Berg, J., Miller, S., Goldberg, K., and Abbeel, P. *Gravity-Based Robotic Cloth Folding.* Springer Berlin Heidelberg, Berlin, Heidelberg, 2011, ch. 6, pp. 409–424.

[166] van Hecke, M. Jamming of soft particles: geometry, mechanics, scaling and isostaticity. *Journal of Physics: Condensed Matter 22*, 3 (Jan. 2010), 033101.

[167] Vasconcelos, R., Hauser, S., Dzeladini, F., Mutlu, M., Horvat, T., Melo, K., Oliveira, P., and Ijspeert, A. Active stabilization of a stiff quadruped robot using local feedback. In *2017 IEEE/RSJ International Conference on Intelligent Robots and Systems (IROS)* (Sept. 2017), pp. 4903–4910.

[168] Vespignani, M. *Challenges in the Locomotion of Self-Reconfigurable Modular Robots.* PhD thesis, 2015.

[169] Vespignani, M., Melo, K., Bonardi, S., and Ijspeert, A. J. Role of compliance on the locomotion of a reconfigurable modular snake robot. In *2015 IEEE/RSJ International Conference on Intelligent Robots and Systems (IROS)* (2015), IEEE, pp. 2238–2245.

[170] VESPIGNANI, M., MELO, K., MUTLU, M., AND IJSPEERT, A. J. Compliant snake robot locomotion on horizontal pipes. In *Safety, Security, and Rescue Robotics (SSRR), 2015 IEEE International Symposium on* (2015), IEEE, pp. 1–8.

[171] VESPIGNANI, M., SENFT, E., BONARDI, S., MOECKEL, R., AND IJSPEERT, A. J. An experimental study on the role of compliant elements on the locomotion of the self-reconfigurable modular robots Roombots. In *Intelligent Robots and Systems (IROS), 2013 IEEE/RSJ International Conference on* (2013), Ieee, pp. 4308–4313.

[172] VILENSKY, J. A., AND LARSON, S. G. Primate Locomotion: Utilization and Control of Symmetrical Gaits. *Annual Review of Anthropology 18*, 1 (Oct. 1989), 17–35.

[173] WEEL, B., D'ANGELO, M., HAASDIJK, E., AND EIBEN, A. E. Online Gait Learning for Modular Robots with Arbitrary Shapes and Sizes. *Artificial Life 23*, 1 (Jan. 2017), 80–104.

[174] WEI, H., CHEN, Y., TAN, J., AND WANG, T. Sambot: A self-assembly modular robot system. *IEEE/ASME Transactions on Mechatronics 16*, 4 (Aug 2011), 745–757.

[175] WEINMEISTER, K., ECKERT, P., WITTE, H., AND IJSPEERT, A. J. Cheetah-cub-S: Steering of a quadruped robot using trunk motion. In *2015 IEEE International Symposium on Safety, Security, and Rescue Robotics (SSRR)* (Oct. 2015), pp. 1–6.

[176] WELLER, M. P., GROSS, M. D., AND GOLDSTEIN, S. C. Hyperform Specification: Designing and Interacting with Self-reconfiguring Materials. *Personal Ubiquitous Comput. 15*, 2 (Feb. 2011), 133–149.

[177] WOLF, S., GRIOLI, G., EIBERGER, O., FRIEDL, W., GREBENSTEIN, M., HÖPPNER, H., BURDET, E., CALDWELL, D. G., CARLONI, R., CATALANO, M. G., LEFEBER, D., STRAMIGIOLI, S., TSAGARAKIS, N., DAMME, M. V., HAM, R. V., VANDERBORGHT, B., VISSER, L. C., BICCHI, A., AND ALBU-SCHÄFFER, A. Variable Stiffness Actuators: Review on Design and Components. *IEEE/ASME Transactions on Mechatronics 21*, 5 (Oct. 2016), 2418–2430.

[178] YE, M., ZHANG, Q., WANG, L., ZHU, J., YANG, R., AND GALL, J. *A Survey on Human Motion Analysis from Depth Data.* Springer Berlin Heidelberg, Berlin, Heidelberg, 2013, ch. 2, pp. 149–187.

[179] YIM, M., AND DUFF, A. D. Modular robots. *IEEE Spectrum 39*, 2 (Feb. 2002), 30–34.

[180] YIM, M., DUFF, D., AND ROUFAS, K. PolyBot: a modular reconfigurable robot. In *IEEE International Conference on Robotics and Automation, 2000. Proceedings. ICRA '00* (2000), vol. 1, pp. 514–520 vol.1.

[181] YIM, M., SHEN, W.-M., SALEMI, B., RUS, D., MOLL, M., LIPSON, H., KLAVINS, E., AND CHIRIKJIAN, G. Modular Self-Reconfigurable Robot Systems [Grand Challenges of Robotics]. *IEEE Robotics Automation Magazine 14*, 1 (Mar. 2007), 43–52.

[182] Yu, C.-H., Willems, F., Ingber, D., and Nagpal, R. Self-organization of environmentally-adaptive shapes on a modular robot. In *2007 IEEE/RSJ International Conference on Intelligent Robots and Systems* (Oct. 2007), pp. 2353–2360.

[183] Zhu, Y., Jin, H., Zhang, X., Yin, J., Liu, P., and Zhao, J. A multi-sensory autonomous docking approach for a self-reconfigurable robot without mechanical guidance. *International Journal of Advanced Robotic Systems 11*, 9 (2014), 146.

# Simon Lukas Hauser

Address: Route du Bois 19
CH-1024 Ecublens
Switzerland
Phone: +41 79 670 55 01
Mail & Skype: simonhauser@hotmail.com
LinkedIn: Simon-Hauser-EPFL
Google scholar: Simon Hauser

---

## Profile

I **design and construct bio-inspired robots** and have hands-on experience with **hardware experiments and data analysis**. My **research goal** is advancing the **understanding of animal locomotion** with the help of robotic tools. I (co-)authored **14 published works**, (co-)supervised over **20 student projects** and served as a **teaching assistant**. I enjoy working in an **international research team** and contribute to a **friendly and productive research environment**.

---

## Education

**since Dec. 2014:** **EPFL Lausanne, Switzerland,** graduation in August 2019

Doctor of Science (PhD); doctoral program in Robotics, Control and Intelligent Systems

- *Doctoral thesis:* Compliance, locomotion and local computation in (self-) reconfigurable modular robots; PhD supervisior: Prof. Auke Ijspeert

**2008 – 2014:** **ETH Zurich, Switzerland**

MSc in Mechanical Engineering; specialization in Robotics; GPA: 5.53 / 6

- *Master thesis:* Automated design and assembly of locomotive robots (Prof. Fumiya Iida)
- *Semester thesis:* From Spontaneous Motor Activity towards walking (Dr. Hugo Marques)

BSc in Mechanical Engineering; specialization in Mechatronics, GPA: 5.07 / 6

- *Bachelor thesis*: Resonance Frequency of Hopping Robots (Prof. Fumiya Iida)

**2011:** **AGH University of Science and Technology in Cracow, Poland**

10-week IAESTE internship; research assistant at the Faculty of Mechanical Engineering and Robotics (IMIR), www.imir.agh.edu.pl

**2008:** **East China Normal University (ECNU) in Shanghai, China**

6-week cultural exchange program *Glimpses of China*, www.foundationprograms.com

**2004 – 2008:** **High School, bilingual matriculation (German – French), Wohlen, Switzerland**

Specialisations in Physics, Mathematics and Biology; GPA: 5.0 / 6

---

## Professional Experience

**since Dec. 2014:** **Research assistant at Biorobotics Laboratory (BIOROB), EPFL, Lausanne, Switzerland**

Hardware and software improvements of the self-reconfigurable modular robot *Roombots*
Development of animal-inspired robots for locomotion research
Integration of compliant materials for control simplifications
Teaching and supervision of students

**2011 – 2012:** **Engineer (7-month internship), Ingenieurbureau H. Gerber, Baden, Switzerland**

*Development, production, consulting, examination and distribution of technical products*

Practical training: CAD, construction, prototyping, assembly, consulting, selling, international negotiations, administration, service

**2009:** **Polymechanic (5-week internship), ABB Turbo Systems, Baden, Switzerland**

*Development and production of turbocharging devices*

Workshop training: CNC, Drilling, filing, milling, grinding, manufacturing, assembly

## Technical Skills

Elective subjects: Control, Dynamic Programming and Recursive Estimation, Computer Science, System Identification, Modeling and Analysis of Dynamic Systems, Multibody and Nonlinear Dynamics, Image Analysis, Computer Vision and Virtual Reality, Bio-Inspired Motor Control, Computational Motor Control, Systems Neuroscience and Neural Networks, Unsupervised & Reinforcement Learning in Neural Networks, Topics in Autonomous Robotics

IT: Windows, LaTeX, Microsoft Office, OpenOffice, Linux

Programming: C, C++, Python, LabView, Mathematica

Design: Inventor, UGS NX 6, 3D printing software, Inkscape, Adobe Premier

Simulation: Webots robot simulator, Blender, Unity, Simulink

Analysis: MATLAB, Mathematica, Ansys Workbench, Flux

Hardware: Motors (Dynamixel, Maxon), force sensors (OptoForce, loadcells), embedded PCs (microcontroller, Arduino, Raspberry Pi, Odroid), electronics debugging (oscilloscope, logic analyser, multimeter), 3D printer, laser cutter, soldering

Entrepreneurship: Business Concept semester course in start-up training: market research, IP, venture capital

Teaching: Teaching assistant for the master course *Computational Motor Control* (3 curriculae)
Supervisor for *Robot Competition* (2 curriculae): consulting of teams of 3 students on how to build a robot from scratch that can collect PET bottles in a challenging arena
Supervision of over 20 student projects (semester and master theses)

## Languages

English: Fluent (C1 written and spoken), Certificate in Advanced English (CAE)
German: Mother tongue
French: Fair (B1 written, B2 spoken)
Chinese: Beginner, 1 year at ETH Zurich and 6-week language stay in Shaghai, China, 2008

## Achievements

since Dec. 2014: Presenter at multiple leading international conferences in the field of robotics
since Dec. 2014: Assembling and maintenance of modular robot system *Roombots*
Oct. 2016: Live coverage of *Roombots* on Swiss National TV during *Cybathlon*, a competition for exoskeletons
Sept. 2016: Invited artist with *Roombots* at *Ars Electronica* in Linz (Austria), European art and technology fair
Oct. 2015: Presenter of *Roombots* in *Tested* and at *Bay Area Science Festival* in San Francisco (US)
Mai. 2009: 2nd place Innovationproject at ETH Zurich (20 teams; robotic solution for sorting objects)

## Extraprofessional Activities

Music: Piano in a band, saxophone in a wind band, composing
Sport: Climbing indoor and outdoor, hiking, skiing
Other: Travelling (5-month world tour in 2012), magic, dancing (lindy-hop, tango)

## References

| | | | |
|---|---|---|---|
| Prof. A. Ijspeert: | PhD supervisor | auke.ijspeert@epfl.ch | +41 21 693 26 58 |
| Prof. F. Iida: | MSc/BSc supervisor | fi224@cam.ac.uk | +44 1223 3 32719 |

## Personal details

Swiss,30, single, Swiss driving licence A1/B

## Publications

### Book Chapters

1. L. Brodbeck, **S. Hauser**, F. Iida, "Robotic Invention: Challenges and Perspectives for model-free design optimization of dynamic locomotion robots", *Robotics Research*, Springer 2018

### Journal Articles

1. **S. Hauser**, M. Mutlu, P.-A. Léziart, H. Khodr, A. Bernardino, A. Ijspeert, "Roombots extended: Challenges of the next generation of self-reconfigurable modular robots and their application in adaptive and assistive furniture", Submitted to *Robotics and Autonomous Systems*
2. H. Khodr, M. Mutlu, **S. Hauser**, A. Bernardino, A. Ijspeert "An optimal planning framework to deploy self-reconfigurable modular robots", *IEEE Robotics and Automation Letters*, 2019, Submitted to *IEEE Robotics and Automation Letters*
3. **S. Hauser**, M. Mutlu, P. Banzet, A. Ijspeert, "Compliant universal grippers as adaptive feet in legged robots", *Advanced Robotics*, 2018
4. M. Mutlu, **S. Hauser**, A. Bernardino, A. Ijspeert, "Effects of passive and active joint compliance in quadrupedal locomotion", *Advanced Robotics*, 2018
5. **S. Hauser**, M. A. Robertson, A. Ijspeert, J. Paik, "JammJoint: A variable stiffness device based on granular jamming for wearable joint support", *IEEE Robotics and Automation Letters*, 2017
6. L. Brodbeck, **S. Hauser**, F. Iida, "Morphological evolution of physical robots through model-free phenotype development", *Plos ONE*, 2015

### Conference Proceedings

1. M. Mutlu, **S. Hauser**, M. Rickert, J. Santos-Victor, A. Ijspeert, A. Bernardino, "Vision-based autonomous docking with self-reconfigurable modular robots", (in preparation)
2. **S. Hauser**, M. Dujany, M. van der Saar, M. Mutlu, A. Ijspeert, "Learning to walk in arbitrary morphologies", *The 9th International Symposium on Adaptive Motion of Animals and Machines (AMAM)*, 2019
3. J. Nguyen-Duc, M. Mutlu, **S. Hauser**, A. Bernardino, A. Ijspeert, "Cooperative bridge building by self-reconfigurable modular robots based on ants' stigmergic behaviour", *The 9th International Symposium on Adaptive Motion of Animals and Machines (AMAM)*, 2019
4. **S. Hauser**, M. Mutlu, F. Freundler, A. Ijspeert, "Stiffness variability in jamming of compliant granules and a case study application in climbing vertical shafts", *IEEE International Conference on Robotics and Automation (ICRA)*, 2018
5. M. Mutlu, **S. Hauser**, A. Bernardino, A. Ijspeert, "Playdough to Roombots: Towards a novel tangible user interface for self-reconfigurable modular robots", *IEEE International Conference on Robotics and Automation (ICRA)*, 2018
6. R. Vasconcelos, **S. Hauser**, F. Dzeladini, M. Mutlu, T. Horvat, K. Melo, A. Ijspeert, "Active stabilization of a stiff quadruped robot using local feedback", *IEEE International conference on Intelligent Robots and Systems (IROS)*, 2017
7. V. Nigolian, M. Mutlu, **S. Hauser**, A. Bernardino, A. Ijspeert, "Self-reconfigurable modular robot interface using virtual reality: Arrangement of furniture made out of Roombots modules", *IEEE International Symposium on Robot and Human Interactive Communication (RO-MAN)*, 2017
8. **S. Hauser**, K. Melo, M. Mutlu, A. Ijspeert, "Fast state-switching of a jamming-based foot", *The 8th International Symposium on Adaptive Motion of Animals and Machines (AMAM)*, 2017
9. M. Mutlu, **S. Hauser**, A. Bernardino, A. Ijspeert, "Effects of joint compliance in quadrupedal locomotion", *The 8th International Symposium on Adaptive Motion of Animals and Machines (AMAM)*, 2017
10. **S. Hauser**, P. Eckert, A. Tuleu, A. Ijspeert, "Fricition and damping of a compliant foot based on granular jamming for legged robots", *IEEE International Conference on Biomedical Robotics and Biomechatronics (BioRob)*, 2016
11. M. Mutlu, S. Bonardi, M. Vespignani, **S. Hauser**, A. Bernardino, A. Ijspeert, "Natural user interface for lighting control: case study on desktop lighting using modular robots", *IEEE International Symposium on Robot and Human Interactive Communication (RO-MAN)*, 2016
12. F. Iida, M. Reis, N. Maheshwari, K. Gunura, **S. Hauser**, "Legged robot locomotion based on free vibration", *The 12th IEEE International Workshop on Advanced Motion Control*, 2012

Ce document a été imprimé au Centre d'impression EPFL,
imprimerie climatiquement neutre, certifiée myClimate.